MULTI-SINES STIMULUS DESIGN FOR THE ASSESSMENT OF NON-LINEAR DEVICES

A thesis submitted to Cardiff University

In candidature for the degree of

Doctor of Philosophy

By

Su Jiangtao

School of Engineering, Cardiff University, United Kingdom

June 2011

DECLARATION

This work has not previously been accepted in substance for any degree and is not being concurrently submitted in candidature for any other degree.

Signed …….. (Candidate)

Date ……

STATEMENT 1

This thesis is being submitted in partial fulfillment of the requirements of the degree of PhD.

Signed …….. (Candidate)

Date ……

STATEMENT 2

This thesis is the result of my own independent investigations, except where otherwise stated. Other sources are acknowledged by footnotes giving explicit references.

Signed …….. (Candidate)

Date ……

STATEMENT 3

I hereby give consent for my thesis, if accepted, to be available for photocopying and for inter-library loan, and for the title and sumary to be made available to outside organisations.

Signed …….. (Candidate)

Date ……

Abstract

The intention of the work presented is to provide novel, accurate and time-efficient way of designing multi-sines stimulus signal to replace real-life modulated signals prevailing within telecommunication networks, hence providing a novel tool for the development of modern RF measurement and design solution.

The work demonstrated that with 50 tones, the multi-sines stimulus excites almost the same level of nonlinearity as real modulated signals do. For this conclusion the investigation of nonlinear behaviour mechanism was taken and a real DUT was measured under designed multi-siness and various types of modulated signals.

It is also demonstrated that this multi-sines stimulus is compatible with the advanced RF measurement systems which are capable of measuring the complete RF waveform including the harmonic and base-band frequencies but demanding a periodical stimulus signal.

Furthermore, a novel and quick sub-sampling algorithm was proposed to efficiently use the memory of Sampling Oscilloscope and therefore allows for accurate multi-sines capturing. An averaging algorithm for multi-sines stimulus was proposed to “stabilize” the captured waveform and a PCA based phase compensating algorithm was also proposed to tackle the problem of frequency shift under multi-sines excitation.

ACKNOWLEDGEMENT

First of all, I would like to thank my supervisors Prof. Johannes Benedikt and Prof. Paul Tasker for their inspiration, support and guidance throughout the duration of this research project. It was Prof. Benedikt's patience and enthusiasm that introduce me to this wonderful research area and it was his richful ideas and wisdom guides me exploring this area. It was Prof. Tasker's valuable advices and helpful discussions that has continuously inspired me exploring the seemingly unlimited knowledge of RF world.

During my time spent in Cardiff, it was a great pleasure to work in High Frequency Centre. Particularly, I would like to say thank you to all my colleagues for their help, advice, and support in my research. It is my honour to work with such an excellent group of talents in microwave engineering.

Finally, I would like to thank my parents for their support both financinally and psychologically. It is your love that excite me climb the mountains. I would specially take this thesis as a present to my son, DongLai Su, it was you who give me the braveness to pick up the flower in the bush mining.

LIST OF PUBLICATIONS

Su Jiangtao, Benedikt, J., Tasker, P.J., "A new method for the design of multi-sine excitations for the assessment of non-linear devices", Microwave Symposium Digest, 2008 IEEE MTT-S International, On page(s): 265 - 268, Volume: Issue: , 15-20 June 2008

M. Akmal, J. Lees, S. Jiangtao, V. Carrubba, Z. Yusoff, S. Woodington, J. Benedikt, P. J. Tasker, “An Enhanced Modulated Waveform Measurement System for the Robust Characterization of Microwave Devices under Modulated Excitation” Microwave Symposium Digest, 2011 IEEE EuMW2011.

LIST OF ABBREVIATIONS

Term	*Description*
ACPR	**Adjacent Channel Power level Ratio**
ADS	**Agilent® Advanced Design System**
AM/PM	**Amplitude-dependent Phase distortion**
BJT	**Bipolar Junction Transistor**
CAD	**Computer-aided Design**
CCDF	**Complementary Cumulative Distribution Function**
CCPR	**Co-Channel Power Ratio**
CDMA	**Code Division Multiple Access**
CF	**Crest Factor**
CW	**Continuous Wave**
DAC	**Data Access Component**
DUT	**Device under Test**
DWLU	**Direct Waveform Look-up**
ESG	**Electronic Signal Generator**
EVM	**Error Vector Magnitude**
FFT	**Fast Fourier Transform**
FOM	**Figure Of Merit**
GPIB	**General Purpose Interface Bus**
GSM	**Global System for Mobile communications**
HOS	**High Order Statistics**
IF	**Intermediate Frequency**
IFT	**Inverse Fourier Transform**
KCL	**Kirchhoff's Current Law**
LDMOS	**Lateral-Drain-Diffusion MOS**
LSNA	**Large Signal Network Analyser**
NVNA	**Nonlinear Vector Network Analyser**
MET	**Motorola Electro Thermal**
MTA	**Microwave Transient Analyser**

NBGN	**Narrow Band Gaussian Noise**
NPR	**Noise Power Ratio**
PA	**Power Amplifier**
PAE	**Power Added Efficiency**
PAPR	**Peak-to-Average Power Ratio**
PHD	**Poly-harmonic Distortion**
PSD	**Power Spectral Density**
RF	**Radio Frequency**
SNAD	**Signal-to-Noise And Distortion**
TRL	**Through Reflective Line calibration**
VNA	**Vector Network Analyser**
VSWR	**Voltage Standing-Wave Ratio**
WCDMA	**Wideband Code Division Multiple Access**

Table of Contents

1 Introduction 1
1.1 Modern communication systems and Power Amplifier 1
1.2 RF power amplifier for wireless communication systems and power amplifier design 4
1.3 Research Motivation 7
1.4 Research Aim 14
1.5 Thesis Structure. 15
1.6 Reference: 18
2 From two-tone to multi-tone: evolution of stimulus signals and overview of multi-tone excitation signals design 22
2.1 Introduction 22
2.2 Distortion in RF power amplifier 23
2.2.1 The nonlinearity of power amplifier 23
2.3 Characterisation of PA nonlinearities 26
2.3.1 Another point of view: Correlated distortion and un-correlated distortion 29
2.3.2 In-band distortion and out-of-band distortion 31
2.3.3 The in-band un-correlated distortion 32
2.4 The evolution from single-tone to multi-tone tests 36
2.4.1 Single-tone test 36
2.4.2 Two-tone test of power amplifier 36
2.4.3 Introduction to multi-sines design 39
2.5 Previous multi-sines designing method 42
2.5.1 Digital Fourier Transformation 42
2.5.2 Engineering phase distributions of multi-sines 45
2.5.3 Matching statistical character of modulated signals 47
2.6 Reference 59
3 Design multi-sines — a novel approach 64
3.1 Designing multi-sines with correlation methods 64

3.1.1 Understanding correlation 64
3.1.2 Modified correlation method to design multi-sines with less number of tones 70
3.1.3 Optimized correlation method with Least-Error Method or Even-tone Method 81
3.2 Limitations of the correlation method 89
3.2.1 Another angle: High-Dimension to Low-Dimension 89
3.2.2 The importance of time-domain statistical properties 96
3.3 New multi-sines design procedure 100
3.3.1 The cause of the CCDF difference 100
3.3.2 Approximating CCDF through waveform summation 102
3.3.3 Optimum 'peak' and 'trough' waveforms 107
3.3.4 The complete design procedure for multi-sines 111
3.4 CAD-based verification 113
3.5 Conclusion 114
3.6 Reference 116
4 FOMs (Figure of Merit) Selection 117
4.1 Common FOMs 118
4.1.1 ACPR 119
4.1.2 NPR 122
4.1.3 CCPR 128
4.1.4 EVM 131
4.2 Choosing ACPR and EVM as the figure of merits 135
4.3 Adaptation of ACPR and EVM 138
4.4 Conclusion 143
4.5 Reference: 145
5 Measurement based verification of multi-sines design procedure 148
5.1 Measurement setup 148
5.1.1 Hardware Architecture 148
5.1.2 Test signal generation 152
5.1.3 Device Under Test 157

5.1.4 Signal Analyser 159
5.2 Experimental verification of multi-sines as stimulus signal 164
5.2.1 Adaptability and accuracy verification of multi-sines with ACPR measurement 164
5.2.2 Further verification of multi-sines performance with EVM measurement 171
5.3 Conclusion 182
6 Applying multi-sines to waveform measurement system -- A case study of the application of multi-sines stimulus 183
6.1 Introduction of Cardiff University's waveform measurement and engineering system..... 184
6.2 Advantages of multi-sines stimulus to waveform measurement system 185
6.2.1 Extension from CW stimulus to modulated signals. . 185
6.2.2 Extending the capability of high power device characterization 188
6.3 Using Multi-sines stimulus in waveform measurement system 192
6.3.1 Multi-sines subsampling 192
6.3.2 Multi-sines averaging 213
6.3.3 PCA based method to correct frequency offset..... 217
6.4 Conclusion 223
6.5 Reference:..... 225
7 Conclusion and future work 226
7.1 Conclusion 226
7.2 Further work 228
7.2.1 Further decrease the number of tones of a multi-sines stimulus 229
7.2.2 Approximating other types of test signal 229
7.2.3 Integration of multi-sines stimulus into a waveform

measurement system 235
7.3 Reference:..... 238

1 Introduction

1.1 Modern communication systems and Power Amplifier

Modern wireless communication started with Guillermo Marconi in 1896, who managed to demonstrate wireless telegraphy by sending and receiving Morse code. Modern mobile communication systems have evolved since the early nineteenth century, when the first attempts of "mobile radio" were used to communicate with vehicles without the use of wire [1]. The first fully automated mobile phone system, called "mobile telephone system A", was developed by Ericsson and released in 1956 in Sweden. The weight of the mobile handset was a significant 40 kg, and the network had 150 subscribers when it was introduced, and only 600 when it was decommissioned in 1983 [2]. From these modest beginnings, there was an explosion in the number of subscribers to mobile phone networks over the last two decades. Figure 1.1 is a plot showing the dramatic rise in subscriptions taken from wireless intelligence, a global database of mobile market information [3].

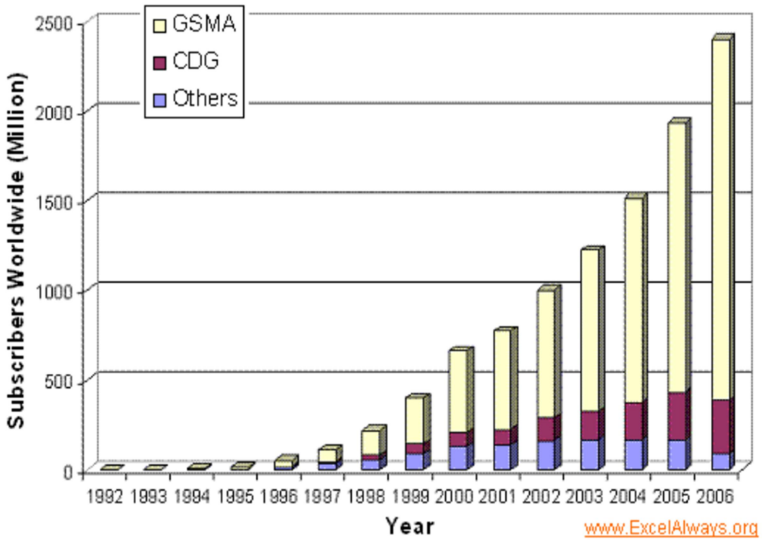

Figure 1.1 The GSM subscribers increasing chart[3]

The wireless communication market expanded far quicker than anybody could have imagined. For example, an estimation from 2006 [4] forecast that the numbers of global mobile subscribers would grow to 3.3 billion by 2010, but actually there were already 4.3 billion wireless communication subscribers in the world by the second quarter of 2009[5].

Moreover, wireless communication is no longer limited to providing verbal telephone services, but also to provide data transmission services. In 1996, Nokia introduced the Communicator, a GSM mobile phone and handheld computer. It had a QWERTY keyboard and built in word processing and calendar programs. Such development has continued in recent years, and the mobile phone has evolved into a personal communications device providing multi-media wireless solutions including voice, video, graphics, audio and broad-band internet access. This development again exceeds people's imagination. In 2008, the smart-phone - a mobile phone offering advanced capabilities - occupied 10% of the overall mobile phones market; a figure estimated to increase to 23% by 2012 [6]. However, a report published by Vodafone in November 2009 has shown that smart-phones already represent 20% of all handsets selling [32]. The report also states that data traffic has risen 300% in the past two years and as such represents 11% of all Europe service revenues. Another report from GSA also states that the number of mobile broadband subscriptions has exceeded 400 million [5] in 2009. It is believed that this development will continue for two reasons: firstly, customers are always expecting quicker data access speed, higher wireless bandwidths, and service providers want to sell high value services beyond voice. Secondly, the cost of the digital signal processing technology required to deploy high bandwidth broadband wireless systems has already dropped to a point where it can now be widely used in smart-phones, MIDs, laptops and other similar devices.

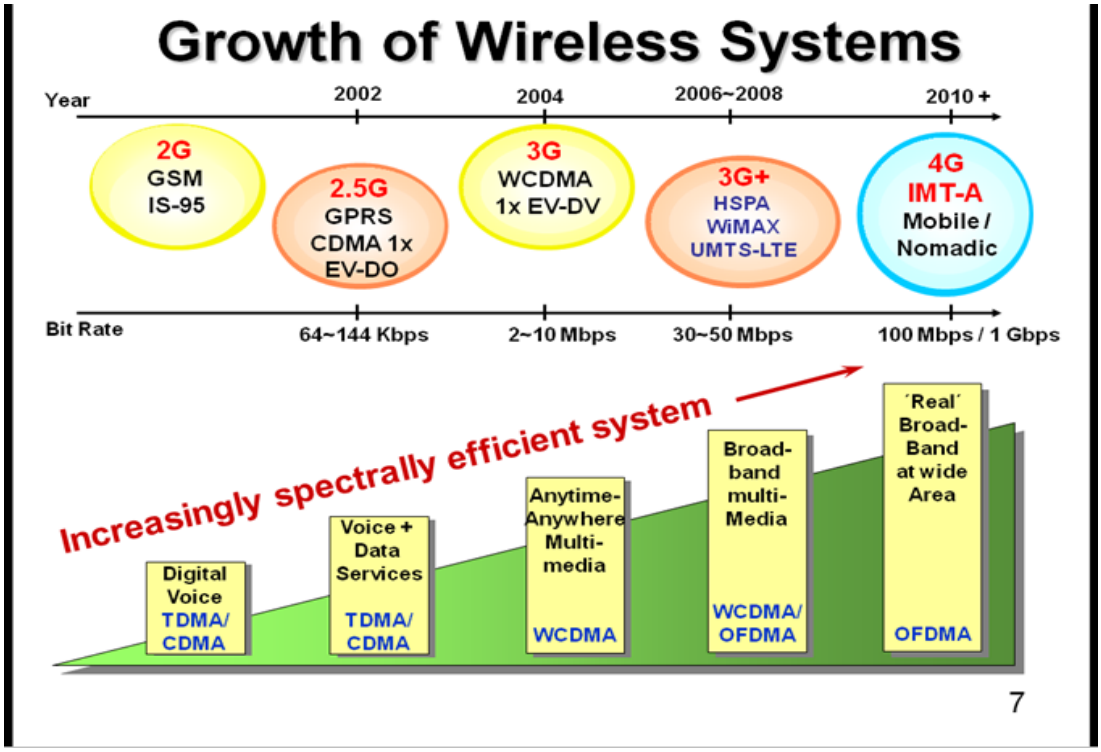

Figure 1.2 *The evolution of wireless communication data access speed[32]*

Thus tremendous efforts are being made to investigate and develop new wireless communication technologies in order to offer competitive multimedia services and cater to as many customers as possible within the limited bandwidth. Figure 1.2 shows the latest, under-development long term evolution (LTE), which illustrates a dramatic increase in the maximum data transfer rate from 384 Kbps to 1Gbps. This is achieved through the utilisation of modulation techniques such as Orthogonal Frequency Division Multiplex (OFDM) and M-QAM, and multiple antennas for the implementation of multiple input, multiple output (MIMO) systems. Such techniques offer high consumer benefits as they provide higher data transmission rates, more reliable transmission performance and higher capability of operating over a range of bandwidths. However, this spectral efficiency is achieved at the cost of power efficiency. For example, it is noted that a base station can only achieve 3.1% efficiency in WLAN (IEEE 802.11a) application [32]. An increase in

signal complexity results in higher wireless system complexity, which leads to ever more stringent wireless system design specifications.

1.2 RF power amplifier for wireless communication systems and power amplifier design

A radio frequency (RF) power amplifier (PA) is a device that converts DC energy into a required amount of RF energy suitable for transmission in response to an input stimulus. PAs are some of the most common constitutive parts of wireless communication systems, meaning their efficient design is vitally important for such applications. Where there is wireless communication, there are power amplifiers: from a mobile phone transmitting hundreds of milliwatts (mW) to a base station transmitting tens to hundreds of watts, or from digital TV transmission to satellite communications. PAs also contribute significantly to the power consumption and the cost of a transmitter system [7]. For example, it is reported that in a WLAN transmission system, PAs consume 70% of the overall power [32].

Hence, PA quality strongly influences the cost, reliability, size and eventually the overall performance of a wireless communication system. There are many figures of merit which can be used to quantify PA performance, with the most important two measures being efficiency and linearity.

Efficiency is, more specifically, a measure of how efficiently a power amplifier can convert DC power into RF power. The efficiency is important since a PA with poor efficiency consumes much more energy to achieve the same result as a more efficient PA. For mobile handhelds, those devices usually use the battery as the primary power source and the poor efficiency directly translates to shorter talk and standby time. For base stations, which employ PAs from tens to hundreds of watts output power capacity, the poor efficiency

not only means larger power consumption but also leads to a large amount of heat dissipation, incurring extra cooling costs.

Classical Class-A and Class-B PAs have respective maximum efficiencies of 50% and 75%. However, when these PAs face a modern modulated signal with 10dB Peak-to-Average Power Ratio (PAPR) [36], the efficiency of these PAs will dramatically drop to only 5% and 28% respectively. It is stated that a typical modern wireless communication system can only achieve 3.1% overall efficiency when PAs with 28% efficiency are employed in this system [32]. This is a contributing factor to why the mobile communication industry accounts for almost 1% of all carbon dioxide emission in the UK, where the average individual mobile subscriber generates 55kg CO_2 per year [8]. Therefore the efficiency of RF PAs imposes a substantial influence on the overall cost, performance and environmental impact of communication systems.

PA linearity refers to how faithfully a power amplifier can amplify an input signal. Unfortunately, inherent PA nonlinearities generate spectral re-growth, which leads to adjacent channel interference and violations of the out-of-band emission requirements mandated by regulatory bodies. It also causes in-band distortion, which degrades the bit error rate (BER) performance. Figure 1.3 illustrates these effects. As PAs always demonstrate some level of nonlinearity, the tolerance of a wireless communication system to the nonlinearity usually depends on the application and system design.

PA design normally involves a compromise between linearity and efficiency. For example, to preserve linearity, PAs are operated with reduced input drive, where the efficiency decreases significantly. Hence RF PAs have to be carefully designed to meet the specific need for various systems. In principle, there are two philosophies for the design of power amplifiers: computer aided design (CAD) and

measurement based design.

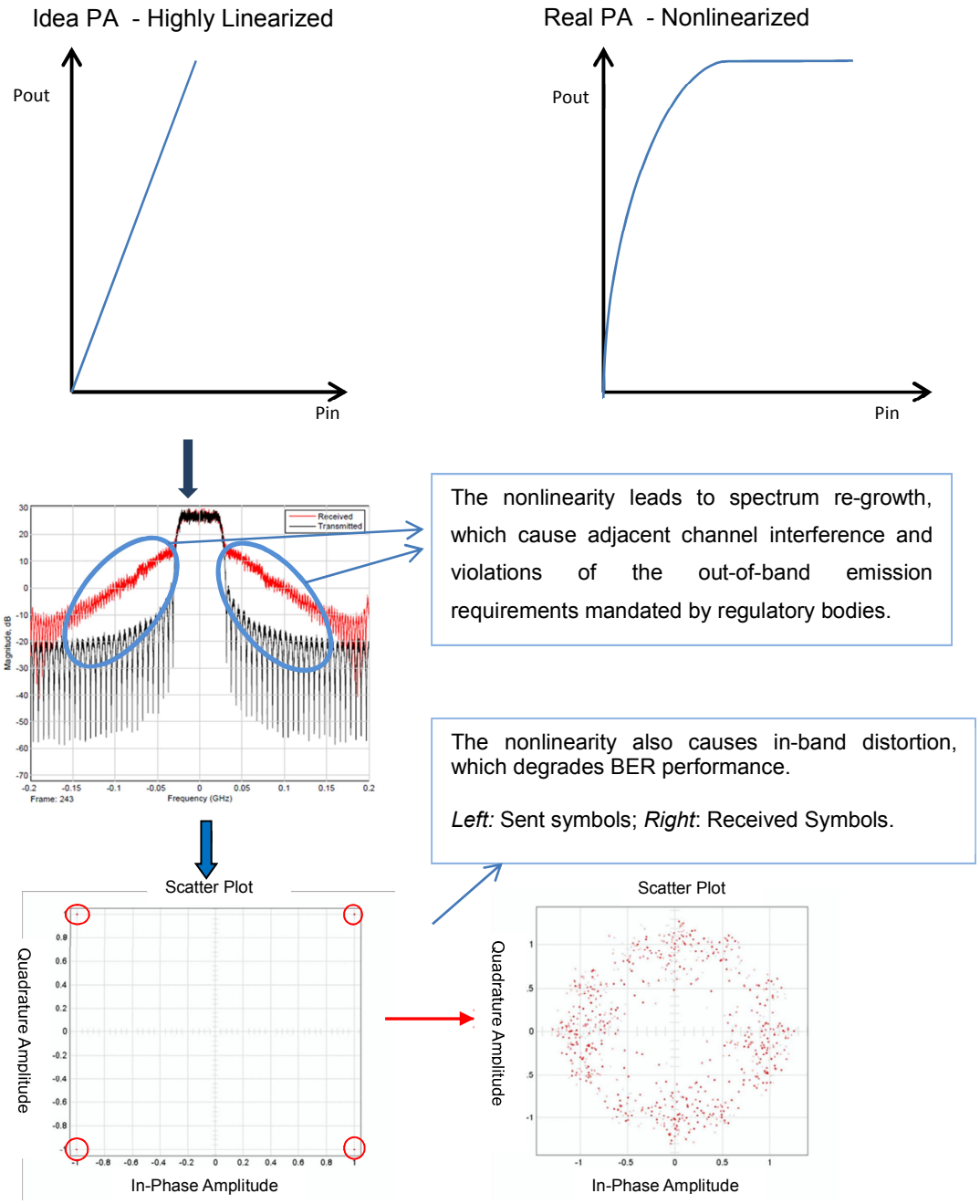

Figure 1.3 *The influence of PA's nonlinearity*

The CAD method uses a model as the primary design tool. In this philosophy, a theoretical device model is developed first. The model extraction procedure is then identified. The target device is subsequently characterised experimentally in order to obtain the necessary measurement data required for the model extraction [37]. By following the extraction procedure, the model can be extracted

and implemented in the CAD environment. The PA designer can start the CAD-based PA design by using the model, and the designed PA will be finalised if all the design specifications can be met at the PA performance testing stage. The accuracy and reliability of the model hence is crucial to the success of PA design by using this method.

The measurement-based PA design philosophy takes the measurement data as the primary resource to design a power amplifier. In this philosophy, a power amplifier transistor device will firstly be characterized to extract key design parameters like the gain, efficiency and load-pull contours. Based on the information, designers start the power amplifier design straightaway. Hence, the accuracy of measurement has great influence on the effectiveness of this philosophy.

1.3 Research Motivation

Newly developed wireless systems put more stringent requirement on the performance of a RF power amplifier. These newer transmission formats are especially vulnerable to nonlinear distortions: random phases of the large numbers of subcarriers can produce instantaneous power levels that cause the amplifier to compress, momentarily causing distortion and ultimately symbol errors. Signals having a high PAPR ratio can cause amplifiers to compress unpredictably during transmission. Table 1.1 [34] shows the PAPR of a signal for some common communication standards. Moreover, the OFDM signals in particular are very dynamic and due to their noise-like nature, compression problems can be difficult to detect.

Table 1.1 PAPR of wireless communication signal standards.

Modulation			Peak-to-Average Ratio (PAPR)	
			Single Carrier	Multicarrier
2G	cdmaOne (IS-95)	QPSK/OQPSK	10.5	11
	TDMA (IS-54, IS-136)	pi/4 DQPSK	3.5	10.5
	GSM	GMSK	0.5	10.5
3G	cdma2000	QPSK/OQPSK/HPSK	9	9
	WCDMA	QPSK/OQPSK/HPSK	7	7
	EDGE	3pi/8 Shifted 8PSK	3	10

At present, both the modelling-based and measurement-based PA design philosophies demonstrate many interesting advantages, but both of them are inherently time consuming. Modelling-based PA design relies on the accuracy of the model in order to achieve a reasonable final design. A special measurement setup and careful experimental design are normally needed to verify the identified model, meaning successive iterations and parameter tuning are expected. This iterative process makes model development very time-consuming and can significantly delay the time-to-market of the final design. Moreover, the special measurement setup is generally designed for extracting a certain type of model and may not be reused if a new modelling approach is employed.

On the other hand, measurement-based PA design has to wait a long time to collect the necessary amount of measurement data to extract the design parameters. For example, to evaluate the device performance over a large impedance range, different loads are applied to the device at each harmonic frequency. If three harmonics

are taken into account, where the load is swept over one hundred different values for each harmonic frequency, we will get 100^3 measurements which will normally take a few months.

This is clearly an undesirable and unsustainable situation in the mobile communications industry where rapid growth and competition has meant that time-to-market has become an absolutely critical factor. Hence many first-pass design methodologies have been proposed to tackle this issue.

One of such methodology is the PA design process based on waveform measurement and engineering, as proposed by Cardiff University [35]. A large-signal measurement system was developed that allows the rapid collection of Continuous Wave (CW) data sets in addition to linearity and memory measurements and engineering. It is capable of characterising the large signal dynamic behaviour up to a few harmonic frequencies, allowing for a time efficient, 'right-first-time' design process that dramatically decreases design time [10][11]. This technology has been demonstrated to be effective for both PA design [12][13] and behaviour modelling [14].

This system, as well as other advanced measurement systems, which allow the complete RF waveform including the harmonic and base-band frequencies to be measured, is still only capable of measuring signals with a limited number of frequency components [15][16]. Obviously, the best excitation signals to be used in the measurement system are those that exactly match the signal that will be input to the system in real operation, or those that place the system into a wide variety of operating states that will occur in practice. However, the measurement of complex non-periodical signals poses a significant challenge for all present measurement systems which are capable of capturing the whole information including the harmonic and base-band frequencies, whether they are sampler-based systems

or mixers-based systems.

For sampler-based systems, the sample rate of oscilloscopes is generally slower than the RF frequency of measured signals, hence sub-sampling techniques have been widely used and therefore only repetitive signals can be measured. In addition, the real modulated signal is non-periodic in the time-domain, so the stimulus signal can no longer be used to trigger the measurement as the pattern is no longer repeatable. Although real-time oscilloscopes capable of capturing non-repetitive signals with wide bandwidth are available today, they have also a significant down side. The dynamic range of real-time oscilloscopes is rather limited, which has a significant impact on the ability to look at both in-band and out-of-band distortion terms.

For mixer-based instruments such as PNA-X from Agilent, a separate frequency conversion is required for each measured spectral line, which is inherently slow for complex signals. In addition, to accurately restore the phase information between the measured spectral lines, the mixer-based approach requires a separate phase reference signal with a spectral component for each measured frequency. In the case of spectrally rich signals spanning multiple harmonics the power requirement of the phase reference becomes unsustainable.

A common solution is to take out a part of the real signal and repeat it. Typical signal durations are 2-5μs. However, these signals still are spectrally rich and cannot be measured easily. Hence, today's PA designs and nonlinear device modelling are mainly conducted at CW excitations and only more recently has the measurement capability been extended to modulated signals with a small number of tones. This poses a valid question as to whether such systems will be ever suitable for measurements with complex signals as currently utilised

by modern communication standards, and furthermore whether it is possible to quantify how complex-modulated signals are interacting with the non-linear characteristics of a PA.

A potential solution to this issue is to employ signals with a limited spectral density whilst keeping the required complexity to obtain a representative response from power transistors, power amplifiers or any other nonlinear circuit. Multi-sines have emerged as a suitable stimulus as they are repetitive but are capable of keeping the complexity of modern modulated signals by combining a finite sum of sinusoids with unique amplitudes and phases. A complex time domain discrete mathematical expression for such a signal can be written as below.

$$x(nT) = \sum_{j=-(N-1)/2}^{(N-1)/2} A_j e^{[2\pi\cdot(f_c + j\cdot\Delta f)\cdot(nT)+\theta_j]}$$

(Equation 1.1)

Where N is the number of sinusoids, A_j the amplitude, f_c the carrier frequency, Δf the frequency spacing, and θ_j is the phase.

The use of multi-sines as excitation signals has only emerged in recent years. Prior to this, two-tone test signals were an extremely popular excitation implementation for assessing RF PA linearity because the narrowband 2G communication signals such as GSM have little amplitude variation. This allows the use of simple two-tone signals is sufficient to characterise the non-linear behaviour of an RF power amplifier. The two-tone test still prevails today as many fundamental concepts regarding nonlinear circuit response, such as inter-modulation distortion, cross-modulation, memory effects [17] and gain compression expansion are clearly illustrated with such an excitation.

Unfortunately, in modern wireless communication signals, the

amplitude, phase, and bandwidth characteristics can no longer be accurately represented by a two-tone test signal. The wireless communication signals of today are wideband and contain significant amplitude variations with a complex statistical distribution, which is a direct by-product of the drive toward spectrally efficiency modulation. Hence the two-tone or even three-tone signals are no longer suitable as excitation in measurement systems. Figure 1.4 clearly shows the difference between a two-tone signal and a WCDMA signal displaying (*a*) the time domain waveform shapes and (*b*) their Complementary Cumulative Distribution Function (CCDF), which is a time-domain statistical description [18]. The existence of significant differences can easily be observed.

Conversely, multi-sines have a periodic, well-characterised waveform that can simulate complex modulated RF signals. By changing the amplitudes and relevant phases of each of the frequency components in the multi-sines, we are able to change the time-domain envelope associated with the multi-sines and manipulate statistical waveform measures such as CCDF of peak-to-average power ratio (PAPR). Hence multi-sines offer sufficient flexibility to simulate a wide variety of complex modulated signals. Therefore, they become the best choice of excitation signal to be used in such a measurement system for complete characterisation including the harmonic and base-band frequencies of a nonlinear signal.

Multi-sines also provide a relatively straightforward method to characterise the harmonic distortion introduced by a nonlinear device. Harmonic distortion, inter-modulation distortion and frequency-selective fading are more straightforward to measure and characterise with multi-sines than modulated signals. Therefore, the use of multi-sines waves could provide an improved insight into distortion-causing mechanisms.

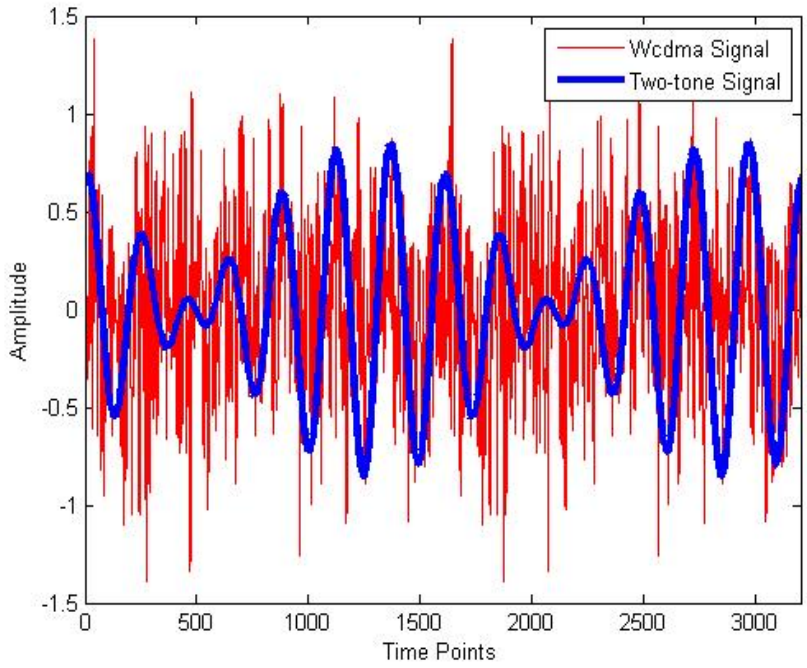

Figure 1.4a The Comparison of waveform *shapes between Two-tone signal and Modern modulated signal.*

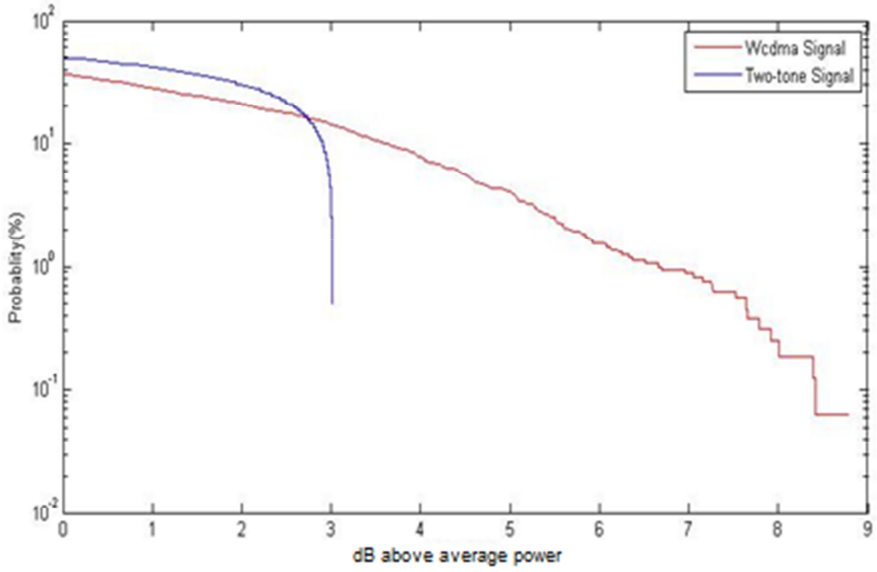

Figure 1.4b The Comparison of CCDF curves between Two-tone signal and Modern modulated signal.

Because of these advantages, multi-sines are becoming more frequently used for system testing [19]–[21], for verifying technology

standard masks [22]–[24], and for device and system modelling [25]–[30] in order to extract robust models for computer-aided design/computer-aided engineering (CAD/CAE) solutions. Recently, their use as calibration signals has also being explored.

1.4 Research Aim

The general research aim of this work is to design multi-sine excitation signals that preserve the properties of the real-world signals using a scalable and manageable number of tones. It is relatively easy to design a multi-sine signal that accurately approximates signals employed in communication systems with an unlimited number of tones. For example, by the definition of Digital Fast Fourier Transformation (DFFT), we can utilise large numbers of tones – for example, 240 tones [31] - to accurately approximate signals that are employed in communication systems. The number of tones needed would get larger with increasing bandwidth of the approximated modulated signal. Too many tones will make any further measurement and analysis impractical. Thus, a compromise between the number of tones and the preserved properties of the real-world signal is required. Hence a large part of this work is addressing the realities of present measurement instrumentation and locating the number of tones needed in the multi-sines within a manageable range. In this work, a sampling oscilloscope employing sub-sampling techniques is used to measure the multi-sine stimulus. This offers high dynamic range as waveforms can be sampled over a number of RF cycles, but offers only a limited memory depth in the region of 4000 points, which corresponds to 2000 frequency components. To accurately measure the 7^{th} order nonlinearity up to the 5^{th} harmonic, the multi-sine signal is expected to contain less than 60 tones.

The design process must be adaptable to most of the signals that are used in real life rather than limited to one or two types of RF

communication signal. There are several mobile communication systems that are widely in use today, such as GSM, CDMA, WCDMA and HSDPA. Even within the same communication system, the modulation schemes, the number of data sub-channels and the orthogonal combination codes may vary depending on the specific application. As a result, the waveform shapes and statistical properties of those signals will significantly differ and influence the nonlinear behaviour and the efficiency of the PA.

It is also necessary that the designed multi-sine signal is able to replace real-life modulation signals in measurement systems. In other words, it is necessary to demonstrate that the designed multi-sine signal is a sufficiently accurate representation of the original signal, so that its utilisation as a stimulus for a non-linear device will produce similar or identical non-linear signal components. However, most of the figures of merit for the evaluation of the level of nonlinear distortion in use today are defined in terms of modulated signal excitation and hence their applicability to a multi-sine signal is questionable. Therefore these figures of merit need to be re-examined and possibly redefined to cater for needs of multi-sine excitation signals.

1.5 Thesis Structure.

This thesis is structured into four major sections.

Chapter 2 is an introduction into multi-sines excitation. Firstly, there is a section that gives an overview of the various types of excitation signals currently being employed to characterise the nonlinear behaviour of the devices, with a focus on the evolution from two-tone stimulus to multi-sines stimulus. After that, a review of recently published research literature related to designing multi-sines excitation signal is provided. These multi-sines design techniques have their own advantages and disadvantages, and none

of them are fully applicable for industry implementation.

Chapter 3 starts with the presentation of the new and effective design method for multi-sines design. Starting with the correlation method, experimental verification and theoretical discussion are used to develop key principles for the approximation of modulated signals. Based on this understanding, a multi-sines design procedure is developed whereby the desired multi-sines waveform shapes are generated through the modification of frequency domain parameters. CAD simulations show that this design procedure is fast, accurate and capable of approximating different types of modulated signals.

Chapter 4 discusses the figures of merit that are to be used to evaluate the similarity between multi-sines and modulated signals. The current lack of universal figures of merit present an obstacle in the successful establishment of multi-sines for device and system characterisations. It is stated in this chapter that ACPR and EVM cannot solely determine the quality of multi-sines design method, but a combination of these two figures of merit is fully capable of evaluating the similarity between multi-sines and target signal. This chapter also presents a discussion of several issues in the measurement of ACPR and EVM for multi-sines stimulus.

Chapter 5 presents a full verification of the realised multi-sines design method utilising nonlinear device characterisations. By measuring ACPR and EVM of nonlinear devices at different power levels, the ability of the new multi-sines design procedure to adapt to various complex modulated signals with different PAPR and bandwidth is highlighted. These investigations also indicate excellent potential for the application of the designed multi-sines to practical large signal measurement systems.

Chapter 6 provides a case-study for the application of multi-sines excitations. The measurement system at Cardiff University is capable of accurately capturing time-domain waveforms at RF and high frequencies, and proved very useful in the areas of RF power transistor characterisation/development and RF PA design/optimization at CW stimulus. Both areas build on the successful utilisation of measured current and voltage waveforms to provide an improved insight into the operation of nonlinear devices, and subsequently inform their optimisation to achieve higher energy efficiencies. In turn, the introduction of designed multi-sines extends the application of this system to new markets requiring device and PA testing not only at CW but also at realistic modulated signals. The measurement system is introduced first, and followed by a discussion on how waveform measurement systems can benefit from multi-sines stimulus. The chapter is concluded by summarising the technical issues arising from the introduction of multi-sines stimuli and provide a PCA-based method to tackle them.

Chapter 7 is comprised of final conclusions and discusses some remaining limitations. Possible future work to expand the application of multi-sines and optimisation of the multi-sines design process is also suggested.

1.6 Reference:

[1] P. B. Kenington, High-Linearity RF Amplifier Design, Boston, MA: Artech House, 2000.

[2] J. S. Kenney and A. Leke, "Design Considerations for Multicarrier CDMA Base Station Power Amplifiers," Microwave J., vol. 42, no. 2, pp. 76-84, Feb. 1999.

[3] K.A. Remley, D.F. Williams, D.M.M.-P. Schreurs, and J. Wood, " Simplifying and interpreting two-tone measurements," IEEE Trans.Microwave Theory Tech., vol. 52, no. 11, pp. 2576–2584, Nov. 2004.

[4] Williams, T. V.; "A large-signal multi-tone time domain waveform measurement system with broadband active impedance control," PhD thesis, December 2007, Cardiff University

[5] GSA, "GSM/3G Market Update October 30, 2009" www.gsacom.com

[6] Juniper Research, "Next Generation Smartphones--- Players, Opportunities & Forecasts 2 008-2013" http://www.juniperresearch.com/shop/viewreport.php?id=171

[7] Cripps, S. C., "RF Power Amplifiers for Wireless Communications", 2nd Edition, Artech House Publishers, 2006

[8] Johannes Benedikt, "take radio frequency power amplifier design to new levels", Engineering, September 2007.

[9] Benedikt, J.; Gaddi, R.; Tasker, P. J.; Goss, M.; "High-power time-domain measurement system with active harmonic load-pull for high efficiency base-station amplifier design," IEEE Transactions on Microwave Theory and Techniques, Volume 48, Issue 12, Dec. 2000, pages: 2617 – 2624

[10] Williams, T.; Benedikt, J.; Tasker, P. J.; "Experimental evaluation of an active envelope load Pull architecture for high speed device characterization," IEEE MTT –S International Microwave Symposium Digest, June 2005, pages: 1509-1512.

[11] Roff, C., Benedikt, J., Tasker, P. J., "Design approach for realization of very high efficiency power amplifiers," IEEE MTT International Microwave Symposium Digest, June 2007, pages: 143-146.

[12] Wright, P. et al., "Highly Efficient Operation Modes in GaN Power Transistors Delivering Upwards of 81% Efficiency and 12W Output Power," IEEE MTT-S Int. Microwave Symp. Digest, June 2008, pp. 1147-1150

[13] Qi, H.; Benedikt, J.; Tasker, P, "Novel Nonlinear Model for Rapid Waveform-based Extraction Enabling Accurate High Power PA Design," IEEE MTT-S International Microwave Symposium, 2007

[14] M. Demmler, P.J. Tasker, and M. Schlechtweg, "On-wafer large signal power, S-parameter and waveform measurement system," in Proc. 3rd Int. Workshop on Integrated Nonlinear Microwave and Millimeterwave Circuits (INMMiC), 1994, pp. 153–158.

[15] J. Verspecht, P. Debie, A. Barel, and L. Martens, "Accurate on wafer measurement of phase and amplitude of the spectral components of incident and scattered voltage waves at the signal ports of a nonlinear microwave device," in IEEE MTT-S Int. Microwave Symp. Dig., June 1995, vol. 3, pp. 1029–1032.

[16] K.A. Remley, D.F. Williams, D.M.M.-P. Schreurs, and J. Wood, "Simplifying and interpreting two-tone measurements," IEEE Trans. Microwave Theory Tech., vol. 52, no. 11, pp. 2576–2584, Nov. 2004.

[17] Agilent, "Charactering digital modulated Signals with CCDF Curves", Agilent application notes, 5968-6875E

[18] G. Simon and J. Schoukens, "Robust broadband periodic excitation design," IEEE Trans. Instrum. Meas., vol. 49, no. 2, pp. 270–274, Apr. 2000.

[19] J.C. Pedro and N.B. Carvalho, "On the use of multitone techniques for assessing RF components' intermodulation distortion," IEEE Trans. Microwave Theory Tech., vol. 47, no. 12, pp. 2393–2402, Dec. 1999.

[20] R. Pintelon and J. Schoukens, System Identification: A Frequency

Domain Approach. New York: Wiley-IEEE Press, 2001.

[21] R. Hajji, F. Beauregard, and F.M. Ghannouchi, “Multitone power and intermodulation load-pull characterization of microwave transistors suitable for linear SSPA’s design,” IEEE Trans. Microwave Theory Tech., vol. 45, no. 7, pp. 1093–1099, July 1997.

[22] K.A. Remley, “Multisine excitation for ACPR measurements,” in 2003 IEEE MTT-S Int. Microwave Symp. Dig., June 2003, vol. 3, pp. 2141–2144.

[23] K.M. Gharaibeh, K.G. Gard, and M.B. Steer, “In-band distortion of multisines,” IEEE Trans. Microwave Theory Tech., vol. 54, no. 8, pp. 3227–3236, Aug. 2006.

[24] J.C. Pedro and N.B. Carvalho, “Designing band-pass multisine excitations for microwave behavioral model identification,” in IEEE MTT-S Int. Microwave Symp. Dig., June 2004, vol. 2, pp. 791–794.

[25] W. Van Moer, Y. Rolain, and A. Geens, “Measurement-based nonlinear modeling of spectral regrowth,” IEEE Trans. Instrum. Meas., vol. 50, no. 6, pp. 1711–1716, Dec. 2001.

[26] J. Verspecht, F. Verbeyst, and M. vanden Bossche, “Network analysis beyond S-parameters: Characterizing and modeling component behaviour under modulated large-signal operating conditions,” in 56th ARFTG Conf. Dig., Nov. 2000, pp. 1–4.

[27] D. Schreurs and K.A. Remley, “Use of multisine signals for efficient behavioural modelling of RF circuits with short-memory effects,” in 61st ARFTG Conf. Dig., Nov. 2003, pp. 65–72.

[28] J.C. Pedro and N.B. Carvalho, “Designing multisine excitations for nonlinear model testing,” IEEE Trans. Microwave Theory Tech., vol. 53, no. 1, pp. 45–54, Jan. 2005.

[29] M. Myslinski, K.A. Remley, M.D. McKinley, D. Schreurs, and B. Nauwelaers, “A measurement-based multisine design procedure,” in Proc. Integrated Nonlinear Microwave and Millimeter-Wave Circuits (INMMiC), Jan. 2006, pp. 52–55.

[30] Minsheng Li, K. M. G., Kevin G. Gard, and Michael B. Steer.

"Accurate Multisine Representation of Digital Communication Signals for Characterization of Nonlinear Circuits." 2004

[31] GSA, “Mobile Broadband growth---Reports from Operators Worldwide, January 14, 2010” www.gsacom.com

[32] Holger. Karl, “An overview of Energy-efficiency techniques for mobile communication system.” TKN Technical Reports. (Available online at http://www.tkn.tu-erlin.de/publications/papers/TechReport_03_017.pdf)

[33] Wangmyong Woo, “Hybrid Digital/RF Envelope Predistortion Linearization For High Power Amplifiers In Wireless Communication Syetems”, PhD Thesis, Georgia Institute of Technology Atlanta, GA 30332, April 2005

[34] Tasker, P.J, “Practical Waveform Engineering”, Microwave Magazine, IEEE Volume: 10 , Issue: 7, 2009, p65~p76

[35] F. Raab, P. Asbeck, S. Cripps, P. Kenington, Z. Popovic, N. Pothecary, J. Sevic, and N. Sokal, "RF and Microwave Power Amplifier and Transmitter Technologies - Part 1," in High Frequency Design, 2003, pp. 22–36.

[36] Williams, T.; Benedikt, J.; Tasker, P.J. “Fully Functional ‘Real Time’ Non-Linear Device Characterization System Incorporating Active Load Control” 36th European Microwave Conference, September 2006, Page(s): 1610-1613

[37] F. Filicori, G. Ghione, C.U. Naldi, “Physics-Based Electron Device Modelling and Computer-Aided MMIC Design,” IEEE Trans. Microwave Theory Tech., vol.40, pp.1333-1352, July 1992.

2 From two-tone to multi-tone: evolution of stimulus signals and overview of multi-tone excitation signals design

2.1 Introduction

RF power amplifiers are inherently nonlinear, and this nonlinearity must be specified by certain figures of merit like gain, power-added efficiency, and 1dB compression point which are determined by accurate characterization procedures. A reliable device characterization is essential for both obtaining an insight into a device or the generation and validation of computer aided design (CAD) models to facilitate circuit design within simulation environments.

During the device characterization and analysis, it is advantageous to utilise a general set of functions as a stimulus signal rather than a complex random signal. Utilizing two-tone signal as stimulus has been popular in the past decades. However, with the advent of modern communication signals it no longer can represent accurately the required amplitude and phase variations over the increasing bandwidth. Therefore it is desirable to investigate the use of multi-sines as excitations in measurement systems.

Various multi-sines design methods have been proposed in the past. However each of them has their limitations which impede their implementation on real RF measurement systems. Therefore, it is necessary to develop new accurate, computationally efficient, and adaptable multi-sines design techniques.

This chapter will firstly introduce the nonlinearity of PAs and the traditional way of utilizing two-tone excitation signals to characterize their nonlinear behaviour. After that, the analysis of multi-sines and its potential to replace complex modulated signals is presented. The advantages and shortcomings of current existing multi-sines design techniques will be reviewed thereafter.

2.2 Distortion in RF power amplifier

2.2.1 The nonlinearity of power amplifier

The perfectly linear ideal memoryless RF power amplifier produces an output that is a multiple of its input. If V_i is the amplifier's input voltage V_o is the amplifier's output voltage, *t* denotes time and *G* the amplifier gain, the linear application can be expressed as:

$$V_o(t) = G \cdot V_i(t)$$

(Equation 2.1)

However, any power amplifier will display a certain degree of nonlinear behaviour. For example, Fig.2.1 and fig.2.2 displays a Cree® 10W power amplifier's input waveform and the distorted output waveform. which are measured by Mesuro®'s MB20 measurement system.

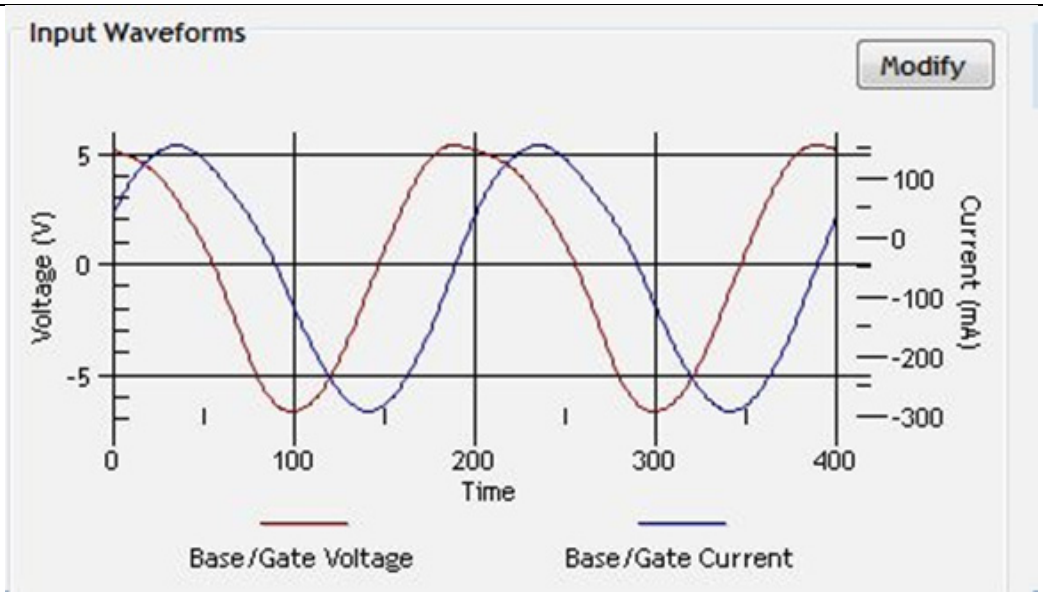

Figure 2.1 An example of input voltage/current waveforms

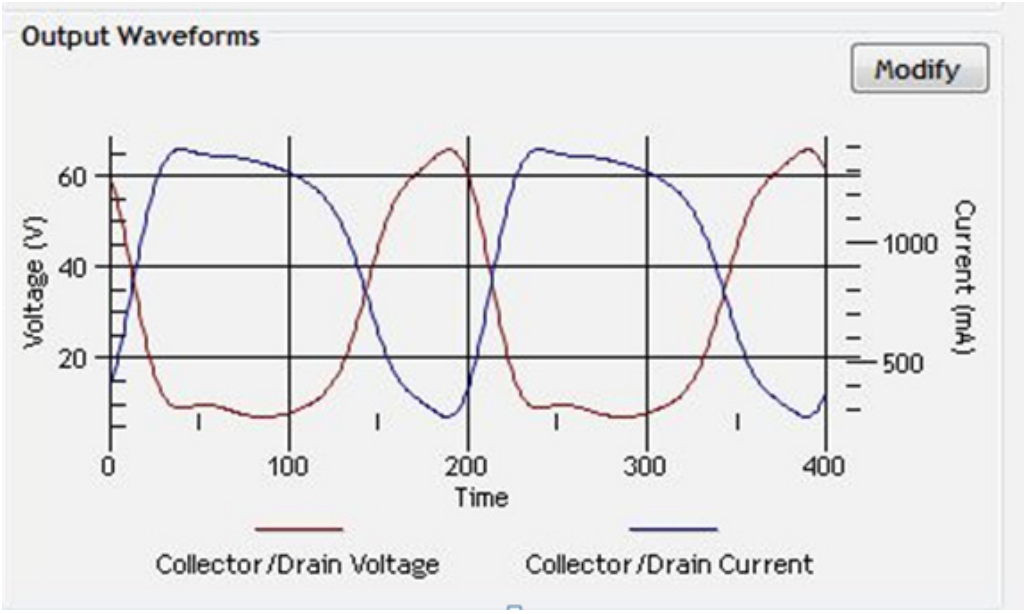

Figure 2.2 The output voltage/current waveforms after passing the DUT

It can be seen from the figure that unlike a pure single-tone sinusoid input, the output waveform is "distorted" which means it contains more than one frequency component and displays imbalance around the fundamental frequency which is often referred to as the memory effect. Such effects can be very troublesome and likely to cause the failure of the PA linearization technique. In the literature some interesting studies about memory effects can be found [1] - [3].

Another phenomenon of the non-linearity in a power amplifier can be observed when input drive is continuously increased: the device's output capacity will approach its limit and eventually stops generating more RF power at the fundamental. This phenomenon is called the clipping effect. Figure 2.3 shows a typical power characteristic of a transistor device. It can be seen that as the input power is increasing, the output power would eventually saturate and cease increasing.

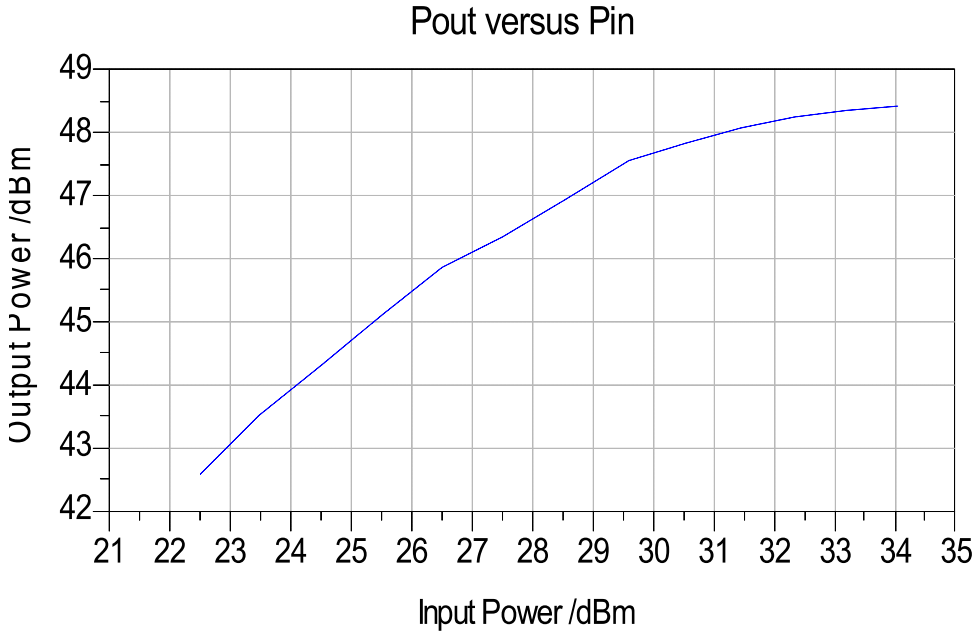

Figure 2.3 A typical power transfer characteristic of power transistor devices

The nonlinearity of a power transistor device has been investigated for decades. Much more comprehensive studies of the nonlinearity and its origins can be found in [4] - [6]. It is certain that in an effort to explain the nonlinearity and characterize it, the simple linear mathematical relationship is no longer sufficient for a power amplifier which works under large signal excitation and at RF frequencies. Thus lots of behavioural modelling has been proposed to more accurately characterise the nonlinearity of power amplifiers. Detailed discussion of these models is out of the scope of this thesis, however, some interesting studies can be found at literature [7] - [13].

2.3 Characterisation of PA nonlinearities

The nonlinearity behaviour of a memoryless PA can be approximated by a power series function that maps input signal to output signal. This function is shown below.

$$V_0(t) = a_1 V_i(t) + a_2 V_i^2(t) + a_3 V_i^3(t) + \cdots = \sum_{k=1}^{n} a_k V_i^k(t) = \sum_{k=1}^{n} W^k(t)$$

(Equation 2.2)

In this equation, a_k are coefficients, V_i (t) is input signal, $W^k(t)$ is the kth order output signal for order k and $V_0(t)$ is the output signal.

If a_k is a real value, equation 2.2 represents a nonlinear and memoryless system in which a nonlinear relationship exists between the magnitudes of the input signal and the output signal. Or in other words, only amplitude distortion is introduced, which is termed as AM/AM conversion of the Power Amplifier. However, if a_k are allowed to be complex valued, then a constant phase shift exists between the input and output signals. In other words, amplitude variation of the input signal leads to the phase variation of output signal. This is so-called AM/PM conversion [40]. Hence a nonlinear system with memory will be modelled.

To better illustrate this, considering an excitation signal of single-tone sinusoid being inserted at the input of the Device Under Test (DUT). This single-tone signal can be expressed as:

$$V_i(t) = A\cos(wt + \theta)$$

(Equation 2.3)

Where A is the amplitude, ω is the frequency and θ is the phase.The distorted output signal $V_0(t)$ will be

$$V_o(t) = f(A)\cos(wt + \theta + g(A))$$

(Equation 2.4)

Where $f(A)$ describes the AM/AM characteristic of nonlinearity and $g(A)$ describe the AM/PM nonlinearity. As it can be seen, beyond the output dependence on frequency, which is also common to linear components and systems, now the output amplitude A_o will no longer be a linearly scaled replica of the input level A_i. The relative phase will be determined by both the input signal amplitude A_i and the frequency w of the input sinusoid.

This output amplitude and phase variation versus drive shows that the nonlinear device could convert input amplitude variations into output amplitude and phase change. AM/AM conversion is particularly important in systems based on amplitude modulation; while AM/PM has its major impact in modern telecommunication and wireless systems that rely on phase modulation formats. Figure 2.4 illustrates the typical AM/AM and AM/PM characteristic of a nonlinear PA versus input drive.

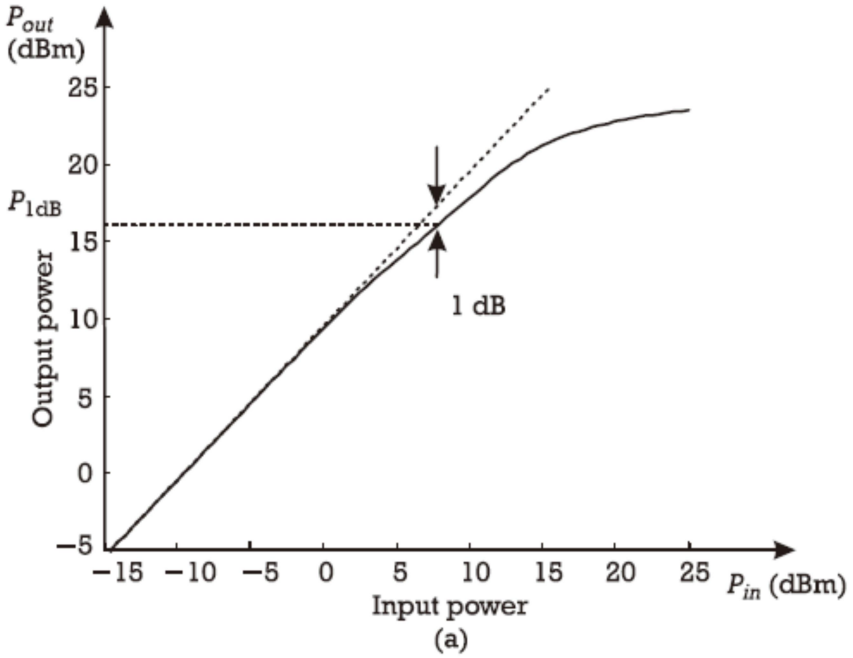

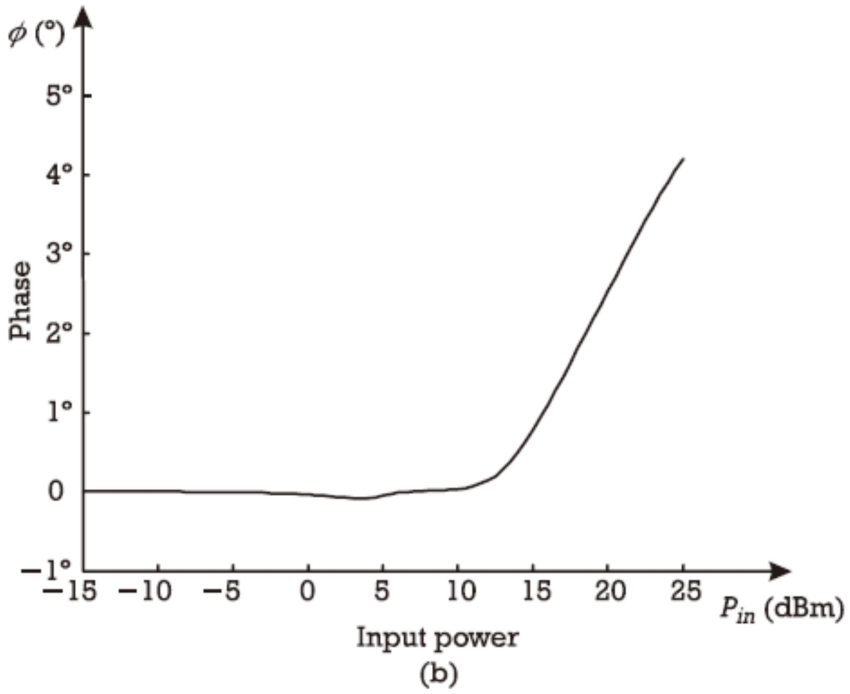

Figure 2.4 A typical amplitude and phase response characteristic of a nonlinear PA versus input drive. [15]

The power series model shown in equation 2.2 is mostly used to approximate quasi-memoryless power amplifiers [41]. A nonlinear power amplifier with memory can be approximated by the Volterra series model.

$$V_o(t) = \sum_{k=1}^{n} \int_{-\infty}^{\infty} \cdots \int_{-\infty}^{\infty} h_k(\tau_1, \tau_2, \cdots \tau_k) \prod_{j=1}^{k} V_i(t-\tau_j) d\tau_1 d\tau_2 \cdots d\tau_k$$

(Equation 2.5)

Where $h_k(\tau_1, \tau_2, \cdots \tau_k)$ are known as kth-order Volterra kernels. However, the Volterra series nonlinear model is in general restricted to weakly nonlinear systems because of the algebraic complexity of determining Volterra nonlinear transfer functions of high order.

It is possible to use an enhanced generalised power series model in the frequency-domain to represent nonlinearity instead of using a Volterra series function, which is a time-domain representation. For this frequency-domain representation, the input signal may be

described as:

$$V_i(t) = \sum_{k=1}^{n} A_k \cos(w_k t + \theta_k)$$

(Equation 2.6)

Where A_k are the real-number magnitudes of the individual frequency components w_n. The distorted output signal $V_0(t)$ will be

$$V_o(t) = X \sum_{j=0}^{\infty} a_j \left\{ \sum_{k=1}^{n} b_k A_k (t - \tau_{k,j}) \right\}^j$$

(Equation 2.7)

Where X is a constant, *j* is the order of the power series, coefficients a_j and b_k are complex and real numbers respectively, and $\tau_{k,j}$ is a time delay term which depends upon frequency and the order of the power series. This power series is related to the Volterra series [44] but is much more efficient than this time-domain representation and is capable of dealing with severe nonlinearities [42] [43].

2.3.1 Another point of view: Correlated distortion and un-correlated distortion

No matter which model we are using to represent the nonlinearity, from the communication system point-of-view, in the receiver side there will be only two types of signal which are the scaled transmitted signal and the noise. Therefore, if part of the measured signal is uncorrelated with the expected waveform, that part of the signal is considered as uncorrelated distortion noise, which contributes to the degradation of a communication system's signal-to-noise and distortion (SINAD) ratio. On the other hand, the remaining component partly consists of nonlinear distortion, which subtracts or adds to the desired output signal and thus causes gain compression or expansion. Here, the term correlation refers not only to the statistical resemblance between the input and output signals, but also to the ability of the receiver to recover useful information

from the transmitted signal. Actually, the nonlinear output is partially correlated with the input signal which leads to gain compression or expansion.

To better illustrate this idea, we consider a memory-less model which is characterized by a power series model shown in equation 2, for a third-order of odd series nonlinearity, the output signal is:

$$V_o(t) = a_1 V_i(t) + a_3 \left(V_i(t)\right)^3$$

(Equation 2.8)

We can define a new set of outputs

(Equation 2.9)

This is correlated to the input signal and can be cancelled by a scaled input signal, and

(Equation 2.10)

this part is uncorrelated to the input signal. In the above two equations, the $\tilde{\alpha} V_i(t)$ can be obtained by Gram-Schmidt orthogonalization process which will be introduced at subchapter 2.2.5

Figure 2.5 illustrates the correlated signal and un-correlated signal geometrically. As can be seen, the third-order output can be partitioned into two components: one in the direction of the linear output and the other orthogonal to it. The correlated distortion output can now be identified in terms of a cancelling process where a scaled replica of the input signal is subtracted from the total nonlinear output. The uncorrelated part is orthogonal to the input signal and therefore cannot be cancelled by a scaled replica of the input signal. The effective uncorrelated distortion contributes to the degradation of system SINAD performance and therefore the degradation of the Bit-Error-Rate (BER) performance (assuming a

digital system), whilst the correlated component of the third-order output represents the correlated distortion that causes gain compression or expansion of the linear output.

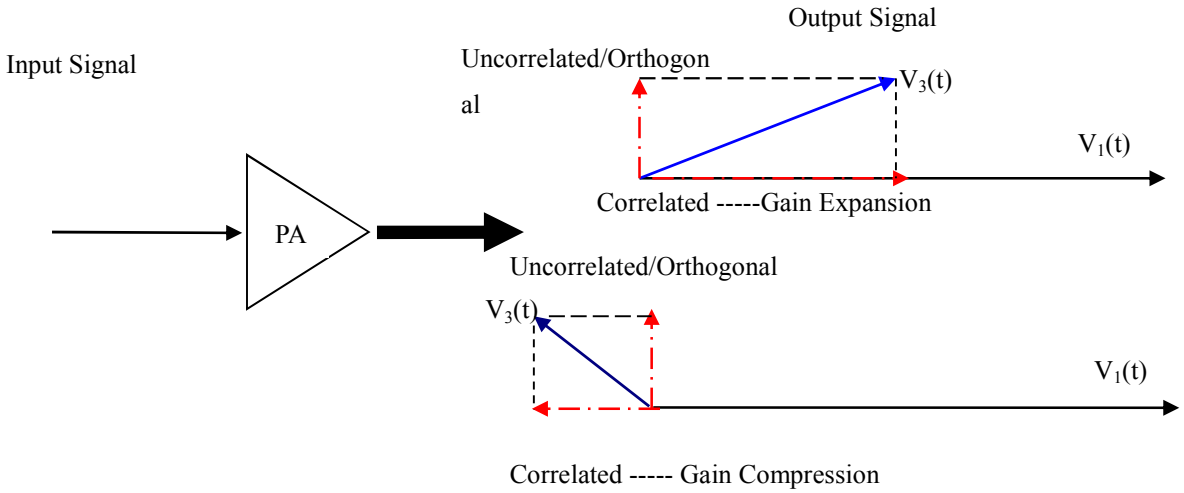

Figure 2.5 Graphic illustration of correlated and un-correlated distortion.

V3(t) refers to $a_3(V_i(t))^3$ *of equation 2.8*

2.3.2 In-band distortion and out-of-band distortion

In this work, the in-band distortion is defined as the component of the nonlinear output that shares the same frequency band as the input signal, but is "uncorrelated" with the ideal transmitter signal. And out-of-band distortion refers to the spectral re-growth of output. Figure 2.6 illustrates these two kinds of distortions in a graphic way.

In figure 2.6, the red waveform is the input and the blue one is the output waveform. The slight difference at the in-band area is the in-band distortion while the spectral re-growth outside the channel is referred to as out-of-band distortion. The problem with characterizing effective in-band distortion is the identification of the effective terms of the nonlinear output that are responsible for in-band distortion inside the main band of the input signal spectrum. The reason for this is that the nonlinear output is partially correlated with the input signal, which subtracts or adds to the desired output

signal causing gain compression or expansion.

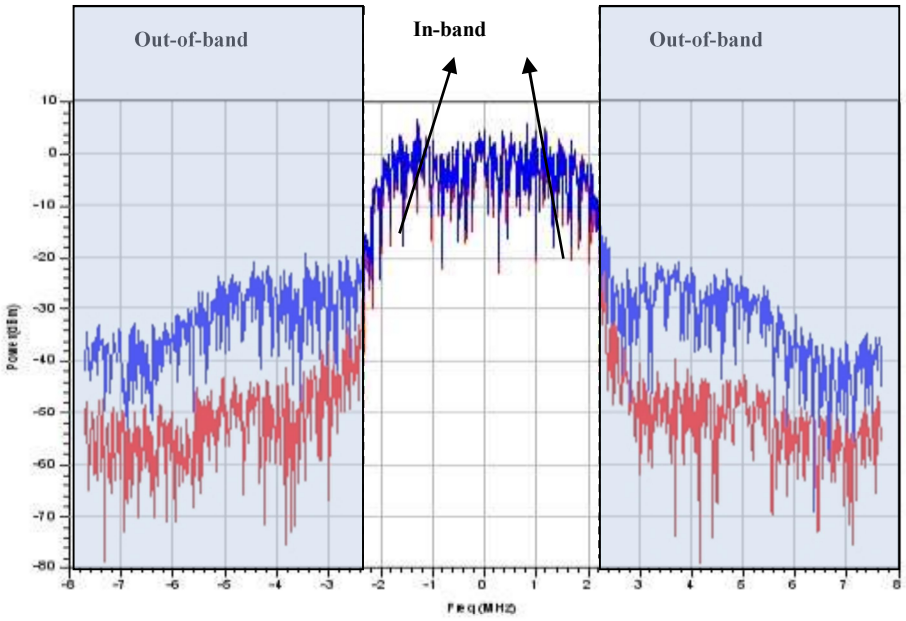

Figure 2.6 Graphic illustration of in-band and out-of-band distortion(Red:Input signal; Blue: Output signal)

2.3.3 The in-band un-correlated distortion

Defining effective in-band distortion as the uncorrelated part of distortion, it is necessary to investigate how to characterise this in-band uncorrelated distortion.

As defined at equation 2.2, where

$$V_0(t) = \sum_{k=1}^{n} W^k(t)$$

As discussed in equation 2.9 and 2.10, this representation generates a large number of mixing terms but is incapable of allowing the in-band distortion, correlated distortion and un-correlated distortion to be separated from the output components. It is therefore necessary to find a way to calculate the values of $\tilde{\alpha}$ in equation 2.9 and equation 2.10.

Gram-Schmidt orthogonalization is such a process. A finite, linearly independent set S $= \{V_1, V_2 \cdots V_k\}$ can be transformed in to an

orthogonal set S' $=\{U_1, U_2 \cdots U_k\}$ that spans the same *k*-dimensional subspace of as S[42]; therefore we can employ this process to separate the different order output components. This allows the separating of the output components to two parts with one correlated to the input signal and the other being orthogonal to the input signal, or in other words, uncorrelated to the input signal. Figure 2.7 illustrates the Gram-Schmidt orthogonalization process graphically.

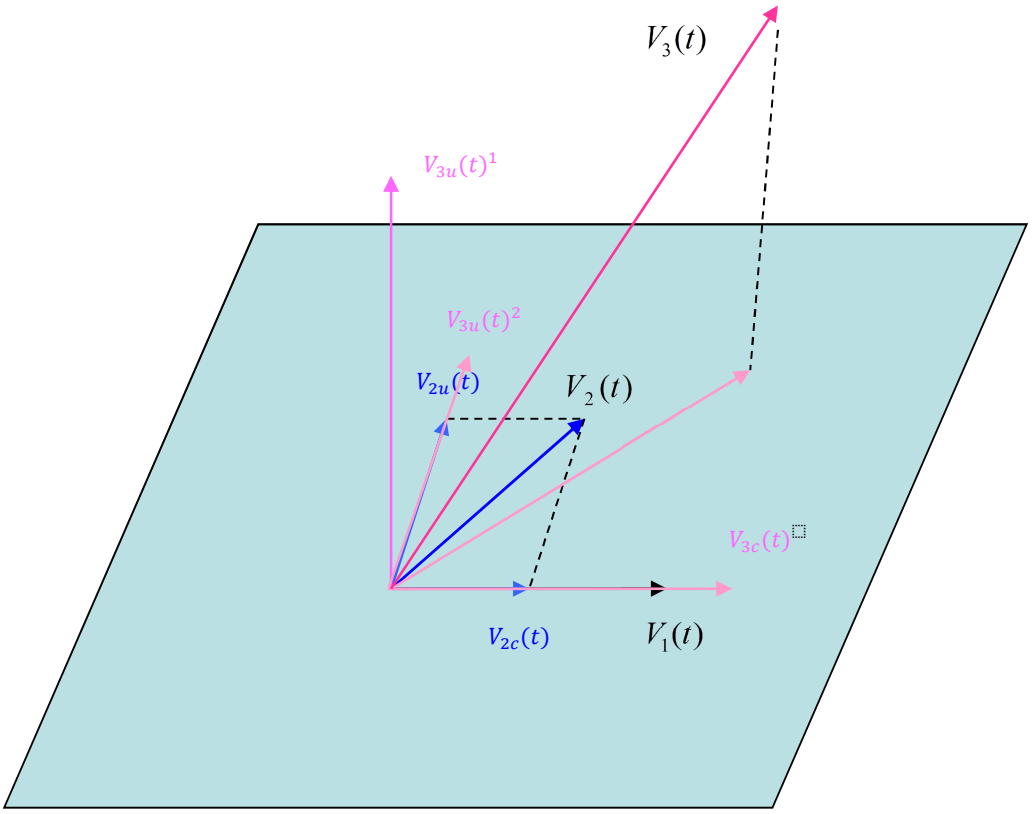

Figure 2.7 Graphic illustration of Gram-Schmidt orthogonalization

In figure 2.7, the second order output $V_2(t)$, depicted by blue arrows, has been divided to $V_{2c}(t)$, which is a scaled replica of input signal and $V_{2u}(t)$, which is uncorrelated with the input signal. The third order output $V_3(t)$, depicted by pink arrows, can be expressed as the sum of uncorrelated components $V_{3u}(t)^1$ and $V_{3u}(t)^2$, which are orthogonal to each other as well, and component $V_{3c}(t)$ which is correlated to input signal $V_i(t)$. Generally, after employing this orthgonalisation process, the output is expressed as a useful component $V_c(t)$ which is correlated with the input signal, and a

series of uncorrelated distortion components $V_u(t)$ where the cross correlation between any two components of the output is zero [2].

To summarize, after Gram-Schmidt orthogonalization, the output components can be written as

$$V_o(t) = V_c(t) + V_u(t)$$

(Equation 2.11)

Where $V_c(t)$ expresses the correlated part and $V_u(t)$ refers to the uncorrelated part. The un-correlated part $V_u(t)$ for *k*-order output component $W^k(t)$ can be calculated by[26]:

$$V_u{}^k(t) = W^k(t) - \sum_{n=1}^{j-1} a_{kn} V_u{}^n(t)$$

(Equation 2.12)

Where

$$a_{kn} = \frac{E[W_k(t) V_u{}^n(t)^*]}{E[V_u{}^n(t) V_u{}^n(t)^*]}$$

(Equation 2.13)

Note that the above analysis is actually using an autocorrelation function to derive the output components, and the output autocorrelation function can also be represented as the sum of the autocorrelation functions of the corresponding terms of the above equation as a result of the orthogonalization process. Therefore, the output autocorrelation of output components can now be written as

$$R_{VV}(\tau) = R_{V_c V_c}(\tau) + R_{V_u V_u}(\tau)$$

(Equation 2.14)

Hence the output power spectral density function (PDF), which is derived from the Fourier transformation of the above equation can also be written as

$$S_{VV}(f) = S_{V_c V_c}(f) + S_{V_u V_u}(f)$$

(Equation 2.15)

From equation 2.15 we can see that the output spectrum is therefore the sum of the spectra of the uncorrelated signal components and the scaled replica parts of the signal components. Figure 2.8 gives the graphic illustration of the correlated spectrum and un-correlated spectrum.

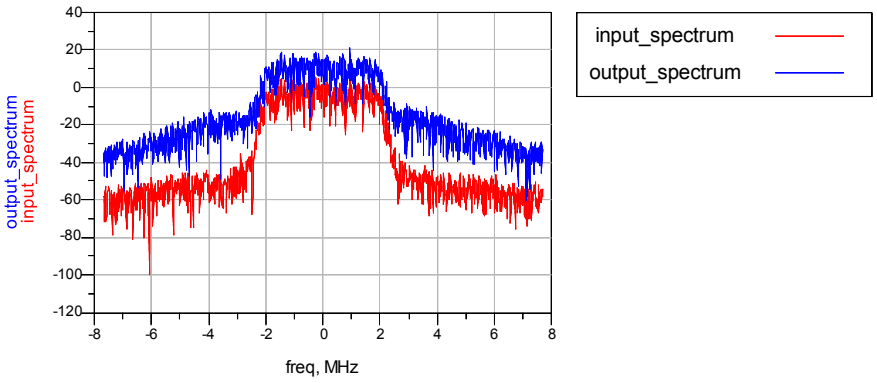

Figure 2.8a The spectrum of input signal and output signal

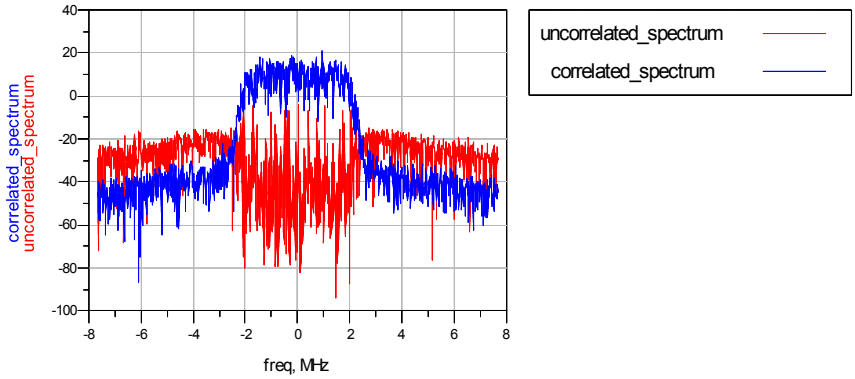

Figure 2.8b The output spectrum shown at figure 2.8a can be further devided as correlated part spectrum and uncorrelated part spectrum

2.4 The evolution from single-tone to multi-tone tests

2.4.1 Single-tone test

In the above analysis, the sinusoid excitation signal corresponds to the standard single-tone test. Figure 2.9 shows the input spectrum and output spectrum of this test. It can be seen that the fundamental output power and phase versus input power are measured, along with the output at a few of the first harmonics related to the input frequency. However, the one-tone test is not suitable as a characterization tool of wireless telecommunication systems as no interference can be measured either inside the tested spectral channel (Co-channel interference) or in any other closely located spectral channel (Adjacent-channel).

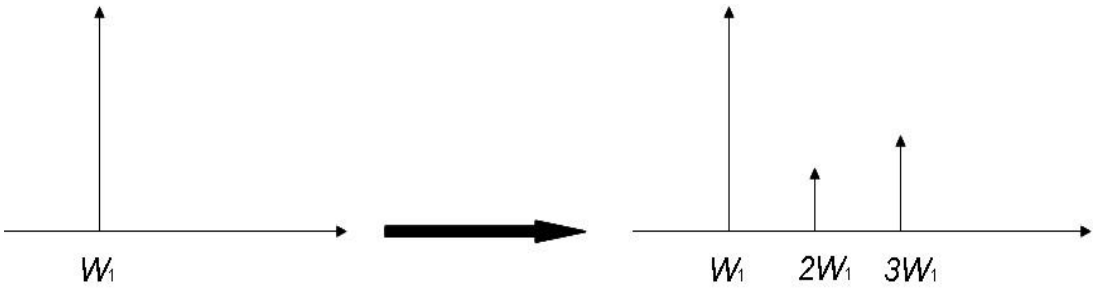

Figure 2.9 A simple illustration of input and output spectrum of single-tone excitation

2.4.2 Two-tone test of power amplifier

To overcome the shortcomings of the single-tone test, it has been replaced by the two-tone test. The two-tone excitation can be expressed as:

$$X(t) = A_1 \cos(w_1 t) + A_2 \cos(w_2 t)$$

The time-domain and frequency domain of the two-tone test signal are shown in Figure 2.10. Under this excitation the output of a nonlinear device characterized by (2) is:

$$y(t) = \sum_{r=1}^{\infty} A_{o_r} \cos(w_r t + \phi_{o_r})$$

$$w_r = m \cdot w_1 + n \cdot w_2,\ m,n \in Z$$

When m+n = 1, the output components are called inter-modulation distortion. For example, the third-degree term produces IM3 at frequency $2w_1 - w_2$, $2w_2 - w_1$, fifth-degree term produces IM5 at frequency $3w_1 - 2w_2, 3w_2 - 2w_1$.

Generally speaking, the even-order distortion terms are of less concern than the odd-order terms, though in recent years researchers have argued that it is beneficial to include even-order nonlinear terms in pre-distorter models [16]. Thus IMR, the Signal-to-Inter-modulation distortion ratio, or simply the Inter-modulation ratio (IMR), is defined as the ratio between the fundamental and IMD output power, and has been widely used as nonlinear distortion standards.

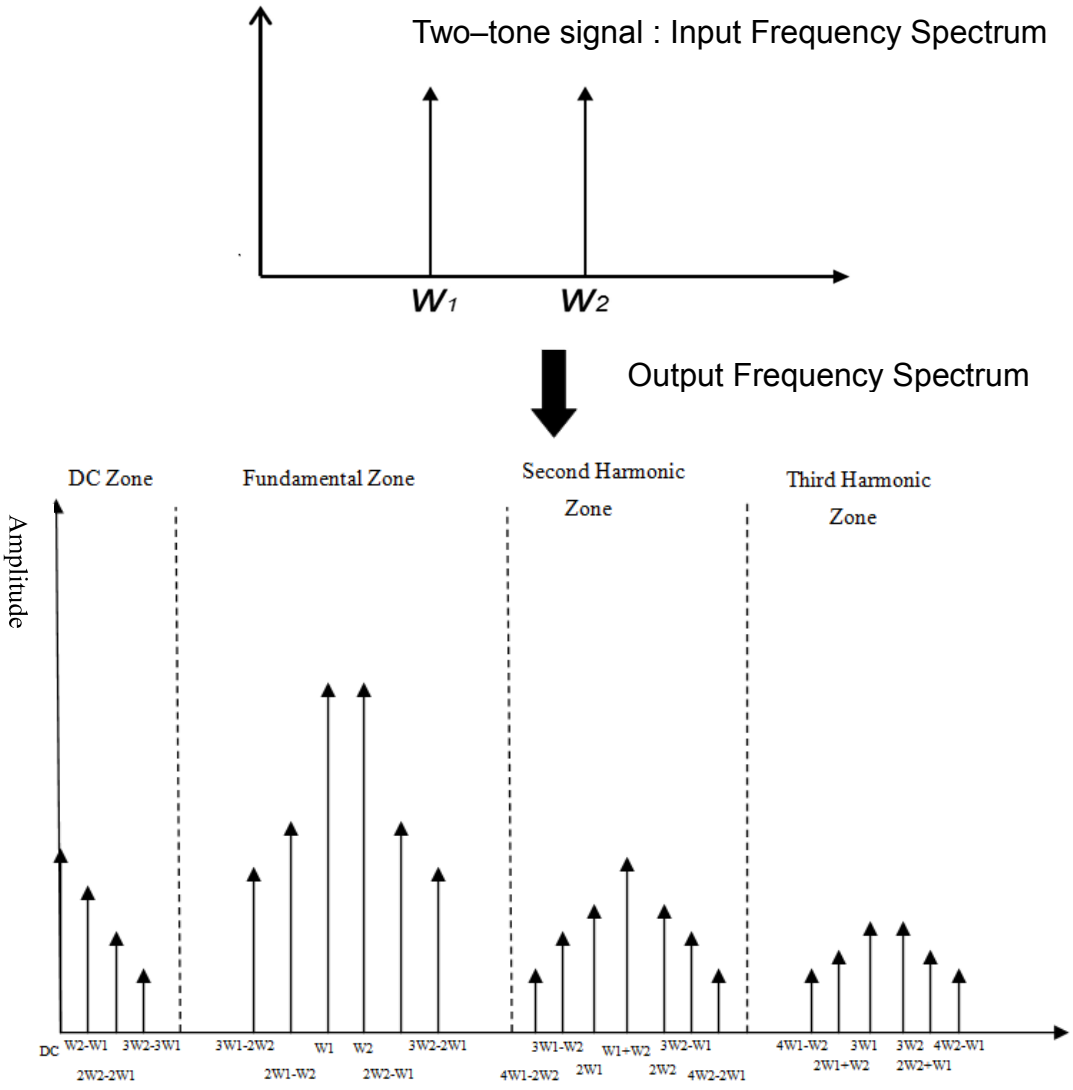

Figure 2.10 Input and output spectrum of two-tone excitation signal

The two-tone test has arguably been regarded as the most severe test of a power amplifier's non-linearity. However, one of the biggest limitations is in the analysis of in-band distortions. This is due to the fact that some of the odd-order mixing terms fall exactly onto the DC or fundamental output terms, as shown in figure 2.11, hence making them difficult to detect. This is further compounded by their small size relative to the linear part. Consequently, the two-tone test is inadequate for evaluating the in-band distortion. [17][18].

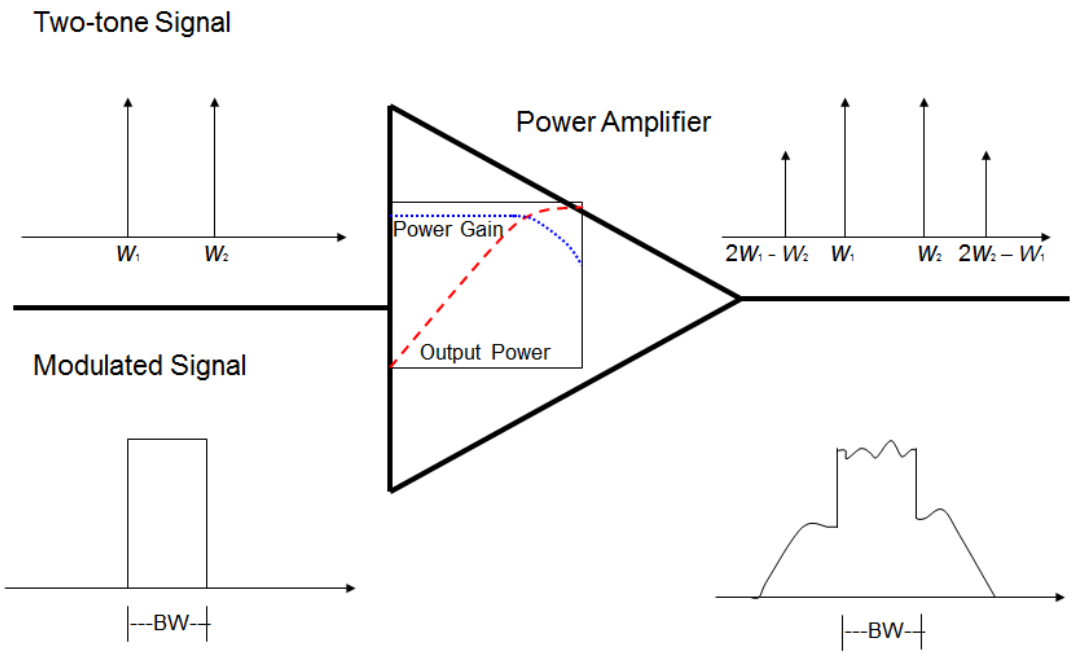

Figure 2.11 PA response of Two-tone signal and Modulated signal. Two-tone signal is inadequate for evaluating in-band distortion

2.4.3 Introduction to multi-sines design

Multi-sines usually refers to a signal with a limited number of *n* tones which sufficiently approximates a more complex signal but avoids the large number of tones that makes any further analysis more complex and even so complex that the signal cannot be measured. Obviously the fewer tones the easier further analysis would be, however the number of tones cannot be completely reduced.

As discussed in the first chapter, one of the key differences between modulated communication signals and two-tone signals is their Peak to Average Power Ratio. Modern wireless communication standards which employed OFDM usually have on average larger amplitude variations in comparison to a two-tone signal. Peak to Average Power Ratio (PAPR) is described as the ratio of a signal's peak power to average power. The PAPR can usually be calculated for units of dB as in the equation below.

$$PAPR = 10\log_{10}(\frac{P_{peak}}{P_{avg}})$$

(Equation 2.16)

For a single-tone signal, the PAPR can be found as[19]:

$$PAPR_{\sin gle-tone} = 10\log_{10}(\frac{A^2}{A^2/2}) = 3dB$$

(Equation 2.17)

where A is the amplitude of the input signal's voltage.

For a two-tone signal, the peak power and average power of this signal are denoted separately as:

$$P_{peak} = (A_1 + A_2)^2$$

(Equation 2.18)

$$P_{avg} = \frac{A_1^{\,2} + A_2^2}{2}$$

(Equation 2.19)

Then the PAPR of the two-tone signal is therefore

$$PAPR_{two-tone} = 10\log_{10}(\frac{2(A_1 + A_2)^2}{A_1^{\,2} + A_2^2})$$

(Equation 2.20)

If $A_1 = A_2$, then

$$PAPR_{two-tone} = 10\log_{10}(4) \approx 6\text{dB}$$

(Equation 2.21)

It should be noted that the above result is the maximum possible PAPR for two-tone multi-sines as the phase information wasn't considered. Compared to modulated signals which normally have a

PAPR larger than 8dB, it can be concluded that the two-tone signals do not approximate the amplitude variations of modulated signals.

Equation 2.20 can be generalized for multi-tone sinusoids if these N tones have equal amplitude, then the PAPR of an N-tone signal is [19]:

$$PAPR_{n-tone} = 20\log_{10}(N)$$

(Equation 2.22)

This result will get extremely large with the number of tones N increasing. However, if one of the amplitudes is much larger than the others, the result is:

$$PAPR_{n-tone} = 10\log_{10}(2) = 3\text{dB}$$

(Equation 2.23)

It can be concluded that theoretically the PAPR of multi-sines will range from 3dB to as large as $20\log_{10}(N)$. As most communication signals have less than 20dB PAPR, therefore any multi-sines containing more than 10 tones has the potential to approximate such modulated signals.

The above observations are just based on a simplified analysis. With the introduction of additional degrees of freedom such as phase information, more randomized frequency locations and amplitude variations the extraction of a generalized PAPR calculation equation for *n*-tone multi-sines will become more difficult and even impossible. As none of these variables are fixed, we will have an infinite multi-dimensional space in which it is difficult if not impossible to find the right combination to match the modulated signal's PAPR. Therefore, designing multi-sines in a purely mathematical way would be the last choice.

2.5 Previous multi-sines designing method

2.5.1 Digital Fourier Transformation

A straightforward approach to designing multi-sines would be the Fourier series transformation of the modulated signal to be approximated. For digital signals with finite duration the Digital Fourier Transformation (DFT) can be employed as:

$$x(n) = \sum_{k=0}^{N-1} A_k \cdot e^{j(2\pi kn/N+\theta_k)} = \frac{1}{N}\sum_{k=0}^{N-1} X(k) \cdot e^{j2\pi kn/N}$$

where A_k and θ_k are obtained from a DFT of the desired time-domain signal. Notice that this DFT process will generate N Fourier coefficients given N time sampling points, which corresponds to the N-tone of a multi-sines waveform. Hence for fixed sample frequency, the increase of signal's length will lead to the increase of the number of sample points, which will further result in an increased number of tones for approximated multi-sines. The multi-sines will more closely approximate the modulated signal in this process.

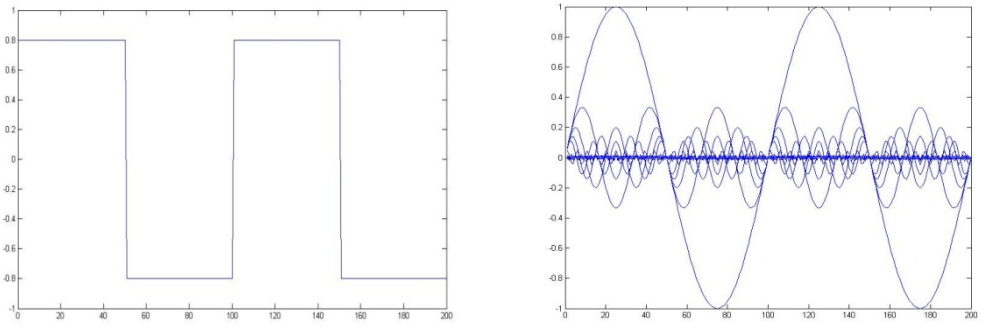

Figure 2.12a A square waveform (left) can be approximated by a set of sinusoid waveforms(right)

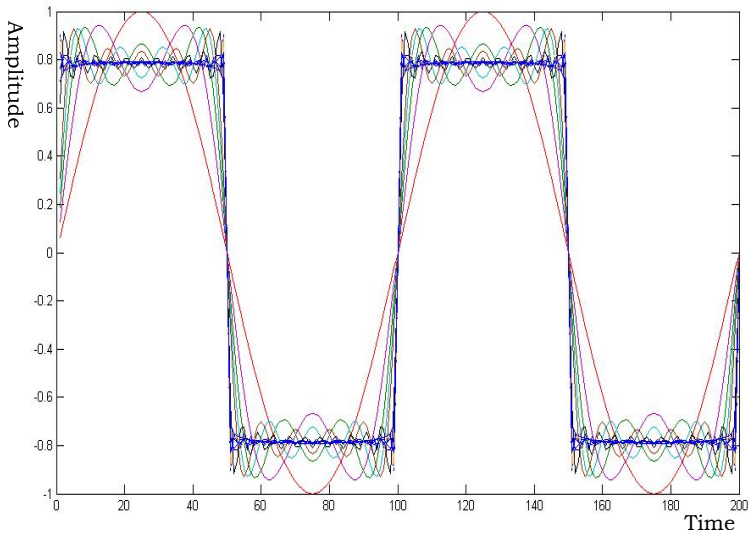

Figure 2.12b The multi-sines will get more and more approximate to the target signal with the increasing number of sinusoids

This can be seen from figure 2.12, suppose the waveform depicted in figure 2.12*a* is the waveform we want to approximate, the DFT algorithm can be used to determine a set of sinusoid waveforms, shown at figure 2.12b. The multi-sines will approximate the target signal more closely with the increasing number of sinusoids, this is depicted in figure 2.12c.

To accurately represent a signal, according to DFT theory, the number of sinusoids should equal the number of sampling points of the target signal which is decided by both the sampling rates and the

length of the represented modulated signals. Obviously, as the sampling rate is relatively constant, the longer the signal length, the finer the frequency resolution and hence the better the multi-sines represents the communication signals. To minimize the number of tones, the frequencies that are outside the bandwidth of the desired signal are removed as the majority of the total signal power is contained within a small fraction of the total bandwidth of the DFT. Figure 2.13 illustrates this idea graphically.

In practice, the truncated bandwidth is usually 20% larger than the actual signal bandwidth to minimize any error between the original signal and the truncated multi-sines representation of the signal [20]. As a result a periodical multi-sines representation of the original signal is obtained.

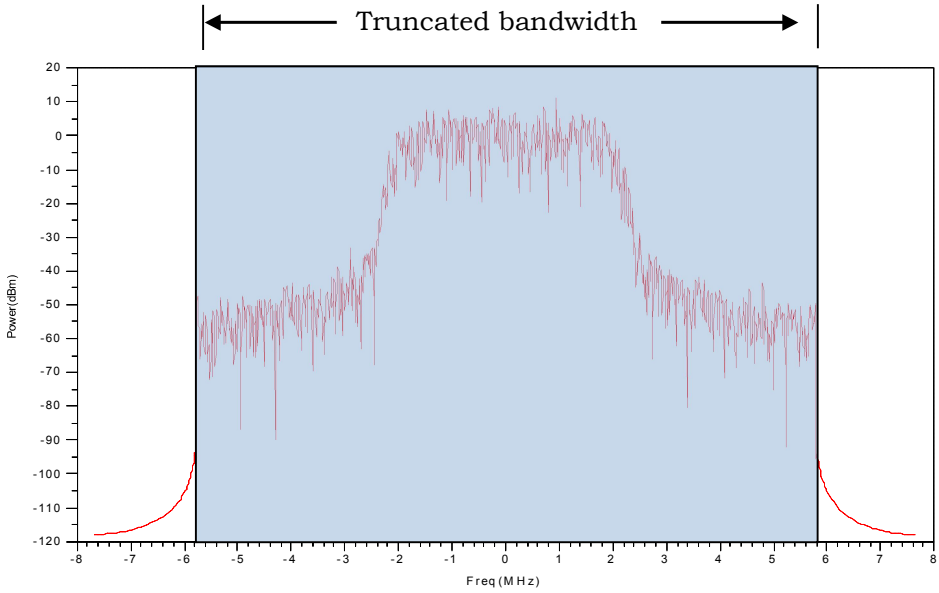

Figure 2.13 Illustration of using truncated bandwidth to design multi-sines

The main drawback of this method is the large number of tones it produces. Though frequencies that are outside the bandwidth of the desired signal have been removed, to accurately represent a 163-μs reverse-link segment of a Code Division Multiple Access (CDMA)

signal under the interim standard IS-95A with the bandwidth of 1.2288MHz, there are still 240 tones required[20]. Actually, with the advent of communication standards like Wi-Max and LTE, which have much wider bandwidths, the DFT algorithm would yield thousands of tones. For example, the bandwidth of a LTE signal ranges from 1.4MHz to 20 MHz. Therefore, to accurately represent a 163~μs segment from a 20MHz LTE signal an accurate representation will require 3912 tones.

In conclusion, the DFT method accurately represents the modulated target signals. However, the resulting high number of tones makes any further analysis difficult. Consequently, there is a clear need for alternative approximation techniques with limited number of tones yet preserving the key characteristics of the original signals.

2.5.2 Engineering phase distributions of multi-sines

During the initial investigations into the design of multi-sines the phase information was not taken into consideration. However the relationship between phases of each sine-wave component of multi-sines will have a particularly significant effect on the behaviour of the composite multi-sines. Hence people have investigated multi-sines with four different magnitude/phase relationships between sine-wave components [21][22]. In this investigation, four types of multi-sines excitations have been considered as: a) multi-sines with constant amplitude and constant-phase spectrum, b) multi-sines with constant-magnitude and random-phase spectrum, c) multi-sines with constant magnitude and Schroeder-phase spectrum [23], and d) multi-sines with random magnitude and random phase spectrum to replace digital modulation employing Quadrate Phase Shift Keying (QPSK) signals.

The obtained results demonstrated the limitations of multi-sines with universal phase distribution for the characterisation of digital systems overestimating the ACPR of digitally modulated QPSK signals. The Schroeder phase relationships between sinusoids can improve ACPR estimation with relatively small error but still a large amount of error existed even at small drive levels.

When using a large number of tones with a random-phase distribution the resulting multi-sines starts behaving like a NBGN (Narrow Band Gaussian Noise) [24], which shares similar stochastic properties with modulated communication signals. Consequently, multi-siness are employed as a substitute for modulated communication signals [26][27] in line with a large number of previous studies[25] in which white Gaussian noise signals were utilised instead. Figure 2.14 depicts as an example a simulated output spectrum of a 16-tone multi-sines with random phase distribution and comparison with a CDMA signal [26]. As can be seen both signals have very similar power spectrum contours.

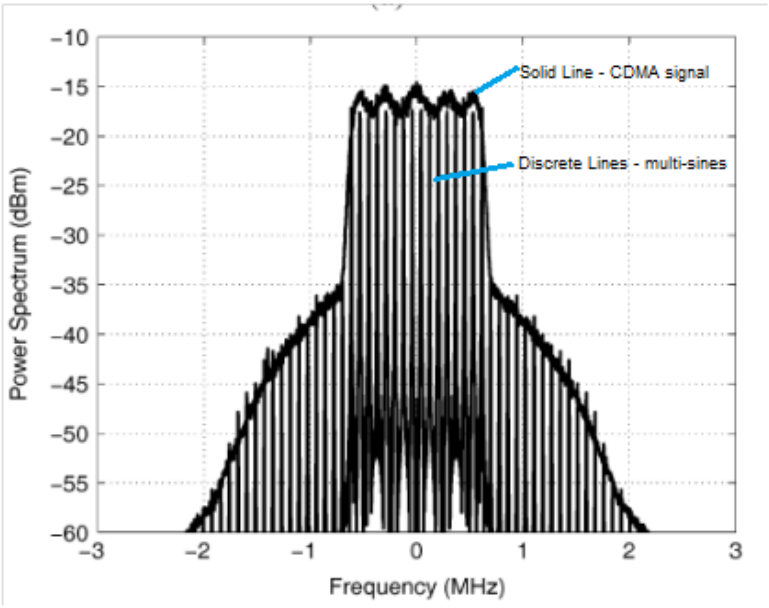

Figure 2.14 Output spectrum of 16-tone random-phase multi-sines(discrete lines) and CDMA signal(solid lines)[26]

When using random phase to approximate modulated signals, the phases of the input tones were generated using a uniform random number generator. Usually with an increasing number of tones the probability of having a uniformly distributed waveform shape increases. However by averaging a large number of phase realizations, a small number of tones multi-sines, for instance 16 tones [26], can approximate a band-limited Gaussian noise process closely enough and the number of averaged realizations depends on when the multi-sines start to converge.

A random-phase multi-sines with random phase distribution is readily calculated and straightforward to implement, providing good approximation for certain types of communication signals. The limitation is due to the fact that Gaussian approximation is only valid for communication links with high data rates, e.g. a forward-link CDMA signal with a large number of Walsh-coded channels transmitted at the same frequency. However, a signal transmitted by a mobile station carries only one channel at a time and does not behave like NBGN. Consequently, the Gaussian approximation of communication links with low data rates, e.g. the reverse-link of a CDMA signal, leads to inaccurate estimates of the cross-modulation distortion in mobile receivers [28]. This will also be demonstrated within the following chapters.

2.5.3 Matching statistical character of modulated signals

One of the reasons why random-phase multi-sines cannot approximate accurately most of the modulated signal is their different PAPR, which strongly varies in modern wireless communication signals according to their modulation methods, spread factors, or orthogonal codes. On the other side, random-phase multi-sines behaves like a Gaussian signal with a constant PAPR of around 8dB rending it unsuitable to approximate the

varying PAPRs of modulated signals [29] - [32]. The work that was published to date was focusing on the crest factor (CF), which is the square of PAPR, of multi-sines to measure the dynamic characteristics of a linear system [33].

The direct application of these techniques to approximate modulated signals [34] does not take into account the range of amplitude values covered by the output and the probability with which they are reached. The latter is of significant importance as what matters is not necessarily the instantaneous amplitude itself, but the value weighted by the probability density function (PDF) of the signal [35]. For instance, although very high instantaneous amplitude can determine the amplitude span of a signal, the resulting distortion caused by the clipping of such a high-amplitude signal will actually become almost irrelevant for the performance of a communication link if it occurs very infrequently.

Therefore, it is necessary to synthesize multi-sines with the PDF of modulated signals rather than the more common PAPR figure of merit. Several methods have been proposed to approximate the PDF of modulated signals by modifying the phase information of multi-sines [36] [37]. One of the more accepted algorithms can be described as follows:

1) Synthesize a modulated signal with a specified PDF statistics pattern and re-order its instantaneous amplitude values in descending order. This creates a vector of PDF bins to be approximated by the target signal.
2) Synthesize an equal-amplitude multi-sines with the prescribed number of frequency positions.
3) Reorder its instantaneous multi-sines waveform amplitude values in descending order, recording their time samples,

hence, creating a vector of PDF bins for the multi-sines.

4) Substitute the amplitudes within the multi-sines PDF vector with the ones from the target modulated signal.
5) Resort the new multi-sines PDF vector according to the stored time samples thus creating a new multi-sines with the desired PDF.
6) Calculate the DFT of this signal, and level off the resulting tone amplitudes so that the same total power is kept, maintaining the phases obtained. This is therefore the desired multi-sines we are looking for.
7) If the amplitude levelling modifies the PDF of the multi-sines unacceptably, repeat the algorithm, using as the starting multi-sines the one synthesized with this technique, until an acceptable error is reached.

This method, theoretically, can generate a multi-sines with the same PDF as the target modulated signal. However, the acquired multi-sines will only have acceptable errors after the algorithm has been repeated until convergence is met. The errors mostly come from step 5 and step 6, where multi-sines with a limited number of tones have been employed to replace the multi-sines generated at step 4 which may possibly have a large number of tones. Moreover, in step 6, only phase information of multi-sines are maintained which results every time in significant changes of the power spectrum. The number of iterations will depend on the target modulated signal and its statistical characteristics. In the case of signals with a low PAPR, the above calculating process becomes very time consuming and difficult to converge because the PAPR is a very complicated function of phases and standard optimising techniques like the above algorithm do not help much with the designing of signals with small PAPR [42].

Furthermore, two waveforms with the same PDF may have

completely different shapes and hence will generate different responses to the characterised device or system. To illustrate this further, two 50-tone multi-sines have been designed employing the above algorithm ensuring that both have the same PDF and power spectrum. Then these two signals were imported to the Agilent Advanced Design System (ADS) environment as excitations of the same nonlinear system and produced different ACPR values for the resulting output signals. Here the DUT used is a Freescale MRF6S21100H MOSFET PA and the calculated ACPR difference was about 2dB.

Figure 2.15a shows the Complementary Cumulative Distribution Function (CCDF) of the two signals. The CCDF is acquired by firstly computing the integral of the PDF to get the Cumulative Distribution Function (CDF) and then subtracting it from unity, i.e. calculating CCDF = 1 – CDF. The two 50-tone multi-sines have exactly the same power spectrum, as shown in figure 2.15b, but different time-domain waveform shapes, which are depicted in figure 2.15c. The power spectrums of the two signals after being imported into the simulation environment are identical at the input of the device under test. The resulting output power spectrums shown in figure 2.16 are obviously different.

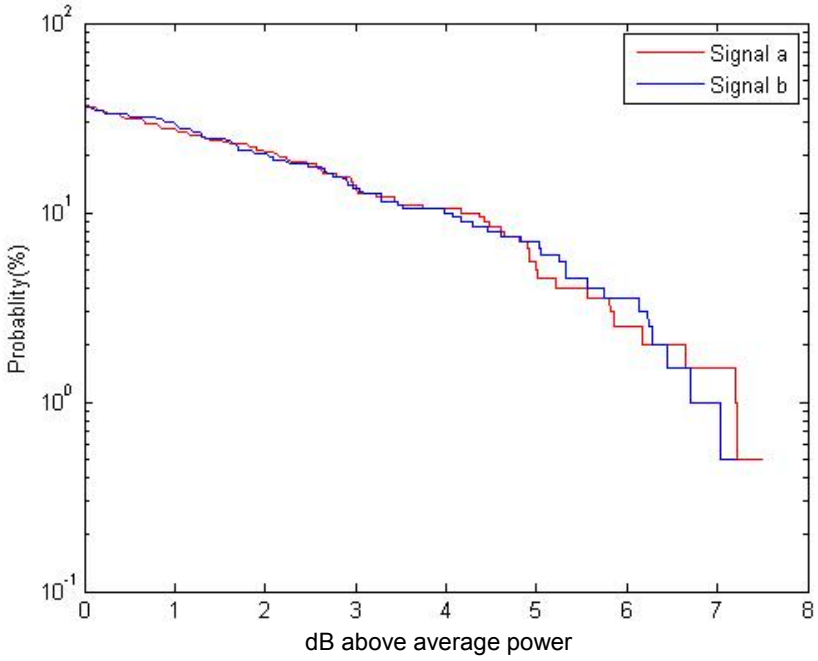

Figure 2.15a The CCDF curves of two 50-tone multi-sines

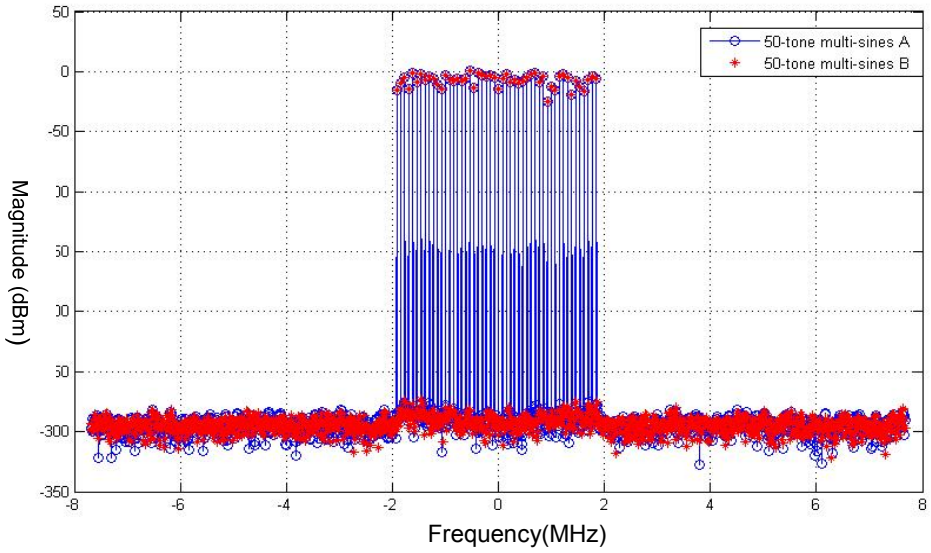

Figure 2.15b The input power spectrum of two 50-tone multi-sines

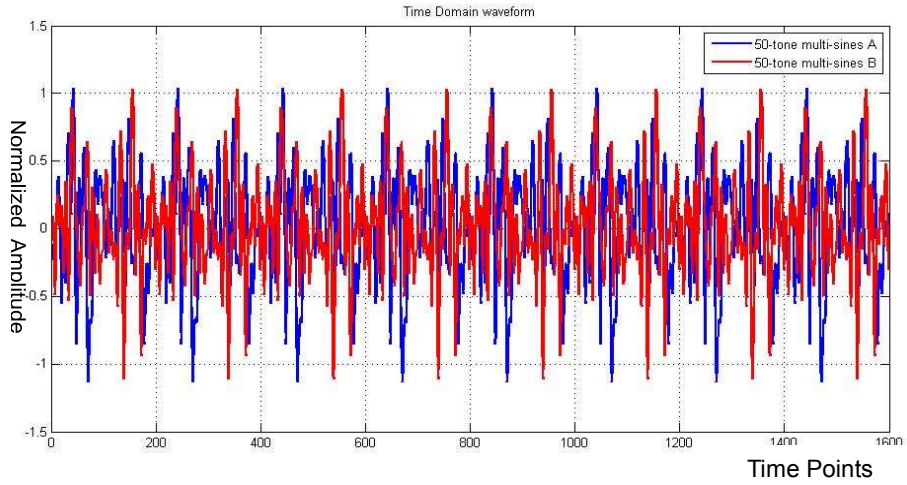

Figure 2.15c The time-domain waveform shapes two 50-tone multi-sines

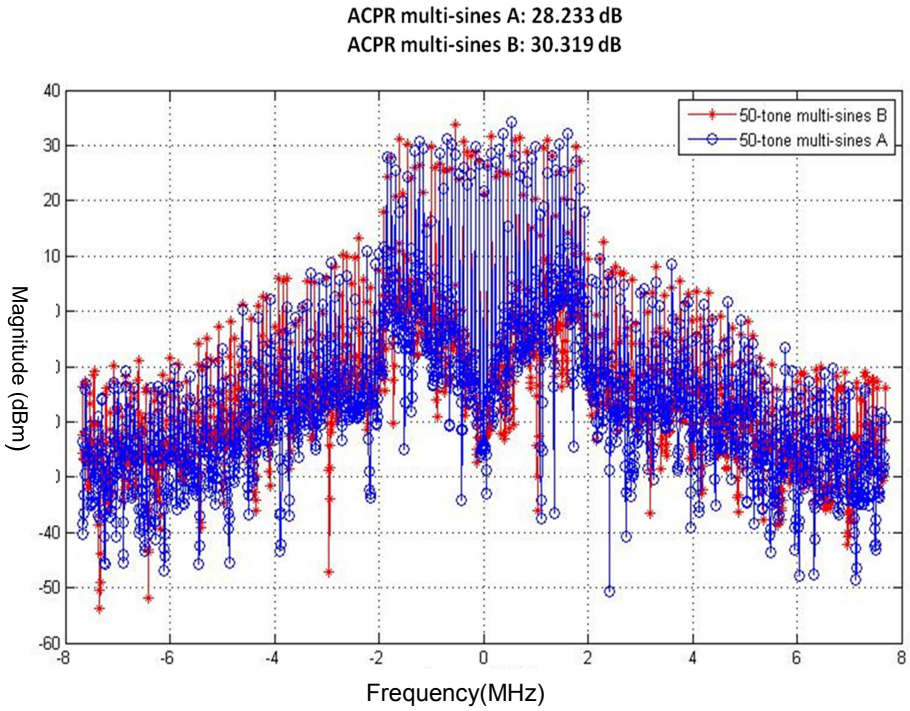

Figure 2.16 The output power spectrum of two 50-tone multi-sines after passing DUT

Similar observations [37] were reported for two signals with the same PDF and power spectrum that passed a memoryless nonlinear system. The resulting distributions of power due to spectrum re-growth generated significantly different output spectra although the ACPR has remained the same. The reported results are summarized

in figure 2.17, with input signals *a* and *b* both having the same PDF and power spectrum but generating a significantly different output response.

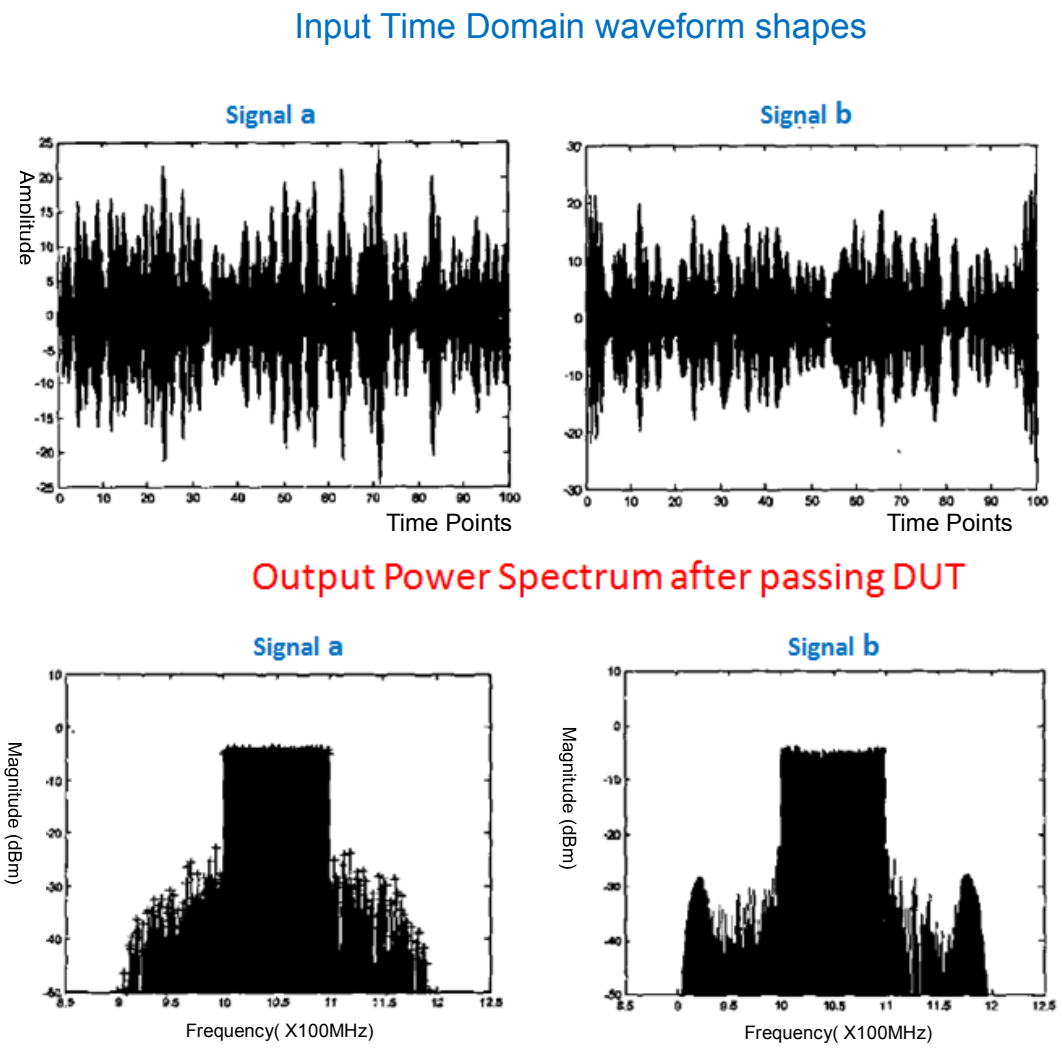

Figure 2.17 Two excitation signals with same PDF and spectrum but different phases could excite completely distinct output power spectrum.[37]

In the above examples, the only difference between the two multi-sines is in the phase relationships between the tones. This also implies that the employed design target parameters such as PDF or power spectrum, being a second-order statistical description, are not sufficient for the accurate approximation of the target signal.

Consequently, subsequent research has employed Higher Order Statistics (HOS) figures recently [38].

High order spectra, also known as poly-spectra, are defined in terms of higher order statistics ("cumulants") [39]. The Fourier transformation of the third order statistics is also called bi-spectra, while the tri-spectra is the Fourier transformation of fourth-order statistics. More specifically, suppose the signal is $V(t)$ and its Fourier Transformation is $X(f)$. The power spectrum is then given by equation (23) given the system resistance is 1Ohm.

$$P(f) = X(f)X^*(f)$$

(Equation 2.24)

The bi-spectrum is defined as follow [38][39]:

$$B(f) = X(f)X(f)X^*(2f)$$

(Equation 2.25)

And the fourth-order spectrum or tri-spectrum is defined as:

$$T(f) = X(f)X(f)X(f)X^*(3f)$$

(Equation 2.26)

As the third order cumulant, bi-spectra, contain phase information This may therefore enable a more accurate approximation through multi-sines by taking into account new and relevant information that is contained within the modulated target signal. Figure 2.18 illustrates this on two of the multi-sines with identical power spectrum, shown in figure 2.15, but different bi-spectra.

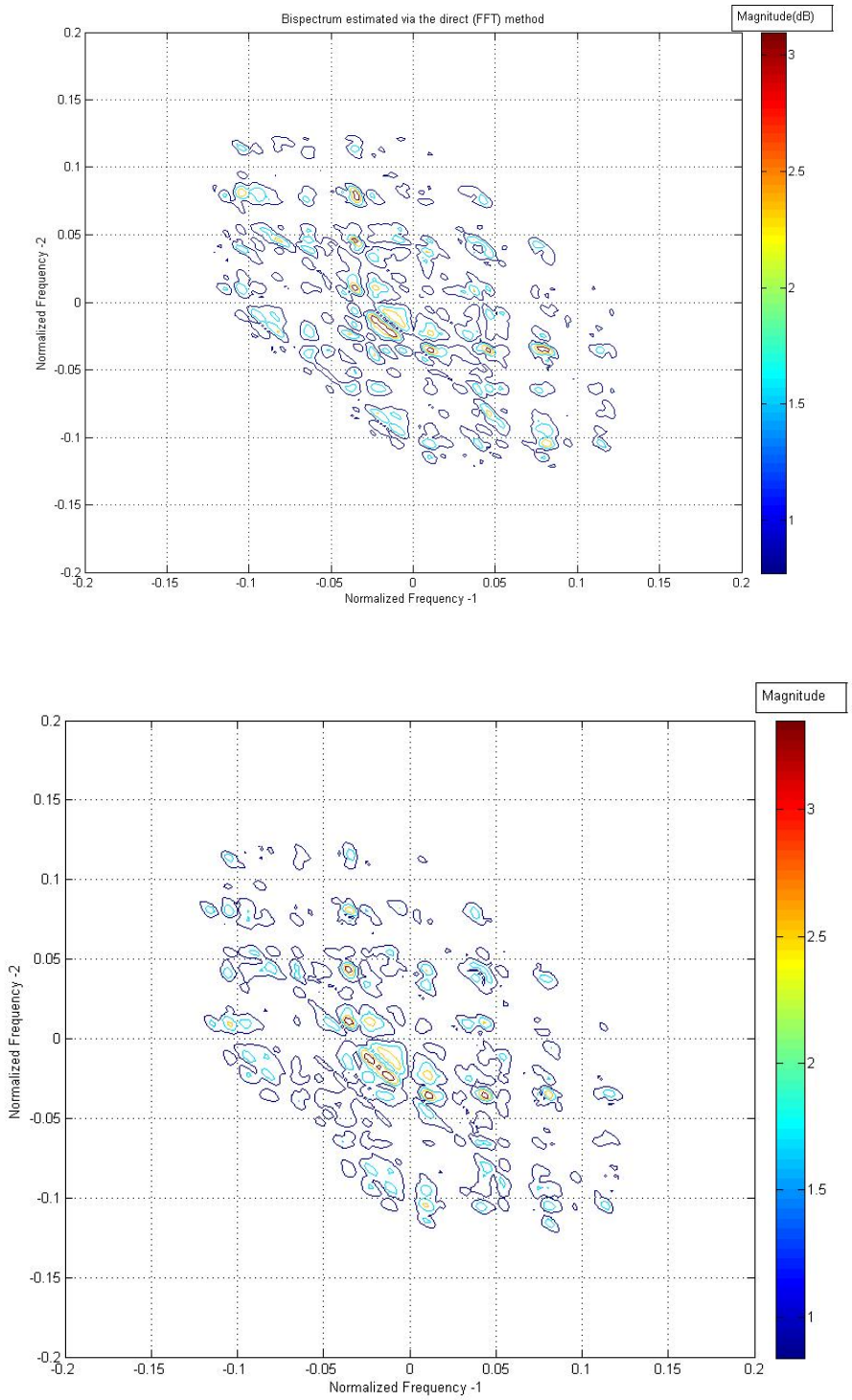

Figure 2.18 The Bispectrum of the two multi-sines with identical power spectrum as shown in figure 2.15. As can be seen, sigificant difference exists

It is clear from the definition of the bispectrum and trispectrum that they enhance the power spectrum by using the second-order and third-order nonlinearity components respectively [38]. Therefore,

higher-order spectrum allows for a more accurate description of a signal, hence the similarity between multi-sines and modulated target can be defined in terms of the similarity between output high-order spectrums. Therefore, utilising the higher order statistics for the multi-sines design is to obtain a maximum match with the high-order PSD of the targeted modulated signal [36].

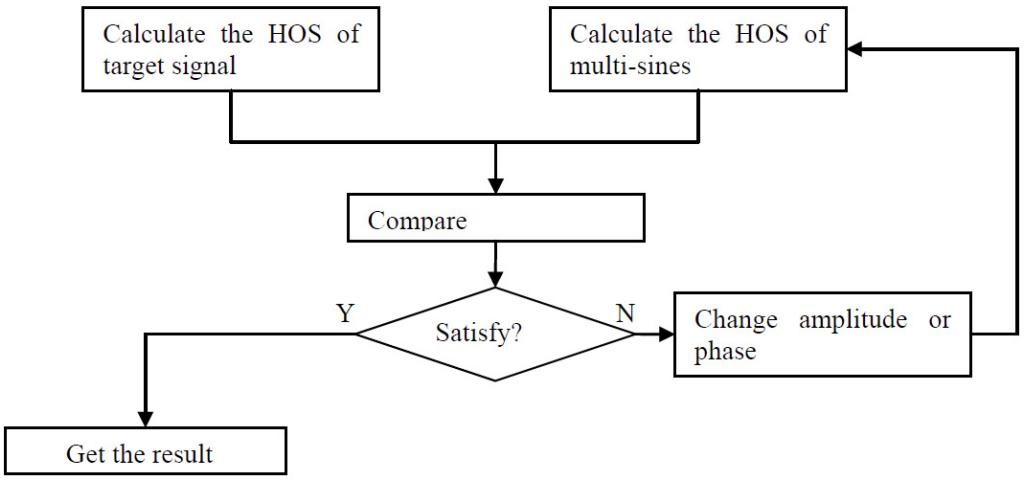

Figure 2.19 A proposed algorithm of designing multi-sines with High Order Spectra

A possible algorithm of this method is proposed in [36], which is summarized in figure 2.19. As it can be seen, to match the higher order statistical descriptions all the possible values of frequency magnitudes and phases need to be iterated until we get a satisfactory multi-sines. Thus, the process results in heavy calculation loads. For instance, for a modulated signal consisting of K sample points, the power spectrum involves on average K complex number Fourier transformations per signal realization. Furthermore, bi-spectrum, a second-order analysis will involve an average over K^3 complex entities while the third-order analysis, which is the lowest nonlinear order responsible for the spectral re-growth, equation (25) must be estimated from averaging complex matrices of size K^5. Moreover,

taking into account that multi-sines consist of n-tones with each tone having m possible amplitudes and m possible phases the number of necessary loops to obtain the multi-sines with the best match would be up to m^{2n} . The resulting number of calculations for K samples is hence up to $K^5 \cdot m^{2n}$.

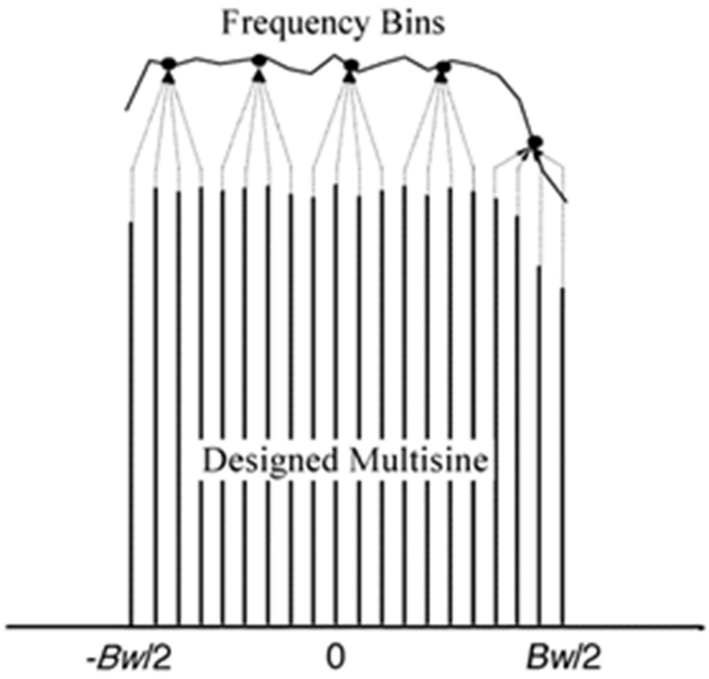

Figure 2.20 Approximating multi-sines by matching higher order PSD(HOS) in a certain number of predefined frequency bins.[38]

An alternative way is to consider a large number of sinusoids, but approximating the PSD only in selected frequency bins. Figure 2.21 illustrates this idea, and the detailed introduction can be found at [38]. This method successfully decreases the complexity of the matrix to calculate the HOS. However, the iteration of n-tones with each tone having m possible amplitudes and m possible phases is a real bottleneck for designing multi-sines. As none of these variables are fixed, we will have an infinite multi-dimensional space in which it is difficult if not impossible to find the right combination to match the modulated signal's HOS. For example, designing a 10-tone multi-

sines with *10* possible amplitude and phase levels will lead to 10^{20} iterations.

Such computational complexity will impose a significant load on both the processor and the storage devices. Hence there is a need to restrict the number of unknowns and thus the degree of similarity between multi-sines and original modulated signals. Moreover, there are still arguments about whether HOS are really necessary or not as the input of a device/transistor responds only to the amplitude and/or amplitude variations.

2.6 Reference

[1] Joel Vuolevi, “Analysis, measurement and cancellation of the bandwidth and amplitude dependence of intermodulation distortion in RF power amplifiers” 2001

[2] Draxler, P.; Langmore, I.; Hung, T.P.; Asbeck, P.M.; “Time domain characterization of power amplifiers with memory effects”, Microwave Symposium Digest, 2003 IEEE MTT-S International, Volume 2, 8-13 June 2003 Page(s):803 - 806 vol.2

[3] Williams, D.J.; Leckey, J.; Tasker, P.J.; “A study of the effect of envelope impedance on intermodulation asymmetry using a two-tone time domain measurement system”, Microwave Symposium Digest, 2002 IEEE MTT-S International, Volume 3, 2-7 June 2002 Page(s):1841 – 1844

[4] Peter B. Kenington, “High-Linearity RF Amplifier Design”,Artech House, 2000

[5] Oapos; Droma, M.S.; Mgebrishvili, N.; Goacher, A.A., “RF power amplifier nonlinearity modelling and intermodulation distortion analysis in OFDM signal transmitter systems”, Microwave Conference, 2004. 34th European, Volume 1, Issue, 11-15 Oct. 2004 Page(s): 185 – 188

[6] K.G. Gard, H.M. Gutierrez and M.B. Steer, "Characterization of Spectral Regrowth in Microwave Amplifiers Based on the Nonlinear Transformation of a Complex Gaussian Process," IEEE Transactions on Microwave Theory and Techniques, Vol. 47, No. 7, July 1999, pp. 1059-1069

[7] J. Verspecht and P. Van Esch, “Accurately Characterizing Hard Nonlinear Behaviour of Microwave Components with the Nonlinear Network Measurement System: Introducing `Nonlinear Scattering Functions',” in Proc. 5th Int. Workshop on Integrated Nonlinear Microwave and Millimeterwave Circuits, Duisburg, Germany, Oct. 1998,pp. 17-26.

[8] Jose C.Pedro and Stephen A .Mass, “A Comparative overview of Microwave and Wireless Power-Amplifier behavioural Modelling Approaches” IEEE Trans. Microwave theory and Techniques. Vol. 53, No 4, April 2005.

[9] D. Schreurs, J. Verspecht, S. Vandenberghe, G. Carchon, K. van der Zanden, and B. Nauwelaers, “Easy and accurate empirical transistor model parameter estimation from vectorial large-signal measurements,” in IEEE MTT-S Int. Microwave Symp. Dig., Anaheim, CA 1999, pp. 753-756.

[10] S. A. Maas, “Volterra Methods for Behavioural Modelling”, IMS 2003 Workshop on Fundamentals of Nonlinear Behavioural modelling, June 2003

[11] S. A. Mass, “Nonlinear Microwave Circuits” IEEE Press,1996

[12] John Wood, David E. Root, “Fundamentals of Nonlinear Behavioural Modelling for RF and Microwave Design”, Artech House, 2005

[13] Qi-Jun Zhang; Gupta, K.C.; Devabhaktuni, V.K., “Artificial neural networks for RF and microwave design - from theory to practice”, Microwave Theory and Techniques, IEEE Transactions on page(s): 1339- 1350, Volume: 51, Issue: 4, Apr 2003

[14] M. Schetzen, “the volterra and wiener theories of nonlinear systems”, New York, John Wiley& Sons, 1980

[15] Jose Carlos Pedro and Nuno Borges Carvalho, “Intermodulation Distortion in Microwave and Wireless Circuits”, Artech House Publishers, August 2003

[16] Kim, J. and Konstantinou, K., “Digital pre-distortion of wideband signals based on power amplifier model with memory,” Electron. Letter, vol. 37, pp. 1417–1418, Nov. 2001.

[17] J.C. Pedro, N. B. Carvalho, ''On the use of multi-tone technique for assessing RF components, inter-modulation distortion,'' IEEE Trans. Microwave Theory Tech, vol. 52, pp. 2395~2402. Dec. 1999.

[18] Gharaibeh.K.M, Gard.K, Steer.M.B, “Characterization of in-band distortion in RF front-ends using multi-sine excitation” IEEE Radio and Wireless Symposium, 2006

[19] Tony Rouphael, “RF and Digital Signal Processing for Software-Defined Radio” Elsevier Science & Technology, ISBN: 9780750682107

[20] M. Li, K.M. Gharaibeh, K.G. Gard, and M.B. Steer, “Accurate multi-sine representation of digital communication signals for characterization of nonlinear circuits,” in Proc. IEEE Radio and Wireless Symp., Jan. 2006, pp. 527–530.

[21] Schreurs, D.; Myslinski, M.; Remley, K. A. “RF Behavioural Modelling from Multisine Measurements: Influence of Excitation Type”, European Microwave Conference, 2003. 33rd Oct. 2003 Page(s):1011 – 1014

[22] K. A. Remley, "Multisine excitation for ACPR measurements," 2003 IEEE MTT-S Intern. Microwave Symp. Digest, 2003, vol. 3, pp. 2141-2144.

[23] R. Pintelon and J. Schoukens, System Identification: A Frequency Domain Approach. New York, NY: IEEE Press, 2001.

[24] K. Vanhoenacker, T. Dobrowiecki, and J. Schoukens, “Design of multisine excitations to characterize the nonlinear distortions during FRF-measurements,” IEEE Trans. Instrum. Meas., vol. 50, no. 5, pp. 1097–1102, Oct. 2001.

[25] Qing Wu. Heng Xiao, and Fu Li, "Linear RF Power Amplifier Design for CDMA Signals: A Spectrum Analysis Approach". Microwave Journal, Vo1.41, No.12, pp.2240, December 1998

[26] K. M. Gharaibeh, K. G. Gard and M. B. Steer, “In-band distortion of multisines,” IEEE Trans. Microwave Theory and Tech., August 2006, pp. 3227–3236.

[27] K. M. Gharaibeh, K. Gard and M. B. Steer, “Characterization of in-band front-ends using multi-sine excitation,” Radio and Wireless

Symp. 2006, Jan. 2006

[28] V. Aparin, B. Butler, and P. Draxler, “Cross modulation distortion in CDMA receivers,” in IEEE MTT-S Int. Microwave Symp. Dig., vol. 3, 2000, pp. 1953–1956

[29] S. Boyd, “Multi-tone signals with low crest factor,” *IEEE Trans. Circuits Syst.*, vol. CAS-33, pp. 1018-1021, Oct. 1986.

[30] S. Narahashi, K. Kumagai, and T. Nojima, “Minimizing peak-to-average power ratio of multi-tone signals using steepest descent method,” *Electron. Lett.*, vol. 31, pp. 1552-1554, Aug. 1995.

[31] D. R. Gimlin and C. R. Patisaul, “On minimizing the peak-to-average power ratio for the sum of N sinusoids,” IEEE Trans. Commun., vol. 41, pp. 631-635, Apr. 1993.

[32] M. Friese, “Multitone signals with low crest factor,” *IEEE Trans. Commun.*, vol. 45, pp. 1338-1344, 1997.

[33] K. Godfrey, Perturbation Signals for System Identification. Englewood Cliffs, NJ: Prentice-Hall, 1993.

[34] J.F. Sevic and M.B. Steer, “On the significance of envelope peak-to-average ratio for estimating the spectral re-growth of an RF/microwave power amplifier,” IEEE Trans. Microwave Theory Tech., vol. 48, no. 6, pp. 1068–1071, June 2000.

[35] M.D. McKinley, K.A. Remley, M. Myslinski, and J.S. Kenney, “Eliminating FFT artifacts in vector signal analyzer spectra,” Microwave J, vol. 49, no. 10, pp. 156–164, Oct. 2006.

[36] J.C. Pedro and N.B. Carvalho, “Designing band-pass multi-sines excitations for microwave behavioral model identification,” in IEEE MTT-S Int. Microwave Symp. Dig., June 2004, vol. 2, pp. 791–794.

[37] J. Schoukens and T. Dobrowiecki, “Design of broadband excitation signals with a user imposed power spectrum and amplitude distribution,” in Proc. IEEE Instrumentation and Measurement Technology Conf., May 1998, vol. 2, pp. 1002–1005.

[38] J.C. Pedro and N.B. Carvalho, “Designing multisine excitations for

nonlinear model testing," IEEE Trans. Microwave Theory Tech., vol. 53, no. 1, pp. 45–54, Jan. 2005.

[39] Nikias, C.L. Mendel, J.M, "Signal processing with higher-order spectra", IEEE Signal Processing Magazine, July 1993 Volume: 10, Issue: 3 pp: 10-37

[40] Joel Vuolevi,Timo Rahkonen, "Distortion in RF power amplifiers", Artech House Publishers, February 2003

[41] R. G. Sea and A. G. Vacroux, "On the computation of intermodulation products for a power series nonlinearity," Proc. IEEE, vol.57, pp. 337-338, Mar. 1969.

[42] Bau III, David; Trefethen, Lloyd N. "Numerical linear algebra", Philadelphia: Society for Industrial and Applied Mathematics, ISBN 978-0-89871-361-9, 1997

3 Design multi-sines — a novel approach

As discussed in previous chapter, all current multi-sines design techniques have their own shortcomings hence limiting their application in industry. This chapter will start with the correlation method for multi-sines design investigating its advantages and limitations. Based on the discussion a new design process is proposed, which can mimic various types of target signals quickly and accurately.

3.1 Designing multi-sines with correlation methods

3.1.1 Understanding correlation

It is intuitive to suggest the use of correlation methods for the design of multi-sines excitations as it describes the difference between various waveforms. To illustrate this point, take the scenario where we are trying to find how much similarity exists among the waveforms 1, 2 and 3 as shown in figure 3.1. To quantify the simliarity, a mathematical method should be employed. Correlation is hereby one of the most widely used methods.

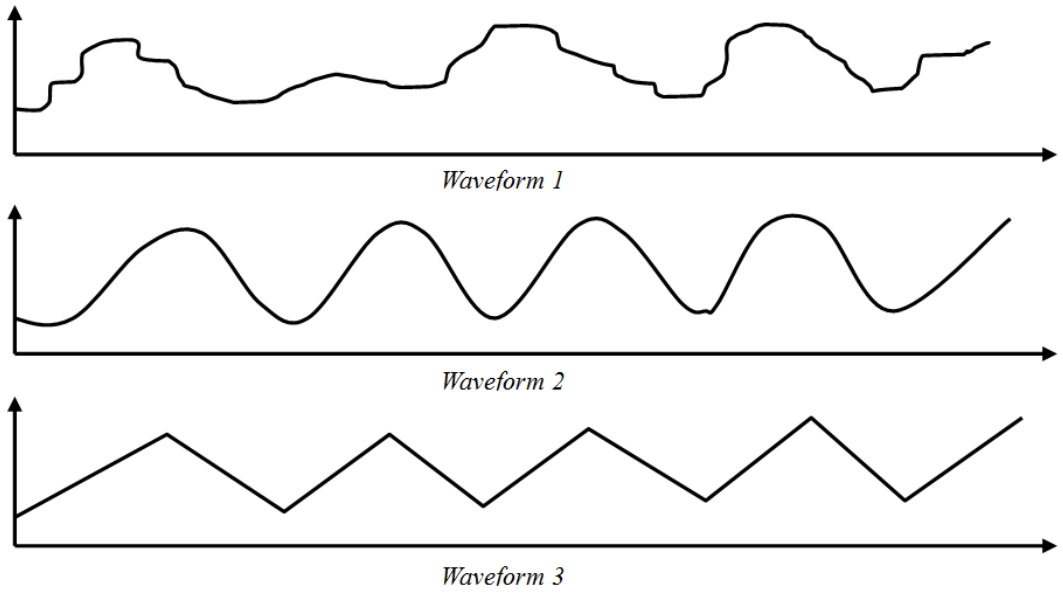

Figure 3.1 Finding similarities between waveforms

The correlation is mathematically described by equation 3.1:

$$y(\tau) = \int_{-\infty}^{\infty} x_1(t)x_2(t+\tau)dt$$

(Equation 3.1)

For periodic functions this equation is modified as:

$$y(\tau) = \frac{1}{T}\int_{0}^{T} x_1(t)x_2(t+\tau)dt$$

(Equation 3.2)

We can now introduce a simplified version of Equation 3.2 in which we take away the time shift t:

$$y = \frac{1}{T}\int_{0}^{T} x_1(t)x_2(t)dt$$

(Equation 3.3)

This definition is generally referred to as spot correlation. The equation 3.3 is simply the average of a product of two periodic

signals over the period and measures the similarity between two signals $x_1(t)$ and $x_2(t)$ without any time shift t between them, i.e. the correlation on the spot. Thus, the spot correlation provides a pattern matching for the two signals. While correlation can be viewed as one function searching to find itself in another, spot correlation can be interpreted as the measure of how much one periodical signal is embedded in another one at a given time[1].

This conclusion can help us designing multi-sines, which can be interpreted as using a series of sinusoid waveforms consisting of different amplitudes, phases and frequencies to represent a target signal, as illustrated in figure 3.2, where two sinusoids are employed for the approximation. In this scenario, spot correlation can be used to find the difference between each sinusoid waveform and the target signal, then assign a weight factor for each sinusoid in regard to their difference to the target signal. Therefore the summation of these two sinusoids will provide best matching to the target signal.

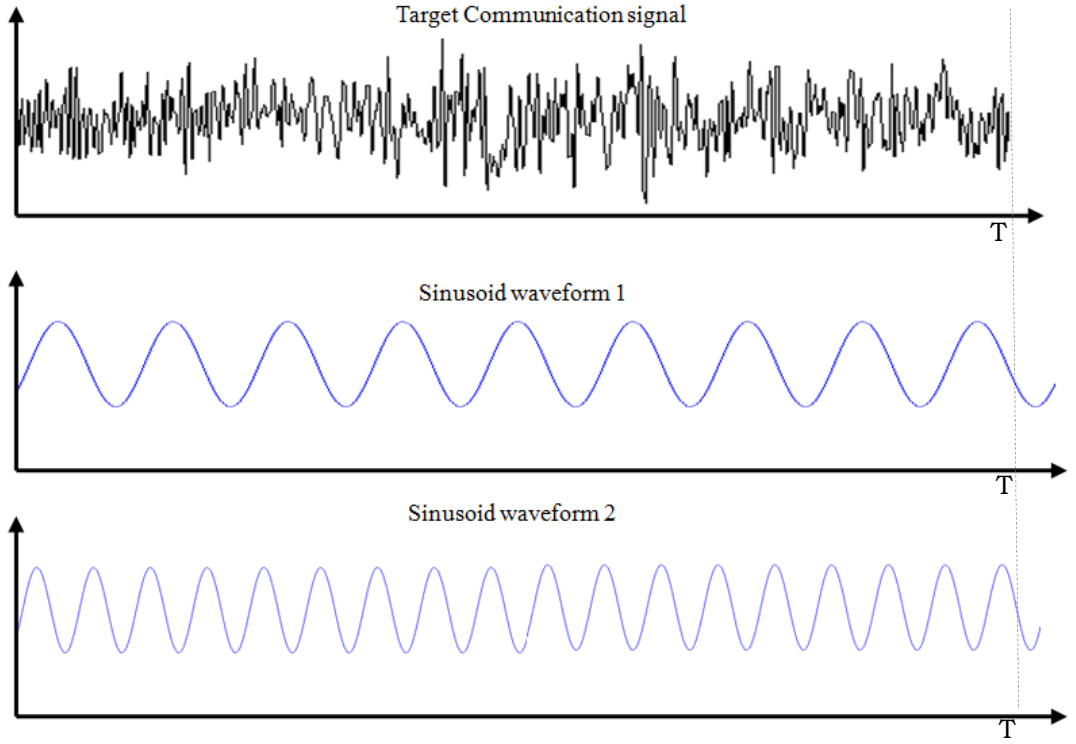

Figure 3.2 Finding the degree of embedding between communication signal and sinusoid waveforms

Actually, the mathematical expression of the spot correlation is equivalent to common DCT (Digital Cosine Transformation), which will be shown in the following paragraphs. As we normally use digitlized signals for signal processing, the spot correlation equation for two discrete-time signals, which consist of N samples with the sampling period of $N\Delta t$, can then be written as

$$y = \frac{1}{N}\sum_{n=0}^{N-1} x_1(n\Delta t) \bullet x_2(n\Delta t)$$

(Equation 3.4)

Where Δt is the sampling time interval between two samples and N Δt = T being the overall time duration of the sampled signal. We can drop the Δt from Equation 3.4 due to the assumed periodicity of our signals and rewrite it as

$$y = \frac{1}{N}\sum_{n=0}^{N-1} x_1(n) \bullet x_2(n)$$

(Equation 3.5)

The traditional DCT of a signal $x(n)$ and its inverse transformation IDCT $y(k)$ can be expressed as:

$$y(k) = w(k)\sum_{n=1}^{N} x(n)\cos\frac{\pi(2n-1)(k-1)}{2N}, k = 1,\ldots, N$$

(Equation 3.6)

$$x(n) = \sum_{k=1}^{N} w(k)y(k)\cos\frac{\pi(2n-1)(k-1)}{2N}, n = 1,\ldots, N$$

(Equation 3.7)

where $w(k)$ is the weight factor which depends on the sampling point k

$$w(k) = \begin{cases} \frac{1}{\sqrt{N}}, k = 1 \\ \sqrt{\frac{2}{N}}, 2 \le k \le N \end{cases}$$

(Equation 3.8)

Equation 3.6 can be rewritten as:

$$y(k) = \sum_{n=1}^{N} x(n) \bullet w(k)\cos\left(2\pi \cdot \frac{(k-1)}{2N} \cdot (n - \frac{1}{2})\right), k = 1,\ldots, N$$

(Equation 3.9)

Equation 3.9 clearly indicates that $y(k)$ are the results of spot correlation between original signal $x(n)$ and a series of sinusoids

$w(k)\cos\left(2\pi\cdot\frac{(k-1)}{2N}\cdot(n-\frac{1}{2})\right)$, where $\frac{(k-1)}{2N}$ are the frequencies of sinusoids. Hence $y(k)$ reflects how well the target signal $x(n)$ been represented by a given set of sinusoids evenly spaced over a given frequency range. On the other hand, equation 3.7 proves that the target signal $x(n)$ can be recovered from a series of sinusoids given the coefficient $y(k)$ is known.

If the original signal is quadrature signal, as is mostly the case for communication signals, we can use the equivalent DFT(Discrete Fourier Transformation) expressions which are

$$y(k)=\sum_{n=1}^{N}x(n)\omega_N^{(n-1)(k-1)}$$

(Equation 3.10)

Where $\omega_N=e^{(-2\pi\cdot j)/N}$

and $$x(n)=\frac{1}{N}\left(\sum_{k=1}^{N}y(k)\omega_N^{-(n-1)(k-1)}\right)$$

(Equation 3.11)

The equation 3.11 can be rewritten as

$$x(n)=\sum_{k=1}^{N}A_k e^{j(2\pi\cdot(k-1)(n-1)/N)}$$

(Equation 3.12)

Where $$A_k=\frac{y(k)}{N},k=1,2,...,N$$

Similar to DCT, the DFT can show how a quadrature communication signal $x(n)$ spot-correlates with a set of complex phasors

$e^{j(-2\pi \cdot j \cdot (k-1)(n-1)/N)}$ with known characteristics like amplitude, frequency and phase. From equation 3.12, we can also see that the sum of all phasors with its relevant weight factor A_k provide a replica of the target communication signal $x(n)$ and the number of phasors is the number of discrete sample points *N*.

In conclusion, equation 3.9 and equation 3.12 tell us that any arbitrary periodic discrete signal can be formed by adding up a limited number of sinusoids with frequencies harmonically related to a fundamental frequency with proper amplitude and phase. To obtain a perfect replica of target signal, the number of sinusoids should equal to the number of sampling points *N*.

However, as none of the communication signals, which we aim to approximate, are periodic, the number of sinusoids needed would be infinite. This infinity is obviously impractical and hence needs to be limited. This will be discussed in the following paragraphs.

3.1.2 Modified correlation method to design multi-sines with less number of tones

In order to represent a communication signal with limited number of tones, a time window is necessary to segment the original signal. Hence, as a first step we examine which duration for the original signal should be chosen for our investigations. As we conclude above, a large number of samples leads to large number of tones, which will ensure accurate frequency resolution and approximation. However, what we need is just an acceptable time duration over which similar

time-domain and statistical metric such as the CCDF curve, can be obtained. This also limits the number of tones that is required to approximate over the target signal.

Taking an example target signal like the WCDMA up-link signal with reference measured channel of 12.2Kbps and a spreading rate of 3.84MHz that is modulated onto a 1.8 GHz carrier. The sampling process was taken place at RF carrier with the usedsampling frequency 3.84MHz×4 = 15.36MHz. The samples are generated within ADS(Agilent® Advanced Design System) EDA environment using ADS standard library which can be found at ADS installed examples directory, as shown in figure 3.2. More information about how to generate WCDMA signals using ADS can be found in reference[3].

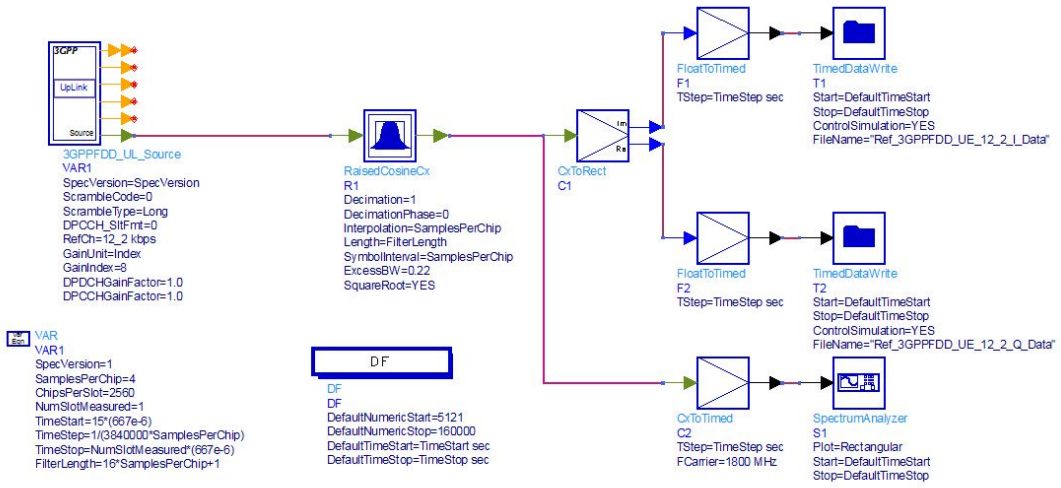

Figure 3.3 The ADS Bench of generating WCDMA signal

The CCDF curves of this signal are plotted for different time durations, as shown in figure 3.4. We can see a strong difference depending on the chosen duration.

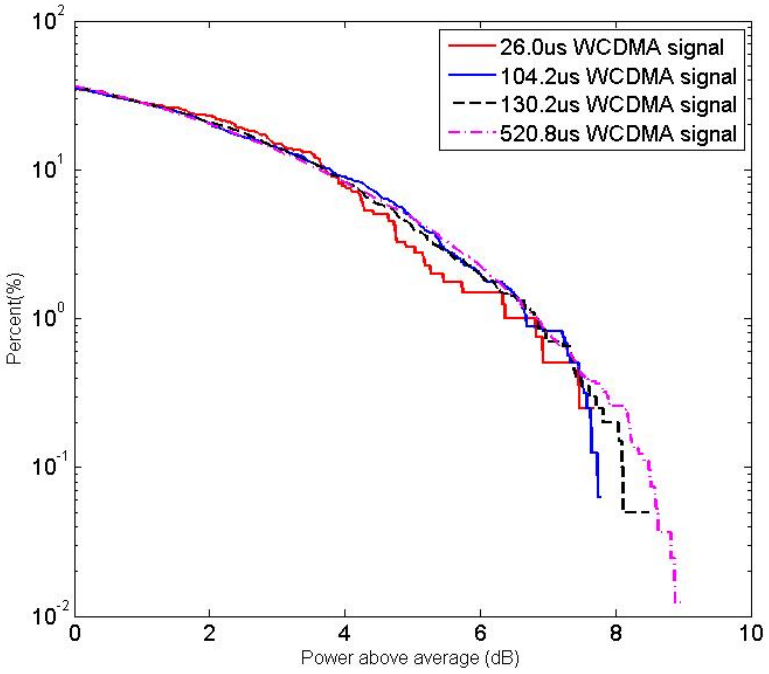

Figure 3.4 Comparison of time-domain CCDF of WCDMA signals with different time durations

To be more specific, the CCDF generated from the shortest duration(26.0*us*) strongly differs from the characteristics of the signals with longer duration. However as the time length increases from 104.2*us* to 520.8*us*, the CCDF characteristics start converging. This leads to the conclusion that a relatively short time duration can accurately represent the statistical properties of a WCDMA signal and provide accurate simulation results for the approximation process using multi-sines signal.

Starting with the 104.2*us* duration WCDMA signal, which contains 1,600 sample points and a 1600-tone multi-sines is required according to equation 3.12 with the frequencies situated evenly in steps of 9.6KHz from -7.68MHz to 7.68MHz around the 1.8GHz center frequency. The resulting number of tones is rather large and

imposes a time consuming task to find the optimum combination for the magnitudes and phases of each tone. Besides, the further analysis is nearly impractical due to the large number of mixing frequencies falling on the same position when passed through a nonlinear device, hence making their separation difficult or even impossible.

Fortunately, when we take a look at the tones being used, we will find that a majority of the multi-sine signal power is contained within the in-band frequency. For example, if we look at the target signal's frequency spectrum, as shown in figure 3.5, we find that the average power spectrum components, located outside of the main channel, are around -50dBc down, hence making them nearly negligible when compared to the in-band spectrum components. This leads us to believe that the total number of tones necessary to represent the signal could be greatly reduced if the out-of-band tones were neglected.

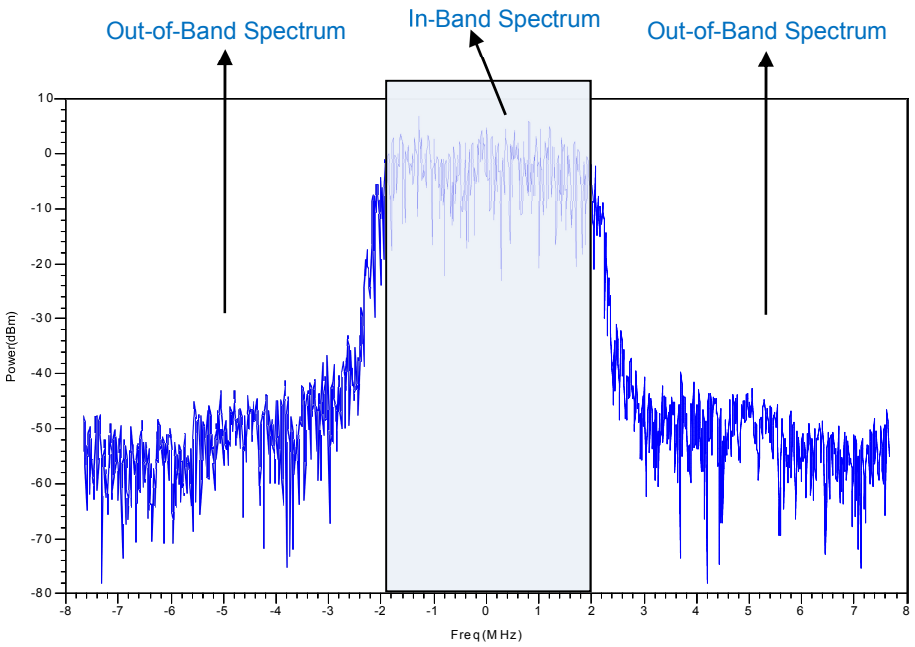

Figure 3.5 The power Spectrum of WCDMA signal. As can be seen, out-of-band spectrum is nearly negiliable if compared to in-band spectrum

To verify this supposition, a number of CAD simulations were carried out. Firstly, three multi-sines approximations were designed using the correlation method introduced in equation 3.12, which are a 400-tone multi-sines consisting of in-band frequency components only, a 500-tone multi-sines with 400 in-band tones and 100 out-of-band tones, plus a 1200-tone multi-sines consisting of 400 in-band tones and 800 out-of-band tones. The spectra of the three different multi-sines are illustrated in figure 3.6. It needs to be pointed out that a noise floor of around -120dBm has been artificially set with the multi-sines, which is different from the actual WCDMA signal's noise floor of around -50dBm. However this difference can be neglected in the simulation as -50dBm is just $0.00001 mW$.

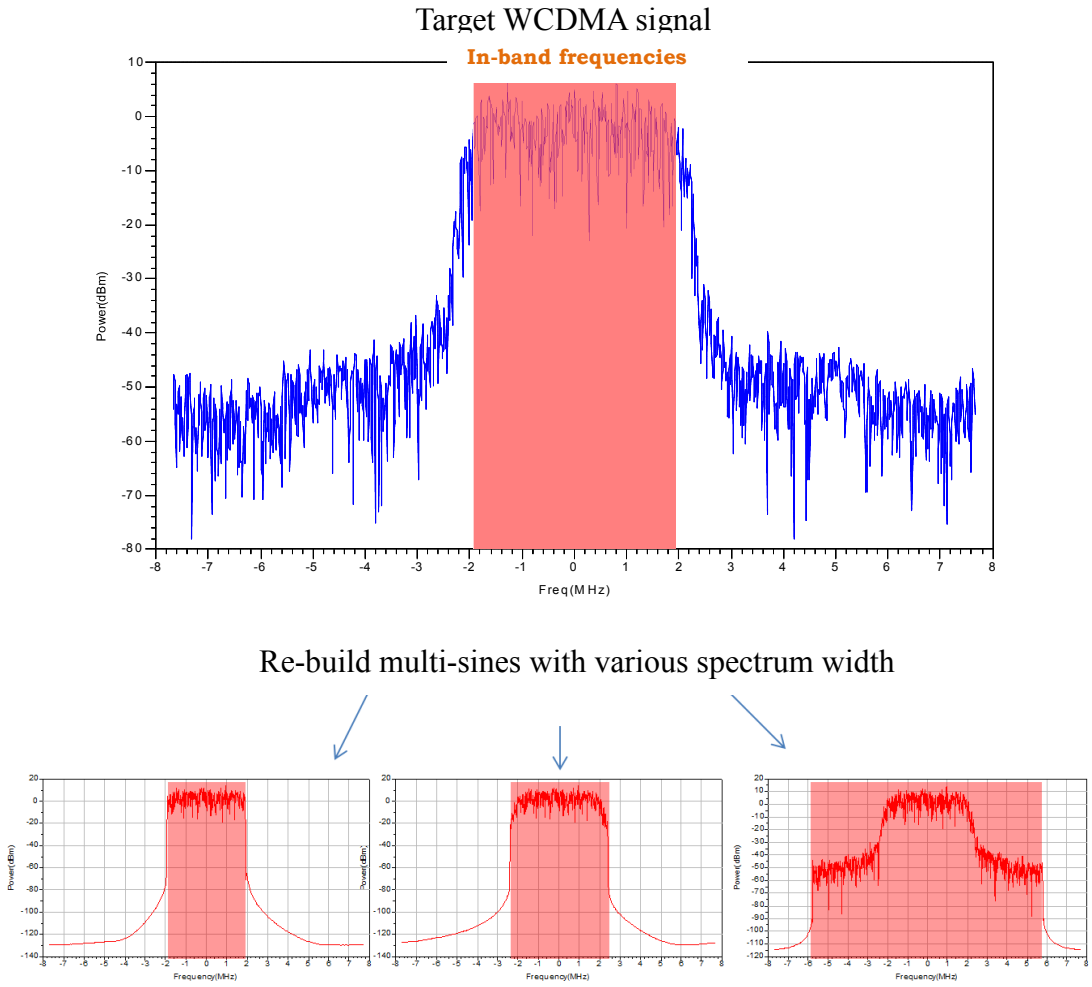

Figure 3.6 Rebuild multi-sines with various spectrum width. Left:using in-band 400 tones only; middle: using in-band 400 tones and out-of-band 100 tones; right: using in-band 400 tones and out-of-band 800 tones.

The multi-sines were caluated using the Matlab® computing environment and exported to the ADS environment together with the target WCDMA signal to drive an amplifier working at 2.14GHz. The simulated power amplifier is based on a FreeScale MET(Motorola Electro Thermal) LDMOS model with 1dB compression point, which is considered as the start of strongly nonlinear effects in power amplifiers, at about 31dBm output power, as shown in figure 3.7. The generated multi-sines signals are thereby scaled to 14~37dBm output power range, which fully covers the weak and strong non-

linear regions of the device. The idea of this experiment was to measure ACPR for the generated excitations and compare them over a range of output power levels. The ADS simulation schematic is shown at figure 3.8.

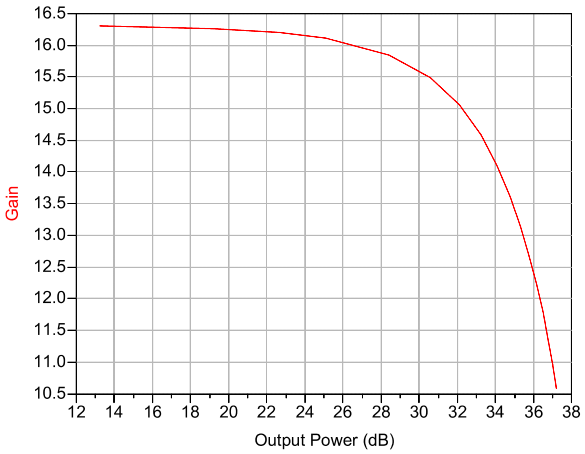

Figure 3.7 PA Compression Charactristics used in this investigation

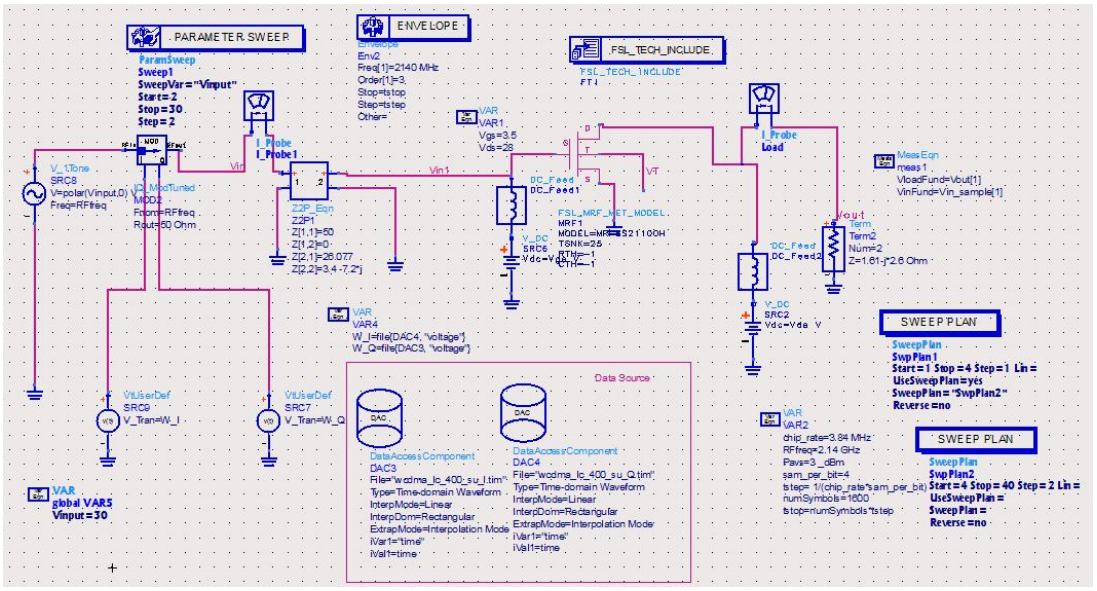

Figure 3.8 The ADS simulation schematic

In this simulation schematic, the in-phase part and quadrature part of the test signal are decided seperately by the “DataAccess” Component. Envelope simulation is used to sample the signal at

2.14GHz frequency. This has the advantage that the sampling frequency required is only need to be be large enough to capture the bandwidth of the modulation envelope instead of the RF carrier[4]. The input power is swept using the component “Parameter Sweep”.

ACPR (or ACLR—Adjacent Channel Level Ratio as it is referred to in UMTS WCDMA specification [2]) measures the amount of power within an adjacent channel caused by frequency mixing between the spectral lines of the input signal when passing through a non-linear device. It has been widely used and is one of the most popular figures of merits to characterize the nonlinear distortion of a given system. Therefore we will use ACPR initalily to observe if the multi-siness have excited the same degree of non-linear response within the device as the original WCDMA signal.

The simulated ACPR values are compared over a range of output power values to account for the DUT’s both weak and strong nonlinear behaviour. It is important to note that in this work, the bandwidth of the adjacent channel when calculating ACPR is the same as the main channel. The resulting comparison is depicted in Fig.3.9.

As can be seen, some obvious differences exist predominantly at the lower drive levels, especially for multi-sines consisting of 400 and 500 tones. These are caused by the artifically introduced low power levels (-120dBm) of the out-of-band spectrum components when compared with the relatively high power levels (-50dBm) contained within the origial WCDMA signal. Actually, the 90dB ACPR at lower

drive level suggest at figure 3.9b and 3.9c exceeds most of the required ACPR specifications defined in the various communication system standards[2] and can hence be assumed as negilible.

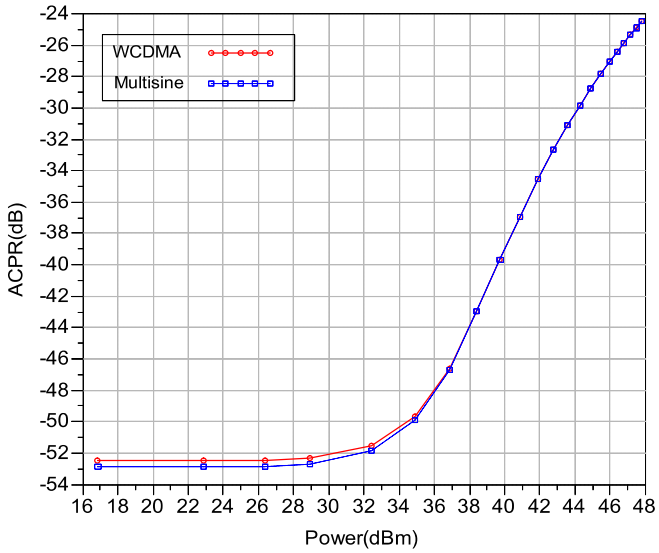

Figure 3.9a ACPR prediction performance of multi-sines with 1200 tones

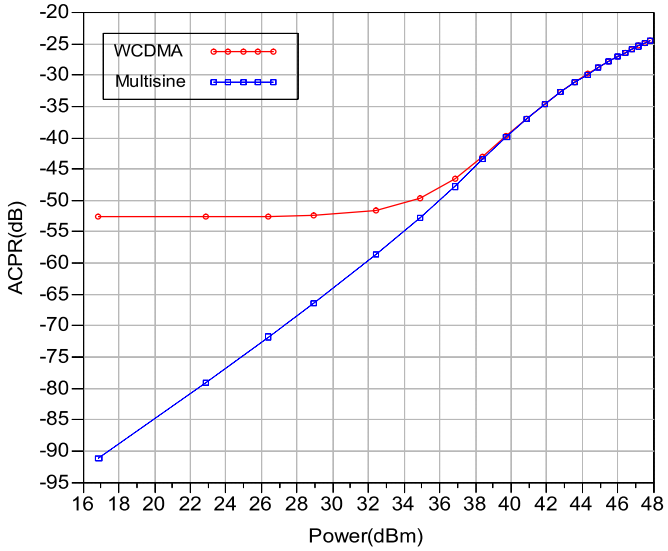

Figure 3.9b ACPR prediction performance of multi-sines with 500 tones

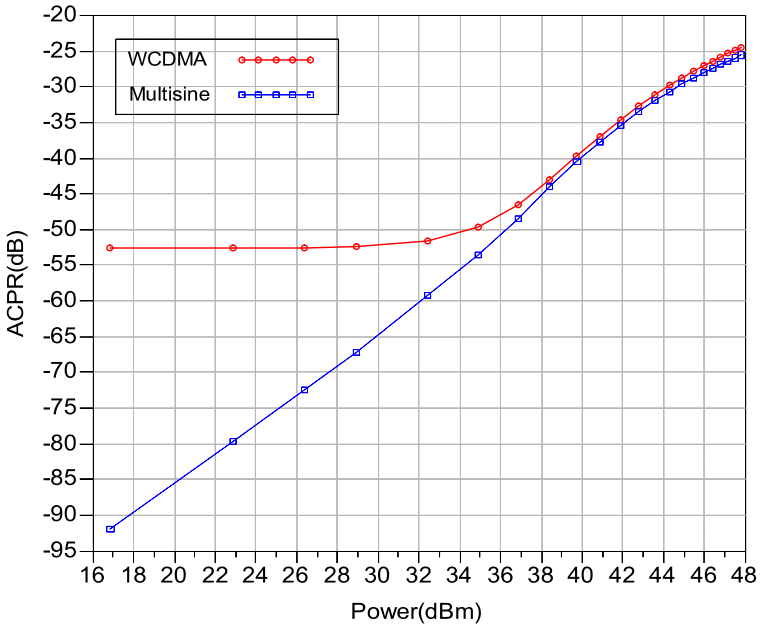

Figure 3.9c ACPR prediction performance of multi-sines with 400 tones

Apart from the obvious difference at low power drive levels, the ACPR difference at the high power drive levels in figure 3.9a and figure 3.9b, where the main nonlinearity starts, is close to 0dB while in figure 3.9c it is almost 1dB. This is further illustrated in figure 3.10c. This confirms our supposition that the out-of-band spectrum components can be dismissed at least intially during the process of building a multi-sines excitation.

The relevance of side-band spectral components is further detailed in figure 3.10a to 3.10c, showing the ACPR prediction error between multi-sines signals and target WCDMA signal. At higher output power levels the 1200-tone multi-sines exhibits no obvious difference when compared with the 500-tone signal. This is shown in figure 3.10a and figure 3.10b respectively. However, the 500-tone multi-sines predicts the ACPR more accurately than the 400-tone versions

with the only difference between these two multi-sines being the additional 100 tones within the out-of-band frequency range.

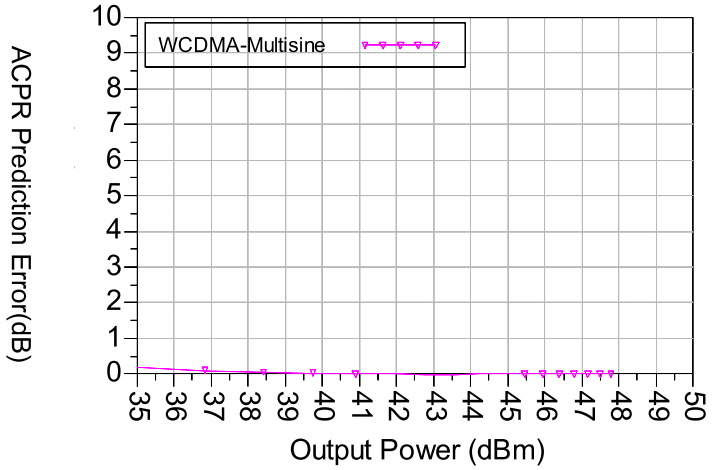

Figure 3.10a The ACPR prediction error(Δ = $ACPR_{WCDMA}$—$ACPR_{multi\text{-}sines}$) of multi-sines with 1200 tones

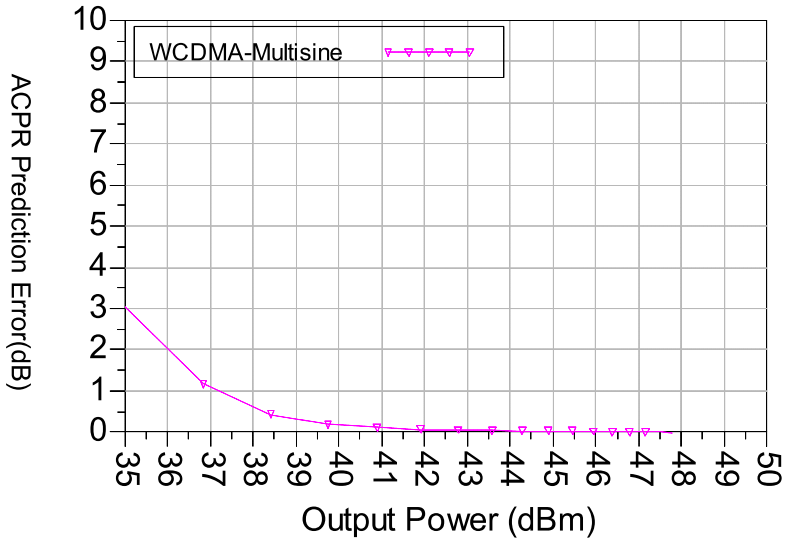

Figure 3.10b The ACPR prediction error (Δ = $ACPR_{WCDMA}$—$ACPR_{multi\text{-}sines}$) of multi-sines with 500 tones

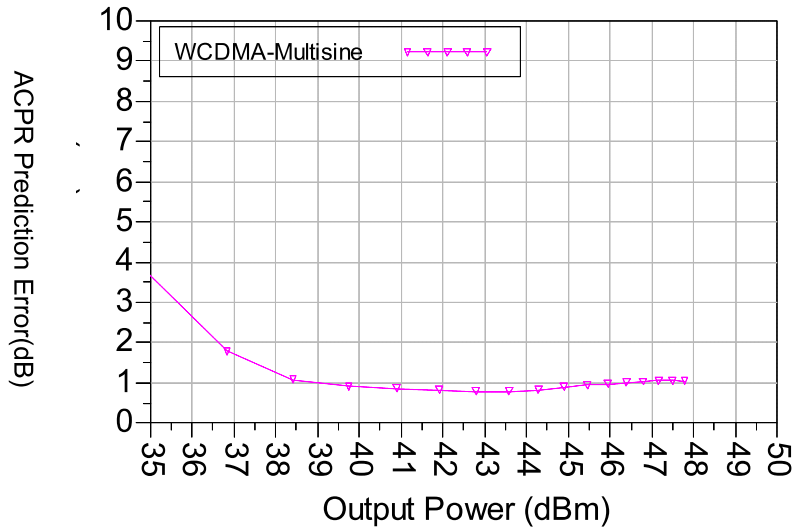

Figure 3.10c The ACPR prediction error(Δ = $ACPR_{WCDMA}$—$ACPR_{multi\text{-}sines}$) of multi-sines with 400 tones

3.1.3 Optimized correlation method with Least-Error Method or Even-tone Method

The results acquired from the above investigations are encouraging and indicated a possible method of using mainly in-band frequency components supplentmented with out-of-band frequency components to reduce the number of tones, which are needed to approximate a communication signal. However, the resulted 500 tones of multi-sines from the above example is still a large number. Furthermore, if the target signals have wider modulation bandwidth than WCDMA signal, an even higher number of tones will be required.

To further reduce the number of tones two optimization methods are proposed here. One method is to minimize the power spectrum errors ε between the multi-sine signals and the original signal. The error ε

can be represented as:

$$\varepsilon = \frac{\sum_{m=1}^{n} S_{xx}(\omega_m) - \sum_{w=1}^{k} S_{xx}(\omega_w)}{\sum_{w=1}^{k} S_{xx}(\omega_w)}$$

(Equation 3.13)

with $S_{xx}(\omega)$ as the PSD(Power Spectral Density) function of a signal, $\sum_{w=1}^{k} S_{xx}(\omega_w)$ being the power of the original WCDMA signal and $\sum_{m=1}^{n} S_{xx}(\omega_m)$ is the power of multi-sine signal which is built by selecting n frequency components from the original k frequency components. Within this work, the PSD of the signals was calculated using Matlab environment from samples obtained in chapter 3.1.2. We refer to this approach as the Least Error method as this method will find the multi-sines which has the least error ε within a target signal.

As Least Error method reduces amount of tones with small amplitudes and might therefore result in a spectrum of multi-sine signals that concentrate at specific frequency locations. Another way is to divide the tones into evenly distributed groups and select tones from every group to avoid this gathering problem. Taking this approach, one tone in every 10 tones been selected using the least error method (as in equation 3.13) from the 500-tone multi-sines to obtain a desired 50-tone signal. We refer to this method as the Even-Space Method.

To verify the suggested approach, 50-tone multi-sines were designed utilising both methods in MATLAB and then exported into Agilent

ADS (Advanced Design System) environment to carry out simulations in which the same PA model was utilised. The results are shown in figure 3.11 and figure 3.12.

As it can be seen from figure 3.11, when passing through a power amplifier, the multi-sines designed with the Least Error method introduces up to 5dB ACPR difference. This poor performance can be explained by the grouping of the spectral components, which can be seen from figure 3.11a as there are an obvious notches in the power spectrum. On the contrary, from figure 3.12, we find that multi-sines designed with the Even-Space Method achieved much better performance as it accurately predicts the ACPR performance of WCDMA signal with less than 1dB difference within the nonlinear drive area of the power amplifier. Therefore, it can be concluded that Even-space Method is better than Least-Error Method for reducing the number of tones.

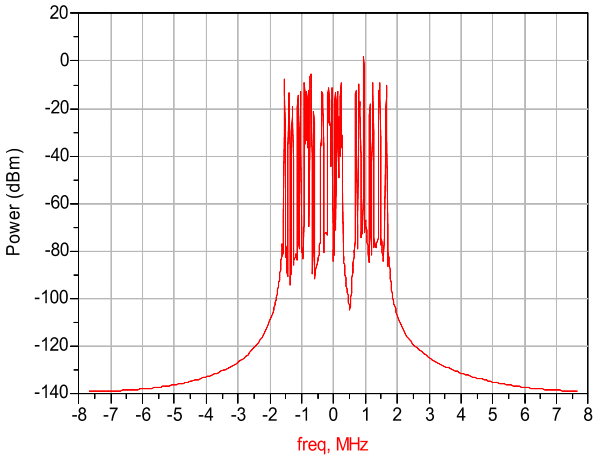

Figure 3.11a. Power Spectrum of 50-tone multi-sines designed with Least Error Method, as can be seen, tones are not evenly distributed

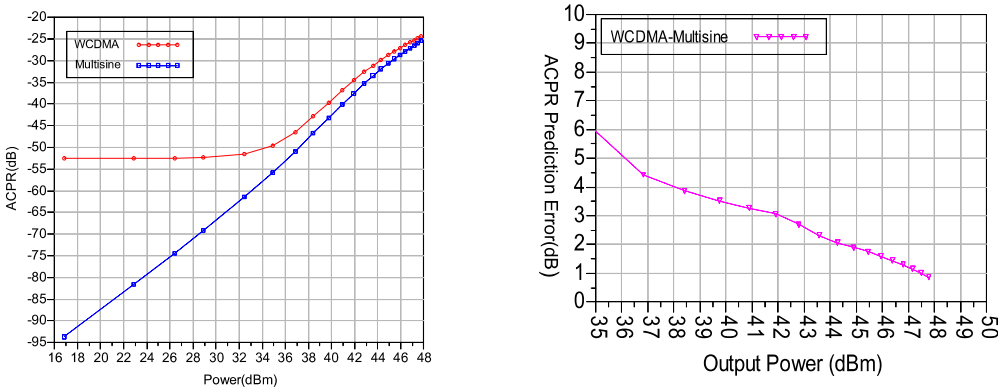

Figure 3.11b ACPR simulation results compared with WCDMA signal --- Using Least Error Method

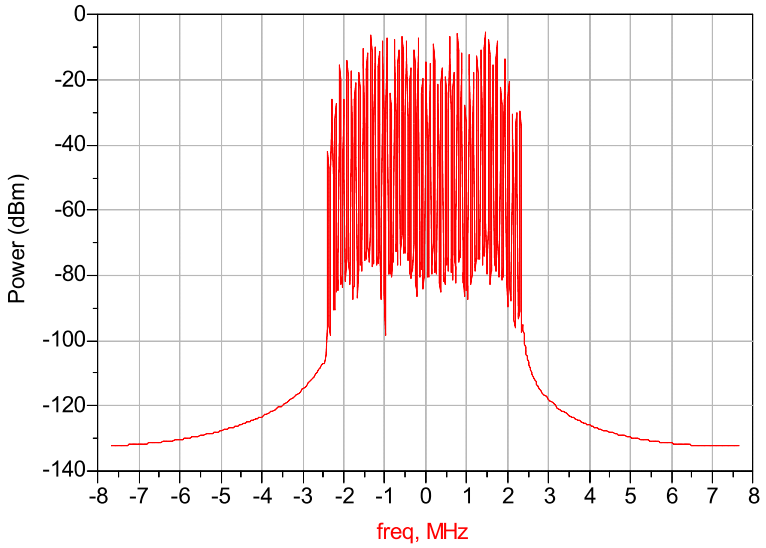

Figure 3.12a. Power Spectrum of 50-tone multi-sines designed with Even Space Method

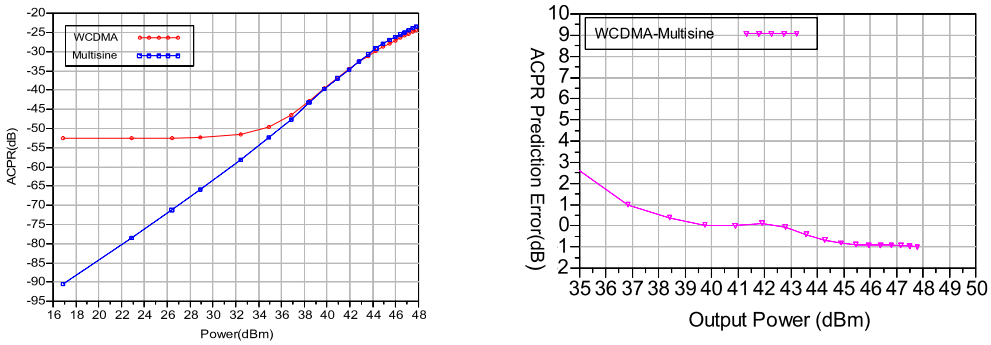

Figure 3.12b ACPR prediction compared with WCDMA signal with Even Space Method

However at this stage, it is too early to conclude that optimizing the correlation method using the even-space method will provide an accurate multi-sines approximation with limited tones, as a single example does not demonstrate the generality of this approach. There are many types of communication signals between which strong variations exist.

To obtain further information as to the generality of the even-tone method, another type of communication signal was set as the target signal to be approximated which is a Test-Downlink WCDMA signal generated by ADS built-in component "WCDMADownlink_Src". The schematic of generating this signal is shown in figure 3.13 and further information of this test signal can be found within Agilent ADS help document. This signal has a low PAPR of 3.7 dB compared to 8.6dB PAPR of the previous WCMDA signal.

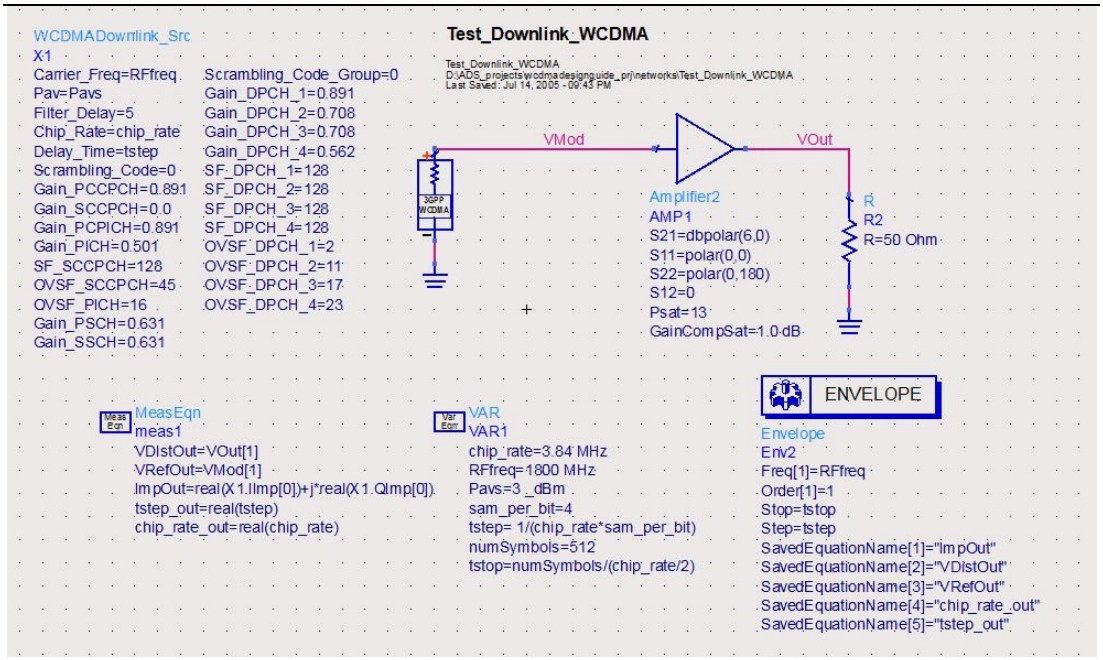

Figure 3.13 The schematic design of generating Low PAPR WCDMA signal

This new WCDMA signal is sampled using the circuit envelope simulation technique, which has been introduced before at section 3.1.2. In line with previous experiments, the same sampling time step is used and the sample duration is kept, consequently the target signal has the same number of sampling points. A 500-tone multi-sines signal, which include 400 in-band frequency component and 100 out-of-band frequency components, is designed using the correlation method introduced in chapter 3.1.1 and then exported into ADS simulation schematic with the results being shown in figure 3.14.

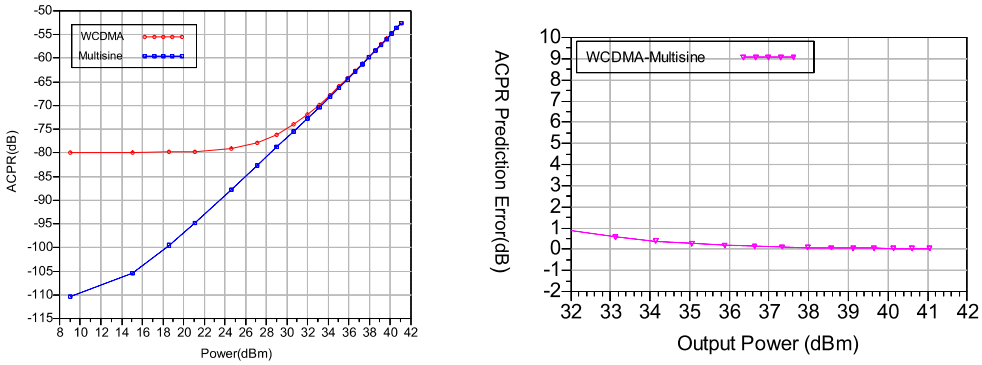

Figure 3.14 ACPR prediction of 500-tone multi-sines and WCDMA signal with Low PAPR

As can be seen, the 500-tone multi-sines precisely predicts the ACPR performance of the low PAPR WCDMA signal(the obvious ACPR difference at lower drive power levels are caused by the lacking of out-of-band noise floor of the designed signal). This again confirms the supposition that a multi-sines, including a combination of in-band and out-of-band spectrum components, can accurately represent original communication signals.

In the next step, both least error method and even-tone methods are employed to further reduce to the number of tones to 50. The results are shown in figure 3.15 and figure 3.16 respectively.

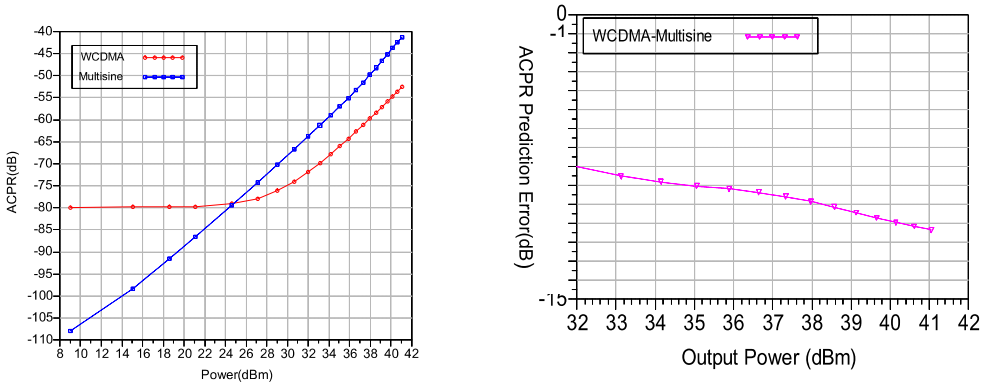

Figure 3.15 ACPR prediction error of 50-tone multi-sines with least error method

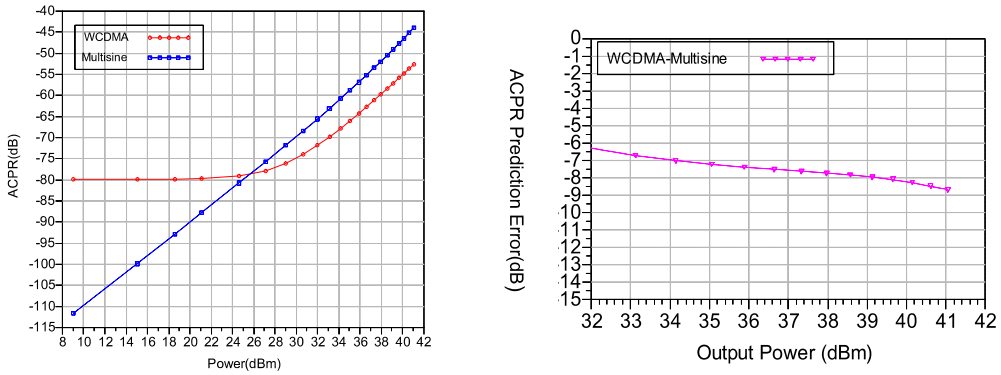

Figure 3.16 ACPR prediction of 50-tone multi-sines with even space method

As in the previous experiment, the multi-sines that was designed with the Least-error method does not predict the ACPR of WCMDA signals accurately. However, in this case also, the multi-sines signal that was designed with the even-space method cannot accurately predicted the ACPR behaviour though the prediction is more accurate than the multi-sines designed with least error method.

These intial results have clearly demonstrated that the even-space method has its limitations though we can't understand the reason. This also leads to the question of whether correlation based method

can solely create multi-sines which are capable of accurately approximating the nonlinear behaviour of a DUT under modulated stimulus.

3.2 Limitations of the correlation method

3.2.1 Another angle: High-Dimension to Low-Dimension

To proceed further, it is necessary to understand why correlation based method cannot be solely used to approximate the communication signals. As discussed before, the designing of multi-sines can be regarded as a signal approximation process utilizing limited number of tones. This process is similar to the definition of IDFT in equation 3.12.

$$x(n) = \sum_{k=1}^{N} A_k e^{j(2\pi\cdot(k-1)(n-1)/N)}$$

Where $$A_k = \frac{y(k)}{N}, k = 1,2,...,N$$

According to this equation, $x(n)$,the target signal, can be accurately represented by N number of points. The coefficient $y(k)$ can be calculated by the DFT as equation 3.10 shows.

Since $e^{j2\pi w_i t}$, with i = 1….N, form an orthogonal set, we can imagine $x(n)$ as a vector in the N-dimensional inner product space R^n consisting of

$$\begin{pmatrix} e^{j(2\pi\cdot\cdot(1-1)\cdot(n-1)/N)} \\ e^{j(2\pi\cdot\cdot(2-1)\cdot(n-1)/N)} \\ \cdots \\ \cdots \\ e^{j(2\pi\cdot\cdot(N-1)\cdot(n-1)/N)} \end{pmatrix}$$

(Equation 3.14)

and A_k for each dimension k. Figure 3.17 shows the new co-ordinate system.

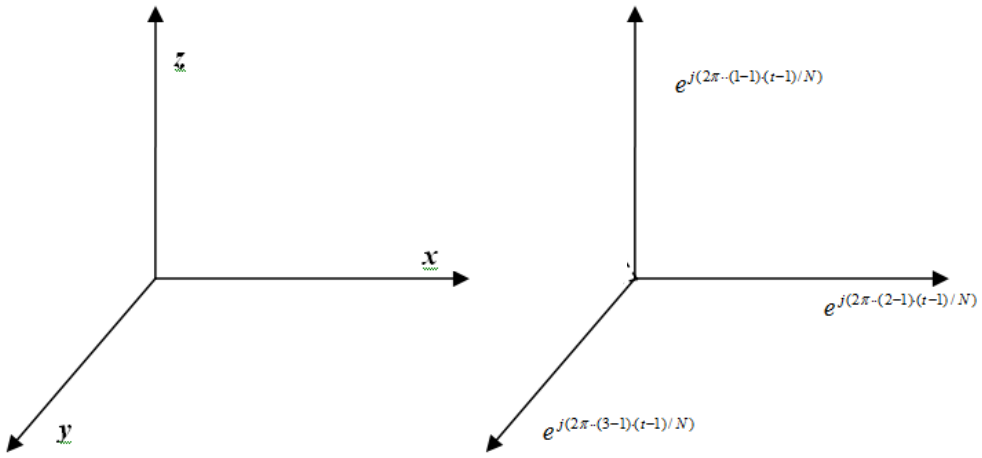

Figure 3.17 The inner product space R^n is essentially an expanded space like the real 3-dimension world but not limited to 3 dimensions.

Hence, the multi-sines design problem can be described as approximating an *N*-dimension vector within an *M*-dimension space where $M < N$. The approximation process should ensure that the new signal stimulate an equivalent response from a nonlinear system as the original. To illustrate this procecss more clearly let us consider a memoryless nonlinear system and represent the output geometrically.

This is shown in Fig 3.18 where a_{in} is a 3-dimension vector and b_{in} is a 2-dimension vector. a' and b' are the two third-order nonlinear components of the output that waere generated by these two vectors. The total output are the vector sum of the linear output components, a and b, and third-order components a' and b'.

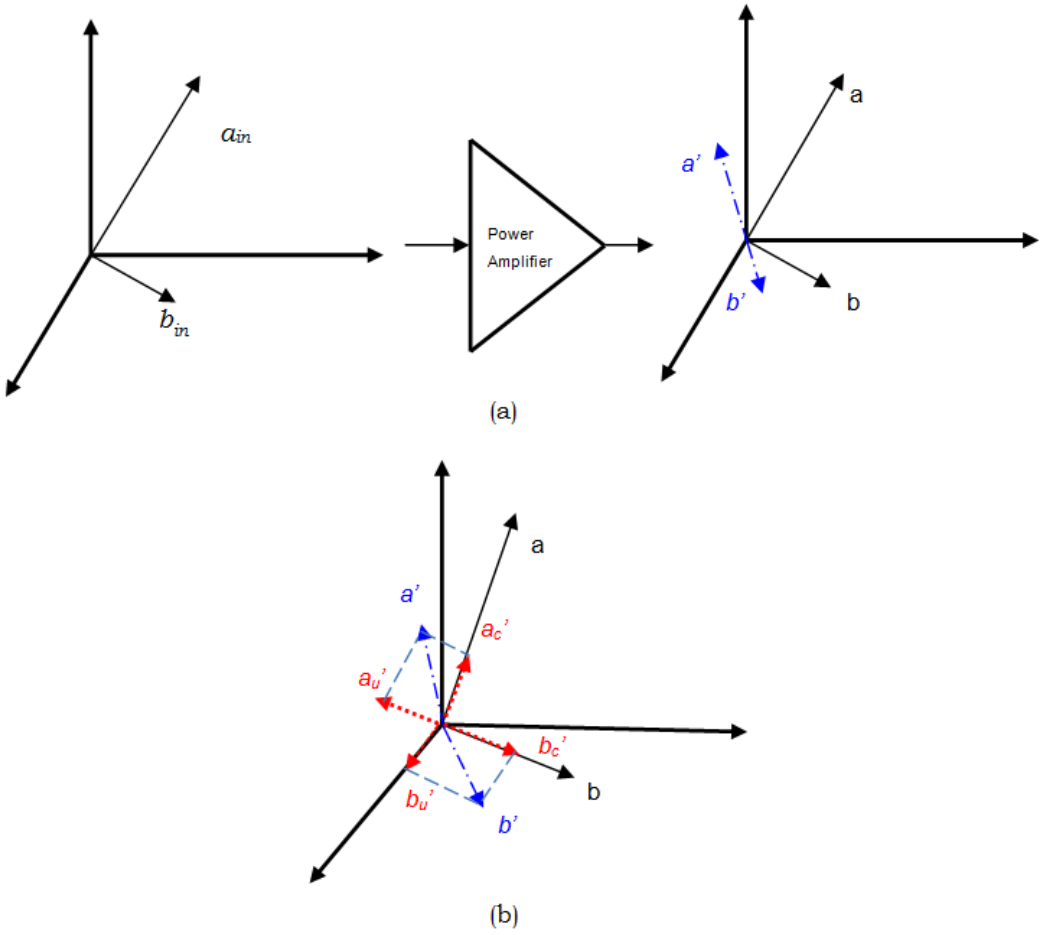

Figure 3.18 Geometrical representation of the nonlinear output

The third-order output can be further partitioned into two components: one in the direction of the linear output and referred as correlated components $a_c'$and b_c'; and the other orthogonal vectors a_u' and b_u' which are refered as uncorrelated components. The uncorrelated distortion output can be identified in terms of a cancelling process where a scaled replica of the input signal is

subtracted from the total nonlinear output. The orthogonal component cannot be cancelled by a scaled replica of the input signal and therefore represents the effective uncorrelated distortion that contributes to the degradation of system SINAD (Signal-to-Noise and Distortion) performance, while the correlated component of the third-order output represents the correlated distortion that causes gain compression of the linear output[6].

The multi-sines design problem is actually much more complicated in real case due to the higher number of dimensions in comparsion with the 3-dimension case show in figure 3.18. To illustrate this point, we use the following analogy: It is obviously impossible to build a house from a plain papersheet without folding it, no matter how large the papersheet is. However, if the target is to replicate the appearance of that house, we can then draw the house on a paper and make it to appear three-dimensional through reasonable adjustment of the proportions between the different lines. In such a case, though the house is not physically existent in three-dimensional space, it reflects the light to our eyes in the same way as a real 3-D object and hence “fool” our mind to thinking it is a real house. Figure 3.19 provides an example of how a 2-D painting has successfully “cheated” our brains.

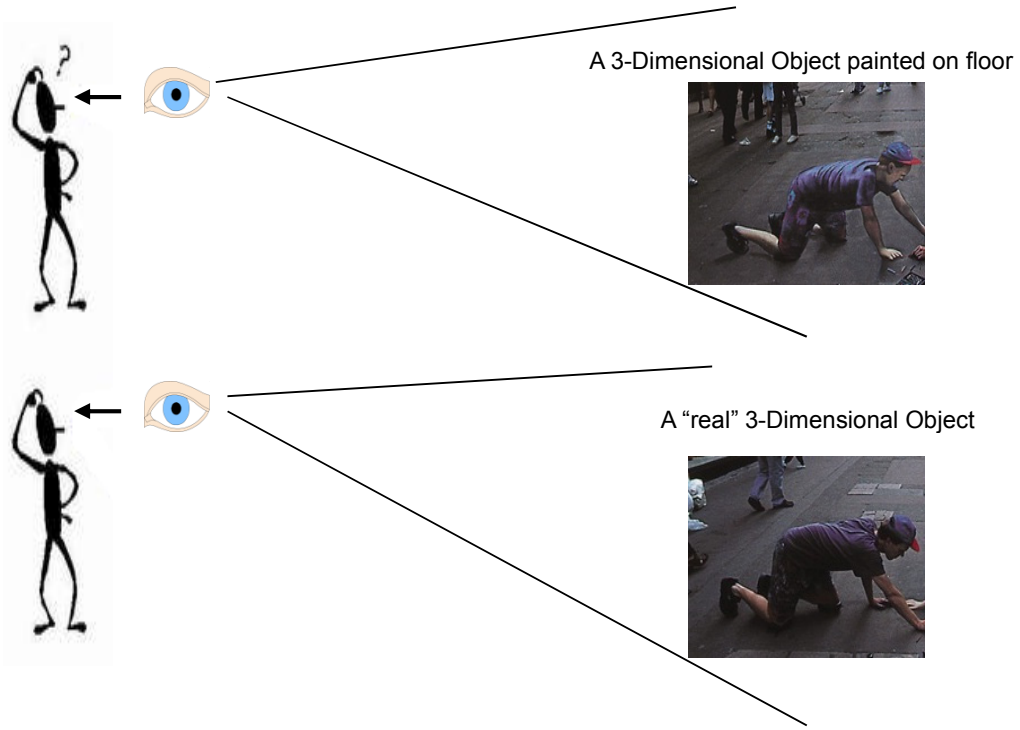

Figure 3.19 Represent a three-dimension object with two-dimension painting. Adjusting the structure of the drawing will "fool" our mind to take both objects as real, three-dimensional ones

Similarly the objective here is to design a multi-sines signal that will "fool" a nonlinear device in behaving the same way as it would encounter a real communication signal. Firstly, we will examine how well is the correlation method suited for this purpose. Simliar to the pre-defined equation 3.10 and 3.11, we can express a new multi-sines *Z(n)* with *M* dimensions that approximates the original signal $X(n)$ with *N*-dimensions as

$$Z(n) = \sum_{k=1}^{M} W(k) e^{-j\cdot(2\pi\cdot(k-1)\cdot(n-1)/N)}$$

(Equation 3.15)

$$W(k) = 1/M \cdot \sum_{k=1}^{M} Z(n) e^{j(2\pi \cdot (n-1) \cdot (k-1)/N)}, n = 1,2,...,N; k \in n$$

(Equation 3.16)

The projection process in high-dimensional space is also defined as

$$Proj_u v = \frac{\langle u, v \rangle}{\langle u, u \rangle} u$$

(Equation 3.17)

This operator projects the vector v orthogonally onto the vector u.

$\langle u, v \rangle$ denotes the inner product of the vectors u and v.

Suppose $v = \begin{pmatrix} \frac{1}{N} e^{j(2\pi \cdot (1-1) \cdot (n-1)/N)} \\ \frac{1}{N} e^{j(2\pi \cdot (2-1) \cdot (n-1)/N)} \\ \cdots \\ \cdots \\ \frac{1}{N} e^{j(2\pi \cdot (N-1) \cdot (n-1)/N)} \end{pmatrix}$ is the original signal $X(n)$ whih can be regarded as a N-dimension vector, while $u = \begin{pmatrix} e^{j(2\pi \cdot (1-1) \cdot (n-1)/N)} \\ e^{j(2\pi \cdot (2-1) \cdot (n-1)/N)} \\ \cdots \\ \cdots \\ e^{j(2\pi \cdot (M-1) \cdot (n-1)/N)} \end{pmatrix}$ defines the M-dimension inner space. According to equation 3.17, the orthogonal projection of vector v onto the vector u is $W(k)$, which is already defined in equation 3.16. Therefore, the multi-sines $Z(n)$ designed using the correlation method equals to the projection of the original signal $X(n)$ into the M-dimensional inner product space R^M.

$$R^M = \begin{pmatrix} e^{j(2\pi\cdot\cdot(1-1)\cdot(n-1)/N)} \\ e^{j(2\pi\cdot\cdot(2-1)\cdot(n-1)/N)} \\ \cdots \\ \cdots \\ e^{j(2\pi\cdot\cdot(M-1)\cdot(n-1)/N)} \end{pmatrix} = u$$

$Z(n) - X(n)$, which is the distance between $Z(n)$ and $X(n)$ in the inner product space R^N will achieve minimum value if $Z(n)$ is the projection of $X(n)$. Furthermore, it can be concluded from equation 3.15 to 3.17 that another *M*-dimmension vector $Z(n)'$, being the third-order component of $Z(n)$, is also the projection of third-order output of $X(n)$. This partly explains why the correlation method works for our first test signal, as section3.1.2 showed.

However, the relationship between the original signal and its third-order nonlinear part has changed after projection. Considering the same process described in figure 3.18 as an example: *b'* is closest to *b*, but it doesn't conclude that *b'/b* is closest to *a'/a*. Furthermore, the ratio of correlated distortion to original signal, and the ratio of un-correlated distortion to original signal also changed as $a'_c/\ a$ and $a'_u\ /a$ could be very different to $b'_c/\ b$ and $b'_u\ /b$ seperately. It's just like for a 3-D object, if the structure of its different parts have been modified, we would easily recognize that it is a simulated painting or image.

This analysis tells us that all the tone-reduction methods based on correlation, which is purely calculated in frequency domain space,

are fundamentally un-reliable as a solution to design multi-sines. Hence any new methods must be capable of modifying the time domain properties like amplitudes and phases of multi-sines that are acquired from the correlation rather than just selecting some of the frequency components as in the even space method.

3.2.2 The importance of time-domain statistical properties

Based on the above discussion, it is important to find a figure of merit that guides the approximation process. From an electrical point of view, RF devices will only respond to the instantaneous amplitude of the excitation signal and possibly a small period of past amplitudes due to memory effects composed of low frequency electrical and thermal response. In other words, it will not recognize or understand the "high-dimension characteristic" of the incident vector we have discussed in the previous chapter, not even to say the high order statistical descriptions. On the other hand, the frequency-domain parameters actually reflect the statistics of the time-domain waveform information over a certain period. It tells us how frequently a waveform is varying and how severe the variation is.

In the process of reducing the number of tones, lots of information is lost so we don't know how often a waveform achieves a certain amplitude. Reducing multi-sines from 500 tones to 50 tones results in a 90% information loss and will therefore have a significant impact on the approximation of the original signal. However, not all of the lost information has the same importance for stimulating the device's nonlinear response. Hence, we have to employ other time-domain statistical descriptions to qualify the importance of the information

loss. Complementary Cumulative Distribution Function (CCDF), being a key criterion for most communication systems, is such a figure of merit that can be employed for guidance.

To illustrate this point, let us first look at figure 3.20, which depicts the CCDF curves of multiple multi-sines that we designed to represent a test WCDMA signal whilst these multi-sines prediction over ACPR performance have been already demonstrated in figure 3.11 and figure 3.12. All of these designed multi-sines signals have nearly the same CCDF curve as the original WCDMA signal with some obvious difference only present in the large amplitude areas. This is in good agreement to the previous results in figure 3.11 and figure 3.12 where these signals have also shown relatively similar ACPR performances.

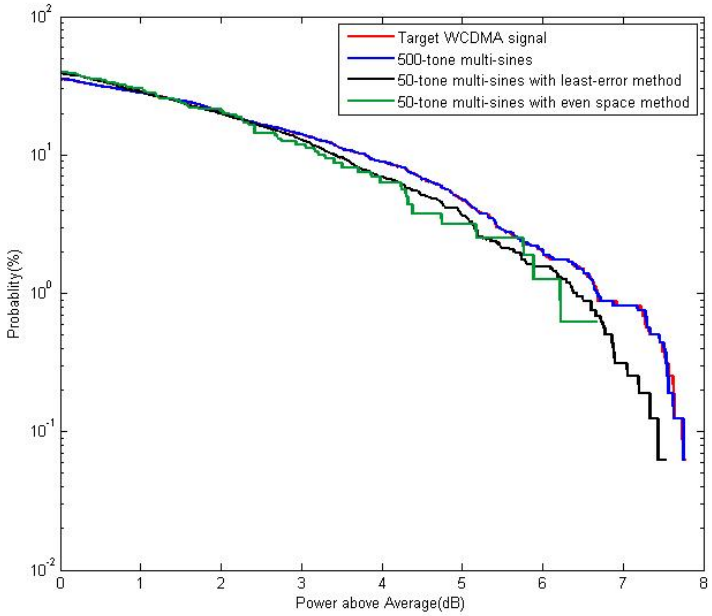

Figure 3.20 The time domain statistical property of the multi-sines in simulating WCDMA signal

Accordingly, we compared the CCDFs of the multi-sines and its

target WCDMA signal with a low PAPR. These multi-sines signal's prediction in terms of ACPR has already been shown before in figure 3.16. As illustrated in figure 3.21, the 500-tone multi-sines, which are generated through deletion of the out-of-band spectrum components, is approximating the target WCDMA signal in CCDF very well. But all the multi-sines with a reduced number of tones exhibit very different statistical properties. This is also in good agreement with the previous discussions in chapter 3.1.3 where these signals have shown very different ACPR performances.

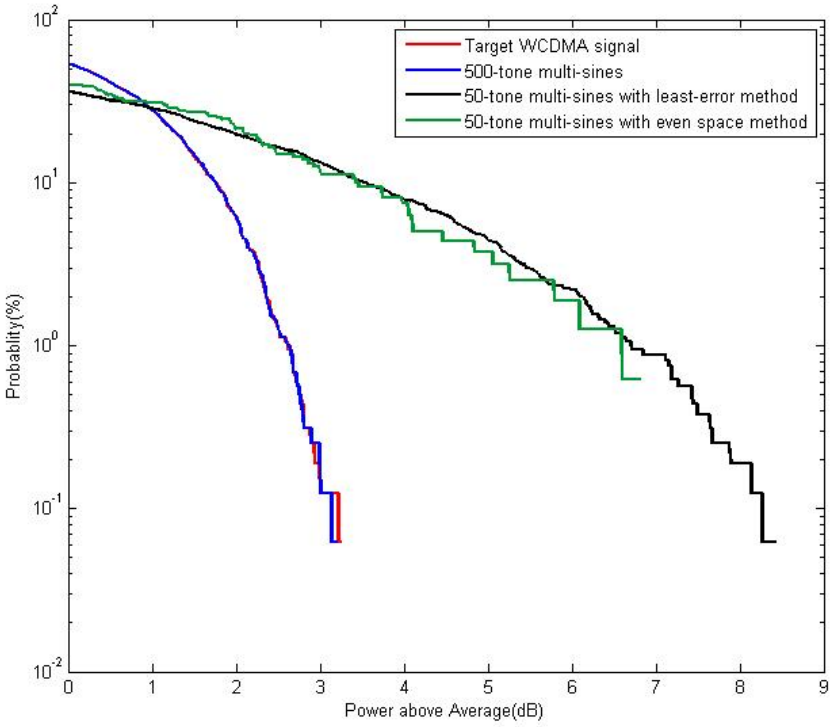

Figure 3.21 The time domain statistical property of the multi-sines in simulating WCDMA signal with low PAPR

This CCDF curve difference is very obivious which implies that a lot of the statistical information was lost in the process of approximating the original WCDMA signal through the limitation of tones. This confirms further our previously established supposition that CCDF

curves strongly influence the spectrum regrowth when passing through a nonlinear device. CCDF is more information rich and therfore more important than the Crest Factor (CF) in predicting the nonlinear distortion[1]as crest factor places too much emphasis on a signal's instantaneous peak values. CCDF gives us more complete statistical information about the high signal levels than the crest factor as it also shows how much time the signal spends at or above a given power level.

The above analysis suggest that with the guidance of CCDF the multi-sines could be modified such that it retains the statistical information of the original signal. However, the above discussion doesn't suggest the time domain statistical information can be employed as a sole indicator for the quality of the approximation process.

Figure 3.22 gives an extreme example of two signals with the same CCDF but very different time-domain waveform shapes. The difference between waveforms *a* and *b* can be easily seen in figure 3.22a, therefore it can be concluded that they will excite very different distortion when passing a nonlinear device. However their CCDF are similiar, as can be seen from figure 3.22b.

[1] CF is the ratio of the peak voltage to its root-mean-square value of a signal and is traditionally a common figure of merit of stimulus signals.

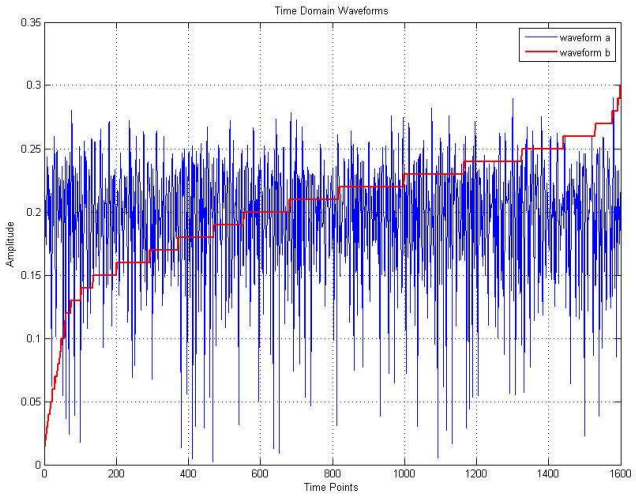

Figure 3.22a Waveform a and waveform b have very different time domain waveform shapes

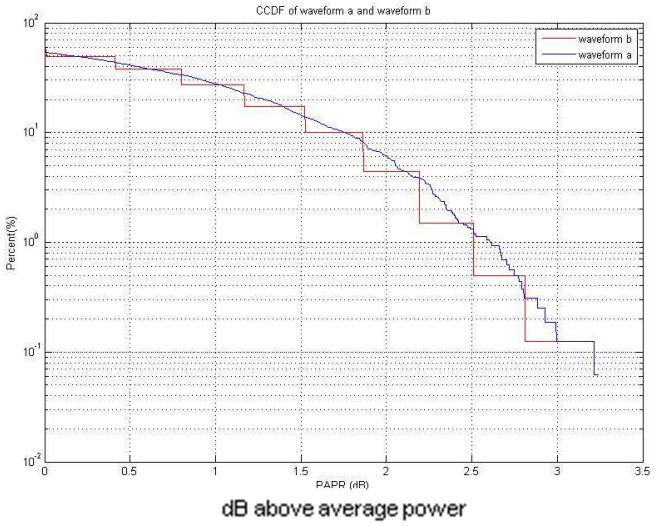

Figure 3.22b However, Waveform a and b have very similar CCDF curves.

3.3 New multi-sines design procedure

3.3.1 The cause of the CCDF difference

As discussed before, the multi-sines acquired from the correlation method followed by further processing may have a significantly different CCDF to the target communication signal. Hence, we need to modify the sinusoids' amplitudes and phases to narrow this

difference. Utilising the amplitudes and phases in the frequency domain the variation of these parameters will not have a straightforward influence on time-domain waveform shape nor its statistical behaviour such as its CCDF. Therefore it is difficult, if not impossible, to accurately adjust the time-domain CCDF by directly modifying those frequency-domain parameters.

As a starting point it might be useful to examine why the multi-sines and original modulated signal exhibit such big differences in CCDF. The WCDMA signal with a low PAPR, and its 50-tone multi-sines approximation from the second experiment in section 3.1.3 are now displayed in an complex In-phase and Quadrante domain as shown in figure 3.23.

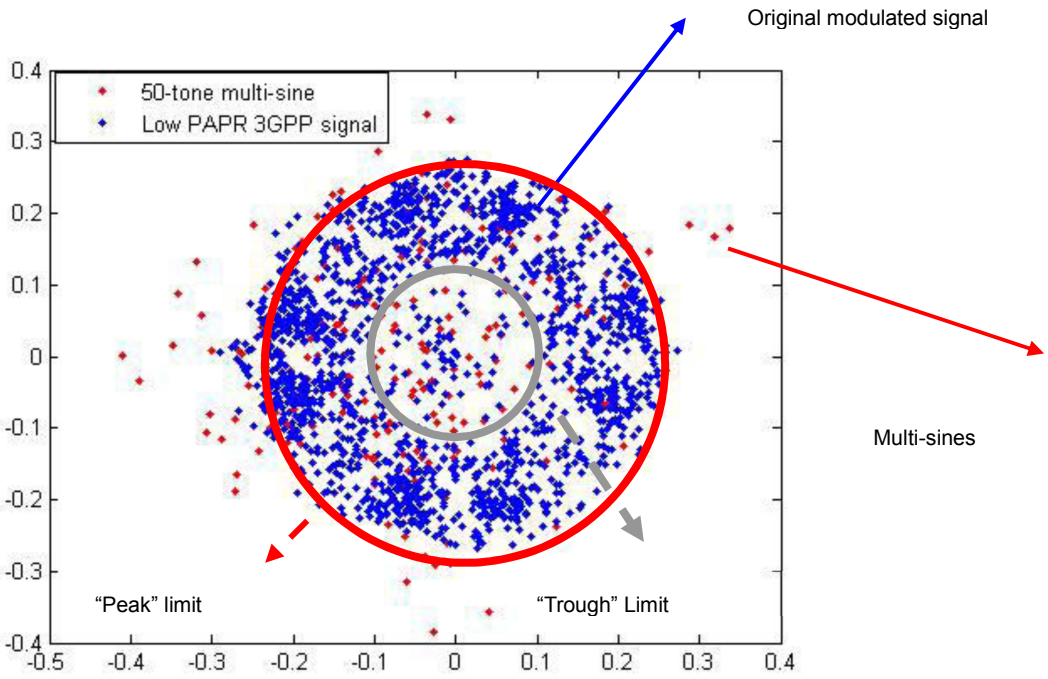

Figure 3.23 Time-domain I-Q diagram of multi-sine (red) and target WCDMA signal (blue)

From the above diagram, we can see that a number of points of the constructed multi-sines are located outside of the range of the 3GPP WCMDA signal, or in other words, beyond the red "Peak" limit. On the other hand, more points are located within the centre area where the values of the original signal are rarely located, i.e, inside the grey "Trough" limit. The "Peak" limit value and "Trough" limit value are not strictly defined here but it is obvious that, as a consequence, these two signals have a very different CCDF characteristic.

3.3.2 Approximating CCDF through waveform summation

The above analysis has also indicated a possible solution to the issue of diverging statistical behaviors of the approximated and original signals: If the excessive peaks could be removed from the approximated signal while at the same time amplifying the troughs to move them further towards the middle zone between central limit and peak limit, the new established waveform should exhibit a CCDF curve that is more simliar to the CCDF curve of target WCDMA signal.

Therefore, once a "peak" value and a "trough" value are defined, we can then extract the "peak" waveform and "trough" waveform from the original multi-sines waveform. Using those waveforms to compress the peaks and extend the troughs within the original waveform, a new waveform could be created with a similar CCDF to the target signal. Figure 3.24 illustrates this process graphically.

I-Q diagram (vertical axis: imaginary; horizonal axis: real)

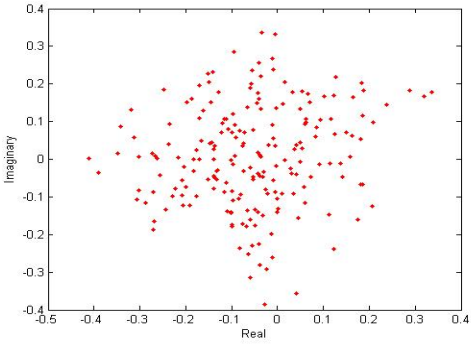

Time-domain real part waveform shape (vertical axis:magnitude; horizonal axis: Time points)

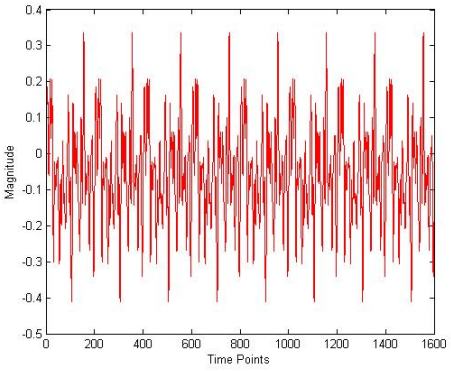

Fig.3.24a The I-Q diagrams and time-domain real part waveform shapes of the 50-tone multi-sines acquired with even space method. The CCDF curve of this signal was depicted at figure 3.18

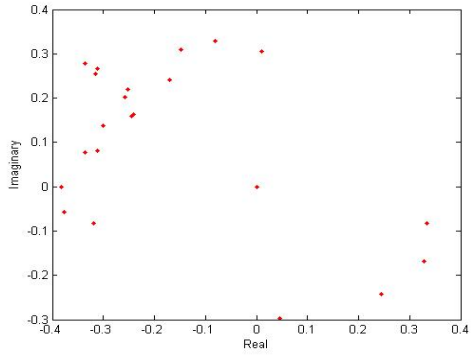

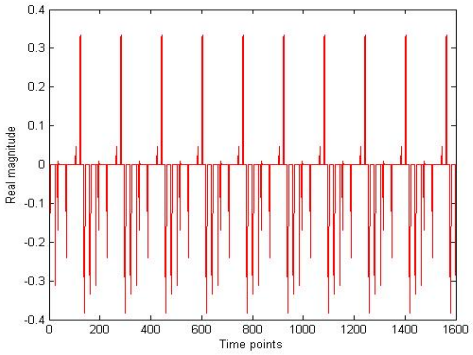

Fig.3.24b The "peak" I-Q diagram and time-domain real part waveform shape of the multi-sines depicted above

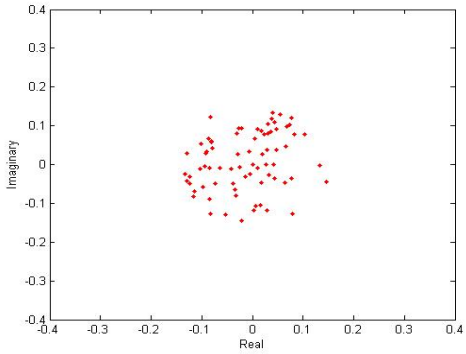

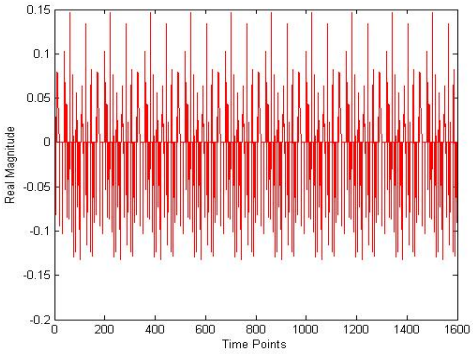

Figure 3.24c The "Trough"I -Q diagram and time-domain real part waveform of the multi-sines depicted at 3.21a

Figure 3.24*a* is the originally designed 50-tone multi-sines. It is obvious that when the peak waveform shown in figure 3.24b has been removed from waveform shown in figure 3.24*a*, the magnitudes of the resulting waveform should have no peaks with more time samples having the maginute close to the chosen "peak" value.

However, if we just simply remove the "trough" waveform shown in figure 3.24*c* from the original waveform, the resulting waveform will have a lot of sampling points with magnitude zero and hence stay below the "trough" limit. Therefore, we choose to amplify the magnitudes of waveform in figure 3.24*c* instead which will push those time points with low magnitude over the "trough" limit. Figure 3.25 shows the I-Q diagram and the CCDF of the newly created waveform after appying this approach using a constant amplifying factor for all samples within the "trough" waveform.

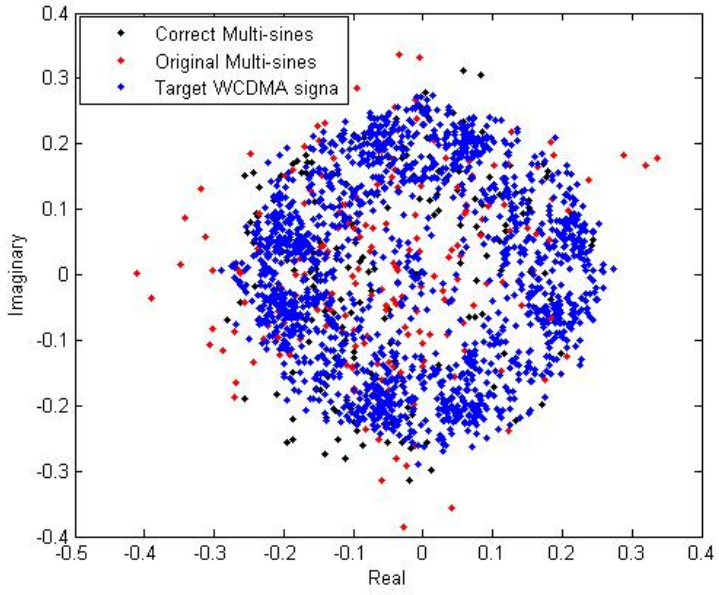

Fig.3.25a The I-Q diagram comparision of corrected multi-sines, original multi-sines and target WCDMA signal

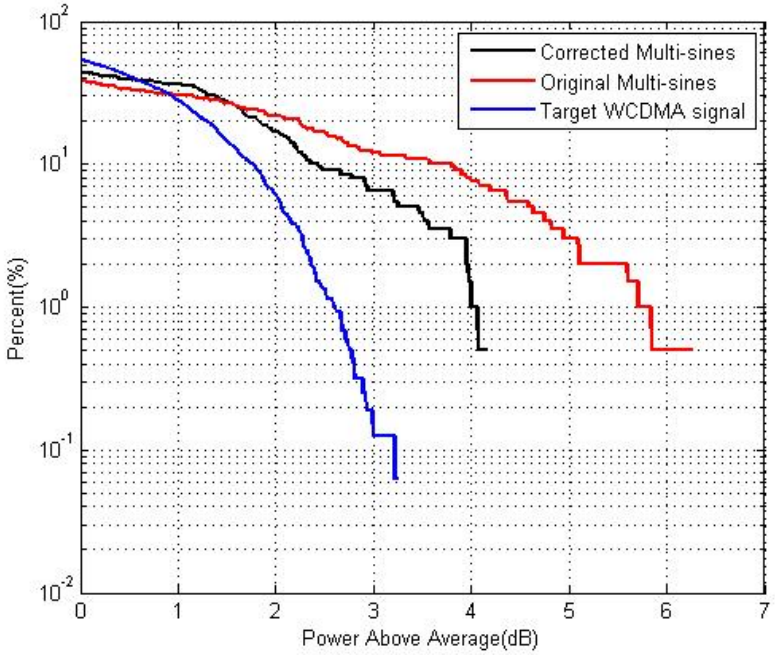

Figure 3.25b The CCDF comparision of corrected multi-sines, original multi-sines and target WCDMA signal

As can be seen from figure 3.25, the modified multi-sines is closer to target WCDMA signal in the IQ diagram and hence approximates the CCDF of the original WCDMA signal more accurately, though some difference still exist. The difference is caused mainly by two reasons. Firstly, in the process of removing peak waveforms, those time points which have the magnitudes over the "peak" limit were given a "peak" value instead of being distributed between "peak" and "trough" limits. Secondly, The process of amplifying "trough" waveform using a constant factor can not push the magnitudes of all those time points climb over the "trough" limit and consequently there are still some points left below the "trough" limit.

The above analysis just provides us the general idea of this novel multi-sines design philosophy. To acquire a more accurate

approximation result, a loop process is required to continusly adjust the statistical character of the desired multi-sines *d(n).* This process can be described by optimizing the four parameters in the following equations:

$$d(n) = a(n) - p_1 a_p(n) + p_2 a_t(n) \qquad n = 1,2,\cdots,N \qquad \text{(Equation 3.18)}$$

where $$a_p(n) = \begin{cases} 0 & ,if\ a(n) < l_1 \\ a(n) - l_1 & ,if\ a(n) > l_1 \end{cases} \qquad \text{(Equation 3.19)}$$

$$a_t(n) = \begin{cases} 0 & ,if\ a(n) > l_2 \\ a(n) & ,if\ a(n) < l_2 \end{cases} \qquad \text{(Equation 3.20)}$$

Where n is the sampling point and *a(n)* is the original multi-sines designed with the even-space method, l_1 and l_2 are the "peak" and "trough" threshold values used to acquire the "peak" sampling waveform $a_p(n)$ and "trough" sampling waveform $a_t(n)$ respectively. The p_1 and p_2 parameters are multiplication factors which represents the peak removing process and trough amplifing process seperately.

Therefore, it is the 4 parameters l_1, l_2, p_1, p_2 which are needed to be optimized in order to get the multi-sines approximate the target WCDMA signal. The optimization process we used in this work is the global search method which steps through all the possible values of these 4 variables. Hence the multi-sines design problem has been simplified from optimizing hundreds of variables, which usually include the amplitudes and phases of a number sinusoids, to the four parameters of equation 3.18 to equation 3.20.

However, the acquired multi-sines signal *d(n)* introduces a number of new tones because $a_p(n)$ and $a_t(n)$ distort the originaly designed multi-sines in frequency domain by introducing a larger number of tones as shown in figure 3.26 which is the DFT transformation of both the original designed multi-sines *a(n)* and the acquired multi-sines *d(n)* after artifical modification process described in equation 3.18. Therefore, in the next step we still need to develop a method to replace these "peak" and "trough" waveforms through multi-sines signals with limited number of tones.

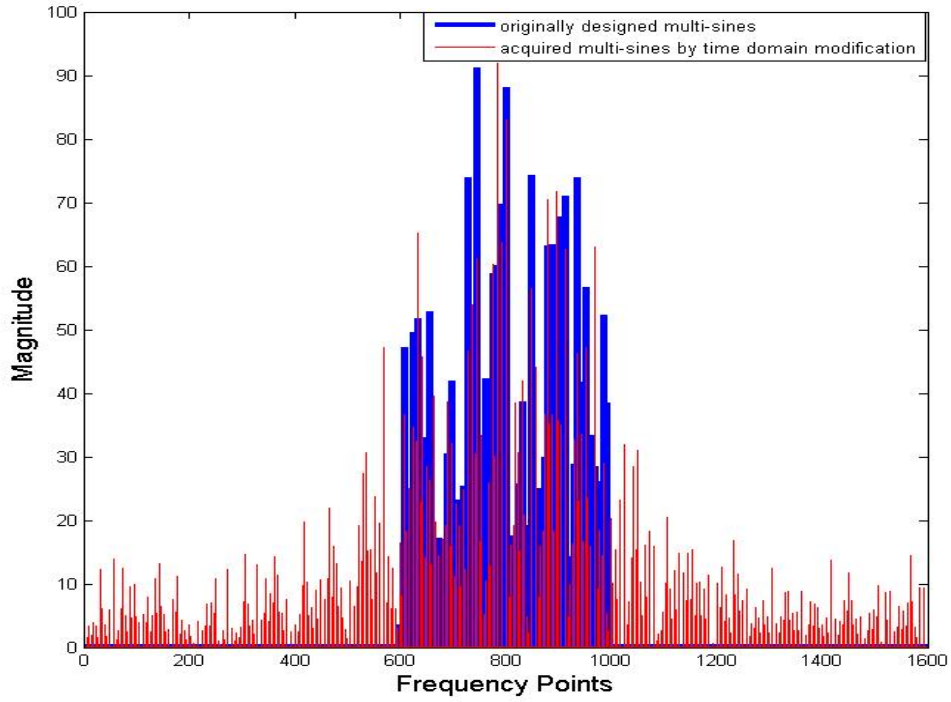

Figure 3.26 The comparation between original the designed 50-tone multi-sines(blue) and the modified signal(red)

3.3.3 Optimum 'peak' and 'trough' waveforms

It is found that the correlation method can also be used here to reduce the number of tones needed. There are two reasons to

support this direction. Firstly, after examining the spectrum of these two “peak” and “trough” waveforms, we find that a few spectral components, whether located in-band or out-of-band, are quite large compared to other components and the difference could be 10 dB or more. Secondly, we know that correlation and further methods for reducing the number of tones are unable to preserve the statistical properties of original signal. However in this case, we do not need to create “peak” or “trough” waveforms with similar statistical information but waveforms that effectively remove the peak and trough points from the multi-sines.

Therefore, we apply the correlation method with the 50 frequency components which were used to get the original multi-sines shown in figure 3.26 to re-create the “peak” and “trough” waveform. The newly created “peak” and “trough” waveforms are shown in figure 3.27 both in frequency domain and time domain.

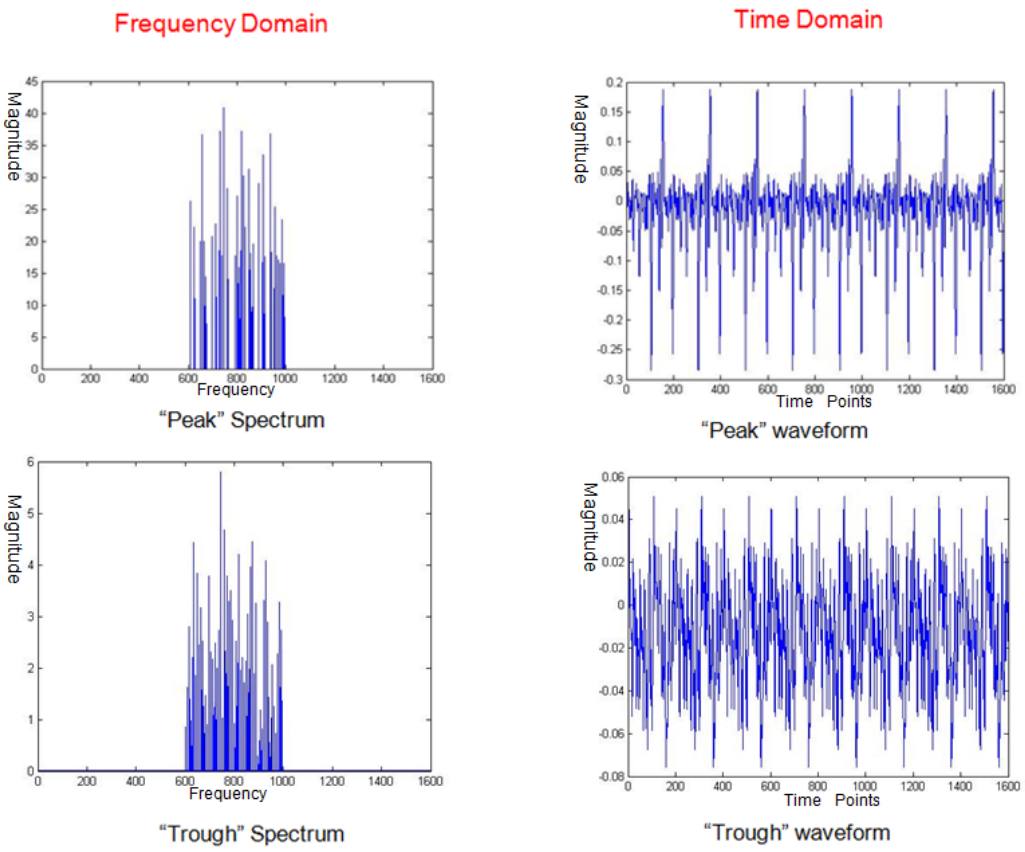

Figure 3.27 The frequency spectrum of multi-sines "peak" waveform and "Trough" waveform and their time-domain real part waveform shapes

The "peak" and "trough" waveforms are obtained using the similar process described in equation 3.18. Therefore the whole looping process can now be expressed as.

$$d'(n) = a(n) - p_1 a_p'(n) + p_2 a_t'(n) \qquad n = 1,2,\cdots,N$$

(Equation 3.21)

The newly created multi-sines is represented as $d'(n)$, $a_p'(n)$ is the multi-sines approximation of the $a_p(n)$ and $a_t'(n)$ is the multi-sines approximation of $a_t(n)$.

Obviously, if we compare figure 3.27 with figure 3.24, we will find that $a_p'(n)$ and $a_t'(n)$ are distorted in time domain, which means the magnitudes of many time points which were located between "peak" and "trough" limits have been modified as well as those "peak" and "trough" waveforms in the modification process. Therefore, the resulting multi-sines $d'(n)$ will be less like the target signal $a(n)$ than the waveform $d(n)$ which is acquired using the original "peak" and "trough" waveforms. Figure 3.28 shows the waveform shape and the CCDF of this newly created multi-sines $d'(n)$ and compares it with the target WCDMA signal and the multi-sines $d(n)$. As can be seen, it still represents the statistical properties of the target signal while maintaining a low number of tones.

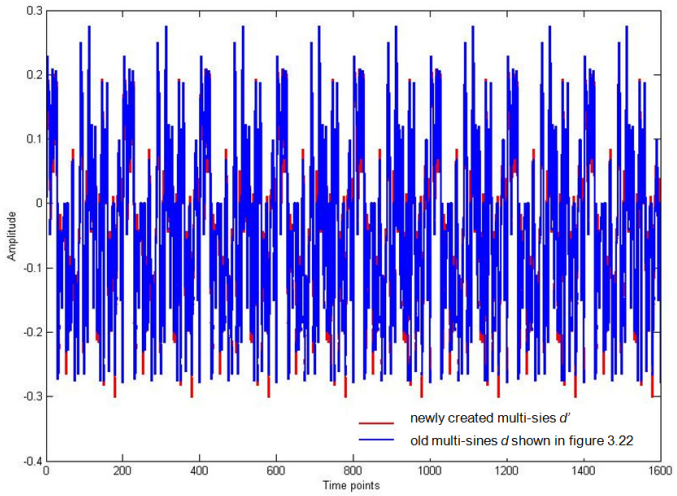

Fig.3.28a Comparison of waveform shapes between the newly created multi-sines d' with 50 tones(red) and old signal obtained through eq3.18(blue)

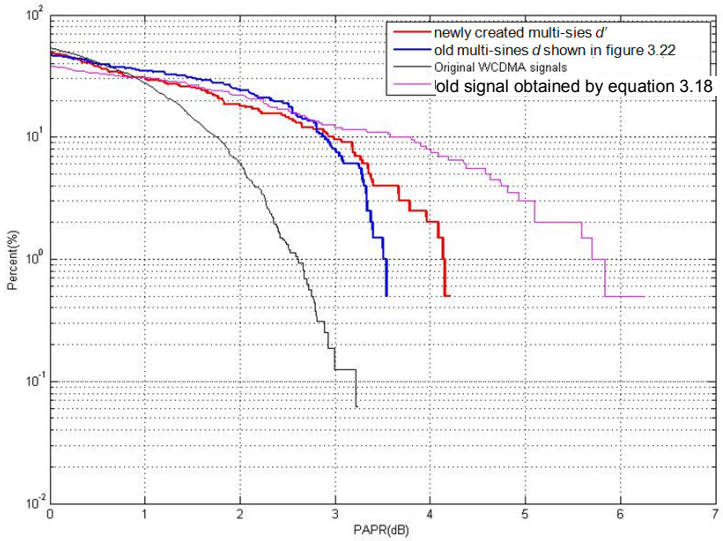

Figure 3.28b Comparison of CCDF between the newly created multi-sines d' with 50 tones(red) and old signal obtained through eq3.18(blue)

3.3.4 The complete design procedure for multi-sines

It is necessary to state that the result shown at figure 3.28 was achieved with optimization of the four parameters l_1, l_2, p_1, p_2 in equations 3.19 to 3.21. The complete multi-sines design procedure can now be concluded by introducing an optimisation loop, as described below to continuously improve the similarity between the multi-sines and target signal according to the identified criteria.

1) Segment a modulated signal by varing time length and analyse their statistical property(i.e, CCDF) until an acceptble level of convergence is accquired. Take this signal clip as the target.
2) Apply spot correlation on the target modulated signal with a defined number of sinusoids using equations 3.15 and 3.16 to accquire a multi-sines signal *a*. The resulting frequencies of these sinusoids are evenly distributed among the in-band area of target modulated signal.
3) Define time domain "peak" clipping level l_1 and "trough"

clipping level l_2 to extract the "peak" waveform and the "trough" waveform from the multi-sines a according to equations 3.19 and 3.20.

4) Rebuild the "peak" multi-sines waveform and the "trough" multi-sines waveform using the correlation method with the same frequencies as the signal a.
5) Calculate the new multi-sines d' by modiying the "peaks" and "troughs" of the multi-sines a using equation 3.21.
6) Calculate the DFT of signal d', and level the total power to the target modulated signal by varing all the magnitudes with the same scaling factor. This provides the first iteration of multi-sines signal to approximate the target signal.
7) If the aggrement between the target signal and approximaed multi-sines is not sufficient, repeat the algorithm, until an acceptable error is reached.

Typically, in step 2 we distribute the frequencies of the multi-sines along a frequency bandwidth that also cover out-of-band frequencies to get a better approximation of target signal. Also in step 3, the clipping level l_1 is normally set between the maximum magnitude and the mean magnitude of the target modulated signal while l_2 is normally be set between the mean magnitude of the target modulated signal and 0. The final value is acquired by looping the design process until an acceptable aggrement between the target signal and the approximated signal is obtained. The same process applies to the sum coefficients p_1 and p_2 which are normally initially set to unity.

Therefore, in total we have only four optimization variables making the process very computationally efficient when compared to previous methods, which introduce hundreds of variables within the design process. This entire design process is relatively straightforward to realize. It only needs a small storage space during computing, thus it can be carried out on most PCs and even laptops or implemented it on embedded DSP chips. In conclusion, the new design process introduces the possibility of designing the multi-sines in real-time during device or system measurements and simulations.

3.4 CAD-based verification

To examine the entire multi-sines design process a CAD simulation was constructed. A Matlab program was written to implement this multi-sines design method. The resulting multi-sines, along with the the target modulated signal, are then imported back to the ADS simulation schematic which was shown before in figure 3.8. The results are compared over a range of input power levels and are shown in figure 3.29.

As can be seen, the two ACPR curves are quite close with less than 2dB difference at the higher drive levels. Compared to the previous figure 3.11b, where the same level of error was acquired with 500 tones based on correlation method, hence the introduced multi-sines design method has dramatically reduced the number of tones needed to stimulate nonlinear device to get very simliar response. Therefore, we can initially conclude that this multi-sines design method has strong potential, hence justifying further investigations to verify its suitability. This will be further discussed in chapter 4 and 5.

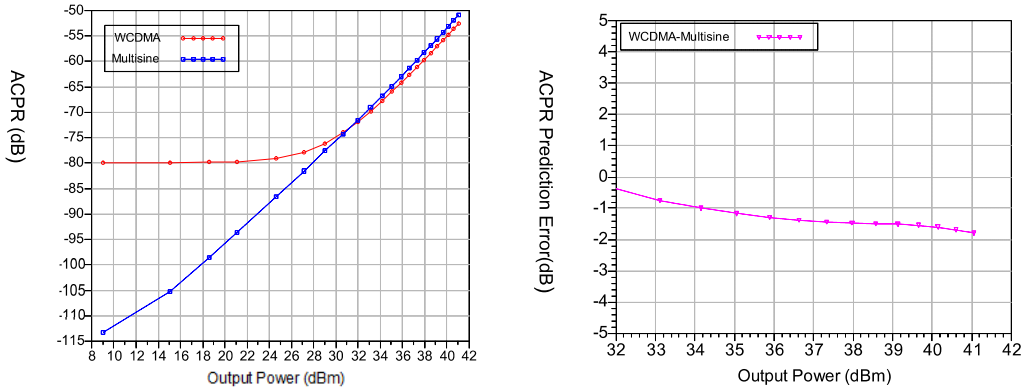

Figure 3.29 The ACPR of the new designed multi-sines and comparison with original WCDMA signal

3.5 Conclusion

In this chapter, we start with the multi-sines design using the correlation method. By definition, the correlation method tells us how many sinusoids with different frequencies are embedded within the original communication signal. Though this method can create an accurate approximation, it leads to a very large number of tones thus making any further analysis of inter-modulation distortions impractical. Further investigations were carried out using firstly only in-band spectrum components and also a fraction of the out-of-band spectrum components. These efforts achieved only partial success for communication signals with a high PAPR only.

Hence, theoretical investigations were carried out to identify the cause of these limitations with the results pointing towards the distribution and relative values of the peak and troughs within waveforms as a cause. The proposed method is therefore based on the idea of removing the “distinguishing” points within the multi-

sines waveform. During this process known and straightforward parameters, such as CCDF curves, can be employed to derive the optimisation parameters. Initial verification of this method utilising CAD simulations have demonstrated its strong potential.

3.6 Reference

[1] R.N. Mutagi, “Understanding the Discrete Fourier Transform”, RF design world, 2004, available online at http://rfdesign.com/mag/401rfdf3.pdf

[2] 3GPP TS 25.141 version 6.6.0 Release 6, Technical Specification, 3rd Generation Partnership Project, Technical Specification Group Radio Access Network, Base Station (BS) conformance testing (FDD) (Release 6).

[3] F. Fernet, "An ADS bench for generating multi-carrier 3GPP WCDMA ACLR test signals," High Freq. Electron., pp. 34-42, Nov. 2002.

[4] How-Siang Yap, “Designing to digital wireless specifications using Circuit Envelope simulation”, Microwave Conference Proceedings, 1997. APMC '97, 1997 Asia-Pacific

[5] [Agilent Application Notes, “Highly Accurate Amplifier ACLR and ACPR Testing”, available online at http:// cp.literature.agilent.com /litweb/pdf/5989-5471EN.pdf

[6] K. M. Gharaibeh, K. G. Gard and M. B. Steer, “In-band distortion of multisines,” IEEE Trans. Microwave Theory and Tech., August 2006, pp.3227–323

4 FOMs (Figure of Merit) Selection

In the chapter 3, a multi-sines design process for preserving the statistical properties of a given modulated signal was developed. It was initially verified by CAD simulation using the resulting ACPR performance of the nonlinear device. However, the question remains whether the new approach allows the design of multi-sines that excite the same nonlinear device response as a real signal. Another unconfirmed question is whether multi-sines are suitable for real device measurements as well as CAD simulations.

The answer to the second question is also dependent on the answer of the first question as the identified figures of merit (FOM) should be measurable. Hence in this chapter, we address the first question by investigating a number of FOMs and their combinations to establish potential applicability and limits for the characterisation and analysis of nonlinear circuits in general. This discussion will involve some theoretical analysis of nonlinear distortion generating mechanisms, so we will use some conclusions and theories introduced in chapter 2.

There are many FOMs which have already been widely accepted, with a number of them developed either for simple excitations like two-tone signals, or for specific modulated signals like QPSK or *n*-QAM. Their applicability to multi-sines therefore needs to be examined and

subsequently re-defined as necessary for the purposes of this work.

4.1 Common FOMs

To evaluate the similarity between the non-linear distortion produced by a modulated signal and that produced by a multi-sine signal, it is necessary to identify a method to evaluate and quantify their quality. In essence, any FOM should directly relate to the nonlinear distortions of the system. In the amplifier design environment, it is relatively straightforward to quantify the PA performance using FOMs such as efficiency, delivered power and bandwidth [1]. Consequently, a designed PA can also be judged against these widely accepted FOMs. However, no such FOMs for the quantification of the quality of a designed multi-sines stimulus currently exist. The need for appropriate FOMs is also essential to create confidence in the use of multi sines and facilitate their wider adaptation and acceptance.

As introduced in chapter 2, there are a number of common FOMs such ACPR, EVM and NPR that have been developed for modulated signals. Often, these FOMs have been developed merely to determine whether distortion exists and eventually compare the distortion levels of different components of modules to a specific communication signal. Therefore, it is important to investigate how well these FOMs describe the nonlinear distortion generated by the nonlinear devices. It is also necessary to analyse the suitability of common FOMs for the evaluation of the designed multi-sines, and the challenges in measuring them.

4.1.1 ACPR

Adjacent channel power ratio (ACPR), or adjacent channel level ratio (ACLR) as it is called in UMTS WCDMA specification [1], measures the amount of power in an adjacent channel due to inter-modulation distortion generated by a digitally modulated signal in the main channel passing through a non-linear device such as a PA. For many of the current and future transmission standards, ACPR is an important test parameter for characterising the distortion of subsystems and the likelihood that a given system may cause interference with a neighbouring channel transmission. In some fields such as PA linearisation techniques, ACPR has become a widely accepted figure of merit for the evaluation of the performance of linearisation.

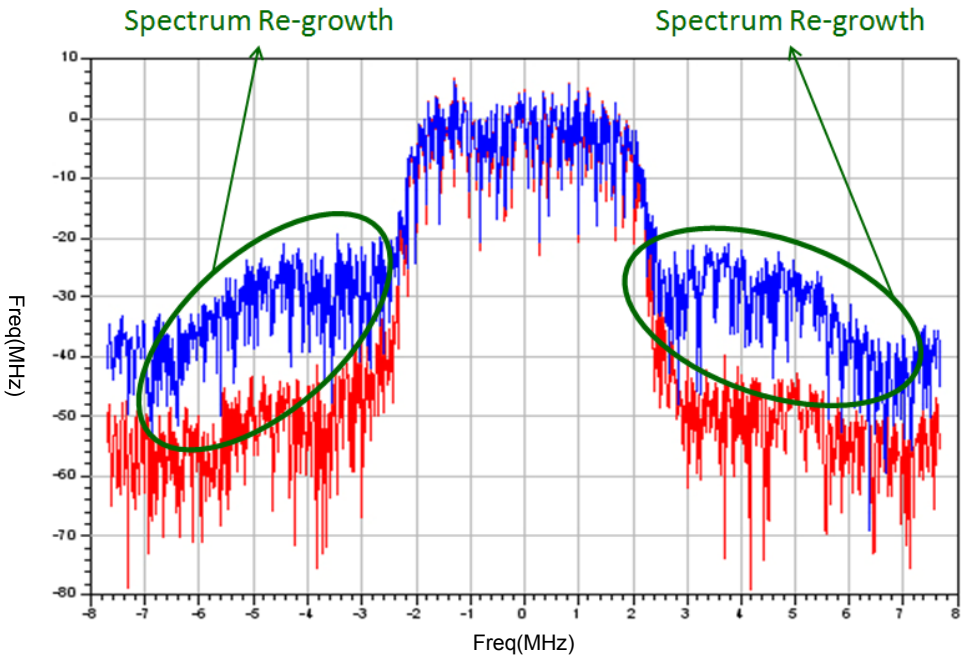

Figure 4.1 Spectral Re-growth when WCDMA signals pass through a nonlinear PA. (Red: input Power Spectrum; Blue: output Power Spectrum.)

ACPR can be seen as an extension of the two-tone signal test for the inter-modulation ratio (IMR). For the case of multi-sines excitation, the complex modulated signals can also be seen as multi-sines as they have thousands of tones. This quantity is essentially the integrated power of the spectral re-growth due to nonlinear distortion related to the output power, as seen in Figure 4.1.

ACPR measurements are relatively simple to achieve as measuring power ratios over some bandwidth can be achieved with a number of readily available instruments such as spectrum analysers or oscilloscopes. These devices can easily lock onto a specific bandwidth over which to make the measurement. The question for and ACPR measurement is then how the power measurement is performed within that bandwidth. For example, the selection of this bandwidth is important as a too narrow bandwidth would result either in a signal that is inadequately sampled or a measurement that takes too long to finish. Too wide a bandwidth, however, might lead to measurement errors at the edges of the channel bandwidth. Nevertheless, such issues are widely known and can be readily addressed, as described by a number of publications [3][4].

It is notable that the channel bandwidths that are used for ACPR measurements are not constant due to the number of different co-existing communication standards. ACPR measurements have been standardised for some time for a number of communication systems with relatively narrowband modulation bandwidths, such as IS-95 CDM. However, the standardisation for systems with wider modulation bandwidth is still in flux. ACPR measurements are

commonly performed for the component, module and system compliance testing within IS-95 CDMA and WCDMA standard definitions. The definitions of the locations of measurement channels and their bandwidths for these two standards are listed at table 4.1.

Type	NB CDMA IS-95 (rev link)	WB CDMA (one approach)
Main channel measurement BW	1.23 MHz or 30 kHz	3.84 MHz
Adj. channel location (from carrier)	± 885 kHz	± 5 MHz
Adj channel measurement BW	30 kHz	3.84 MHz
Alt channel location (from carrier)	± 1.98 MHz	± 10 MHz
Alt channel measurement BW	30 kHz	3.84 MHz

Table 4.1 Definitions of locations of measurement channels and their bandwidths for different signal sources

Although ACPR is fully capable of assessing the spectral re-growth due to a nonlinear device response, it does not provide a full picture of its nonlinear behaviour. This can be concluded from the following discussions.

ACPR can be expressed mathematically as:

$$ACPR = \frac{P_{in}}{P_L + P_U} = \frac{\int_{in-band} S(f)}{\int_{out-of-band} S(f)}$$

(Equation 4.1)

where P_{in} is the total integrated power of the entire in-band bandwidth, P_L and P_U refer to the integrated power in lower and upper adjacent channels, and $S(f)$ is the Power Spectral Density (PSD) function of the output signal.

An alternative method to define ACPR using the definitions of correlated and un-correlated distortion is shown in equation 4.2.

$$ACPR = \frac{S_{y_c y_c}(f) + \int_{in-band} S_{y_u y_u}(f)}{\int_{out-of-band} S_{y_u y_u}(f)}$$

(Equation 4.2)

According to our discussion in chapter 2, the correlated distortion is located in-band while the uncorrelated distortion exists both in-band and out-of-band. As can be seen from equation 4.2, as long as the in-band and out-of-band part of the signal form a constant ratio, the ACPR will remain constant. This means that the ACPR is unable to differentiate between the transmitted signal and the in-band distortions. In other words, the main drawback of ACPR is that it is unable to assess in-band distortions.

4.1.2 NPR

Noise power ratio (NPR) is defined as the ratio of output power of a nonlinear system within the bandwidth of a notch located at some in-band frequency, to the output power without the notch in the same notch bandwidth. Therefore, NPR represents the ratio of total

output power to the effective in-band distortion power. This definition is illustrated in figure 4.2.

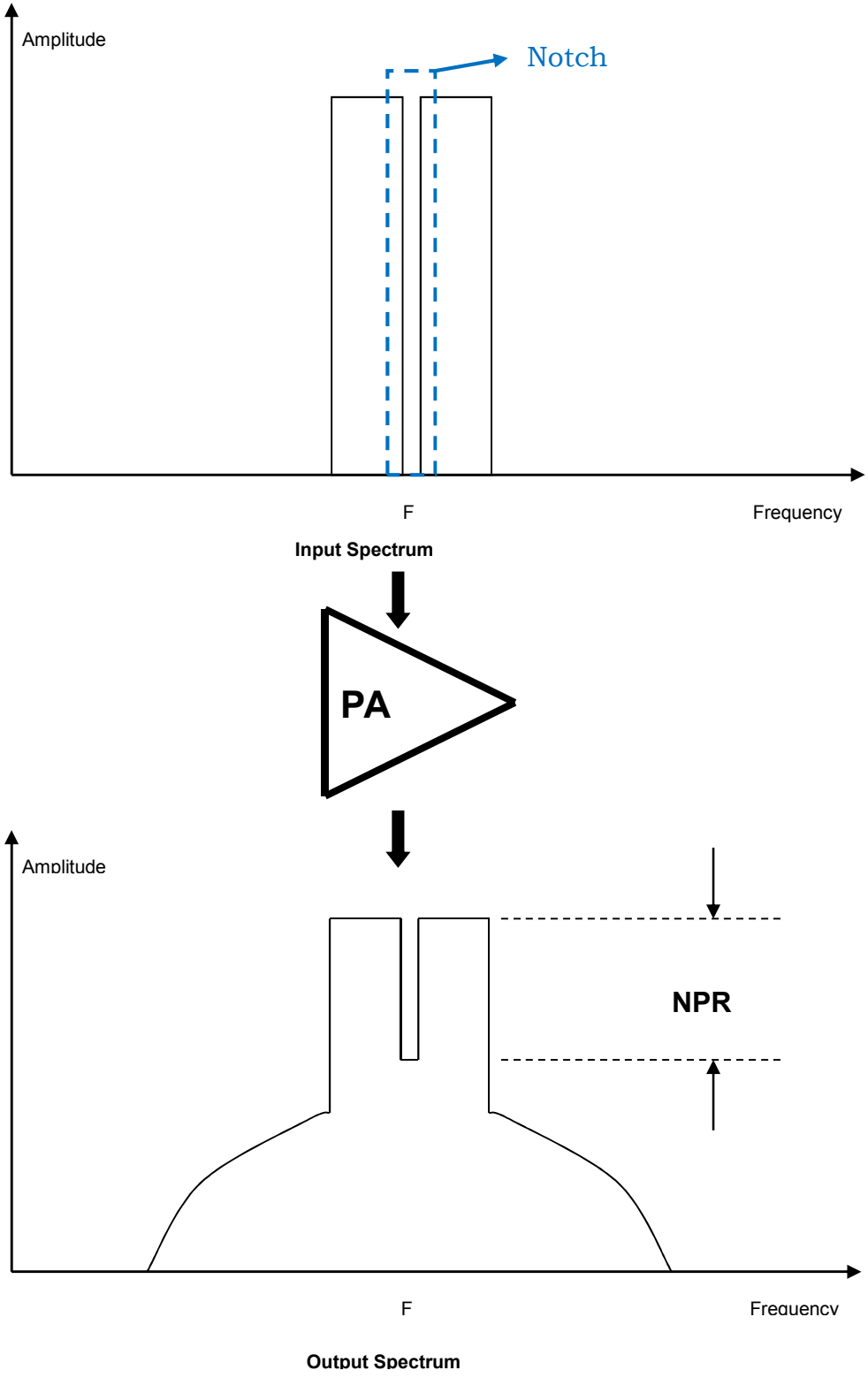

Figure 4.2 Definition of NPR

When measuring NPR, the input excitation signal is the same as the real signal except for the notch where only the residual thermal noise is present. Therefore, at the output, the nonlinear distortion noise will appear at the notch and thus can be measured. NPR is similar to IP3 of a two-tone test. However, due to the utilised communication signals, large signal peaks are created that stress the communications channel more than a two-tone measurement. Because of the nature of this stimulus, the NPR method was widely regarded as the most accurate method for reproducing multi-carrier inter-modulation effects and predicting the system BER performance under real broadband traffic conditions.

Many factors influence the result of an NPR measurement. These include the characteristics of the stimulus used and the specifics of the measurement technique. The measurement can be carried out by either digital or analogue methods. While the two approaches are equivalent, analysis shows that the digital approach is superior in repeatability and execution time.

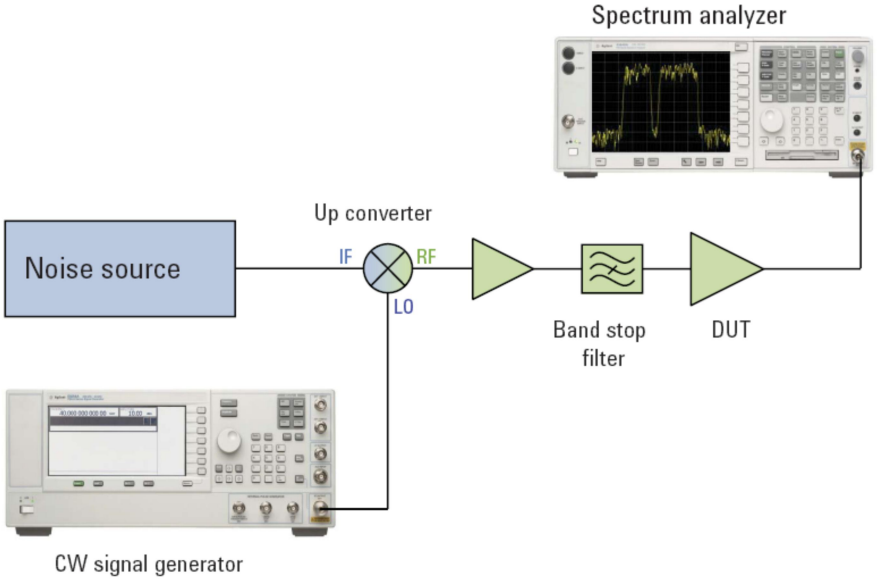

Figure 4.3 Measuring NPR by analogue method

Figure 4.3 shows the traditional analogue method of measuring NPR. The stimulus is generally created by taking the output of a noise tube or noise diode and conditioning it with amplification, frequency translation and band-pass or band-reject filtering. The spectrum of such a signal is continuous and its spectral shape is highly dependent on the actual filters used. A frequency selective instrument like a swept spectrum analyser is typically used for the measurement. This provides an accurate measurement of the peak of the noise power of the stimulus down to power levels at the bottom of the notch. The resolution bandwidth selected should be as wide as possible while still maintaining a capability to resolve the notch precisely.

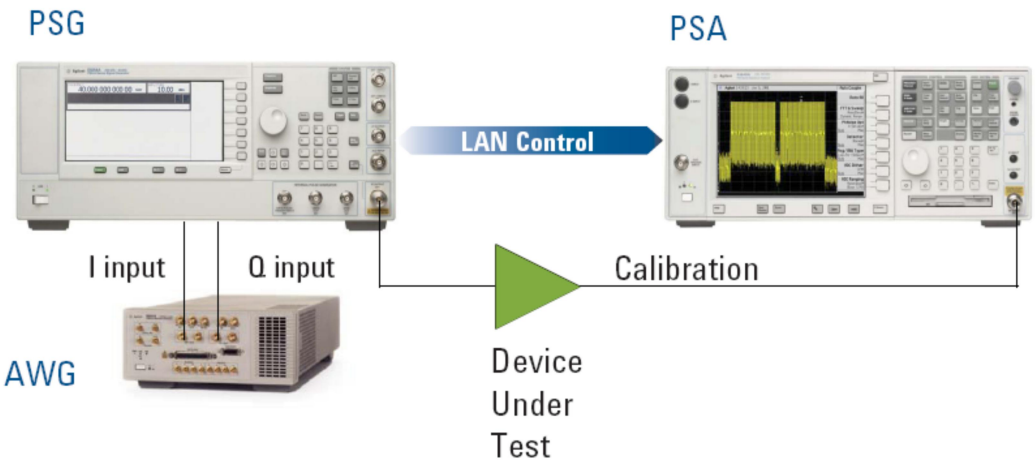

Figure 4.4 Measuring NPR by digital method

Figure 4.4 shows the digital way to measure NPR. In this technique, the measurement system is comprised of an Arbitrary Waveform Generator (AWG), an RF/microwave synthesizer with a broadband I/Q modulator, and a spectrum analyser that can be programmed as a receiver. The AWG is programmed to generate the baseband noise pedestal signal with the necessary characteristics. The synthesizer is used to up-convert the noise signal pedestal to the DUT's operating frequencies. The spectrum analyser is used to calibrate the noise signal pedestal and the notch for optimum performance and to obtain a reference NPR of the input signal. The digital NPR measurement provides higher accuracy and faster averaging to improve measurement repeatability and throughput. It also allows for the implementation of more advanced signal processing techniques.

The mathematical expression for NPR can be defined as [4]:

$$NPR = \frac{\int S_{yy}(f)}{\int S_{yy'}(f)}$$

(Equation 4.3)

Where $S_{yy'}(f)$ is the output PSD with the notch and $S_{yy}(f)$ is the output PSD without the notch. Obviously if the system is linear and completely noise free, then NPR reaches infinity.

NPR can be also defined using the definition of correlated and uncorrelated distortion [4]:

$$NPR = \frac{\int S_{yy}(f)}{\int S_{y_c y_c'}(f) + \int S_{y_u y_u'}(f)}$$

(Equation 4.4)

Where $S_{y_c y_c'}(f)$ refers to correlated distortion and $S_{y_u y_u'}(f)$ refers to un-correlated distortion. If it is assumed that the notch is very narrow, $S_{y_c y_c'}(\omega_0)$ = 0. Thus, equation 4.4 can be expressed as:

$$NPR = \frac{\int S_{yy}(f)}{\int S_{y_u y_u'}(f)}$$

(Equation 4.5)

Therefore, NPR is defined in terms of the ratio of uncorrelated spectrum of the notched output $S_{y_u y_u'}(f)$ to the output PSD without the notch $S_{yy}(f)$. However, the true effective in-band distortion should be calculated with the uncorrelated spectrum of the original output $S_{y_u y_u}(f)$, so the validity of NPR as a good measure of in-band distortion is doubted [3][4].

Furthermore, the analysis of NPR is usually based on exploiting the properties of a Gaussian noise signal which produces closed form expressions of NPR as a function of noise power, notch filter characteristics and the coefficients of the nonlinear polynomial model. Therefore, if the PDF of the input signal is not Gaussian, NPR does not represent the effective in-band distortion. This has been discussed in [5] where NPR measurements were complicated by the deviation of the input signal from Gaussian nature due to the nonlinearity of an overdriven preamplifier. In further investigations [6], three different types of signals with different statistical properties were studied (NBGN, WCDMA and Multi-sines) and used to demonstrate that the orthogonal model is useful in showing the effectiveness of the NPR as a measure of effective in-band distortion. It has also shown that NPR, when measured using NBGN, overestimates the NPR of some WCDMA signals and multi-sines with fixed phases.

4.1.3 CCPR

As NPR is exclusively defined in terms of uncorrelated distortion and implicitly ignores in-band correlated distortion, CCPR (Co-Channel Power Ratio) has been introduced as a new figure of merit for measuring in-band distortion [7]. The idea of CCPR is to eliminate the linear part of the measured output [8] (or the underlying linear system), as well as the part of the output distortion that has some correlation with the input signal. In other words, it is defined as the ratio of the linear part of the output to the uncorrelated distortion part of the power. Figure 4.5 presents the overall idea.

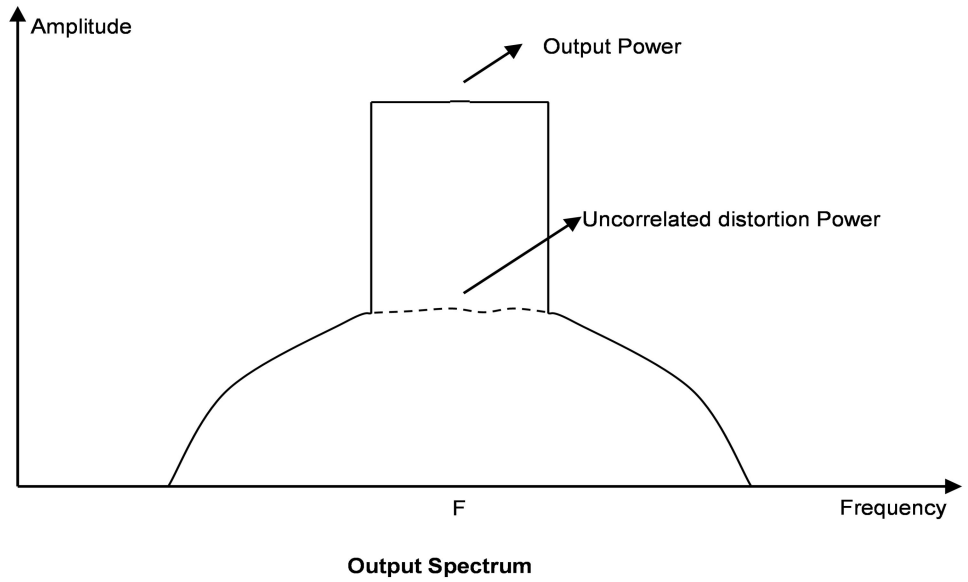

Figure 4.5 Graphic illustration of CCPR

Thus, it can be shown that CCPR can be represented in terms of the correlated spectrum and un-correlated spectrum as:

$$CCPR = \frac{Output\ \ Power}{Uncorrelated\ \ distortion\ \ power} = \frac{\int S_{yy}(f)}{\int S_{yy}(f) - \int S_{y_c y_c}(f)} = \frac{\int S_{yy}(f)}{\int S_{y_u y_u}(f)}$$

(Equation 4.6)

Where $S_{y_c y_c'}(f)$ refers to correlated distortion and $S_{y_u y_u'}(f)$ refers to un-correlated distortion. A CCPR measurement setup has been introduced in [9] where a feed-forward cancellation loop was tuned to small signal cancelation. In this setup, the device under test (DUT) is excited with its full input spectrum, while the linear components are subtracted from the output, using a scaled version of the stimulus provided by the bridge linear auxiliary arm. Firstly, an error signal was generated in a signal cancellation loop to subsequently correct the PA output in the distortion cancellation loop. Therefore, this error signal must be a replica of the amplifier-induced noise-plus-

distortion perturbation. Thus, a visualisation of this error signal constitutes a true distortion (plus noise) measurement system. This procedure is illustrated in Fig 4.6.

However, a feed-forward cancellation loop is sensitive to the variation of the components characteristics, which may change due to aging, temperature or other environment influences. The matching of circuit elements over the working bandwidth will also influence the performance of this feed-forward cancellation loop. Therefore, more components have to be added which then increases the complexity and cost of the feed-forward set-up.

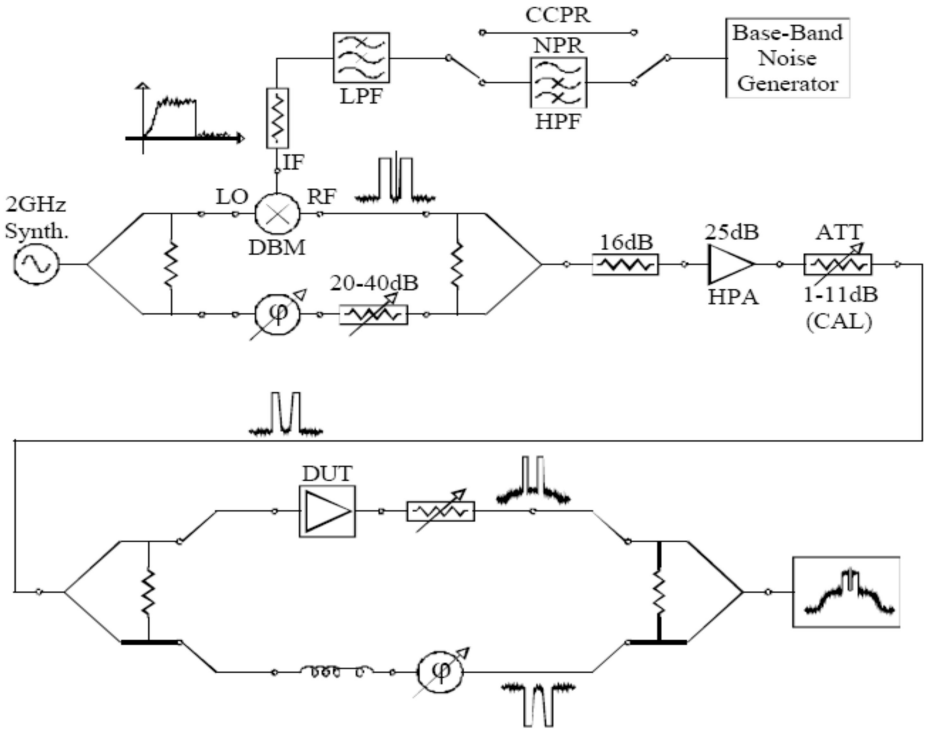

Figure 4.6 Experimental setup for the measurement of CCPR [9]

Besides that, this approach also faces the question of whether to consider signal correlated distortion as an additive noise component or as part of the useful signal. This was studied in [10] [11] where it

was shown that CCPR in certain situations does not represent a useful measure of in-band distortion.

Another similar figure of merit to measure in-band distortion is the signal to noise and distortion ratio (SNDR), which is defined as the ratio of the power containing the useful part of the output signal to the summed power of the uncorrelated distortion and the additive Gaussian noise [7]. However, this figure assumes the nonlinear output consists of uncorrelated components and so the analysis depends on the statistical properties of the input signal. In addition, the measurement of SNDR is still complicated as it also needs the proper tuning of a cancellation loop in a feed-forward cancellation system.

4.1.4 EVM

Error Vector Magnitude (EVM) is a common figure of merit for characterising system linearity in digital wireless communication standards (including GSM, NADC, IS-95 and WCDMA systems). It provides an insight into the signal's quality that other performance measurements such as the eye diagram or BER measurements do not cover. Normally a maximum level of EVM is defined at different stages of a communication system to help the designer to troubleshoot specific problems.

As illustrated in figure 4.7, the Error Vector Magnitude is based upon the difference between the reference waveform and the measured waveform, where difference is called the error vector. When measuring EVM, the measured waveform and the reference

waveform must pass through the same filter with the same bandwidth. Both waveforms should then be further modified by selecting the frequency, absolute phase, absolute amplitude and chip clock timing so as to minimize the error vector. After that, the EVM result is defined as the square root of the ratio of the mean error vector power to the mean reference power expressed as percent. A measurement interval is required to cover a total power dynamic range [2].

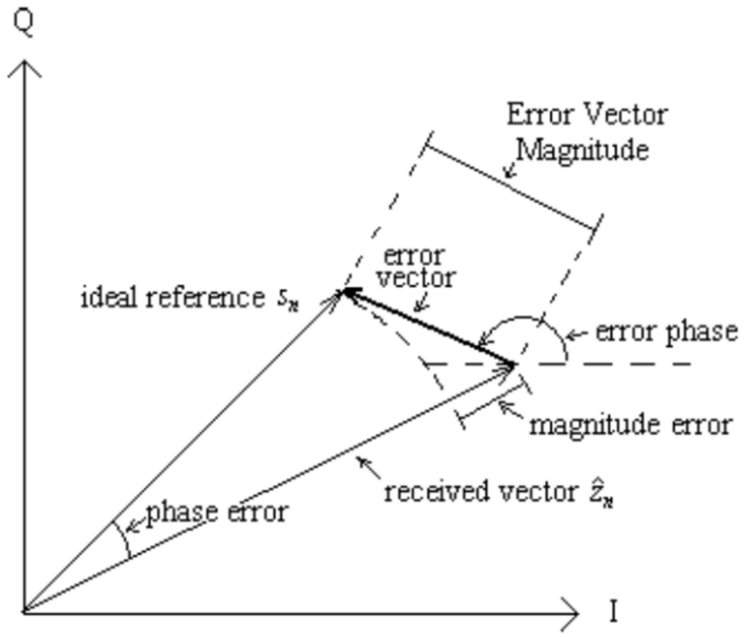

Figure 4.7 Graphic illustration of error vector magnitude

EVM measurements are often performed on vector signal analysers (VSAs), real-time analysers or other instruments that capture a time record and internally perform a Fast Fourier Transform (FFT) to enable frequency-domain analysis. In practice, this usually involves the calculation of the difference between the expected demodulated symbol and the value of the actual received symbol. Software processing of the signals facilitating the down-conversion and demodulation are made internally within these instruments. Figure

4.8 provides constellation diagrams that represent digital bits in terms of symbols for common modulation standards.

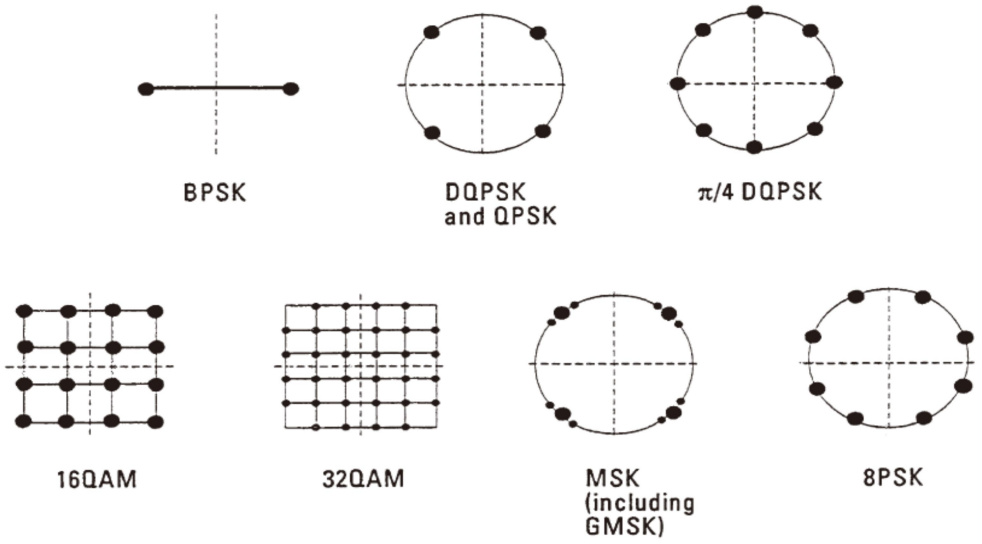

Figure 4.8 Constellation diagram of commonly used modulation standards[16]

Besides demodulation, the EVM calculation process also includes normalisation, re-sampling to find optimal measurement position, and frequency offset compensation. To find the EVM, we must compare the ideal symbol values from the ideal constellation diagram to the arbitrary voltage values that are measured; hence normalisation is required for both the measured and ideal symbols to make a comparison. Also, the received signal is typically unknown and no specific synchronization signal or predetermined sequence is supplied. Therefore, the received signal needs to be re-sampled at the vertical lines to identify the instant with the smallest distortion in order to minimise the contribution to EVM. Figure 4.9 shows the eye diagram of a QPSK signal divided into I and Q components. This eye diagram is acquired with Matlab Simulink CAD environment. The red

vertical line indicates the instant with the smallest distortion and therefore minimises the contribution to EVM.

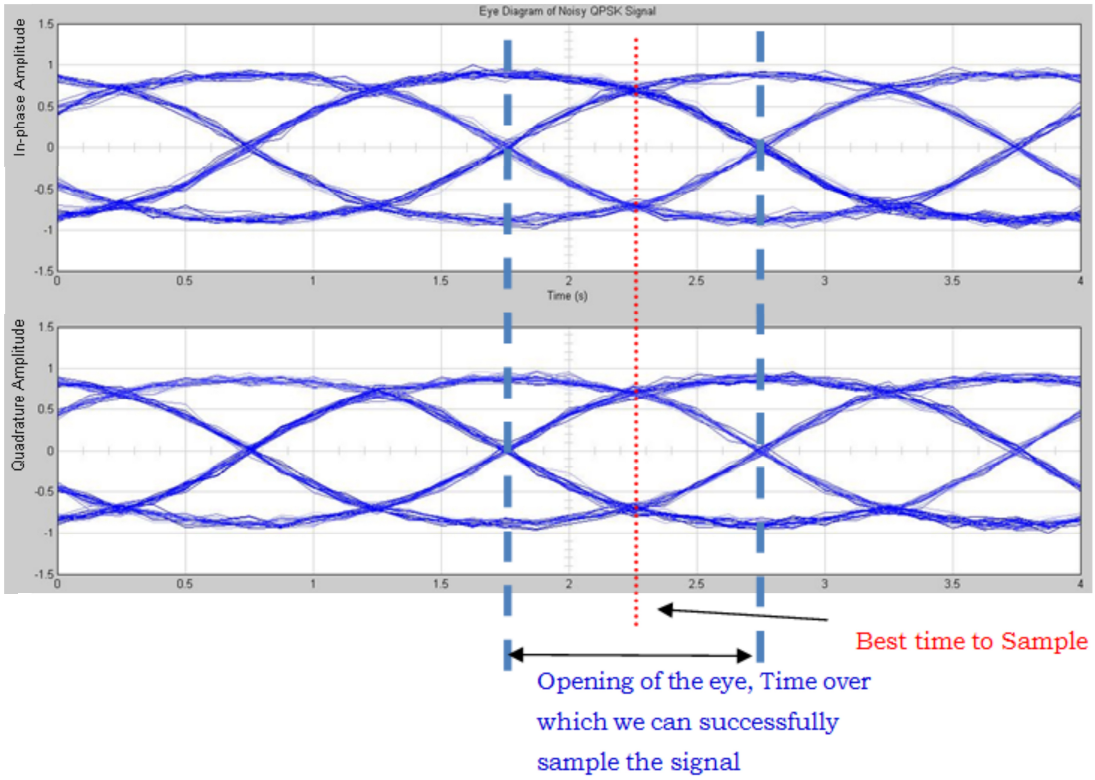

Figure 4.9 Finding the optimal measurement position using eye diagram

The re-sampling process might become difficult if the sent RF signal is down-converted by an unlocked RF local oscillator (LO) which will introduce frequency offsets. These frequency offsets affect the signal, hence making it impossible to calculate the EVM without a prior compensation. More detailed discussion about measuring EVM can be found in[12]-[14].

When using a mathematic equation to calculate EVM, the differences between the two vectors in terms of root mean square EVM is defined as:

$$EVM_{RMS} = \sqrt{\frac{\sum_{n \in N} |Z_n - S_n|^2}{\sum_{n \in N} |S_n|^2}}$$

(Equation 4.7)

Where S_n is the ideal reference signal whose magnitude has been normalised to one. Z_n is the distorted version of the measured signal. In terms of correlated distortion and uncorrelated distortion, it can be defined as[15]:

$$EVM = \frac{\sqrt{E_{y_u y_u}(t)^2}}{\sqrt{E_{y_c y_c}(t)^2}} = \sqrt{\frac{\int S_{y_u y_u}(f)}{\int S_{y_c y_c}(f)}}$$

(Equation 4.8)

Where $E(t)^2$ is the power of a signal, $S_{y_c y_c}(f)$ refers to the PSD of correlated part of the output signal and $S_{y_u y_u'}(f)$ refers to the PSD of un-correlated distortion. In theory, this represents the ratio of un-correlated distortion, whether in-band or out-of-band, to transmitted signals. However, as the uncorrelated distortion is composed of in-band uncorrelated distortion and out-of-band un-correlated distortion, EVM still fails to recognize the effective in-band un-correlated distortion.

4.2 Choosing ACPR and EVM as the figure of merits

Obviously, it is neither necessarily useful nor practical to measure all the figure of merits just for the purpose of verifying that a multi-sines signal had excited the nonlinear device in the same way as the

original communication signals might. However, any single figure of merit is incapable of fully accessing the nonlinear distortion. Hence, we need a combination of FOMs to accurately access the nonlinear behaviour of the device. Additional underlying conditions are that the measurement bench for these figures of merit should ideally be easy to set up and the measurement process is time efficient.

ACPR is relatively easy and quick to measure. In addition, it has widely been accepted as a figure of merit within the industry. However, as discussed above, it is unable to recognize the in-band distortion. This is actually the reason why NPR has emerged to resolve this problem. The drawback of NPR is its incapability of truly addressing the nonlinear distortion for those excitation signals whose statistical properties are different from the property of a Gaussian signal.

CCPR and SNDR measure the in-band distortion by using a feed-forward loop to eliminate the input signal part from the output signal. However, they have their own limitation as the feed-forward setup is not as a widely accepted standard for device characterisation such as single semiconductor transistors or power amplifiers. Besides, the measurement results suffer from poor repeatability. Further questions also remain such as the analytical treatment of correlated distortion; either as an additive noise component or as a part of the useful signal. All of these drawbacks have prevented the large scale application of CCPR and SNDR in industry.

EVM, on the other hand, has been widely used for decades for testing the performance of communication systems. However, as EVM represents the ratio of the correlated part of the output signal part to the un-correlated distortion it fails to quantify the effective in-band distortion.

Based on the above analysis, a supposition is proposed that the combination of ACPR and EVM would for an effective assessment of both in-band distortion and out-of-band spectrum regrowth. In this way, each components of the output signal can be identified including the correlated distortion, in-band un-correlated distortion and out-of-band distortion and therefore encapsulate a holistic assessment of the nonlinear behaviour. This idea can be further illustrated using the following equations of ACPR and EVM:

Let us quote equation 4.2 and equation 4.8 here:

$$ACPR = \frac{S_{y_c y_c}(f) + \int\limits_{in-band} S_{y_u y_u}(f)}{\int\limits_{out-of-band} S_{y_u y_u}(f)} \qquad \textbf{(Equation 4.2)}$$

$$EVM = \frac{\int S_{y_u y_u}(f)}{\int S_{y_c y_c}(f)} \qquad \textbf{(Equation 4.8)}$$

As can be seen from the above equations, once EVM is defined, the ratio between the correlated part and uncorrelated distortion, which exists both in-band and out-of-band, will thereafter be defined as well. Furthermore, with a given ACPR, the ratio between in-band

spectrum and out-of-band spectrum will be defined. Hence with these two equations, $\int_{in-band} S_{y_u y_u}(f) \Big/ \int_{out-of-band} S_{y_u y_u}(f)$, which is the ratio between in-band uncorrelated distortion and out-of-band uncorrelated distortion is defined. As a consequence, $\int S_{y_c y_c}(f) \Big/ \int_{out-of-band} S_{y_u y_u}(f)$ and $\int S_{y_c y_c}(f) \Big/ \int_{in-band} S_{y_u y_u}(f)$, which are separately the ratio of correlated part to out-of-band uncorrelated distortion, and the ratio of correlated part to in-band uncorrelated distortion will be further decided. Hence with a given ACPR and EVM, the relationship among in-band distortion, in-band correlated part of signal, and out-of-band distortion will be completely defined. The full nonlinearity will be completely characterised in an analogous fashion to how we can access a cuboid's dimension once we know the ratio between the width, length and height of this cuboid and one of three such parameters.

Furthermore, the measurement setup required for the measurement of ACPR and EVM is relatively straightforward and common as both of these FOMs have been widely used in industry. However, as EVM is proposed for modulated excitation signals with pre-defined symbols initially, a modified EVM measurement standard and procedure will have to be defined for a multi-sines stimulus that has no such symbols.

4.3 **Adaptation of ACPR and EVM**

Based on above analysis, EVM and ACPR are selected as FOMs for further investigations into the achieved similarity between designed multi-sines the original communication signal. However, these two

figures of merit were originally not proposed for multi-sines, making it challenging to measure EVM and ACPR with multi-sines as the stimulus signal. For example, EVM is calculated by comparing a measured signals' symbol constellation diagram with an ideal or "reference" constellation diagram, which is calculated from a known transmitted data stream, the symbol clock timing, and baseband filtering parameters. These parameters are only defined in the context of modulated signals and not necessarily defined for multi-sines. Figure 4.10 gives a comparison of the constellation diagrams.

Hence a modification of ACPR and EVM measurement standard is necessary. For ACPR, it is relatively easy as multi-sines have a similar power spectrum to that of a communication signal. The only required modification is change of the measurement bandwidth within neighbouring channel; with specified bandwidths in table 4.1. Taking the IS-95 CDMA specification as an example it uses a bandwidth of 30KHz. However, the space between multi-sines spectrum components is often larger than 30 KHz. Taking this into account, the same bandwidths will be used for the main and adjacent channel for further investigations within this work, e.g. using a 1.23MHz bandwidth for signals approximating the IS-95 CDMA standard.

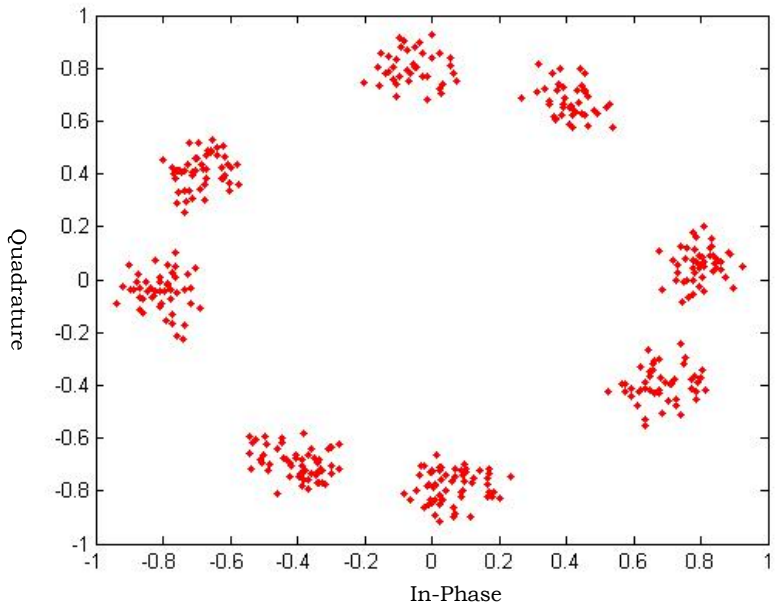

(a)

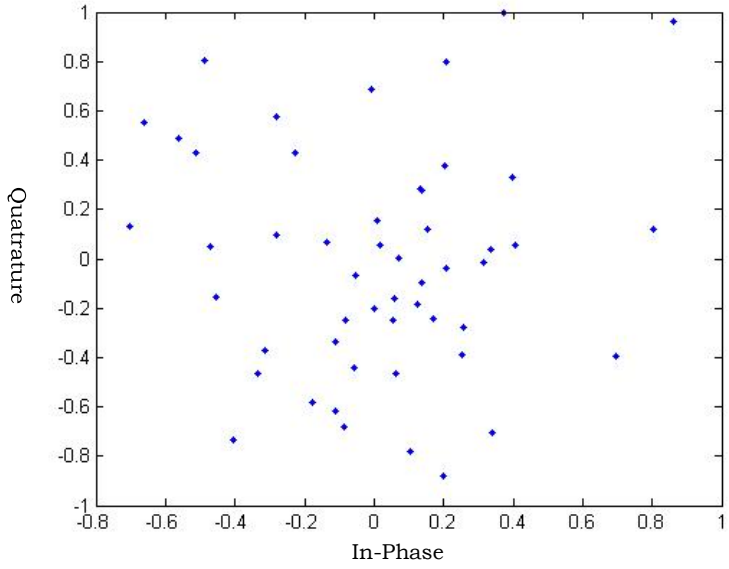

(b)

Figure 4.10 Symbol constellation diagram for a 8PSK signal(a) and multi-sines(b). Obviously multi-sines has no pre-defined symbols which leads to the difficulty of EVM measurement

For the adaptation of the EVM measurements, one possible solution is to directly use the sampling points instead of the instance at which the symbol occurs. This change would be very suitable for the

investigations of multi-sines because of two main reasons. Firstly, according to our previous analysis, as long as we are measuring $EVM = \frac{\sqrt{E_{y_u y_u}(t)^2}}{\sqrt{E_{y_c y_c}(t)^2}}$ we will fully assess the distortion of a nonlinear device, and hence be able to evaluate if both the multi-sines and the original communication signals provide similar results. Secondly, this new definition is also compatible with the 3GPP standard definition, which does not necessarily require that EVM will be calculated utilising symbol constellations [2].

Taking a closer look at the multi-sines constellation diagram shown in figure 4.10, it can be seen that the multi-sines "symbols" are randomly located within the constellation plane. This is rather different for symbol constellations of N-PSK, common for present mobile communication standards, with well defined and constant amplitude values. Hence, when these multi-sines are used as a stimulus for nonlinear devices the received signals will have various degrees of distortion for symbols at different magnitude scales. This is illustrated at figure 4.11 where it can seen that symbols at larger magnitude scales will probably exhibit more severe distortions and therefore result in larger EVM values for multi-sine signals.

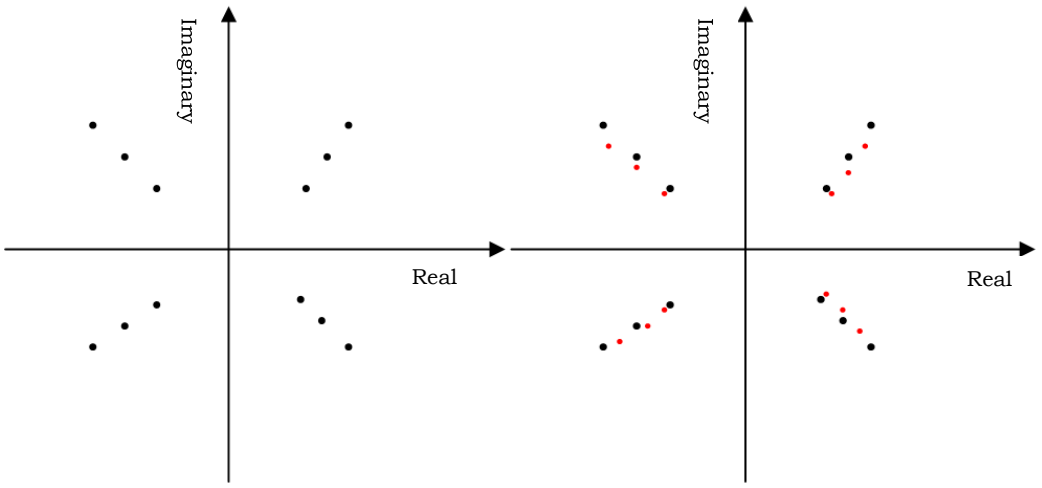

Figure 4.11 Error Magnitude constellation diagram.

(Black: Reference Signal Constellation diagram; Red: Distorted Signal Constellation diagram)

Moreover, when calculating EVM some of the error vector is due to the un-correlated distortion and the correlated distortion such as gain compression. Hence, a simple RMS average over all the sampling points will also obscure the difference between both distortion parts. To further demonstrate this effect mathematically, the un-correlated distortion $E_{y_u y_u}(t)$ that is acquired during EVM measurements can be also expressed as the output signal $y(t)$ minus a linearly scaled version of input signal $k \cdot W(t)$ with k representing here the gain of the measured device or amplifier. Thus, the EVM expression can be written as

$$E_{y_d y_d}(t) = y(t) - k \cdot W(t) \qquad EVM = \frac{\sqrt{(y(t) - k \cdot W(t))^2}}{\sqrt{(k \cdot W(t))^2}}$$

(Equation 4.9)

Unfortunately, the amplifier gain is not constant and might vary during the measurement process. As it is difficult to acquire the exact instantaneous gain of the non-linear system (a feed-forward loop is not easy to setup and may not follow the distortion instantly), the acquired $S_{y_u y_u}(t)$ may either underestimate or overestimate the un-correlated distortion. In other words, the correlated distortion will be either considered as an additive noise component that is increasing the uncorrelated distortion or as a useful part of the signal.

A possible solution to address this issue is to calculate the EVM according to the signal's time domain instant output power to minimise the impact of gain compression. This solution is based on the assumption that the gain of power amplifier will keep constant for the same output power. Hence the correlated distortion will be seen as a useful part of the signal and EVM will only assess the additive noise component, i.e, the un-correlated distortion. This solution will be further investigated in the following chapter employing EVM results using both the traditional and amplitude-related methods.

4.4 Conclusion

In this chapter, common FOMs were described and their function for the evaluation of nonlinear distortions was examined including a brief introduction of required measurement setups for their characterisation. According to the analysis, a combination of both ACPR and EVM will provide a clear determination of the correlated in-band distortion, uncorrelated in-band distortion and uncorrelated

out-of-band distortion. Therefore, the combination of both FOMs will allow for a full assessment of the excited distortion.

As EVM was initially proposed especially for modulated signals with pre-defined symbols, its adaptation for multi-sines is suggested by taking every sampling point within the multi-sines instead of the symbol instant. The applicability of these changes will be verified through a number of measurements that will be carried out within the next chapter.

4.5 Reference:

[1] Cripps, S. C., "RF Power Amplifiers for Wireless Communications", 2nd Edition, Artech House Publishers, 2006

[2] 3GPP TS 25.141 version 6.6.0 Release 6, Technical Specification, 3rd Generation Partnership Project, Technical Specification Group Radio Access Network, Base Station (BS) conformance testing (FDD) (Release 6).

[3] J. C. Pedro and N. B. Carvalho, "On the use of multitone techniques for assessing RF components' intermodulation distortion," IEEE Trans. Microwave Theory Tech., vol. 47, pp. 2393–2402, Dec. 1999.

[4] J. C. Pedro and N. B. Carvalho, "A novel set-up for co-channel distortion ratio evaluation," in IEEE MTT-S Symp., Boston, MA, June 2000.

[5] L. West, "The effect of preamplifier compression on measured noise power ratios," IEEE Photonics Tech. Let., vol. 12, pp. 924–926, July 2000

[6] Khaled M. Gharaibeh, "On the relationship between the noise-to-power ratio (NPR) and the effective in-band distortion of WCDMA signals". International Journal of Electronics and Communications.

[7] J. C. Pedro, N. B. Carvalho and P. M. Lavrador, "Evaluation of signal-to-noise and distortion ratio degradation in nonlinear systems," IEEE Trans. Microwave Theory Tech, vol. 52, pp. 813–822, March 2004

[8] R. Pintelon and J. Schoukens, System Identification: A Frequency Domain Approach. New York: Wiley-IEEE Press, 2001

[9] J.C.Pedro, Nuno Borges de Carvalho , "A novel set-up for co-channel distortion ratio evaluation," IEEE MTT-S Int. Microwave Symp. Dig., Boston, MA, June 2000, pp.1851–1854.

[10] A. Geens, Y. Rolain, W. Van Moer, K. Vanhoenacker and J. Schoukens, "Discussion on fundamental issues of NPR measurements," IEEE Trans. Inst. and Meas., vol. 52, pp. 197–202, Feb. 2003.

[11] J. C. Pedro, N. B. Carvalho and P. M. Lavrador, "Modeling nonlinear behavior of band-pass memoryless and dynamic systems," Int. Mic. Symp., vol. 3, June 2003, pp. 2133–2136.

[12] Michael D. McKinley, Kate A. Remley, Maciej Myslinski, J. Stevenson Kenney, Dominique Schreurs, and Bart Nauwelaers2, "EVM Calculation for Broadband Modulated Signals" 64th ARFTG Conference.Digest, Orlando, pp 45-52, Dec.2004

[13] Agilent Application Notes, "8 Hints for Making and Interpreting EVM Measurements", available on Agilent Website.

[14] Osvalod.Mendoza, "Measurement of EVM (Error Vector Magnitude) for 3G Receivers". Master Thesis of Chalmers University of Technology, 2002, available online at: http://citeseerx.ist.psu.edu/viewdoc/download?doi=10.1.1.16.1325&rep

[15] Khaled M. Gharaibeh, Kevin G. Gard and Michael B. Steer, "Accurate Estimation of Digital Communication System Metrics — SNR, EVM and ρ in a Nonlinear Amplifier Environment", 64th ARFTG Conference.Digest, Orlando, pp 41-44, Dec.2004

[16] Agilent, "Digital Modulation in Communications Systems — An

Introduction" Agilent application notes 1298,available online.

5 Measurement based verification of multi-sines design procedure

The previous chapter introduced the two figures of merit, ACPR and EVM, for the evaluation of the device's nonlinear behaviour and also to re-define these figures for multi-sines excitations. According to the discussion, combined ACPR and EVM will provide us with a complete insight into nonlinear behaviour; hence, in this chapter we will measure ACPR and EVM for the same nonlinear device under both multi-sines and its approximated communication signal exitations. The idea is that if the desired multi-sines are capable of replacing communication signals in nonlinear device measurement systems we should acquire similar ACPR and EVM values for both multi-sines stimulus and modulated signal stimulus at different power levels. This chapter will firstly introduce the necessary measurement setup, after that the measurement results will be shown which clearly demonstrate that our designed multi-sines have accurately approximated our communication signals.

5.1 Measurement setup

5.1.1 Hardware Architecture

There are a number of instruments based on the National Instrument (NI) PXI system that we are using as the platform to obtain measurements in this chapter. This is firstly because all the other instruments that were present in our laboratory, during these investigations, can only generate multi-sines with a maximum of 64

tones. This is not enough to accurately approximate modulated signals; the resulting multi-sines will require a larger number of tones. Secondly, the NI instruments employing a "Virtual Instruments" technique, which means we can readily create a measurement system, which meets our exact application needs.

The main instruments we are using in this work are a NI PXI-5441 AWG, which will generate the baseband signal, a PXI-5610 Up-Converter is used to shift the baseband signals to an RF frequency. On the signal receiver side, a NI PXI-5600 Down-Converter combined with a PXI-5142 DSP unit acts as a vector signal analyser. Apart from these main instruments, the measurement system also includes a PXI-1045 chassis and a PXI system embedded controller. The whole system is shown in figure 5.1.

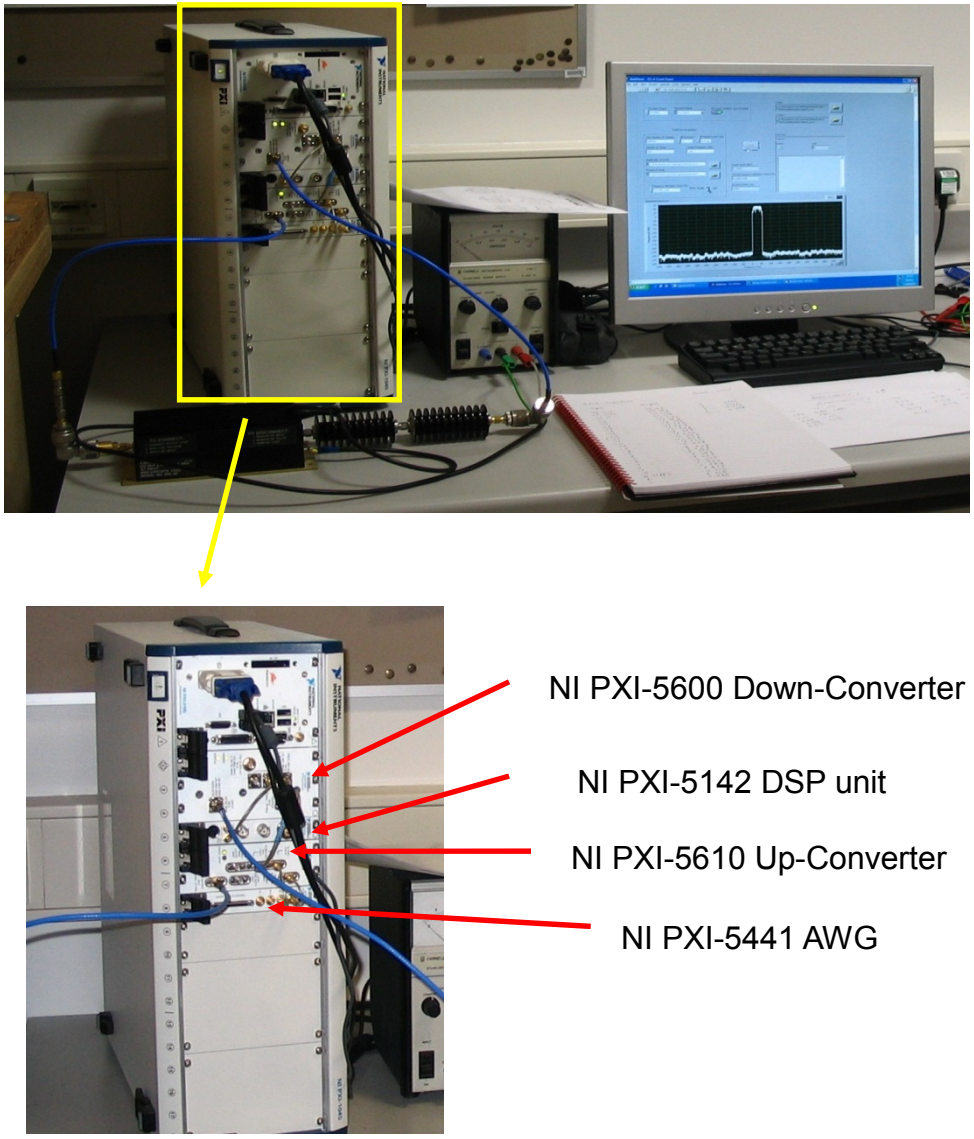

Figure 5.1 The Photos of NI measurement instruments.

The user-defined measurements are realized using NI Labview, which is a program development application much like various commercial C or Matlab development systems. However, it is different from those applications as most other programming systems use script-based languages to create lines of code while Labview uses a graphical programming interface to create programs in block diagram format. The created programs are called virtual instruments (VI) because their appearance and operation imitate actual instruments. As a

result, software that is based on user requirements defines general-purpose measurement and control hardware functionality, so we can create our own systems that meet our exact application needs. This is especially advantageous for these investigations as it allows the calculation of the re-defined ACPR and EVM, which is slightly different from the traditional algorithms. Figure 5.2 graphically illustrates the relationship between Labview and NI instruments.

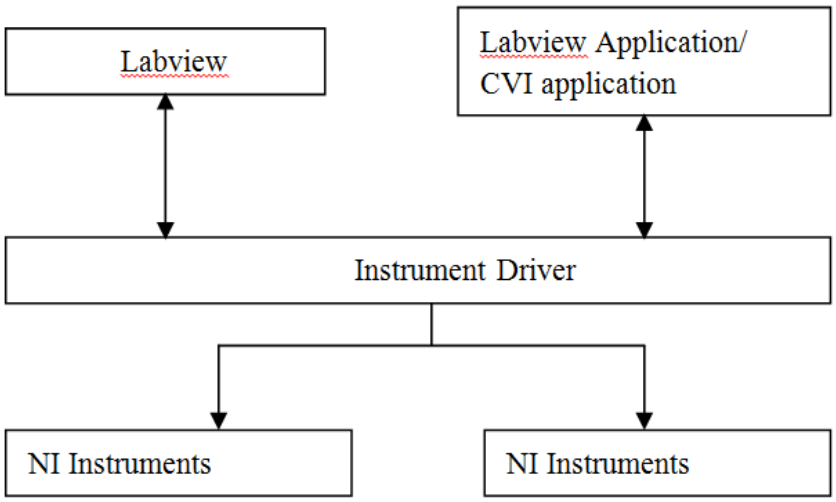

Figure 5.2 The relationship between Labview and National Instruments devices

NI Labview application consists of two interfaces, Block Diagram and Front Panel. Block Diagram is where all the programming codes are implemented as a graphical programming environment while the Front Panel is a Graphical User Interface (GUI) where all required tests are controlled, such as the start and conclusion of tests and presentation and analysis of data. Figure5.3 gives a quick snapshot of the developed Labview programs.

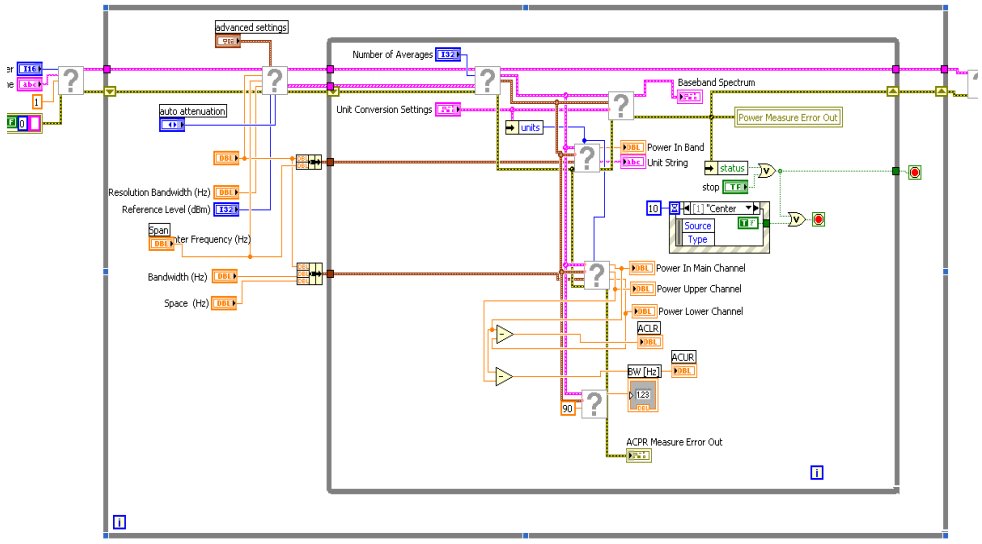

Fig 5.3a Labview Application: Block Diagram

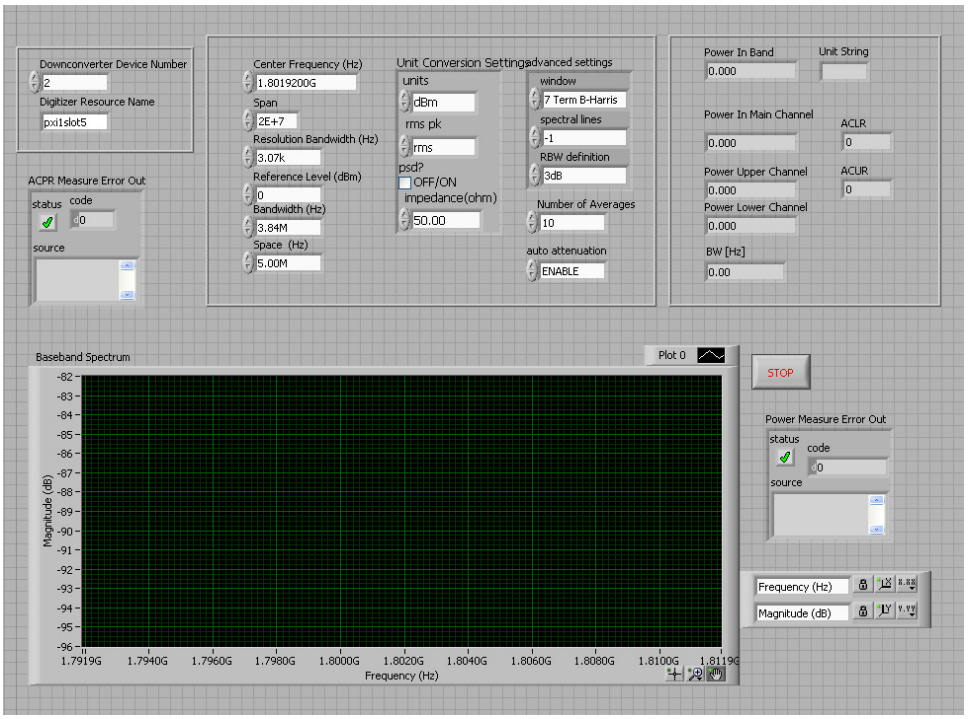

Figure 5.3b Labview Application: Front panel

5.1.2 Test signal generation

To investigate the capability and the adaptability of the proposed multi-sines design approach, we employ three different

communication signals as target signals for multi-sines. Table 5.1 summarizes their Power Peak to Average Ratio (PAPR) and bandwidth.

	Type	PAPR	Band-Width
Signal 1	3GPP uplink signal	3.6dB	3.84MHz
Signal 2	IS-95 CDMA signal	5.53dB	1.2288MHz
Signal 3	3GPP WCDMA test model 1	8.7dB	3.84MHz

Table 5.1 the specification of test signals

As the modern modulated signals usually have high PAPR, it might be considered as insignificant to employ a stimulus signal with low PAPR as is the case with signal 1. However, the often-utilised two-tone signal has a 3dB PAPR and as such a communication signal with 3.6dB PAPR is considered to represent the lower PAPR boundary of the investigated multi-sines design approach. Despite many of the communication signals having a PAPR as high as 16dB or even 20dB actually many researchers within the communication system field are investigating PAPR reduction techniques as high PAPR can seriously affect the power efficiency of the whole communication system. These techniques have been matured enough to successfully reduce the signal's PAPR to less than 9dB. Therefore, a communication signal with 8.7dB PAPR is chosen as the high PAPR boundary of our multi-sines design approach. Finally, to test multi-sines' ability to approximate modulated signals with medium amplitude variation, a third test signal was selected with a 5.53dB PAPR.

The selected test signals will test the new multi-sines approach for various bandwidths. The selected signals include a relatively narrow-band signal with a bandwidth of 1.288MHz and the wideband signals 1 and 3. The idea is that our selected test signals should cover most of the modulated signals, which a nonlinear device would process in a real-world scenario.

The test signals were generated in Agilent Advanced Design System (ADS) with the help of the communication signal library. This library and its demo examples are usually situated under ADS installation directory with the name "WCDMA_3G_SignalSource_prj". The detailed introduction of this library and other specifications about generating real WCDMA signals can be found in references [1]-[4]. Figure 5.4 gives a snapshot of the ADS schematic and the more detailed schematics can be found in the appendix.

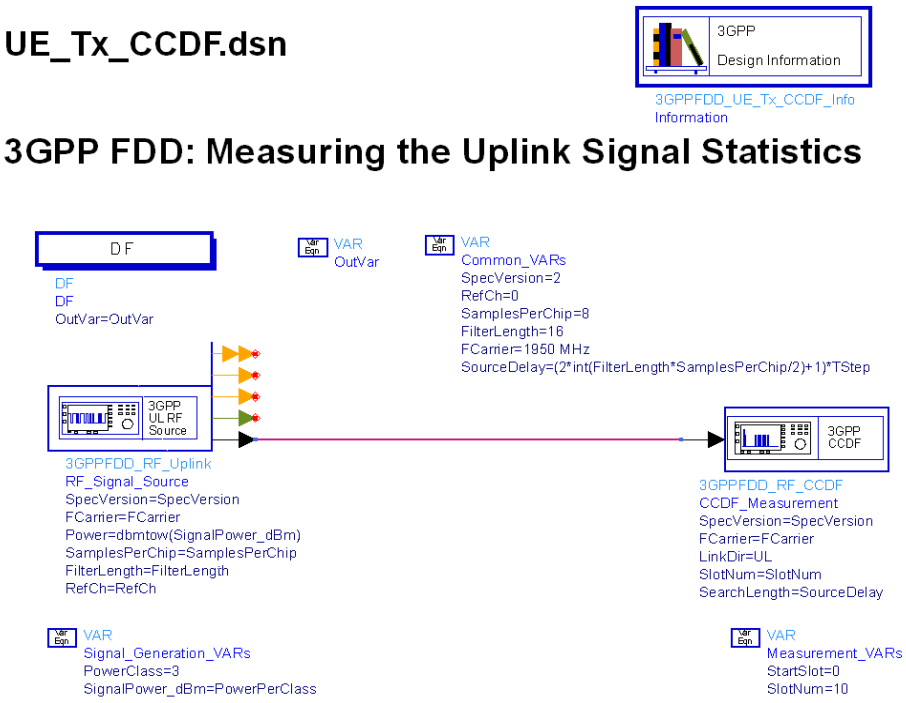

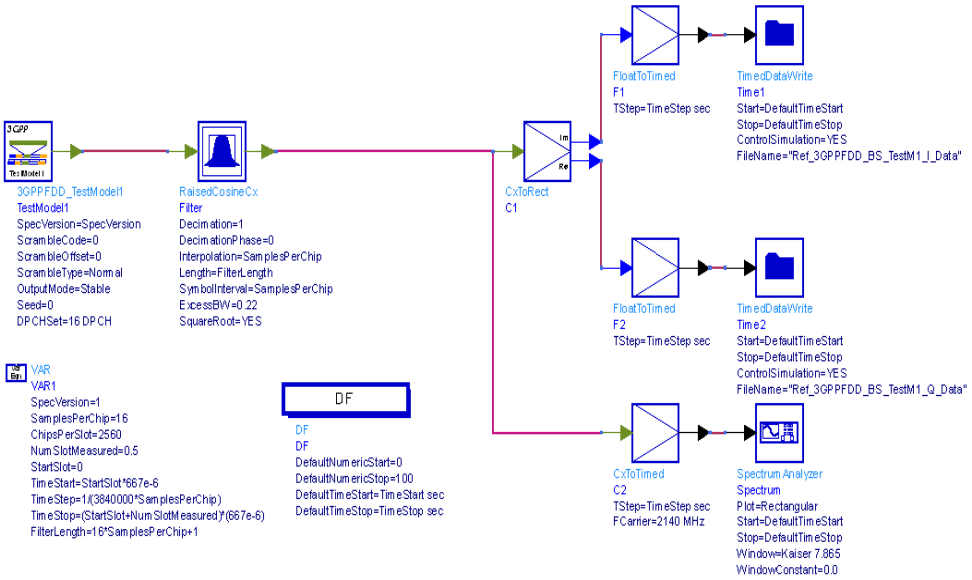

Figure 5.4 The ADS schematic of generating target modulated communication signals

The generated signals are discrete digital signals with the sampling frequency being four times higher than their bandwidth to provide an accurate representation. Due to the random nature of communication signals, determination of a suitable duration of the truncated communication signal is necessary. This can be tackled by continuously increasing the durations of the original signal until the statistical characteristics of the signals, such as CCDF, converge.

The ADS design schematic also saves the generated signals into text files. Those files are then imported to Matlab since the multi-sines design algorithm is implemented within the Matlab environment. The Matlab algorithms provide a series of multi-sines, which have the same number of sampling points as the communication signals.

Unfortunately, the Matlab software is unable to communicate with National Instruments (NI) hardware directly. Hence two VIs (Virtual Instruments) have been developed to translate the generated signals into waveforms that the NI signal generator can understand. These two VIs have different functions. The first directly reads I and Q waveform information from text files exported by Matlab and uploads these waveforms to the signal generator. The second VI passes the multi-sines parameters such as the amplitudes, phases and frequencies to the signal generator enabling the gereration of the multi-sines. These parameters, before being sent to the NI signal generator, have been converted into the format that the NI signal generator understands. For example, the amplitudes of each tone within the multi-sines need to be converted from the linear domain into logarithmic domain ,i.e. dBm, to facilitate a correct interpretation by the instruments. A translation of the phase parameters, from radians to degrees, is also needed. All these VI files are included in the appended CD as reference. Figure 5.5 provides a flow graph to illustrate the test signal generation process.

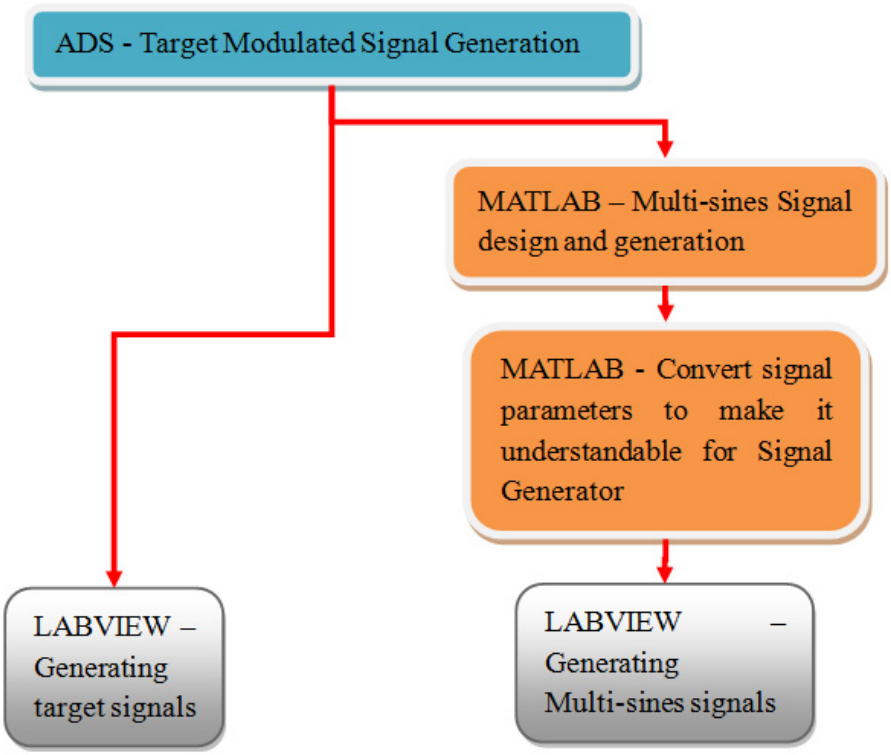

Figure 5.5 The flow graph of generating test signals

5.1.3 Device Under Test

An ideal PA should be as linear as possible within a given bandwidth. However for this project, we need a PA which would display both light and strong distortion during its operation, or in other words, we need a "bad" PA from the traditional point of view. With this PA, we are able to observe the nonlinear behaviour gradually getting more pronounced for an increasing stimulus of both multi-sines and wireless modulated signals. Another criteria for choosing the PA was the stability as some PAs, if not being destoried, would behave with degraded performance after working in severe nonlinear modes of operation. With this in mind, an unlinearized HP Power Amplifier

83020A was employed as the DUT (Device Under Test). The gain compression characteristic of this PA is displayed at figure 5.6. It can be seen that it works upto the 12dB compression point, with the 1dB compression point located at 30.6 dBm output power.

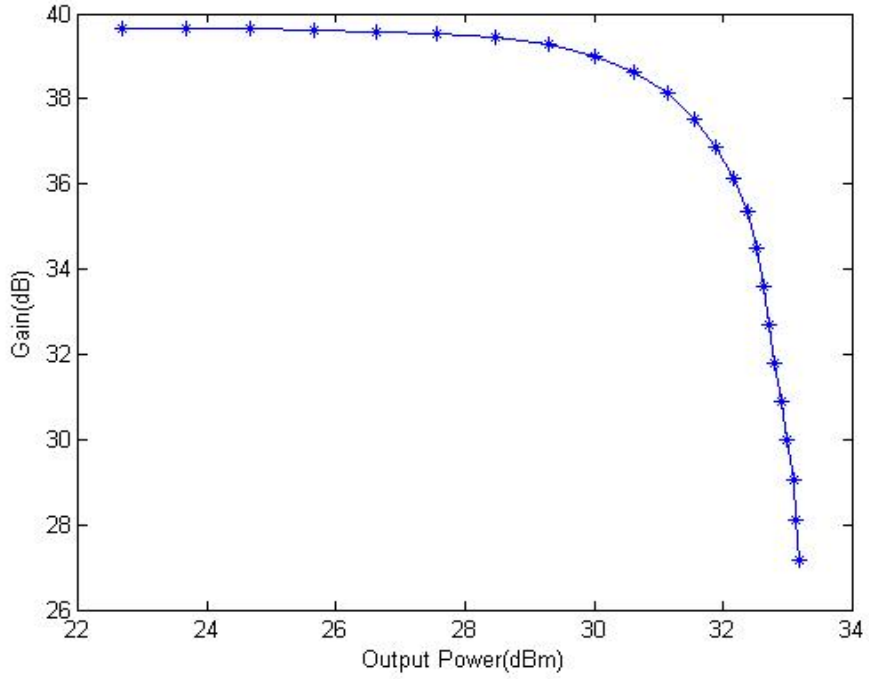

Figure 5.6 The Compression Characteristics of the DUT HP83020A

It is noticed that this DUT is not the only component in the measurement system which can introduce nonlinear distortions. Many other components, such as the attenuators, couplers, and RF components inside the signal generator and signal analysers introduce different degrees of nonlinear distortion at the same time. This is not even including the impedance mismatch, system frequency response and leakage signals. All of these factors would lead to a certain amount of distortion and hence influence the accuracy of the measurement. However, as our objective in this project is characterizing of the RF system's nonlinear distortion it is not necessary to distinguish between the various distortion factors.

Furthermore, the measurements can be directly compared as long as the two stimulus signals are exciting the same measurement system under the same condition.

5.1.4 Signal Analyser

As discussed in chapter 4, we modified the definition of the ACPR figure-of-merit for the analysis of the multi-sines exitation. To make this analysis practical the adjacent channel bandwidth is the same as the main channel bandwidth. This is a relatively simple modification and can be easily implemented in the Labview Virtual Instruments. However for EVM measurements, more work needs to be done to cater for the requirements of multi-sines excitation.

One issue is the synchronisation between the reference signal and the measured signals. The modulated signals have pre-defined symbols, so no matter where we start to sample the signals, the positions of acquired symbols in the symbol constellation diagram are constant. However for multi-sines, which have no predefined symbols, an algorithm must be designed to find the optimal observing position to minimise the EVM, otherwise two completely different constellation diagrams will appear which will leads to the wrong EVM measurement results.

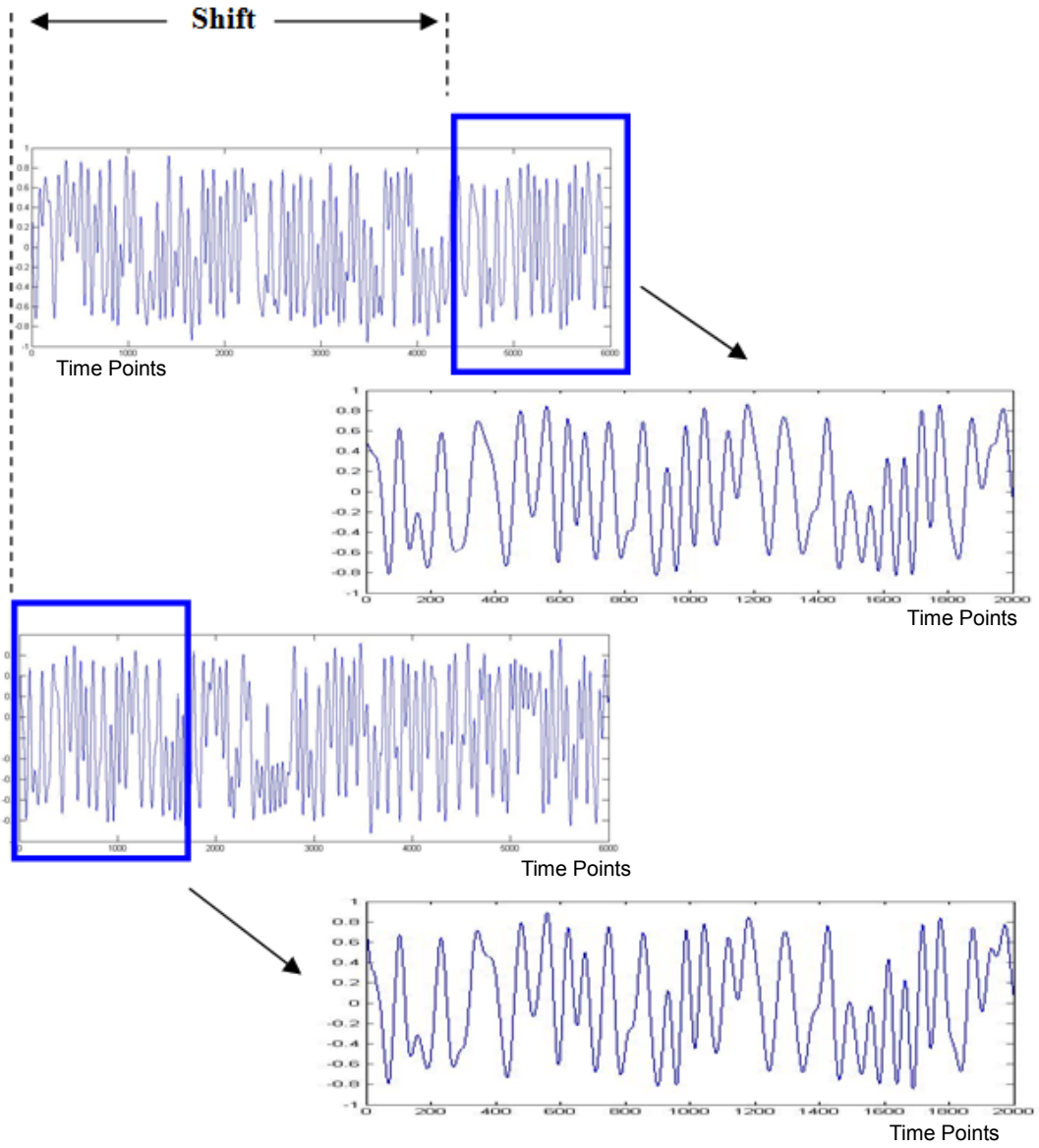

Figure 5.7 A synchronization process is needed to synchronize the time window between reference signal and measured signal

Figure 5.7 shows the non-synchronous reference signal and measured signal in the time domain. Figure 5.8 shows the comparison in I-Q constellation diagram between these two signals. As can be seen in figure 5.8a, the reference signal and measured signal are non-synchornized hence the Error Magnitude cannot

reflect nonlinear distortion of DUT. Figure 5.8b shows the measured signal and reference signal after synchronization process by which Error Magnitude has been minimised in accordance to 3GPP organization's definition of EVM measurement.

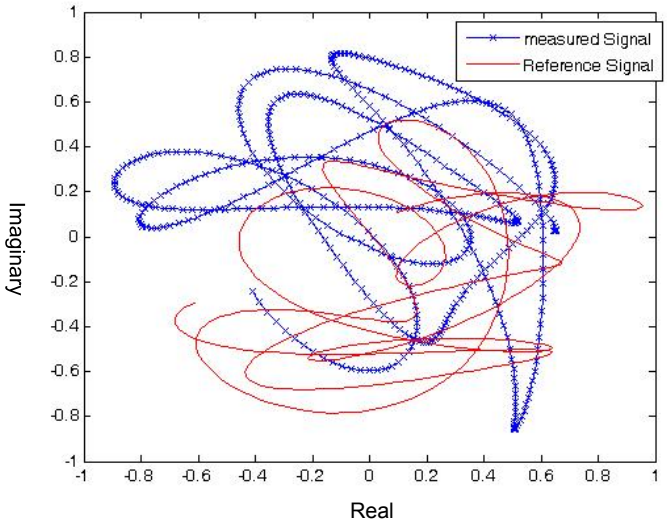

Figure 5.8a The constellation diagram between received signal and reference signal

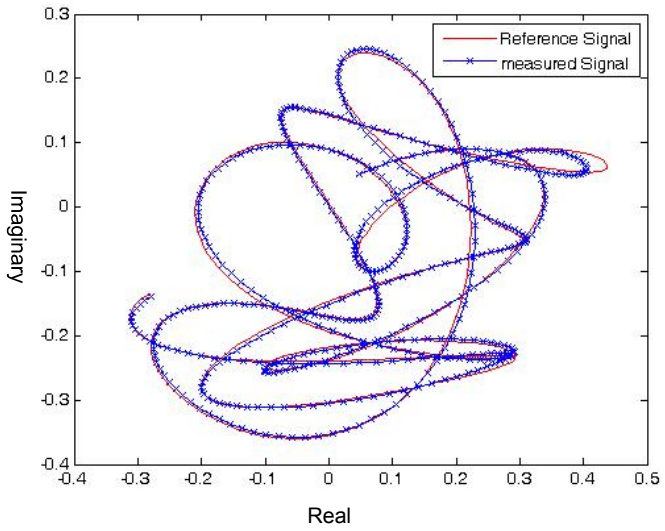

Figure5.8b The constellation diagram after synchronization process

Secondly, the RF signal is up-converted to an RF frequency to excite the DUT and then is down-converted by an RF local oscillator (LO). If

the LO's frequency is not locked frequency offsets would be introduced. To eliminate those, we utilize the frequency shifting property of the Fourier transform, which can be written as:

$$F^{-1}\{F(w-w_o)\} = f(t)\exp(jw_o t)$$

(Equation 5.1)

It states that if F(ω) is shifted by w_o its inverse transform is multiplied by exp(j $w_o t$). Therefore, compensating for frequency offsets in the frequency domain can be achieved through phase rotation in the time domain.

It can be seen from the above discussion that the compensation algorithm is aiming to find the offset frequency w_o. To provide maximum accuracy, a global searching algorithm is employed to find the time shift and frequency offset. The drawback of this method is that it is probably the slowest method, especially compared to other adaptive convergence methods. However, as the target in this chapter is not to propose a fast and accurate measurement solution allowing for large-scale industry application but to verify that multi-sines stimuli are able to replace modulated signal stimuli in system testing, we decided to adopt this approach.

This post-measurement modification process is implemented in Labview along with the other necessary EVM calculation steps. Figure 5.8 also shows that the reference signals and measurement signals' I-Q diagram before and after adjustment. It is clearly shown that our synchronization and phase compensation process achieves

very good results. The overall signal processing flow is illustrated on figure 5.9

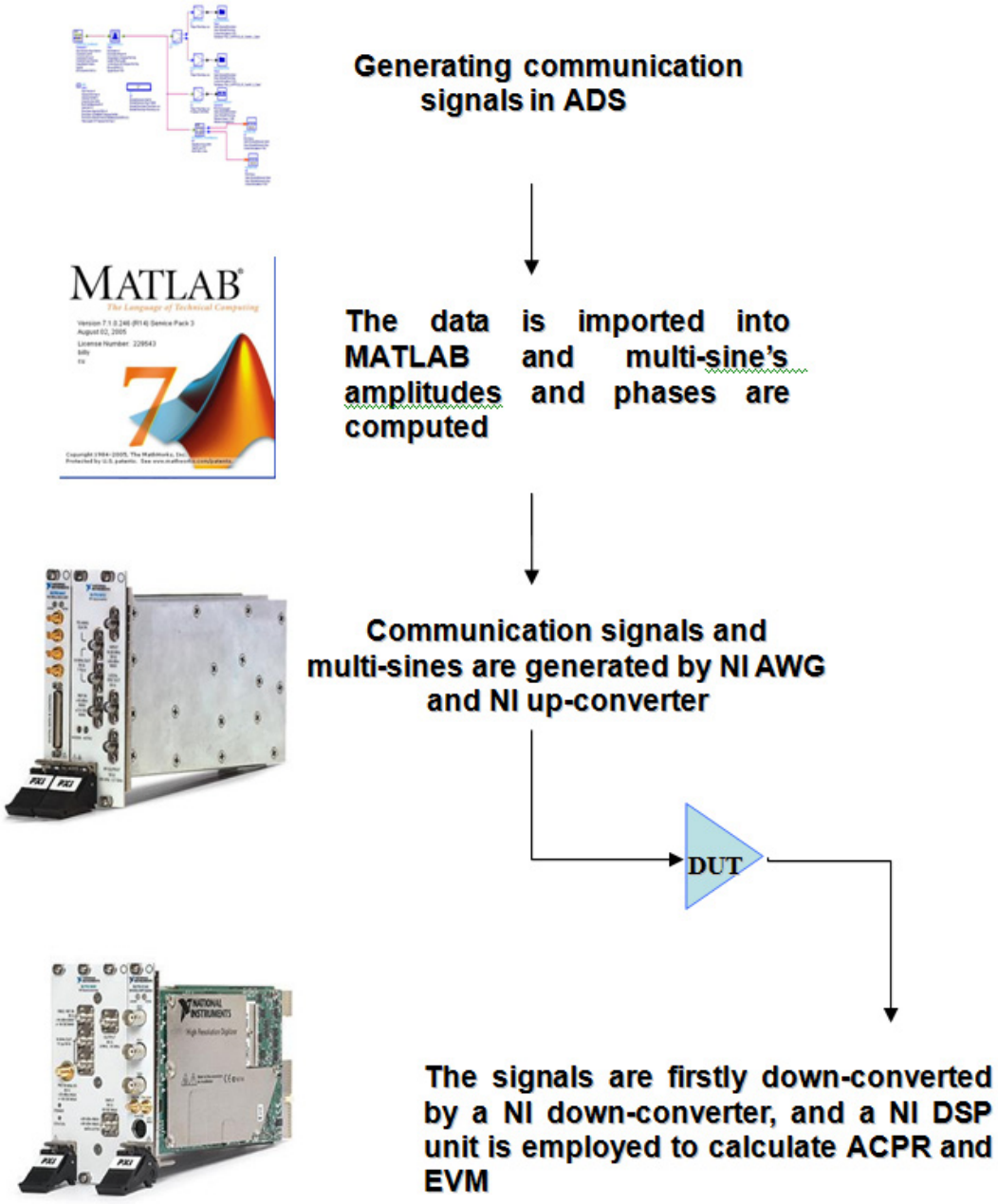

Figure 5.9 Measurement procedure and setup

5.2 Experimental verification of multi-sines as stimulus signal

5.2.1 Adaptability and accuracy verification of multi-sines with ACPR measurement

We have discussed various multi-sines design methods in chapter 2. As noted the random-phased multi-sines represent a relatively straightforward way to approximate communication signals with a Gaussian probability distribution. As a consequence, it has been widely used to investigate the nonlinear behaviour of devices. However, multi-sines generated with this method theoretically are incapable of approximating the modulated signals, which are statistically different from the Gaussian signals. To better illustrate that our multi-sines design method is capable of adapting to modulated signals with various shapes, we will generate a series of multi-sines using the random-phase method as a comparison.

We will start with signal 3, which is theoretically easier to approximate with random phase multi-sines than the other two signals since it has a Gaussian probability distribution. The initial analysis compares the statistical properties, such as CCDF, of test signal sets with the, multi-sines that are designed in two different ways; namely utilizing the random phase method and the approach as proposed in this work. The results are shown in figure 5.10. As can be seen, all these three test signal sets have similar CCDF curves. According to our previous analysis in chapter 3.2, this statistical similarity leads to comparable levels of nonlinear distortion, hence the three stimulus signals should have very similar ACPR results

when passed through the same DUT.

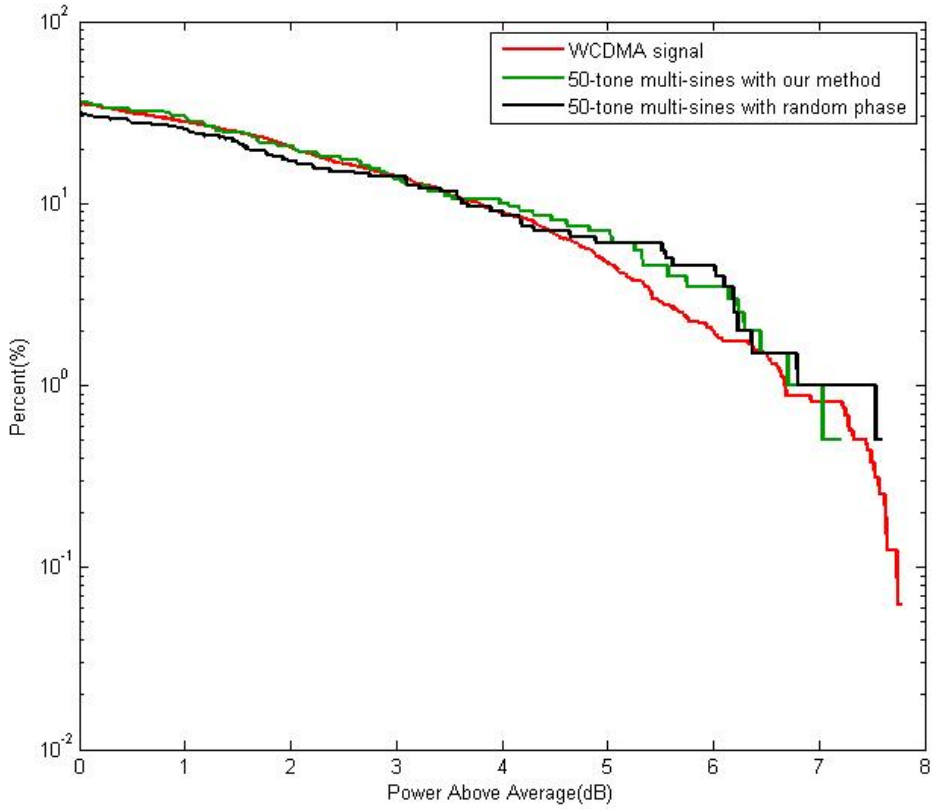

Figure 5.10 CCDF curves for signal 1 and its approximated multi-sines

This supposition is verified by the performed measurement with the ACLR for all three signals depicted in figure 5.11. As it can be seen, the output signals' ACPR at different output power levels agree with each other very well.

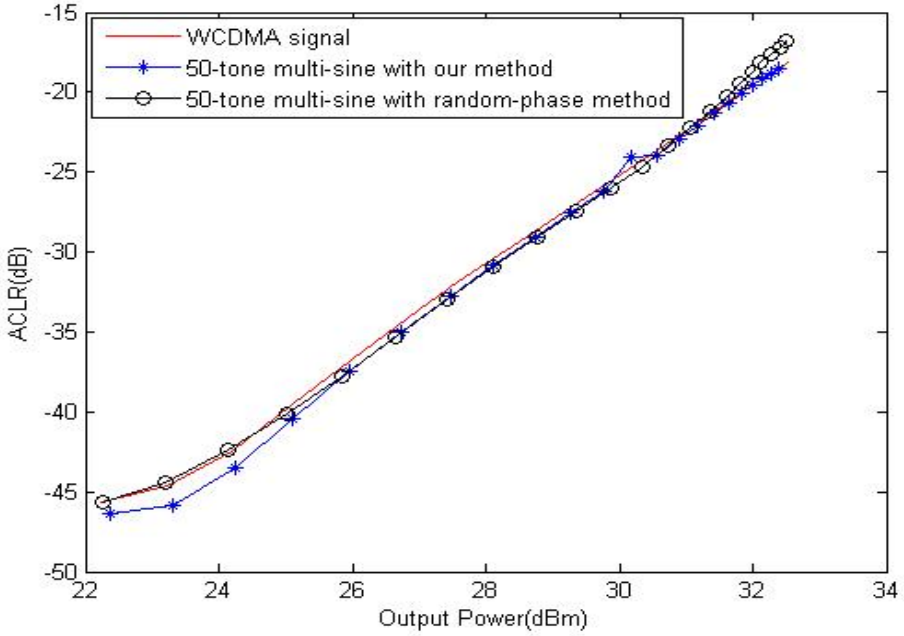

Figure 5.11 ACPR measurement results for signal 3 and its approximated multi-sines

Then we take signal 2 as the target signal to approximate. This signal has PAPR of 5.53dB and is therefore quite unlike Gaussian noise signals. A 50-tone multi-sines with our proposed method and a 50-tone random phase multi-sines were designed to approximate the target signal. Then these two multi-sines and original signal 2 have been set as stimulus of the DUT with the results shown in figure 5.12.

As it can be seen, the multi-sines designed with our method have closer CCDF curves to the target signal than the random-phase multi-sines, as it has not only the same maximum PAPR as the target signal, but the overall distribution of PAPR also agrees with the target signal very well. According to our previous analysis, the

statistical properties of PAPR will matter greatly for the nonlinear distortion, so our multi-sines would be expected to be a more accurate prediction of the ACPR than random-phase multi-sines. The measurement results shown in figure 5.13 verified our expectation.

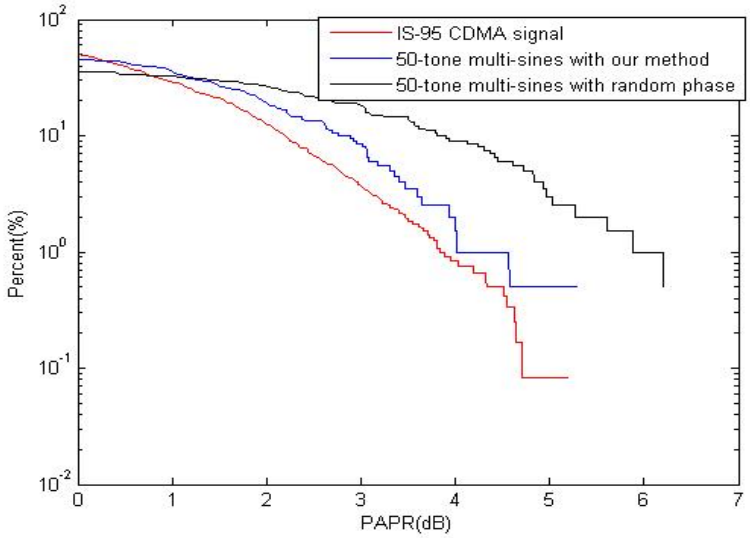

Figure 5.12 CCDF curves for signal 2 and its approximated multi-sines

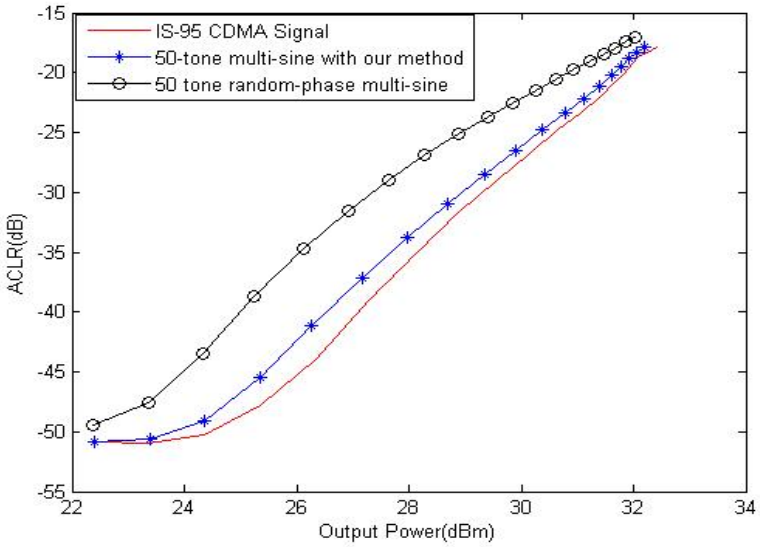

Figure 5.13 ACPR measurement results for signal 2 and its approximated multi-sines

Designing a multi-sines to approximate signal 1 is more difficult, as signal 1 has extremely low PAPR, which is very different from the

Gaussian signal. This is also demonstrated in figure 5.14 showing that the CCDF curves of multi-sines designed by random-phase method and target modulated signals are more separated. The multi-sines designed by our method is more similar to the target signal at lower PAPR values while at higher PAPR values there is still a clear difference. The following ACPR measurement results are shown in figure 5.15 and illustrate that the random-phase multi-sines is rather incapable of predicting the ACPR of the target signal while the second designed signal is predicting the distortions levels much better over the entire output power range.

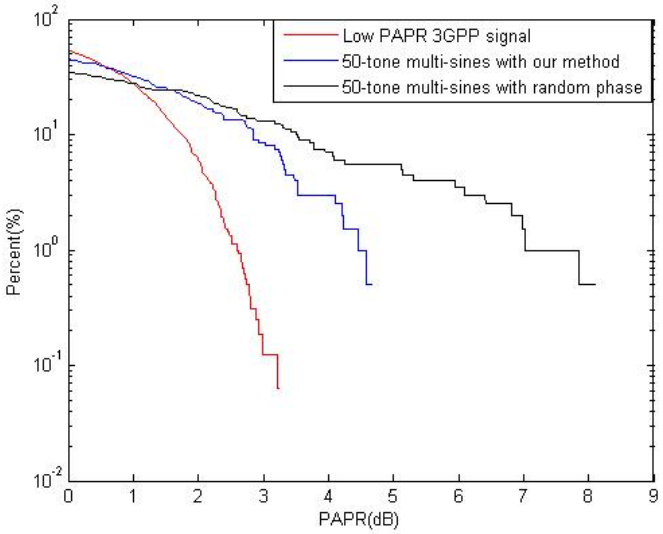

Figure 5.14 CCDF curves for signal 1 and its approximated multi-sines

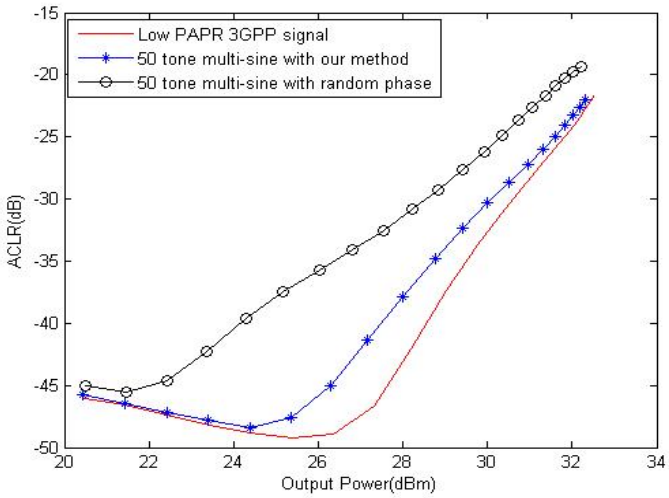

Figure 5.15 ACPR measurement results for signal 1 and its approximated multi-sines

So far there are 9 different signals that have been used to stimulate the DUT. By analysing their CCDF and resulting measured ACPR values over a range of power levels, our supposition that a signal's statistical descriptions, like the CCDF, have direct impact on the nonlinear distortion has been verified. Hence, the design of multi-

sines under the guidance of the statistical properties of the target signals has been confirmed as a correct approach.

From the above analysis, it can be seen that our multi-sines design procedure shows good adaptability to different target signals. Signal 3 is a CDMA signal with a wide bandwidth, high PAPR and CCDF that is similar to the statistical properties of Gaussian signal. For this signal, both the random phase method and our method predicted the ACPR very well. Signal 2 is an IS-95 CDMA signal with low bandwidth, low PAPR and a CCDF that is dissimilar to the characteristics of a Gaussian signal. Our method still accurately predicts the ACPR results with better than 2dB accuracy while the signal which is designed using the more common random-phase distribution generate differences of up to 10dB. Signal 1 is a wideband modulated signal with a wide bandwidth and very low PAPR, thus it is statistically very different to the Gaussian signal. For this signal, our method still achieved a relatively good approximation with maximum 5dB variation between the ACPR curves. In addition, the trend of the predicted ACPR curve follows the target signal well. This demonstrates the advantage of our multi-sines design procedure especially when compared with the more common random-phase multi-sines, which seems to be unable to predict the ACPR results of modulated signals.

5.2.2 Further verification of multi-sines performance with EVM measurement

According to our previous analysis, ACPR is not capable of fully assessing the device's nonlinear behaviour, hence EVM measurements are necessary to further verify if the designed multi-siness have excited similar, if not identical, nonlinear distortions.

For this investigation, the same stimulus signals have been utilized to measure EVM. As we discussed in chapter 4, a simple average of all error vectors when calculating the EVM of a multi-sines would produce erroneous results, the EVM is calculated using the instant amplitude level of the excitation signal. To illustrate this point, we will calculate the EVM employing both the traditional way of averaging all the error vectors and the new approach utilising the instantaneous amplitudes of the excitation signal.

Firstly, we measure the EVM with the test signal 1 and the two 50-tone multi-sines approximating it, which were designed with the random-phase and our own approach. The three signals, as we have shown earlier in figure 5.14, have very different CCDF curves. Hence, it can be expected that these three signals will excite different in-band distortions and thus lead to different EVM values. The results are depicted in Fig.5.16 over an increasing average input power. The figure shows that for the same average input power, the random phase multi-sines has higher EVM than the other two signals.

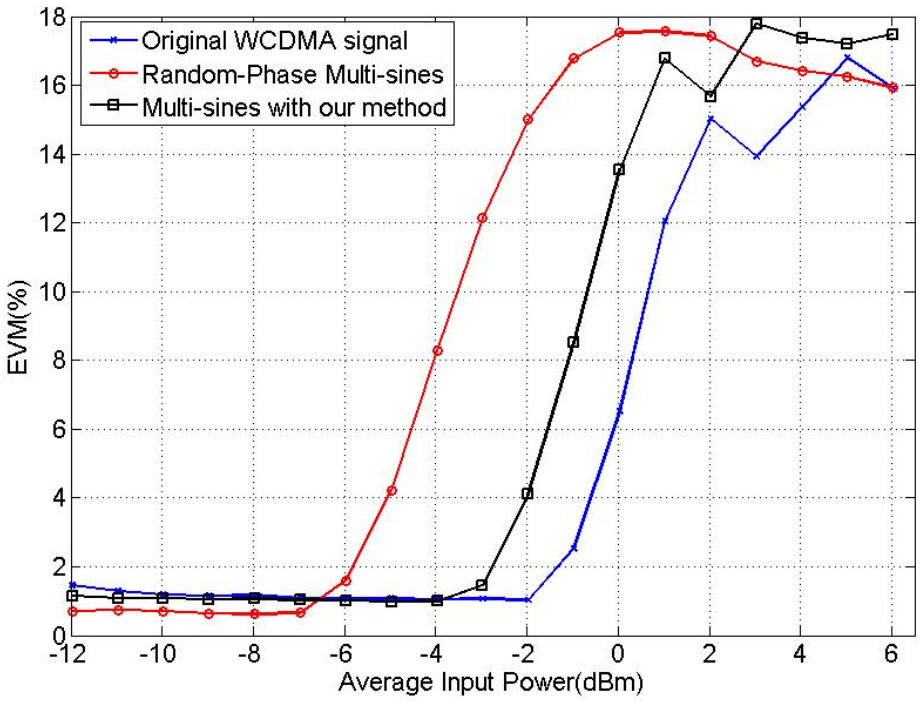

Figure 5.16 EVM measurement for Signal 1 and its approximated multi-sines drawn with average input power

However, drawing the EVM values according to the average input power may cover the fact that signals with higher PAPR, with respect to the same average input power value, will go into the compression zone earlier and hence cause higher EVM resulting in the strong separation between the three EVM curves in Figure 5.16. In this situation, the Error Vector is mainly caused by gain compression, which is the correlated part of the in-band distortion, with the consequence that the effective in-band distortion, as the uncorrelated part of distortion, is difficult to determine.

Hence, we also investigated another approach to display EVM results and plotted them over the signals' instant input peak power. The

acquired results are shown at figure 5.17. As we can see, this time the three stimuli lead to very similar EVM results, though theoretically the excited in-band distortions, which are introduced by these three stimulus, are very different.

This observation can be explained by the existing gain compression at peak levels, which tends to be the largest cause of in-band distortion. In addition, it is similar for all three signals and is effectively re-positioning the three curves at the same EVM values and therefore potentially covering any EVM differences due to the effective(un-correlated) in-band distortions.

In conclusion, we can see that no matter how we plot the EVM using the traditional ways of calculating we face difficulty in accessing the effective in-band distortion.

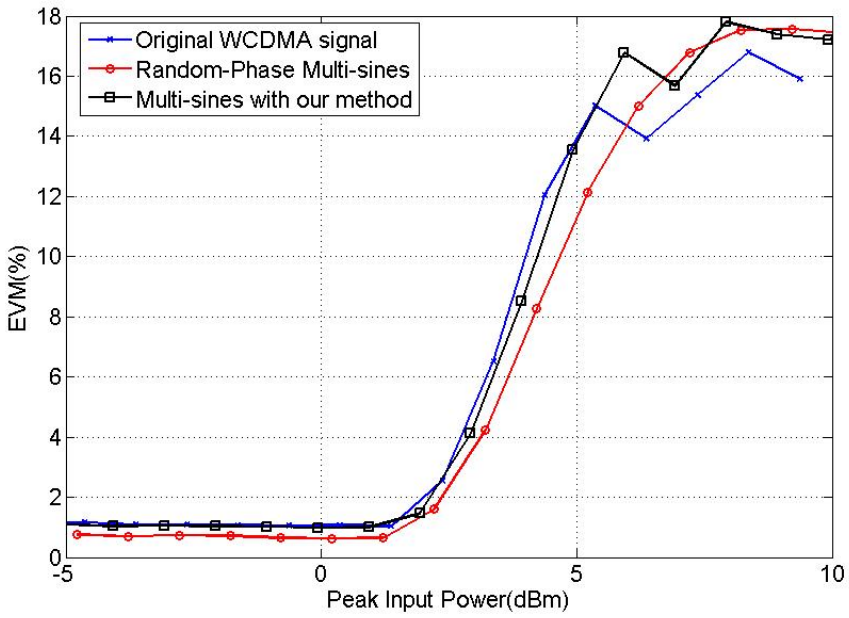

Figure 5.17 EVM measurement for Signal 1 and its approximated multi-sines drawn according to peak input power

As we discussed in chapter 4, a better way is to calculate the EVM according to their instant-power to average-power ratio, which is calculated as the power ratio between a waveform sample point and the average level of all sample points. This allows then also to access the impact of the power levels change.

The supposition here is that the gain will keep relatively constant within each power level hence the influence of gain can be neglected and the true un-correlated in-band distortion will become visible. The introduction of this calculation process can be found at chapter 4.3 and Figure 5.18 provides an illustration of how to split the signal according to its instant power.

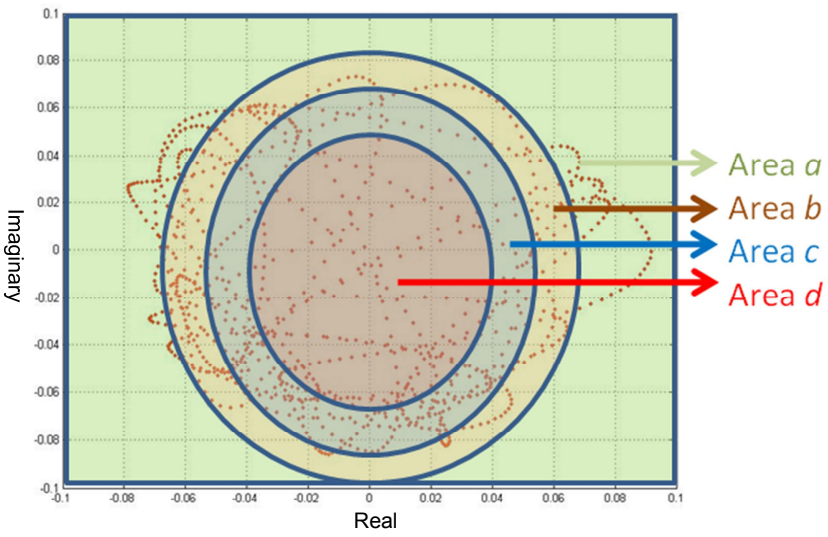

Figure 5.18 A rough illustration of the constellation diagram showing the spliting of the signal according to its instantaneous power

The results with this method are shown in Fig.5.19. Here, the impact on EVM has been grouped for all waveform samples into different levels, which are larger or smaller from the average values less than 1dB (Fig 5.19a), between 1 and 2dB (Fig 5.19b), between 2 and 3dB (Fig 5.19c) and between 3 and 4dB (Fig 5.19d). This calculated EVM results are obtained for a continuously scaled output power signal.

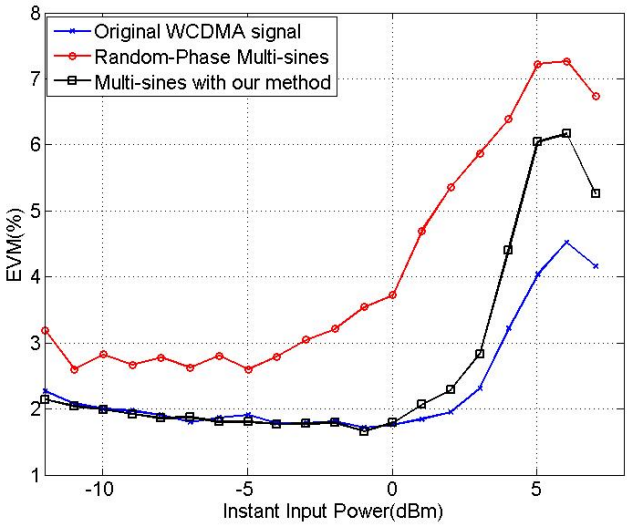

Figure 5.19a The EVM results of signal 1 and its approximated multi-sines with instant peak-to-average output power ratio less than 1dB

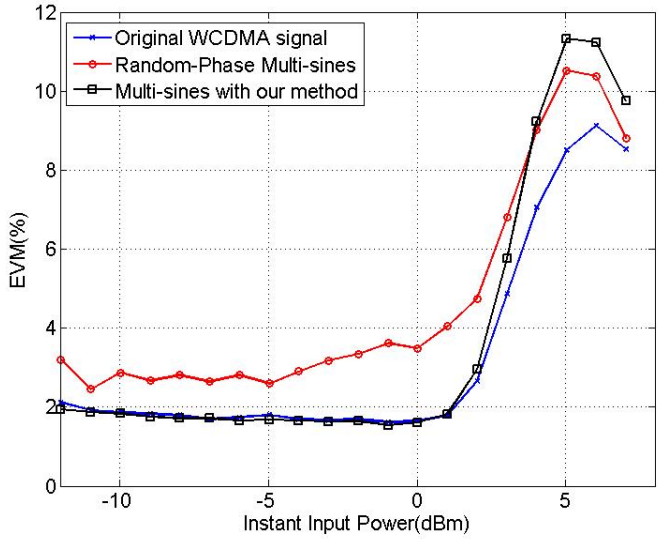

Fig.5.18b: The EVM results of signal 1 and its approximated multi-sines with instant Peak to average output power ratio between 1dB and 2dB

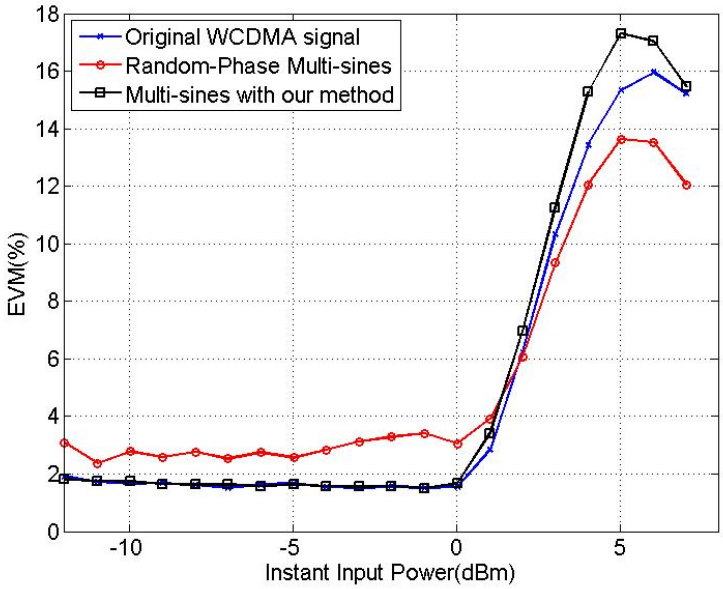

Fig.5.18c:The EVM results of signal 1 and its approximated multi-sines with instant Peak to average power ratio between 2dB and 3dB.

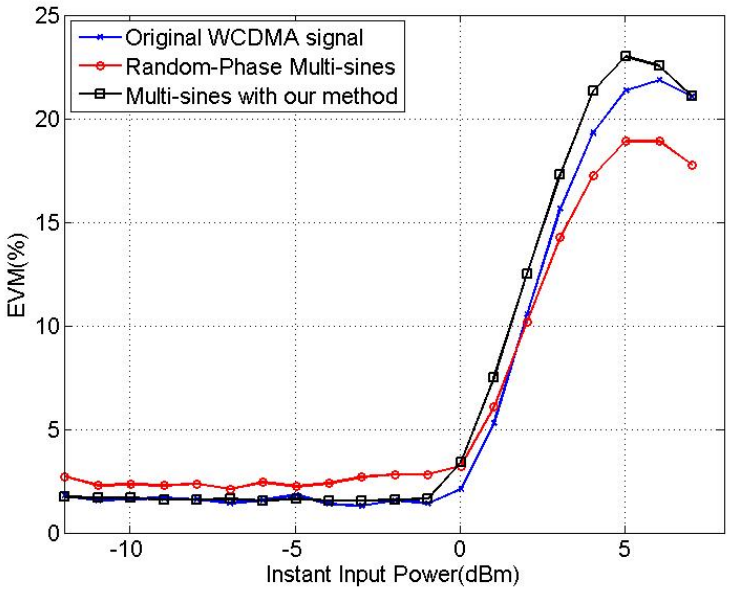

Fig.5.18d:The EVM results of signal 1 and its approximated multi-sines with instant Peak to average power ratio between 3dB and 4dB

As we can see, with the DUT entering into the compression zone the un-correlated distortion will become severer and hence we will see higher EVM values. However, the above figures clearly show that for different stimuli, the nonlinear device will behave differently even under the same level of gain compression. As can be seen, the EVM values are starting to rise almost at the same power level for these three stimuli, which means the DUT went into compression at almost the same drive level for each stimulus. However, their EVMs are well separated at higher output power levels. At lower drive levels there is only little difference between the traces from the original WCMDA and the 50-tone multi-sine signal while the random phase multi-sines trace exhibits an offset at all drive levels. This clearly indicates that the random-phase multi-sines stimulus will excite the device under test to generate more nonlinear response.

These figures verify that our multi-sines are suitable for replacing modulated signals as stimulus in a system testing over a large output power range. Our multi-sines achieved good results when compared to predicted EVM values and with actual modulated EVM values and are therefore capable of accurately predicting the un-correlated distortion that the device will generate under modulated stimulus.

To further verify the adaptability of our multi-sines design procedure, we will use test signal 2 and its approximate multi-sines as stimulus to re-measure the EVM. Signal 2 has 5.53dB PAPR, so the EVM measurement looks at 6 different instantaneous power levels, which are shown in Fig.5.19a-f. The shown results confirm again that our proposed design method allows to accurately predict the EVM performance of a DUT over a larger range of drive levels in comparison to previous multi-sines design approaches.

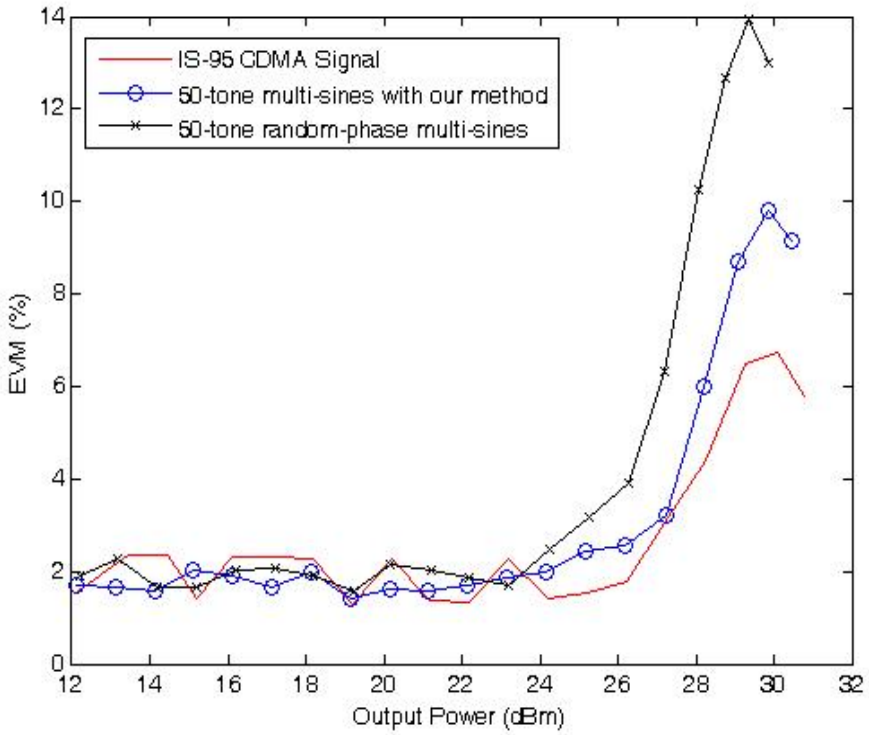

Fig.5.19a: The EVM results of signal 2 and its approximated multi-sines with instant Peak to average power ratio less than 1dB

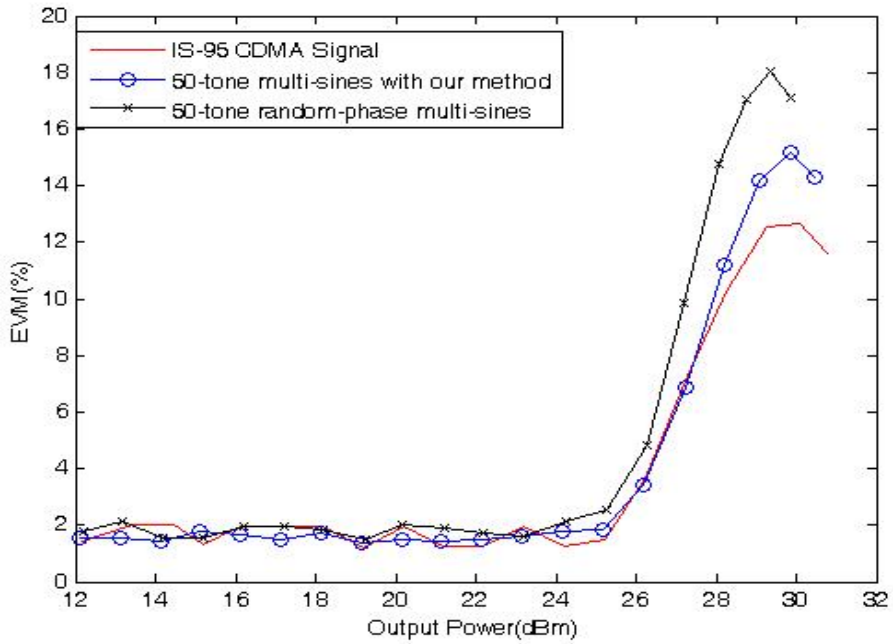

Fig.5.19b: The EVM results of signal 2 and its approximated multi-sines with instant Peak to average power ratio between 1dB and 2dB.

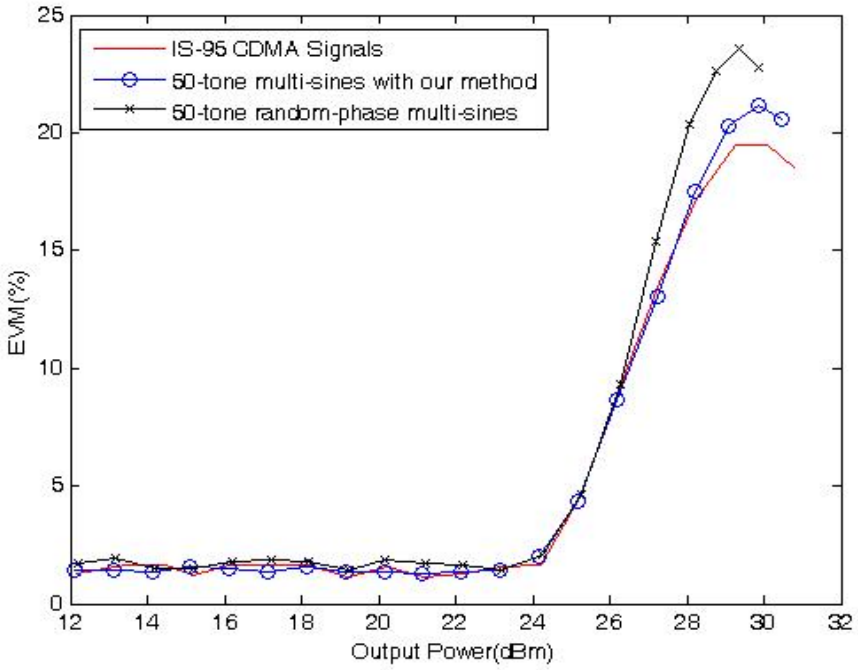

Fig.5.19c: The EVM results of signal 2 and its approximated multi-sines with instant Peak to average power ratio between 2dB and 3dB.

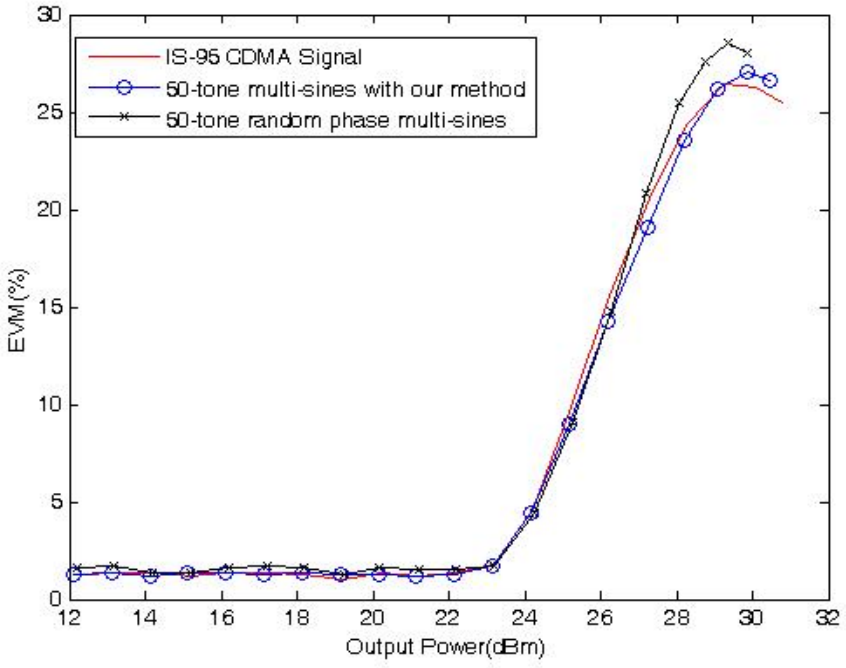

Fig.5.19d: The EVM results of signal 2 and its approximated multi-sines with instant Peak to average power ratio between 3dB and 4dB

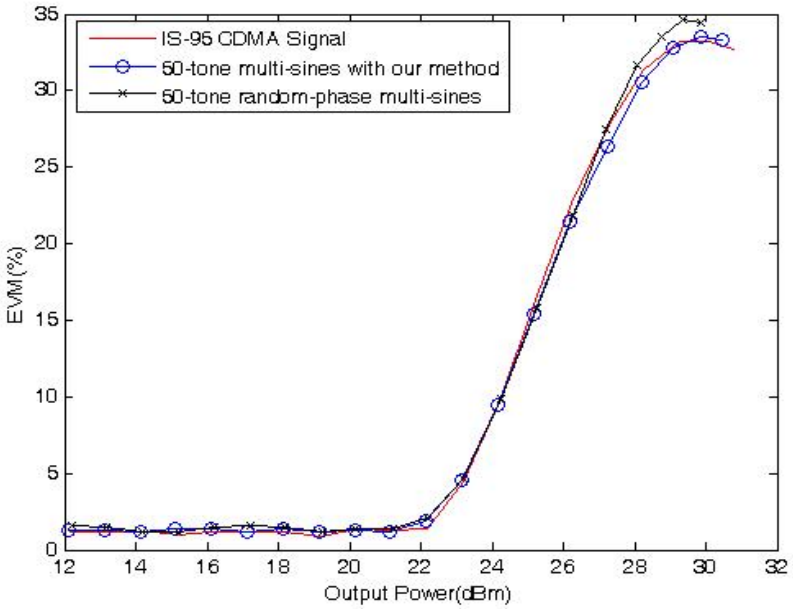

Fig.5.19e: The EVM results of signal 2 and its approximated multi-sines with instant Peak to average power ratio between 4dB and 5dB

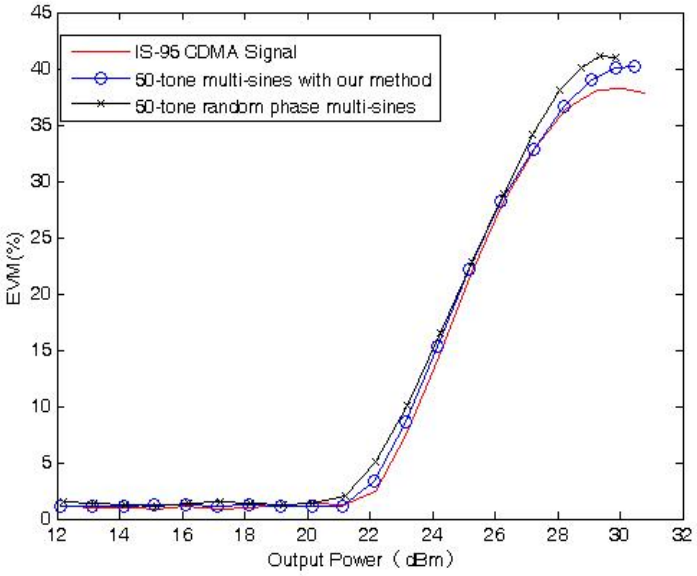

Fig.5.19f: The EVM results of signal 2 and its approximated multi-sines with instant Peak to average power ratio between 5dB and 6dB

5.3 Conclusion

In this chapter, we have experimentally verified that our proposed multi-sines could accurately predict both the ACPR and EVM performance of a nonlinear device when it is excited by a real modulated signal. In this experiment, communication signals with various PAPR are used as the target signals to test the adaptability of our multi-sines design approach. With communication techniques progressing rapidly, our proposed multi-sines design procedure is not only able to approximate modulated signals with current modulated schemes, but also capable of approximating future unknown modulated signals as long as their time-domain statistical descriptions are known.

6 Applying multi-sines to waveform measurement system --- A case study of the application of multi-sines stimulus

The primary aim of this research was to design and validate a multi-sines stimulus which is a sufficiently accurate representation of the original signal, such that its utilisation as a stimulus for non-linear devices will produce very similar non-linear signal components. It is however important to highlight a number of applications that have been extended through the implementation of multi-sines stimulus.

One such applications is waveform measurement and engineering, which aims to observe and modify in a quantified manner the time varying voltage and current components present at all terminals of the DUT, is becoming popular in the areas of RF power transistor characterisation/development and RF PA design/optimization. However, waveform engineering is mainly conducted at CW excitations and only more recently the measurement capability has been extended to modulated signals with a small number of tones. Hence the introduction of multi-sines would extend the application of this system to new markets requiring device and PA testing not only at CW but also at realistic modulated signals. This chapter starts with the introduction of the evolution of the waveform measurement system and then the advantages of employing multi-sines as the stimulus in this system will be explained. Finally, an accurate multi-tone subsampling method has been introduced as well as a multi-

sines averaging technique.

6.1 Introduction of Cardiff University's waveform measurement and engineering system

The communication industry is demanding faster, more flexible and more accurate turnaround in the design and realisation of RF devices, circuits and systems to meet the recent growth of mobile communication systems. However this can only be achieved if the accurate knowledge of the target semiconductor device characterization obtained.

A reliable device characterization is essential for gaining an insight into a device. Therefore, all measurement activity should ideally be robust and accurate as the measurement results will in future be used in the generation and validation of computer aided design (CAD) models, allowing the design and optimisation of devices and circuits to be conducted within simulation environments.

The measurement of time domain waveforms, along with the resulting characterisation, is establishing itself as an optimum design approach for a number of reasons. The first reason is that though most of the fundamental electronic theory is based abound time domain waveforms which typically developed at much lower frequencies, such theorems are still valid at high frequency. Secondly, the ability to analyse the shape of the waveforms can form a vital part of the design process. Theoretically, it is the time varying voltage $V(t)$ and current $I(t)$ waveforms present on the terminals of the transistor that contribute to the performance of that transistor.

Actually in many cases it is virtually impossible to determine the class of operation of an amplifier without analysis of the waveforms. For example, to make Power Amplifiers work in Class-E mode, which is a highly efficient switching mode of operation, the fundamental and harmonic load impedances must be engineered to ensure that when the voltage appears, no current flows at the device plane, and when current flows there is no voltage, thus limiting dissipated power and leading to a highly efficient operation. However, the only way to truly convince oneself that the device is in this class of operation is to view the voltage and current waveforms that exist at the device plane. Thirdly, it has been shown that through waveform engineering, it is possible to systematically maximise device performance in terms of efficiency, linearity or gain by analysis and manipulation of the waveforms instead of employing a blind, trial and error design approach.

The waveform engineering philosophy has been successfully adopted by Cardiff University to develop the waveform measurement system which has been domonstrated to great advantage over many application areas. The detailed introduction can be found in appendix.1.

6.2 Advantages of multi-sines stimulus to waveform measurement system

6.2.1 Extension from CW stimulus to modulated signals.

Th waveform measurement system however has the limitation of only supporting time-domain continuous stimulus, i.e, excitation signals with a discrete spectrum. More specifically, the stimulus can only be

CW waves or multi-tone signals with limited number of tones.

Back to 10 years ago, i.e, around 2000, this drawback was not as severe as it is now because the main communication standard at that time was still GSM, which has low amplitude variations hence can be approximated by a CW stimulus. Wireless communication signals with complex modulation schemes, such as W-CDMA, only occupied a small amount of market share at that time, as can be seen in figure 6.1. However communication techniques have developed faster than anybody could image, and today 3G or more advanced communication techniques are being widely used around the world. It is estimated that there are 329 million WCDMA subscribers at the first quarter of 2009, which is a large share in the communication market, also as shown in figure 6.2.

It is concluded in chapter 2 that multi-sines excitation signal are able to approximate these next-generation high PAPR modulated signals, hence waveform engineering and measurement techniques would reach a higher level of maturity if it is capable of supporting multi-sines stimulus. This will further boost the competitiveness of these commercialized measurement solutions in the market.

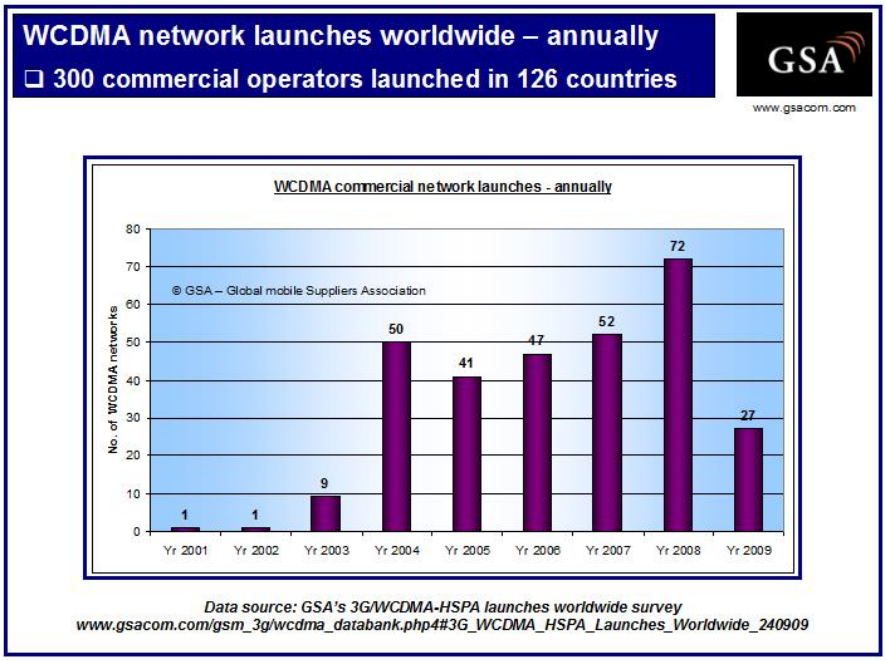

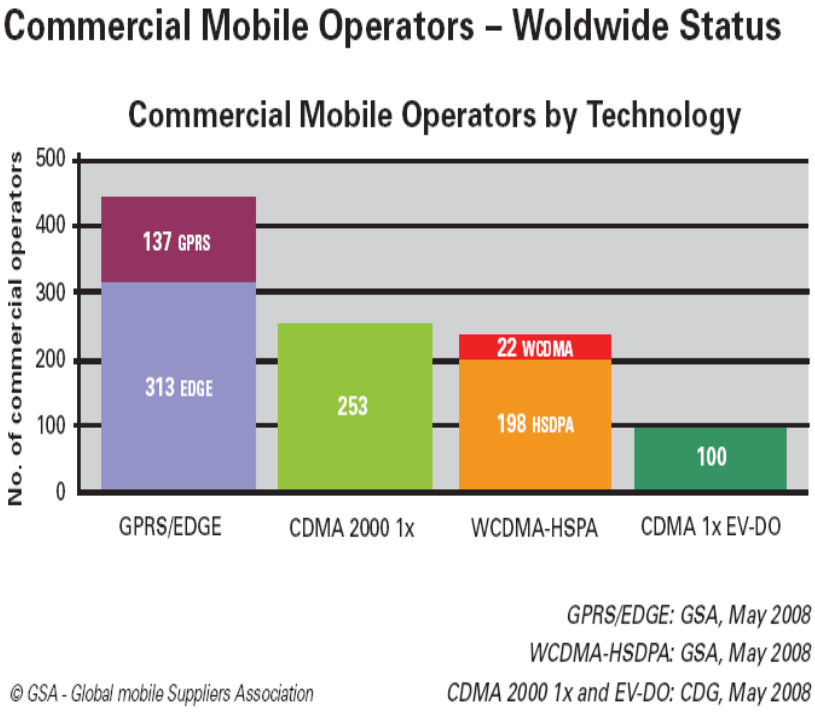

Figure 6.1 Development of WCDMA network. As it can be seen, wireless communication signals with complex modulation schemes occupies larger share in market [1].

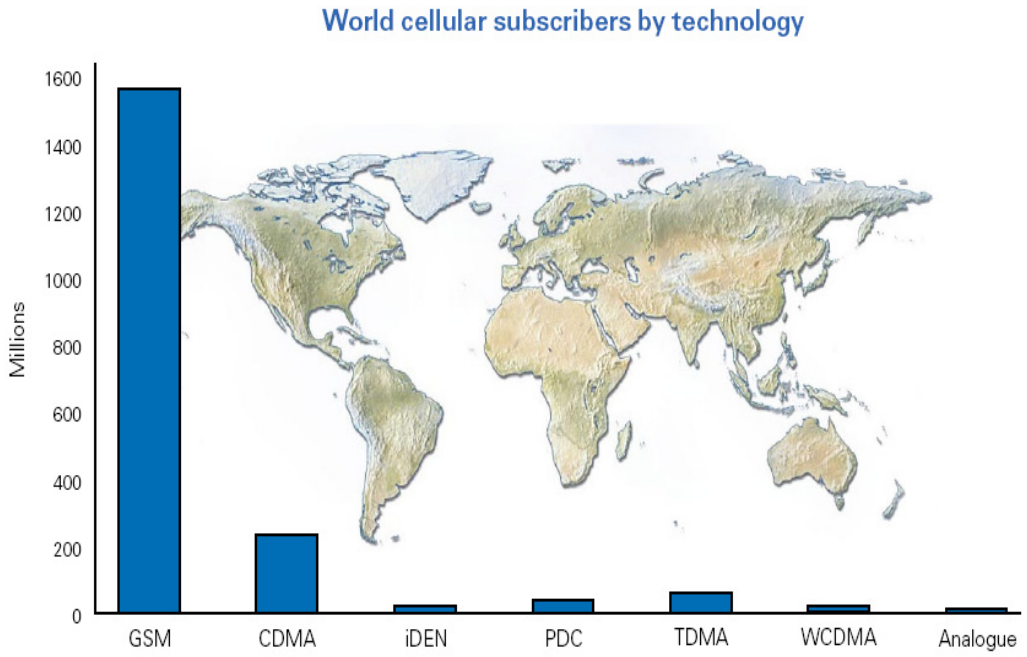

Figure 6.2 Mobile subscribers by technology at September 2005[22]

6.2.2 Extending the capability of high power device characterization

Currently, there are only few commercially available measurement systems which are capable of detecting broadband signals over 100W, and those measurement systems are very expensive. The reason not only lies in the fact that components with required performance are lacking or high-priced due to the low-volume demand for such components, but also caused by the added supplementary components required like a larger DC supply, impedance transformer, and additional pre-amplifiers.

Firstly, generating high-power signals is rather expensive. An increase of 2dB on a 100W signal would necessitate an additional production cost of more than generating a signal of 50W. One

solution to address the increased requirement on output power is to insert an additional RF high-power transistor in parallel. However, a single high-power transistor operating at frequencies around 2 GHz and delivering more than 50W costs more than £100.

Another cost is added from supplementary components required such as a larger DC supply, the bias networks, or a drive stage. The resulting material costs amount to several hundreds of pounds. It is noticed that the DC voltage at the DC source is usually not the same as the dc biasing voltage at device ports since the system components sitting in between have non-zero resistance. For relatively low power devices, the dc current when the device is operating in normal condition is small. The resultant voltage drop on the DC resistance can be neglected without seriously affecting the accuracy of the measurement but for high power devices, the dc current can go as high as 8A. By simple mathematical calculation this indicates that more than a 2 volt drop would happen across the DC resistance and hence the power lost cannot be neglected.

Thirdly, the single tone waveform measurement system has the potential of characterizing transistor devices ranging from mW to a hundred Watts. However, as high power transistor devices usually possess very small optimum impedance for maximum output power or gain, high mismatch between the optimum impedance and system characteristic impedance is expected. High mismatch implies the power reflected from the load to DUT is massive and sometimes the reflected power is even higher than the actual power delivered into the load. On the other hand, as most of the massive RF power

injected from the active load would be converted to heat, it brings the problems of heat dissipation. This issue can be tackled by inserting a broadband impedance transformer, which is shown at figure 6.3, into the measurement system. However this will further increase the cost of high power measurement systems.

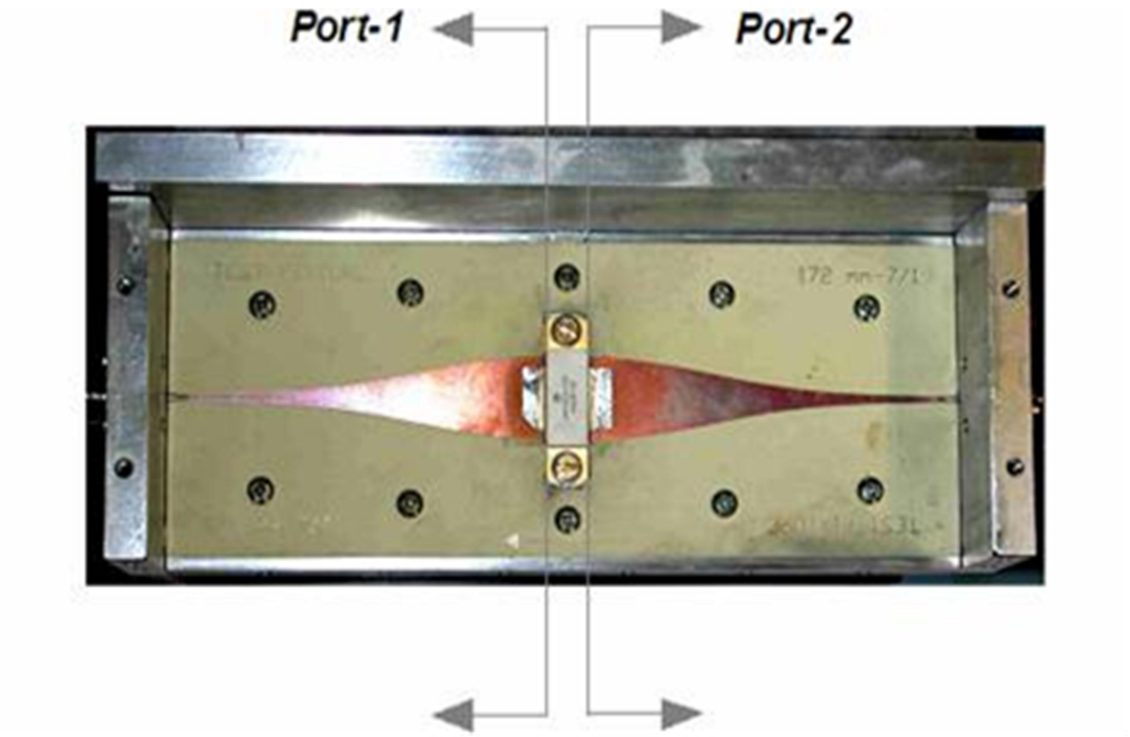

Figure 6.3 An impedance transformer used to tackle the impedance mismatch issue in high power measurement

Another possible solution is using pulsed signals as stimulus to decrease the total amount of power needed. However, during load-pull iterations, the power from signal source is adjusted until the desired load reflection coefficient is achieved. Since the characterization of high power devices always involves a quite large power variation, the risk of damaging the DUT during load-pull convergence increases as the DUT is usually vulnerable to a sudden increasing of power injected from the output.

Applying multi-sines stimulus would be a much better choice. The high power transistors are not actually suffering from high power drive levels continually in real applications. For example, if we look at the CCDF curves of a typical WCDMA signal, which is shown in figure 6.4, we will find that 90% of the time the WCDMA signal is 5dB less than the peak power, and 99% of the time, the signal is 2dB less than the peak power. Therefore, a high power transistor which is designed for 52 dBm(158.49W) in a WCDMA transmission system will actually suffer less than 50dBm(100W) power 99% of the time and even less than 47 dBm(50W) at 90% of the time period. Hence a CW test signal which continually outputs 52dBm power is not only a waste of energy but also incompatible with the real world conditions. On the contrary, multi-sines stimulus is closer to the real world signals thus the delivered power is less than 100W most of the time. This will lead to a much cheaper and more reliable measurement system as a 47dBm (50W) measurement system is easier to implement with cheaper, currently off-the-shelf devices. Therefore the whole measurement system will be more competitive in the market.

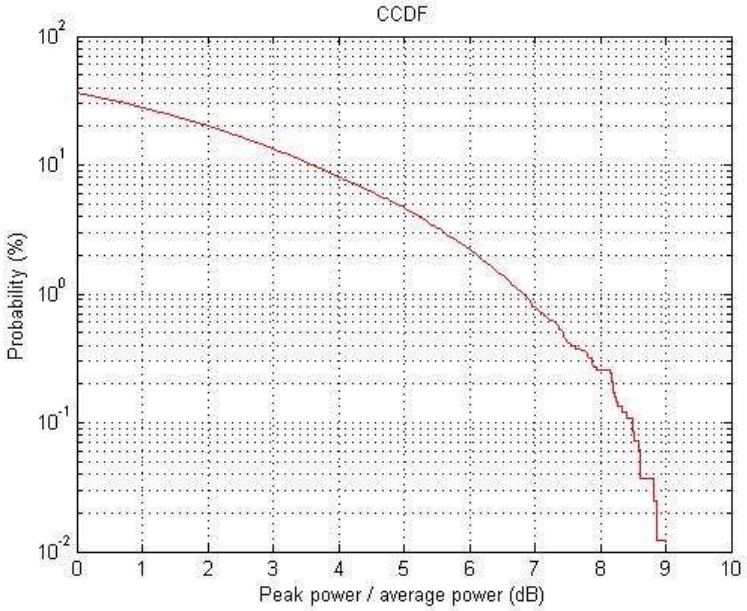

Figure 6.4 Typical CCDF of W-CDMA signal

6.3 Using Multi-sines stimulus in waveform measurement system

6.3.1 Multi-sines subsampling

The magnitude and phase generated by the DUT must be captured when applying the multi-sines as stimulus in the presented waveform measurement system. Such captured data allows a true 'envelope' representation of the modulated signals being generated that provides for meaningful device characterisation relative to the device boundary conditions. It is therefore clearly essential for the measurement system to capture information at the base-band, the fundamental-band and all significant harmonic bands.

However today's available high-frequency Oscilloscopes are often problematic in dealing with this requirement. Real time oscilloscopes

have a sufficiently large memory depth but have limited RF bandwidth. Moreover, these instruments have insufficient dynamic range due to limited (typically 8 bits) analogue to digital converter A/D bit resolution. On the other hand, sampling oscilloscopes employing sub-sampling techniques offer much higher dynamic range as waveforms can be sampled over a number of RF cycles, which means A/D converters with around 16 bits can be employed. But the shortcoming of these instruments is they offer only a limited memory depth like 4000 points[23] which corresponding to 2000 frequency components, by contrast the output of multi-sines stimulus often contains huge number of spectral components as we discussed in chapter 2.

Consider a 39-tone multi-sines signal with frequency spacing of 100kHz and which has been modulated to 1GHz carrier. To capture the information from DC to harmonics up to the 3rd order, a frequency grid from 100kHz with a step of 100kHz to 3.0117GHz is needed, which in turn would require the capture of 30,117 frequency points and corresponds to 60,234 sampling points. Figure 6.5a illustrates this standard sampling process.

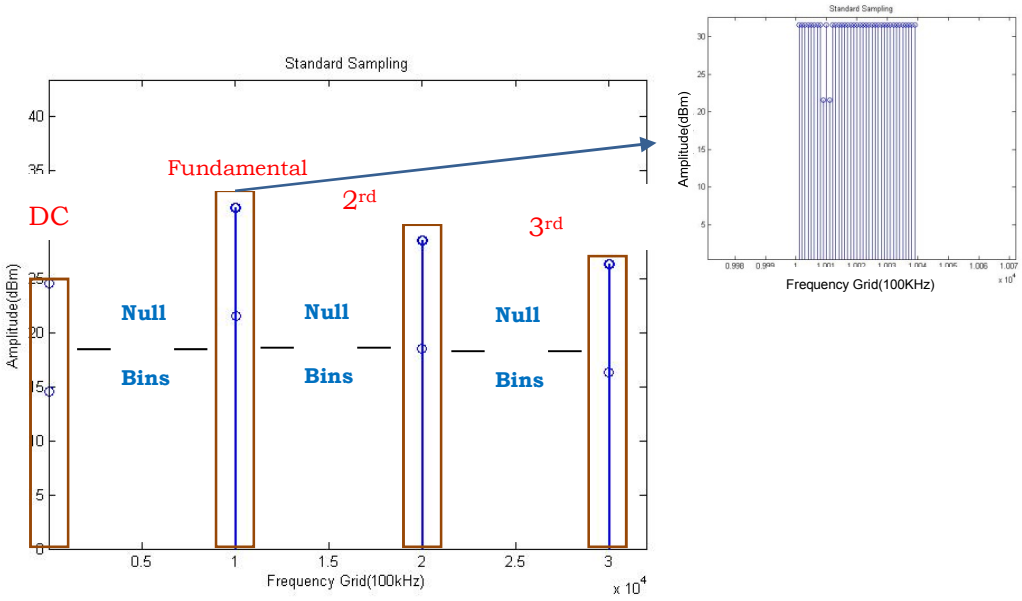

Figure 6.5a Standard sampling process need more than 30,000 frequency points.

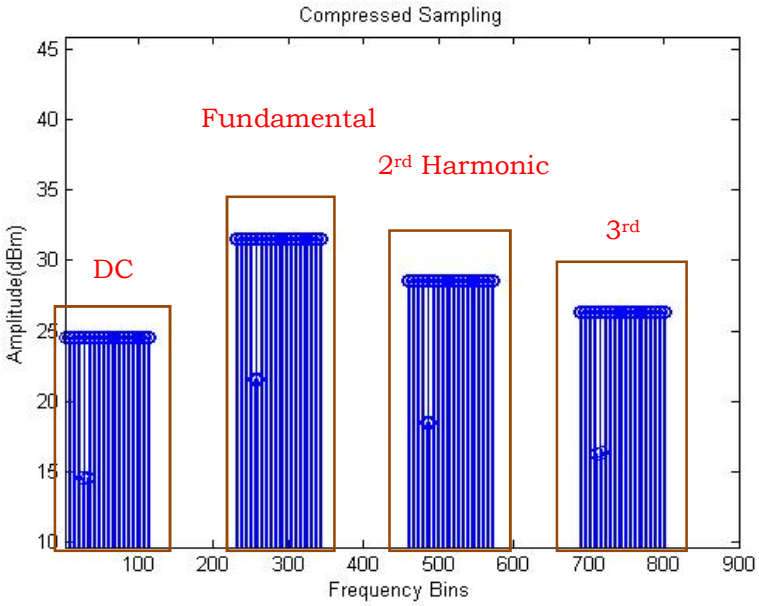

Figure 6.5b: The removal of null bins significantly reduce the number of frequency bins needed while keeping the fundamental and harmonic spectral information unchanged

Notice that there are a lot of null frequency bins in between the DC, fundamental, 2nd harmonic and 3rd harmonic, which means this

multi-sines waveform was captured in a spectrally inefficient way as can be seen from figure 6.5a, this shows that there are only less than 2000 “effective” frequency bins. Hence it can be concluded that the removal of null bins would make it possible for the sampling oscilloscope to capture the full spectrum information. This process can be understood as a compressed frequency sampling approach, as it is hinted in figure 6.5b.

This compressed sampling can be achieved by the sub-sampling process in which a sampling frequency much less than the RF frequency will be employed. This sampling technique seems disobey with the Nyquist sampling theorem, but as long as the sampling frequency is higher than the bandwidth of the signal to be sampled, the frequency information can still be recovered without loss. Figure 6.6 explains this technique in a graphic way by applying this technique to a simple 2-tone signal.

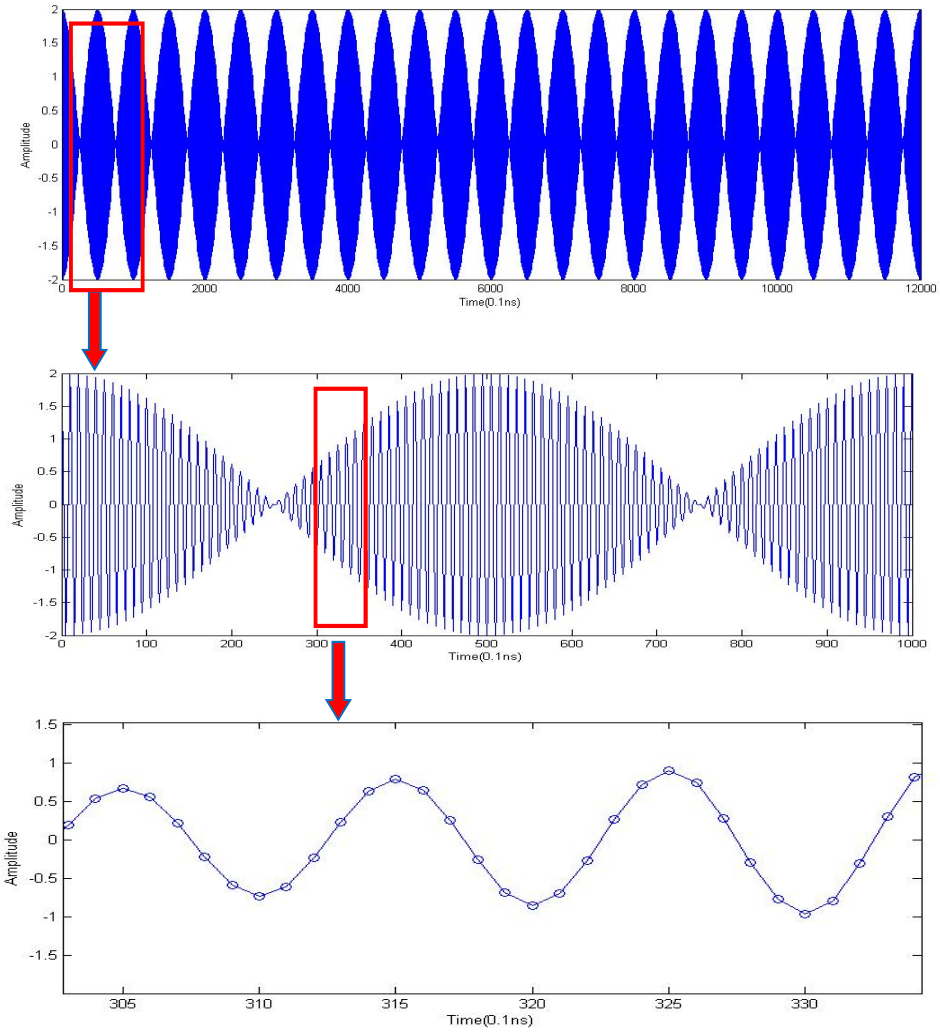

Figure 6.6a A standard two-tone signal modulated to 1GHz with sampling frequency 10GHz. This corresponds to 10 sample points over one RF period

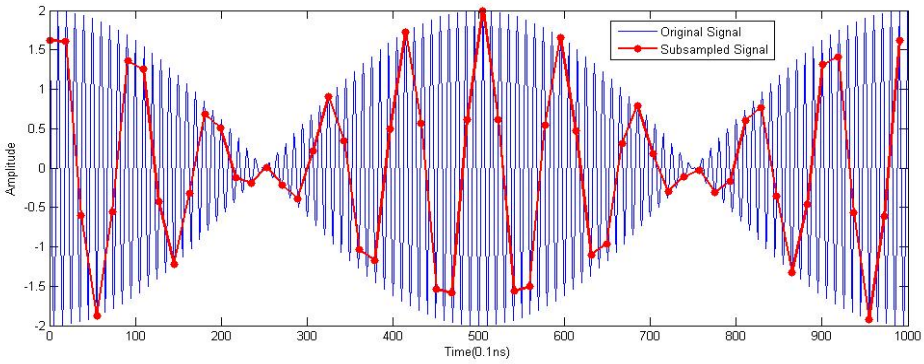

Figure 6.6b: The idea of subsampling two-tone signal. In this case, the subsampling frequency is 555.6MHz and 18 times lower than the standard sampling frequency. This subsampled signal is shown with red lines.

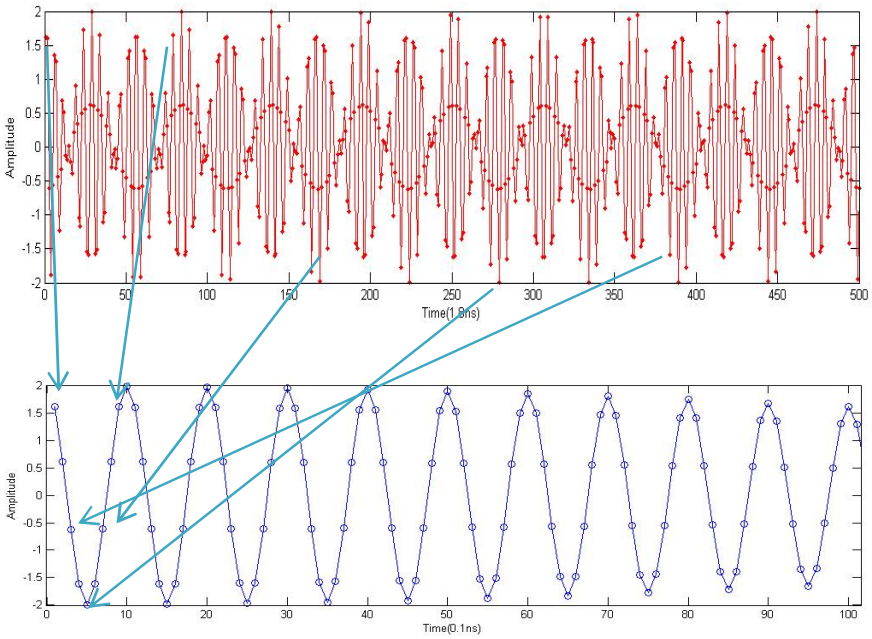

Figure 6.6c: The time domain waveform information of original signal (blue) has been well maintained after subsampling process (the red waveform) by sampling over multiple envelope periods.

Considering a two-tone signal with tone space 10MHz and been modulated to 1GHz carrier frequency. The 5th harmonic will be centred at 5GHz hence the standard sampling frequency is normally higher than 10GHz according to Nyquist sampling theorem. Under the 10GHz sampling frequency, there will be 10 sampling points every 1*ns.* Figure 6.6a shows the huge number of sampling points of this two-tone waveform after the standard sampling approach.

Figure 6.6b, shows that after the subsampling process, some waveform points have been dismissed and as a result, much waveform information lost because we only sampled over one envelope cycle. This also implies that sub-sampling technique can only be applied to a periodical signal.

However, if multiple envelope cycles are sampled, the original waveform can still be recovered without loss. This is demonstrated at figure 6.6c, where we can see each original sampled point (blue) corresponds to each subsampled point (red). On the other side, figure 6.6d demonstrates that the frequency information of the two-tone signal has also been well maintained after the subsampling process, though it has been moved from a centre at 1GHz to a centre at 440MHz. We will further discuss this frequency translocation phenomenon in the following paragraphs.

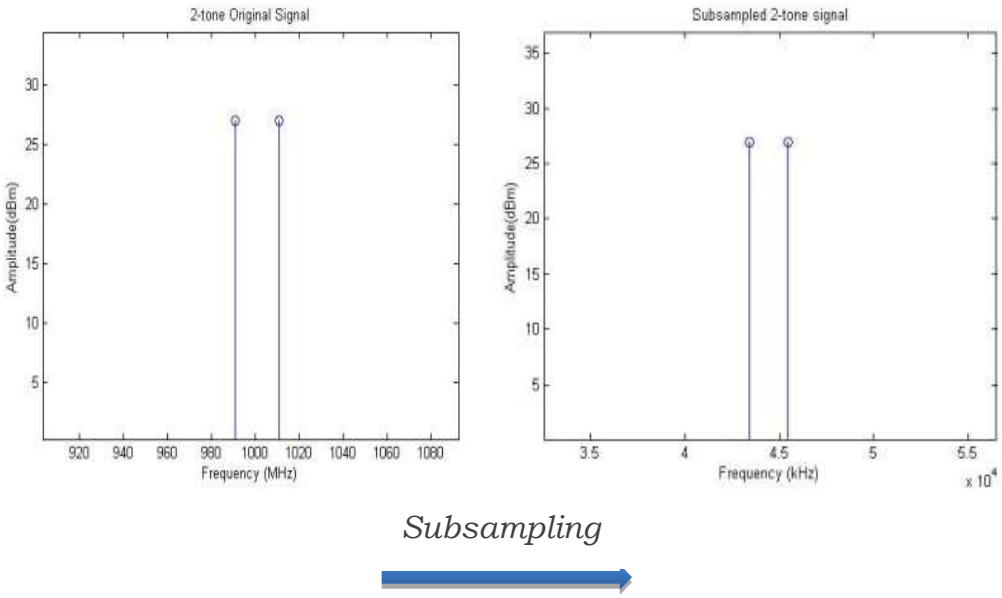

Figure 6.6d: The frequency domain waveform information of the original two-tone signal (left) has been well maintained after subsampling process (right). However the centre frequency has been moved from 1GHz to 170MHz

The internal mathematic mechanisms of subsampling are explained in figure 6.7. Suppose f_1 and f_2 are the start frequency and end frequency of the RF signal. After being subsampled by frequency fs which has a much lower frequency than the centre frequency of RF signal f_c, a series of mapping spectrums f_1' to f_2' and its "mirror" spectrums f_1" to f_2", will be generated.

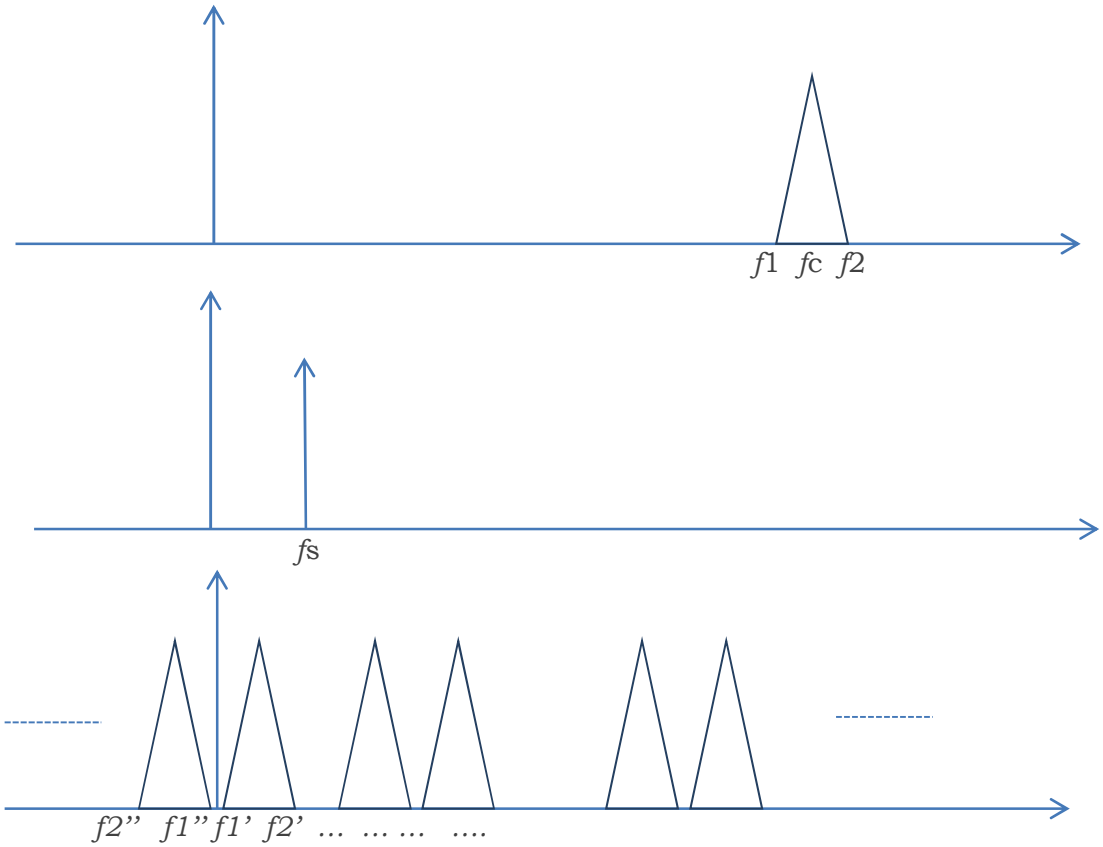

Figure 6.7 f1 and f2 are the start frequency and end frequency of the RF signal. After subsampled by fs which has much lower frequency than fc, the f1 to f2 has been moved from f1' to f2' and f1'' to f2''

*f*1' and *f*2' are given by:

$$f1' = n \times fs + f1 \qquad f2' = n \times fs + f2$$

(Equation 6.1)

and *f*1'' and *f*2'', which are the "mirror" of *f*1' and *f*2' are given by:

$$f1'' = n \times fs - f1 \qquad f2'' = n \times fs - f2$$

(Equation 6.2)

Where is *n* in these two equations are any integer number.

It can be seen from the above equations that it is possible to move all

the frequency information which is located around *f*c to a much lower frequency location without losing any spectrum information. Actually, though there are a series of mapping spectrum that are generated theoretically, only the mapping spectrum below subsampling frequency fs can be collected by the Oscilloscope due to the bandwidth limitation of subsampling. To make sure the subsampled spectrum contains all the spectrum information we interested in, the subsampling frequency fs should allow all of the spectral components we are interested in to be well separated from each other after the subsampling process. Mathematically, suppose $f1 \dots fk$ are our interested spectrum components, the generated $f1' \dots fk'$ after the subsampling process should be situated in a unique position. Otherwise they will collide with each other and thus lead to difficulty in further analysis. Figure 6.15 illustrates the frequency collision graphically. For a 29-tone multi-sines with three harmonics, a proper selection of subsampling frequency will provide us with a clean spectrum with separated fundamental, second harmonic and third-harmonic information, which is shown in Figure 6.8a. However, an improper subsampling frequency will cause fundamental components and third-order harmonic components to collide with each other, which will make further analysis of nonlinear behaviour difficult. This is shown in Figure 6.8b.

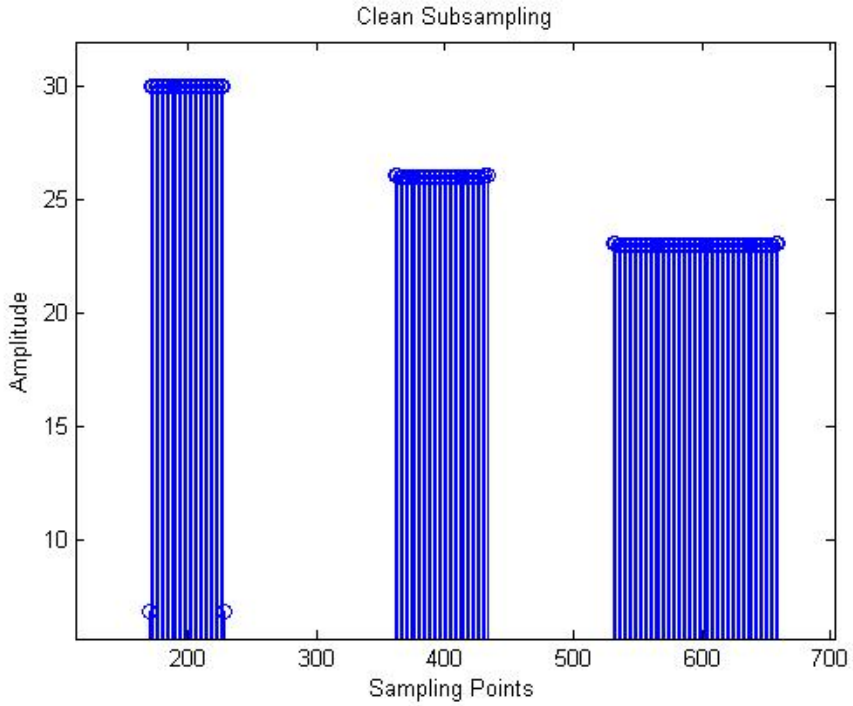

Figure 6.8a Subsampling with proper subsampling frequency

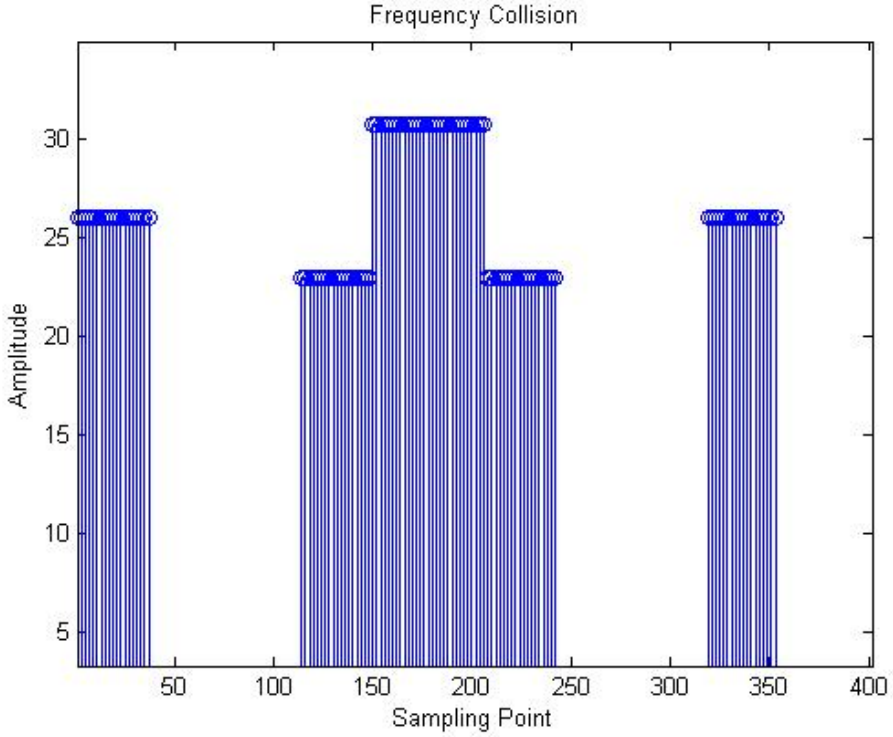

Figure 6.8b: Subsampling with improper subsampling frequency, fundamental and third harmonic components are colliding

It will be very time consuming and inefficient to calculate all the

possible subsampling frequencies to choose the subsampling frequency and make sure no frequency collision happens. Actually, if we look at the time domain waveform data, we will find that it is important for the time interval sampled points be a prime number to make sure every collected point is unique and contains different frequency information. For example, if a waveform has 1000 sample points over a modulated cycle, a subsampling interval of 20 points will lead to the same waveform information been collected again and again whilst a subsampling interval of 19 points ensures all the 1000 sample points information will be collected if given long enough sampling period Figure 6.9 explains this conclusion with a simple three-tone signal scenario. As it can be seen, when sampling over a non-prime time interval, the subsampled waveform (red) repeats with the modulated cycles, therefore only a small part of the original waveform information has been collected. Or in other words, only part of the collected points contains useful waveform information. On the contrary, with prime numbers of time interval (magenta), the sampled waveform is different with each modulated cycle and hence all the collected sampling points are useful as every sampling point contains different waveform information.

Therefore, a more time-efficient way is to choose the sub-sampling time-interval rather than directly choosing sub-sampling frequency. While the number of prime numbers is quite limited, the scope of possible subsampling frequencies is greatly narrowed, as a result, we can now find a proper subsampling frequency much quicker.

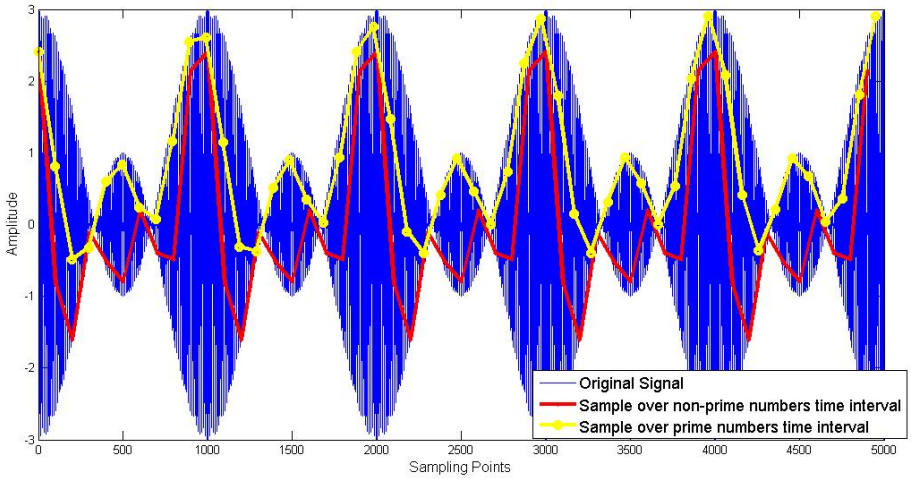

Figure 6.9 Subsampling over prime numbers time intervals will make sure all the sampled frequency components are unique hence the sampled points are used most efficiently

As well as the sub-sampling frequency, the frequency bins resolution is another parameter we need to engineer to accurately display the harmonic spectrum information of designed multi-sines. Back to the two-tone signal which is used at figure 6.7, the original two tones are located at 990MHz and 1010MHz. With the subsampling frequency of 555.6MHz, the following frequency components will be generated within the band from 0 MHz to 555.6 MHz:

Number	*location*	*Description*
1	101.1111MHz	$2 \times fs - f2$
2	121.1111MHz	$2 \times fs - f1$
3	434.4444MHz	$-1 \times fs + f1$
4	454.4444MHz	$-1 \times fs + f2$

Table 6.1 The generated frequency after subsampling approach

As the frequency locations are infinite decimals, the frequency resolution needs to be engineered otherwise the two-tone spectrum

information would hide among other frequency components. For example, 500 frequency bins leads to the frequency resolution of 1.111MHz which allows for the above four frequency components to be situated at integer frequency bins shown in figure 6.10a. In this scenario, the two-tone information will be correctly displayed. However 800 frequency bins will lead to a frequency resolution of 694.4kHz, as a result, the two tone sub-sampled spectrum will be located in the middle of two frequency bins, which will lead to the acquired spectrum being distorted, as can be seen at 6.10b.

This issue can be tackled by decreasing the number of sub-sample points, which decreases the number of frequency bins, gradually until all harmonic components are located at the integral number of bins. The number of sub-sampling points must be at least over one entire RF cycle to make sure all the harmonic information has been collected.

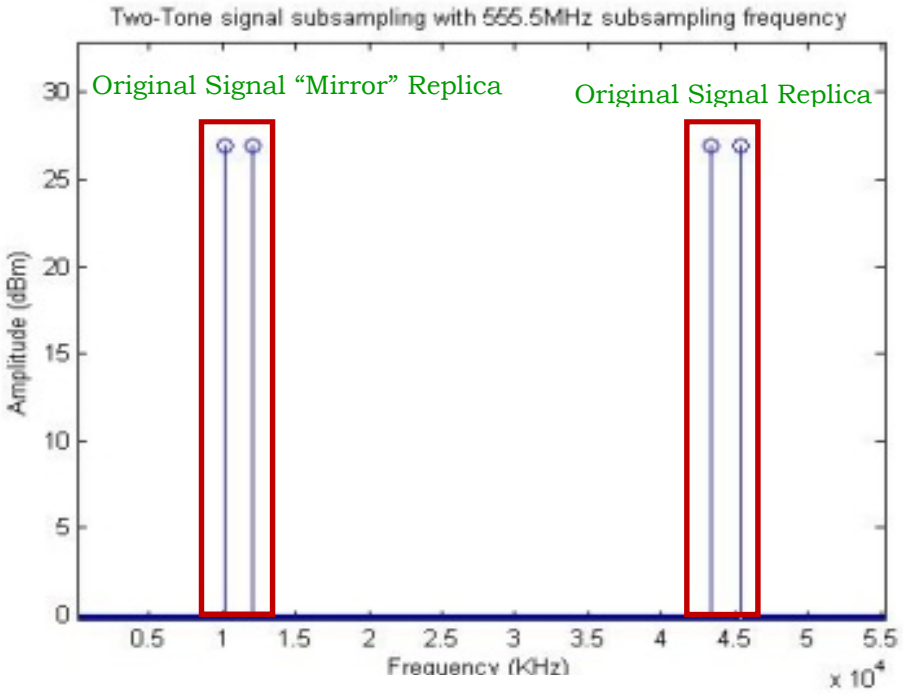

Figure 6.10a Subsampled Spectrum with Frequency resolution of 1.111MHz

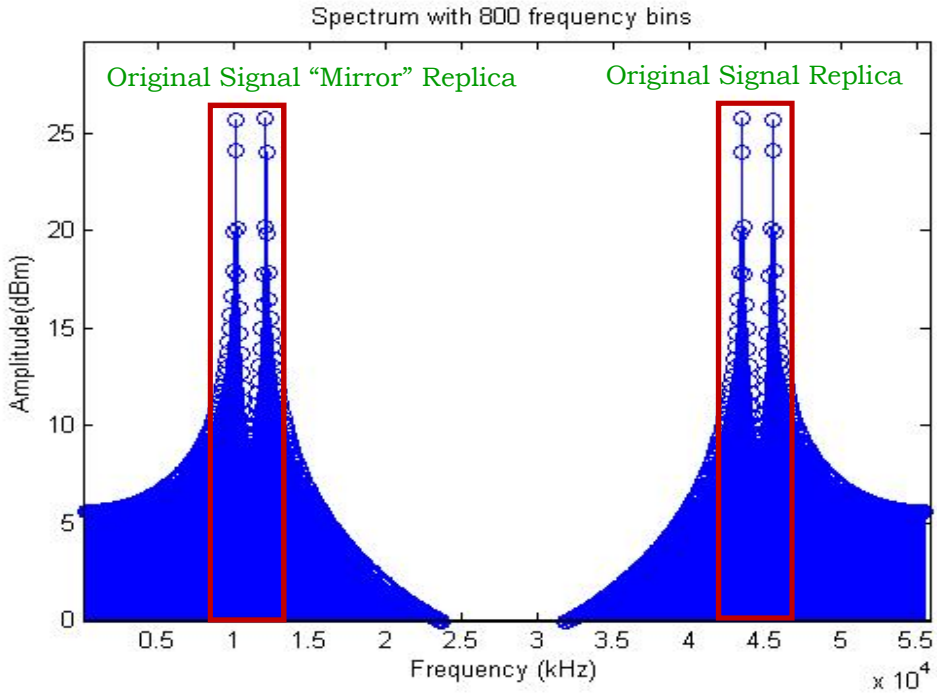

Figure 6.10b: Subsampled Spectrum with Frequency resolution of 694.4kHz

To summarize, sub-sampling frequency and the number of frequency

bins are the two most important parameters that need to be engineered in applying the sub-sampling technique. The proposed sub-sampling algorithm can be summarized as:

- The start sub-sampling frequency is one which could cover one modulated cycle for the specified number of points.
- Calculate frequency spectrum after subsampling.
- If frequency collision exists, increase the period of sub-sampling (which corresponding to decreasing the subsampling frequency) to next prime number, and calculate the subsampled spectral components again.
- Once a satisfactory subsampling frequency is acquired, calculate whether every spectral component is located in the integral number of frequency bins.
- If not, start from the specified number of sampling points, decrease the number of points used in order to increasing the frequency resolution between frequency bins until every spectral components are located in the integral number of frequency bins.

The flow diagram of this subsampling algorithm is concluded in figure 6.11.

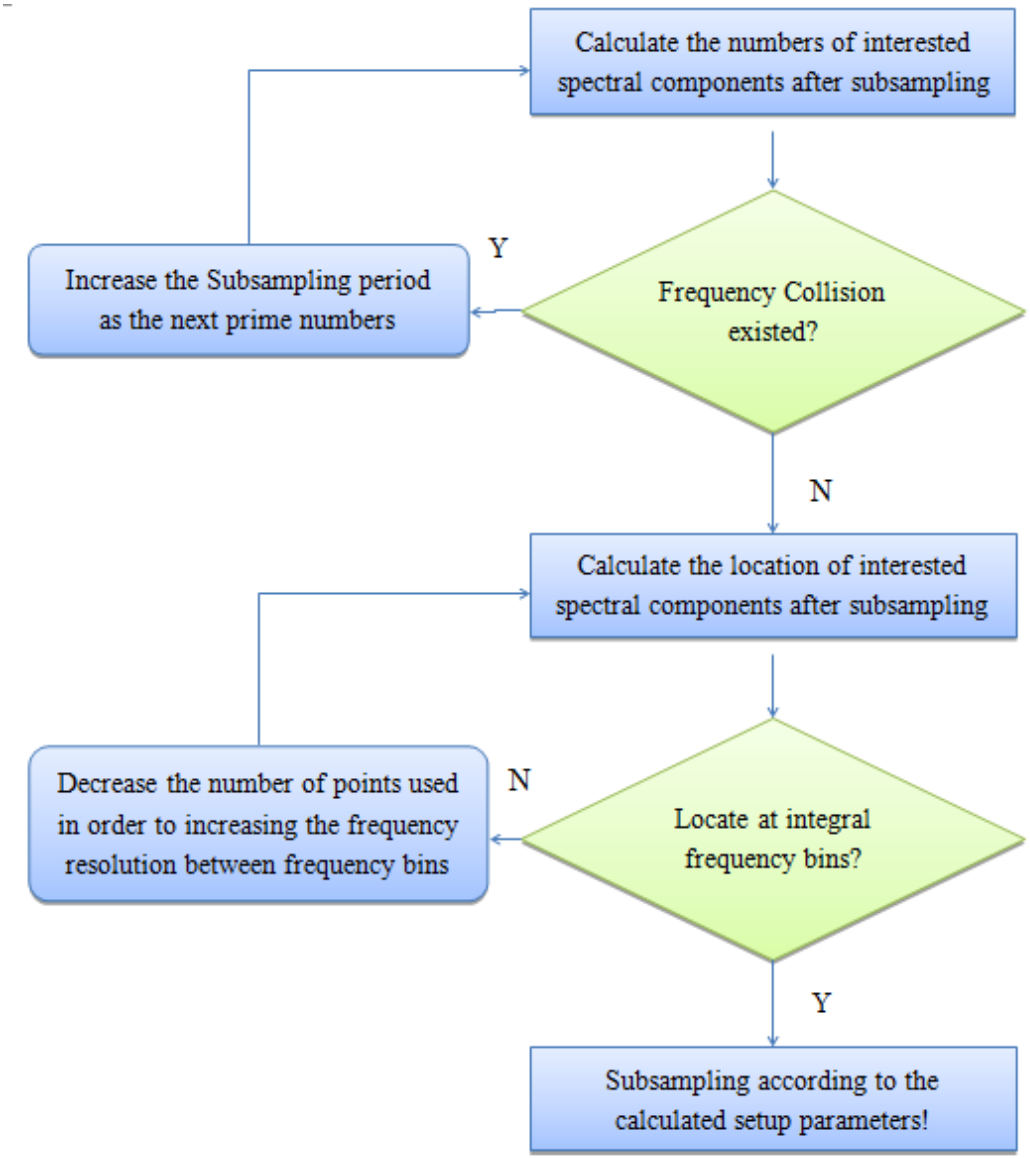

Figure 6.11 The proposed algorithm to calculate subsampling parameters

To verify the performance of this multi-sines subsampling algorithm, we start with a 3-tone multi-sines modulated to 1GHz with 1MHz tone spacing. This signal was generated by a Tektronix AWG7000 series signal generator with 10Gs/sec sample rate. Hence the modulation cycle is 1,000ns which corresponding to 10,000 sample points and the time interval between two points is 1/10GHz = 0.1ns.

The generated signal by AWG is shown at figure 6.12a.

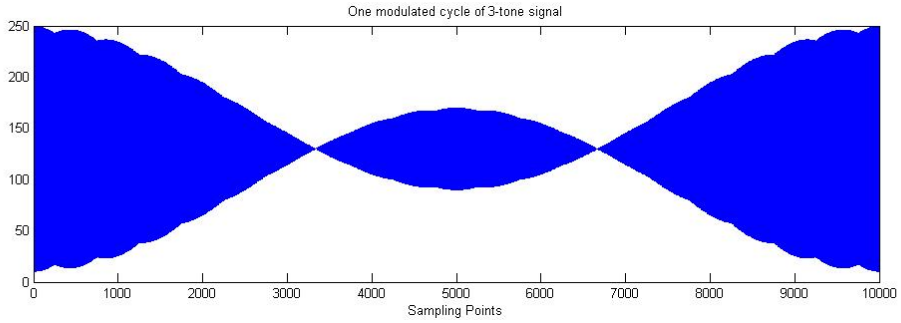

Figure 6.12a Original 3-tone signal. This figure refers to 1 modulated cycle, i.e.1us period, which corresponding to 10,000 sampling points.

A trigger signal was generated at 1MHz frequency to enable the Oscilloscope to measure this signal. However, the Tektronix DSA 8200 series Oscilloscope we are using in this work has a minimum 5us trigger re-arm time, which means there are 50,000 points between two triggers. This apparently exceeds the memory limitation of this Oscilloscope which can only record a maximum of 4,000 points. Hence the sub-sampling technique is necessary.

A 4.3*ns* sampling period, which equals 232.5581MHz subsampling frequency, combined with 3720 sample points is calculated after running the algorithm described in figure 6.18. It is important to point out that though this algorithm looks a bit complicated, the result is acquired almost instantly when running on a PC. The Horizontal Resolution on this DSA8200 Oscilloscope setup menu refers to the 1/10 of the whole sampling period, therefore it is calculated that we should set 4.3*ns*×400 = 1720*ns* and also set the number of samples as 4,000 to achieve the 232.5581MHz subsampling frequency.

The collect waveform is shown at figure 6.12b. As calculated, 3,720 points of these collected 4,000 points has been used to calculate the spectrum of the measured 3-tone signal, which is plotted at figure 6.12c. As can be seen, the 3-tones have been accurately measured and the dynamic range of this signal is well over 40dB.

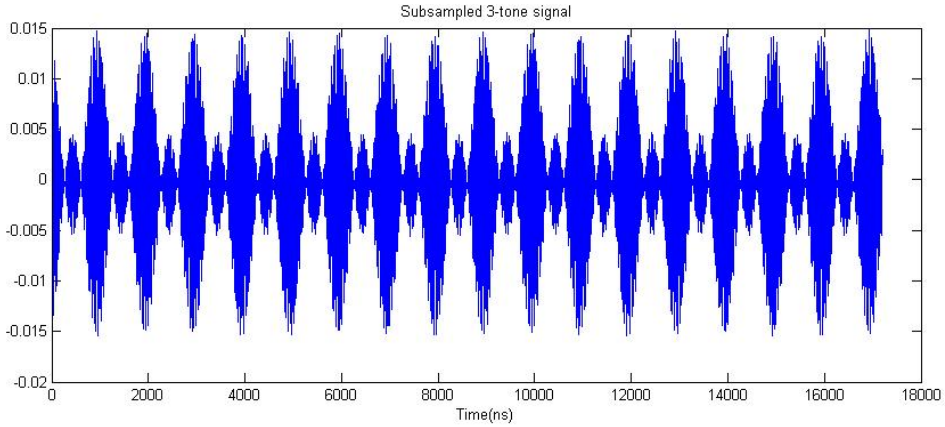

Figure 6.12b: Subsampled 3-tone signal. By subsampling, 4,000 points have been collected over 18 us.

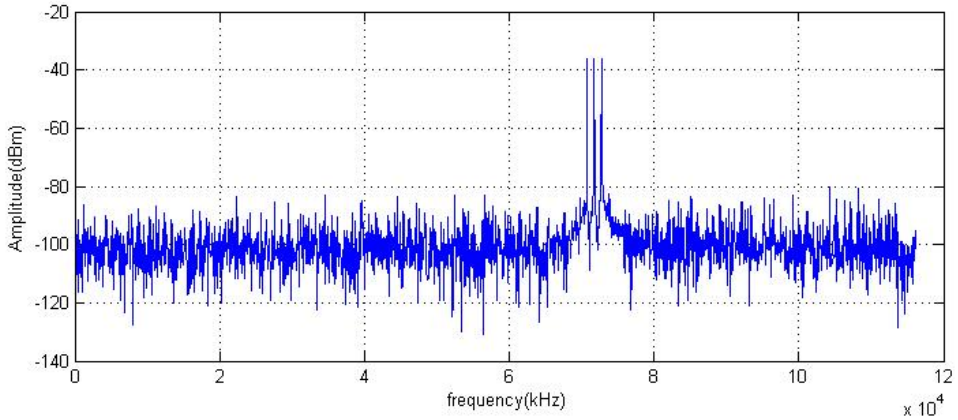

Figure 6.12c: The spectrum of 3-tone signal measured by sub-sampling technique

We further apply this subsampling technique into a real PA to verify its validity. Here a Cree 10W device is used as DUT and we modulated this three-tone signal to 900MHz carrier thus three tones are situated at 901MHz, 902MHz and 903MHz. The spectrum locations of nonlinear components excited by this three-tone signal

have been calculated up to 7th order and 7th harmonics, which is shown below in table 6.1 (there are possibly more than one mixed nonlinear terms situate at the same frequency location, this table just shows one of the terms). To accurately sample all the generated nonlinear harmonic components, a time resolution of 1800ns, which corresponding to 1/(1800ns/40) = 22.2MHz subsampling frequency, has been acquired by running the algorithm we introduced at figure 6.12.

The spectrum after subsampling is shown at figure 6.13. As can be seen, the subsampling technique acts as a down-converter from a certain point of view, hence the three-tone signal and its harmonics have been converted to below 22.2MHz.

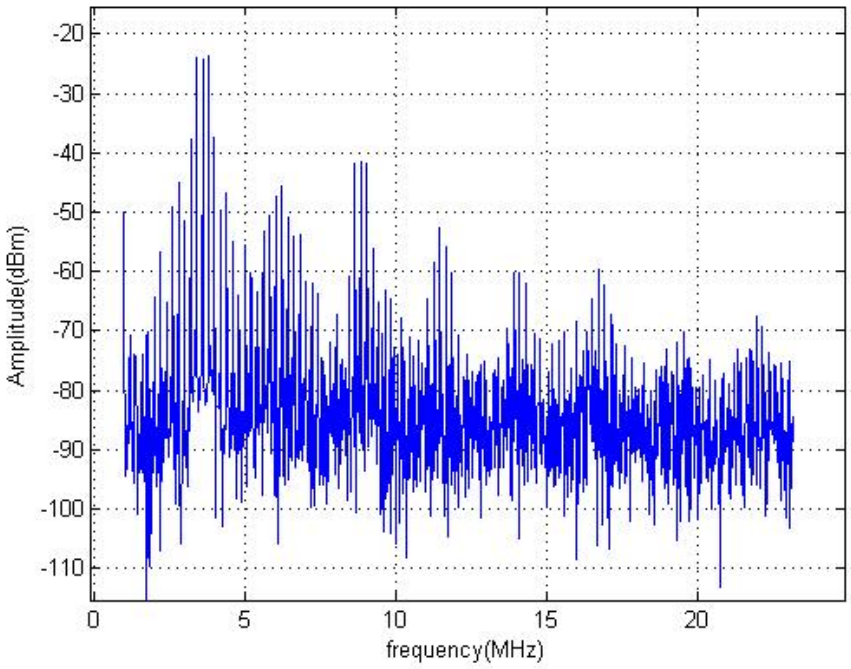

Figure 6.13 The spectrum of 3-tone stimulus passing through a PA and sampled using the sub-sampling technique.

Mixed Terms	f(MHz)	Mixed Terms	f (MHz)	Mixed Terms	f (MHz)
w1-3w2+2w3	1	2w1+w2+w3	1803	4w1-1w2+1w3	3605
-2w2+2w3	2	2w1-2w2+2w3	1804	3w1+1w3	3606
-3w2+3w3	3	1w1-1w2+2w3	1805	3w1-1w2+2w3	3607
-1w1-2w2+3w3	4	1w1-2w2+3w3	1806	2w1+2w3	3608
-2w1-1w2+3w3	5	-1w2+3w3	1807	2w1-1w2+3w3	3609
-3w1+3w3	6	-2w2+4w3	1808	w1+3w3	3610
4w1-3w3	895	-w1-w2+4w3	1809	w1-1w2+4w3	3611
4w1-w2-2w3	896	-2w1+4w3	1810	4w3	3612
4w1-2w2-w3	897	5w1-2w3	2699	-1w2+5w3	3613
4w1-3w2	898	5w1-w2-w3	2700	-w1+5w3	3614
3w1-2w2	899	5w1-2w2	2701	6w1-w3	4503
3w1-3w2+w3	900	4w1-1w2	2702	6w1-w2	4504
2w1-2w2+w3	901	4w1-2w2+w3	2703	5w1	4505
2w1-3w2+2w3	902	'3w1-w2+1w3	2704	5w1-w2+w3	4506
w1-w2+2w3	903	3w1-2w2+2w3	2705	4w1+w3	4507
w1-3w2+3w3	904	2w1-w2+2w3	2706	4w1-w2+2w3	4508
-2w2+3w3	905	2w1-2w2+3w3	2707	3w1+2w3	4509
-3w2+4w3	906	w1-w2+3w3	2708	3w1-1w2+3w3	4510
-w1-2w2+4w3	907	w1-2w2+4w3	2709	2w1+3w3	4511
-2w1-w2+4w3	908	-w2+4w3	2710	2w1-w2+4w3	4512
-3w1+4w3	909	-2w2+5w3	2711	w1+4w3	4513
4w1-2w3	1798	w1-w2+5w3	2712	w1-w2+5w3	4514
4w1-w2-w3	1799	-2w1+5w3	2713	5w3	4515
4w1-2w2	1800	5w1-w3	3602	-w2+6w3	4516
3w1-w2	1801	5w1-w2	3603	-w1+6w3	4517
3w1-2w2+w3	1802	4w1	3604		

Table 6.2 The generated nonlinear components up to 5th order and 5th harmonic

For the future nonlinear analysis, it is necessary to remap these subsampled frequency components to their original location. This can be achieved by the inverse-calculation of equation 6.1 and

equation 6.2. This remapped spectrum is plotted at figure 6.14.

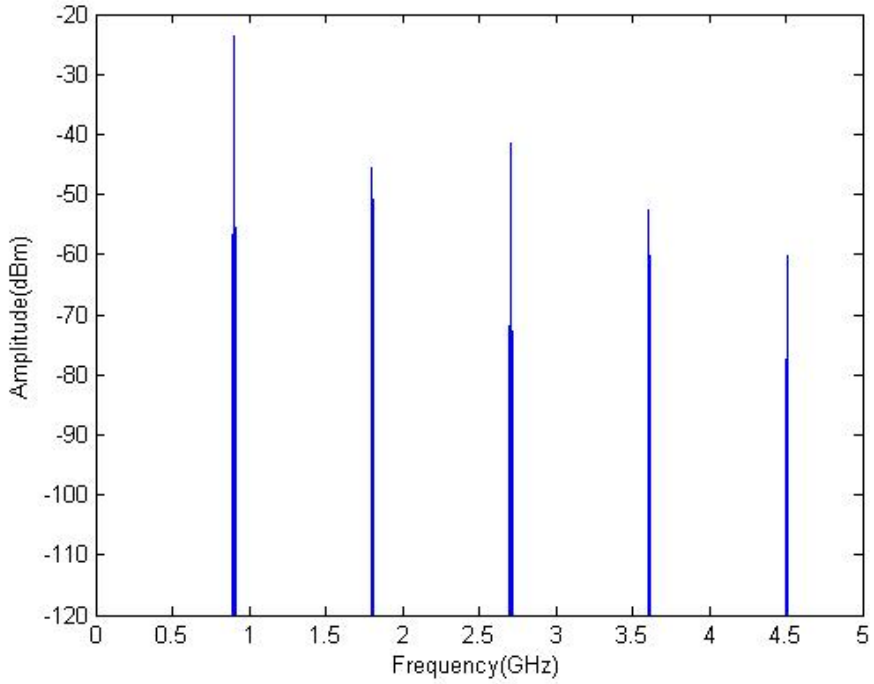

Figure 6.14a Overview of the spectrum of 3-tone stimulus passing a PA after remapping

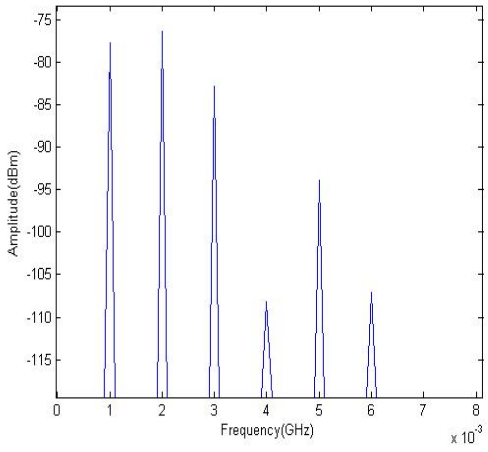

Figure 6.14b: DC Components

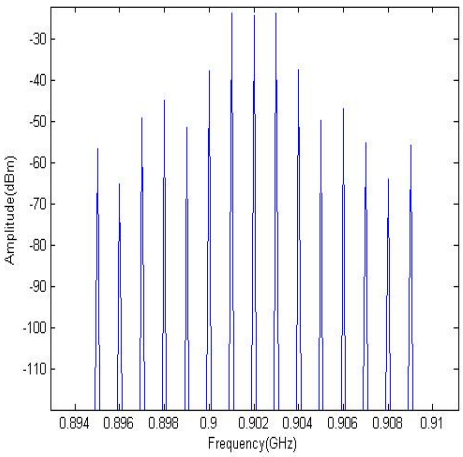

Figure 6.14c: Fundmental Components

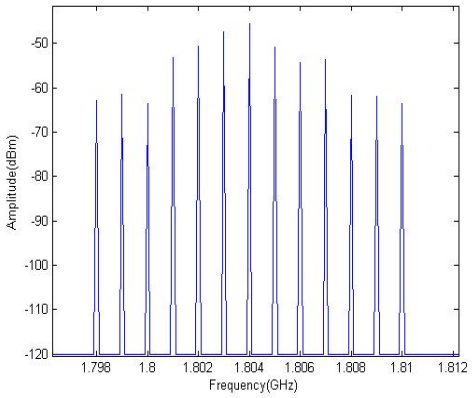

Figure 6.14d:

Second Order Harmonic Components

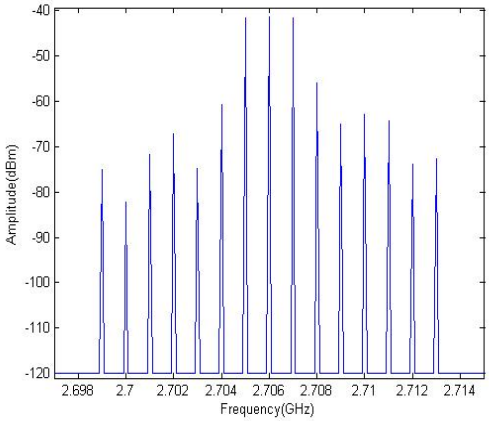

Figure 6.14e:

Third Order Harmonic Components

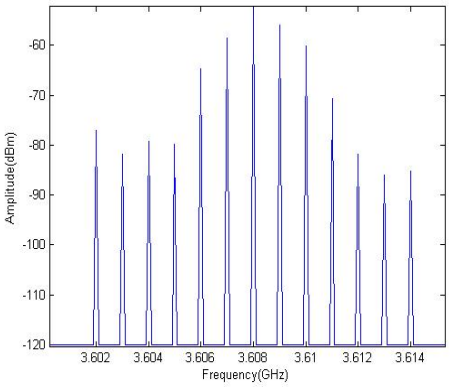

Figure 6.14f:

Fourth Order Harmonic Components

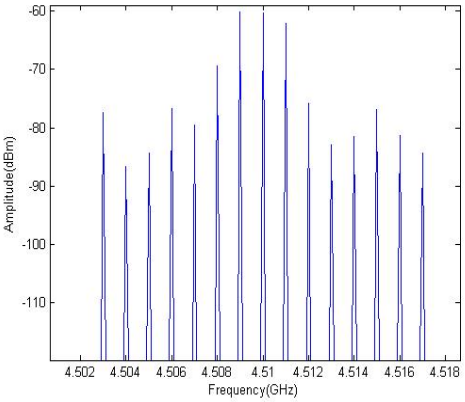

Figure 6.14g:

Fifth Order Harmonic Components

6.3.2 Multi-sines averaging

The sub-sampling technique we introduced above is incapable of "freezing" the display of the sampling-oscilloscope. The reason is because the collection of each new multi-tone waveform is in itself a valid measurement, and captures all of the relevant information, but consecutive measurements do not occur with a coherent time reference. More specifically, although the oscilloscope coherently samples across the selected time window, when the end of the time

window is reached the data must be processed and displayed. This leads to an unknown and unpredictable number of clock edges being ignored, thus each new waveform collection begins at a different time-point in the repetitive waveform. Hence software post-processing is required to accurately time align the collected waveforms in order to allow the averaging that is necessary to improve the overall quality of the measurements to an acceptable level rather than directly using the on-board averaging of the oscilloscope.

The required software processing is relatively trivial for a sampled CW signal as each consecutive captured waveform is simply a time shifted version of its predecessor. In this case, averaging can be achieved by simply using the first waveform as a reference with all other waveforms time-shifted to align. This approach allows for simple yet effective time-domain averaging. However, as soon as we modulate the excitation, a simple time shift is no longer sufficient as the RF and Modulation naturally have different down-conversion ratios, which means that consecutive waveform collections are no longer just time shifted versions of each other. The envelope changes and RF changes occur on totally different time scales. This is illustrated in figure 6.15 below, which shows two instances of a captured five-tone waveform. It can be seen that a straight forward time shifting is incapable of aligning these two waveforms.

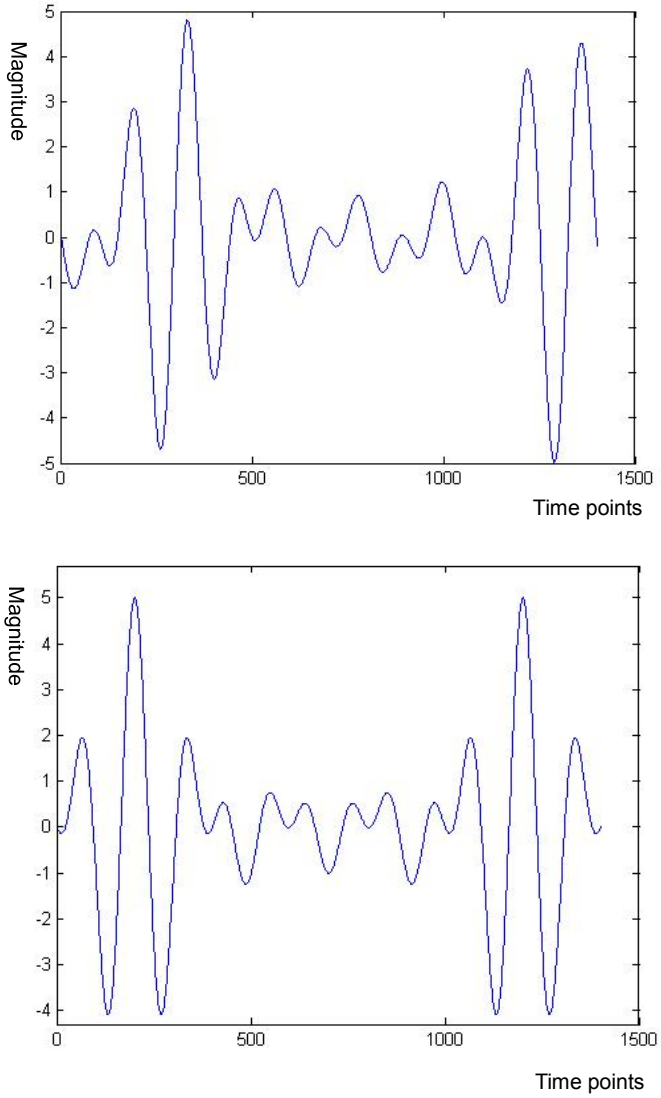

Figure 6.15 Two captures of consecutive five-tone waveform

This issue can be tackled by using an FFT to convert the waveform into a polar format which contains the magnitude and phase information for each spectral component. As we can see in figure 6.16, the time-delay of the captured waveforms will lead to an increase in the difference between the phases of each spectral component. This can also be intuitively understood as a "flower" opening because of the time delay. Hence we can first calculate the phase of the envelope ϕ_E by averaging the phase difference between

the upper sideband phase ϕ_U and lower sideband phase ϕ_L .

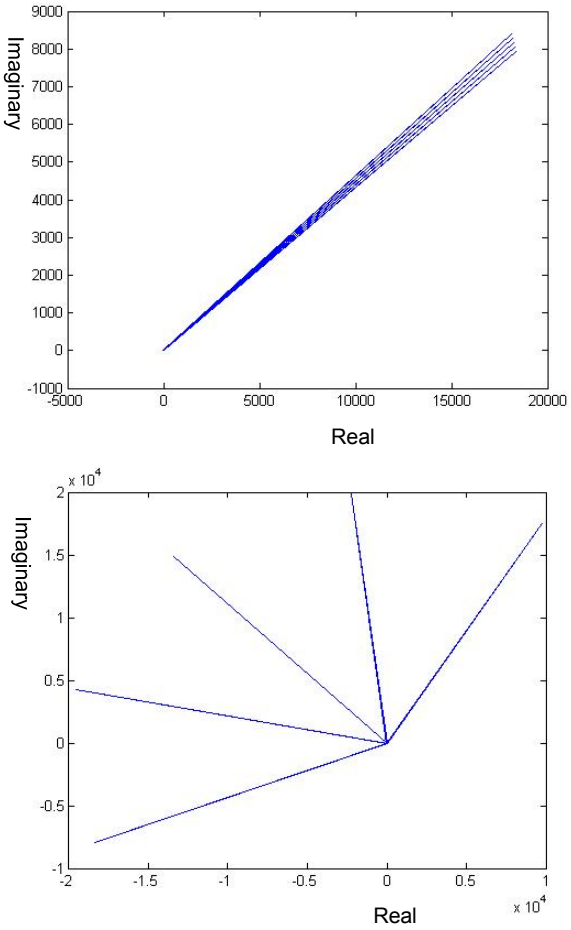

Figure 6.16 The frequency domain constellation diagram of five-tone multi-sines with a time delay. upper: initial waveform; below: imposed a time delay

The mathematic expression is:

$$\phi_E = average\,(\phi_U - \phi_L)$$

(Equation 6.3)

After the envelope phase of the captured waveform is calculated, it will then be compared to the envelope phase of the reference waveform to calculate an equivalent time-shift. This is given by equation 6.4, where T_{Mod} is the period of the modulated signal.

$$T_{shift} = \frac{\phi_E}{360} \times T_{Mod}$$

(Equation 6.4)

6.3.3 PCA based method to correct frequency offset

The signal generator and signal analyser in the measurement system often have different up-converter and down-converter frequencies. If these two frequencies are not locked to synchronize, the demodulated signal will have a phase shift ϕ_f with the original signal. Suppose $W_R(t)$ is the multi-sines which will be modulated to the carrier frequency w_c . The acquired signal $W_A(t)$ which has been demodulated by frequency w_d is:

$$W_A(t) = W_R(t) \times e^{jw_c t} \times e^{-jw_d t} = W_R(t) \times e^{j\phi_f}$$

(Equation 6.5)

From the above equation, it also can be seen that compensating for frequency offsets in the frequency domain can be translated as compensating for phase rotation in the time domain. Because of this phase shift, the captured multi-sines waveform shapes will keep changing with time. For example, the 5-tone multi-sines shown in figure 6.17*a* may have lost its waveform shape because of the frequency shifting, as figure 6.17*b* shows. Also, figure 6.18 shows this frequency-domain offset can actually be translated to time-domain phase shift.

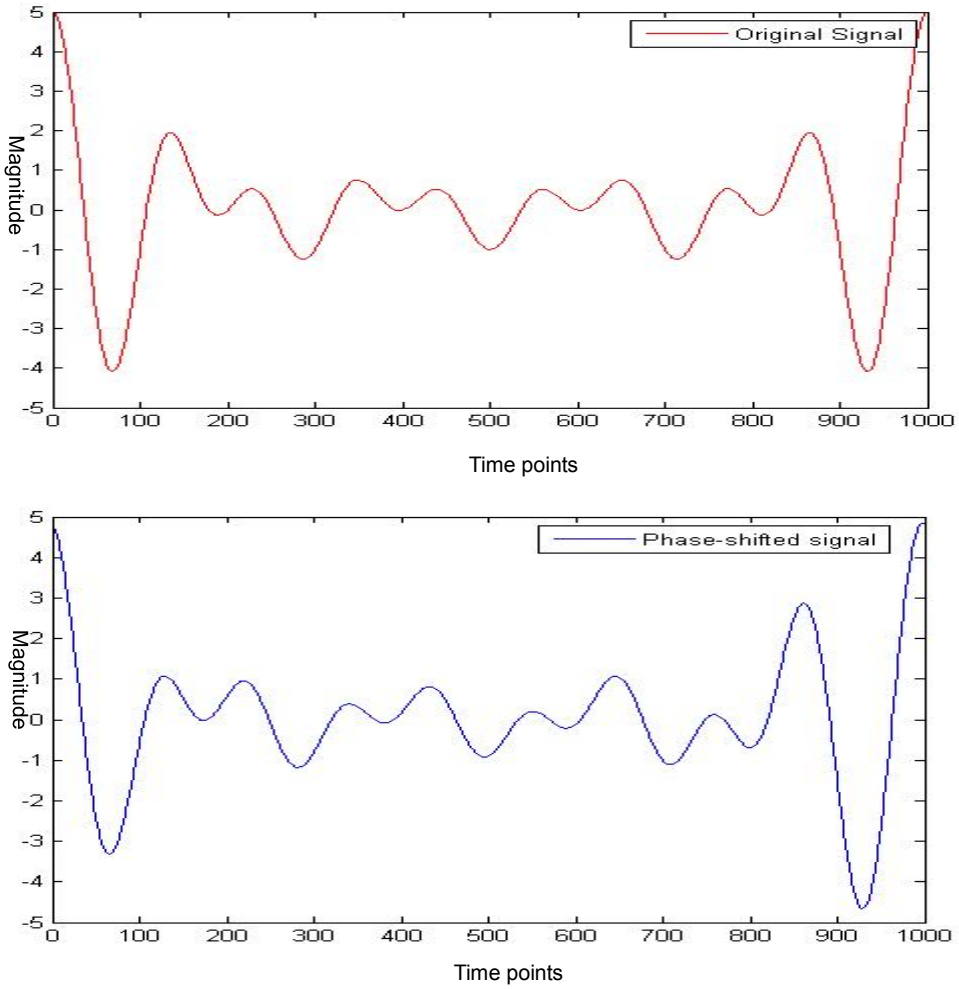

Figure 6.17 The multi-sines waveforms are changing because of the frequency shift. upper: original signal; lower: the signal with frequency shift

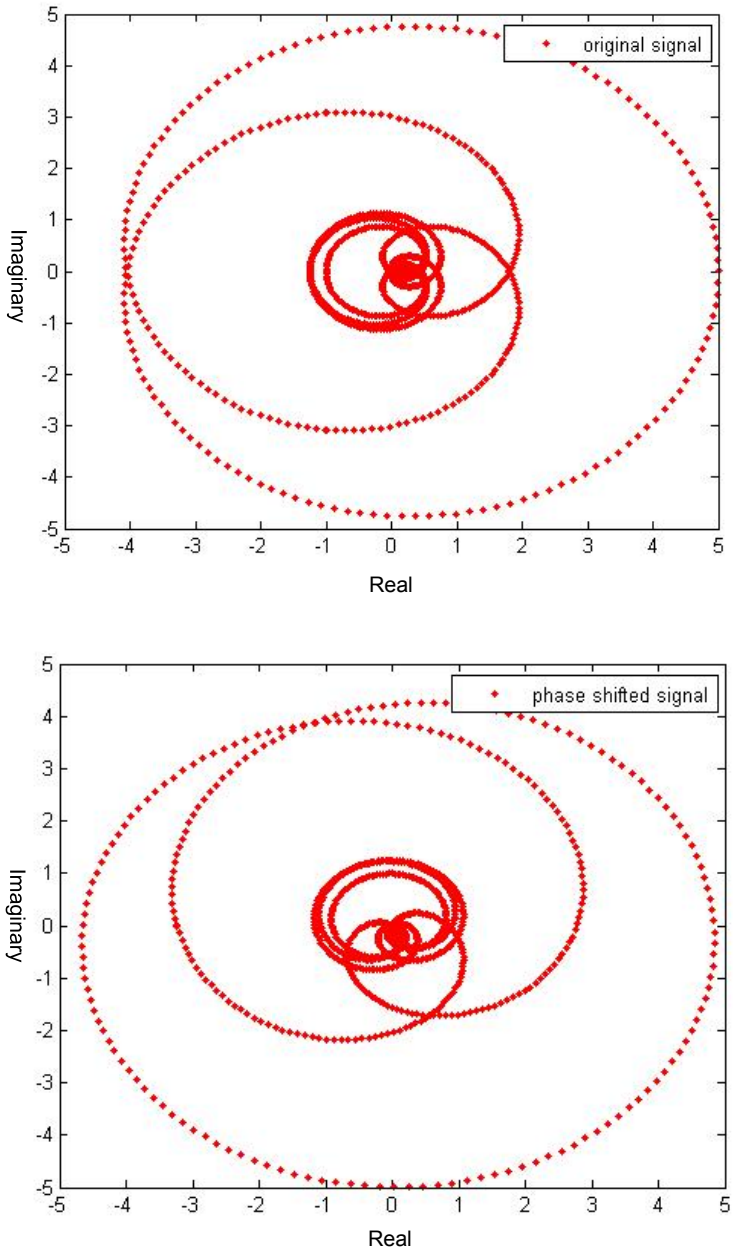

Figure 6.18 The frequency shift shown in figure 6.17 can be seen as time-domain phase shift in the time domian IQ constellation diagram.

For a modulated signal or two-tone signal it will be easy to calculate this phase shift and carry out frequency offset compensation. However for multi-sines as shown in figure 6.18, it is obviously difficult to calculate the exact phase shift. Hence a Principal Component Analysis (PCA) based procedure has been designed. PCA is mathematically defined [24] as an orthogonal linear transformation

that transforms the data to a new coordinate system such that the greatest variance in the projection of the data comes to lie on the first coordinate (called the first principal component), the second greatest variance on the second coordinate, and so on. For example, for given data sets as shown in figure 6.19, a new coordinate system can be drawn to get the vector where the projection of all the points are minimised.

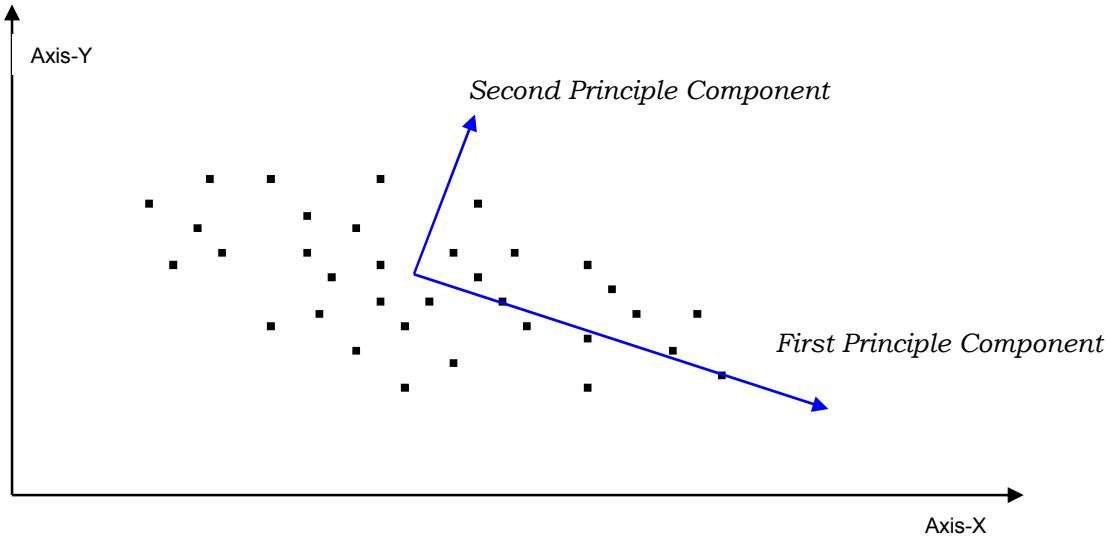

Figure 6.19 The illustration of Principle Component Analysis. The first principle component is a vector at which all points get minimized projection

Therefore, the phase shift compensation procedure can be derived as:

- Calculate the First Principle axis of the acquired waveform and reference waveform.
- Calculate the phase difference of the acquired two axes.
- The phase shift is therefore the phase difference

Figure 6.20 shows the corrected waveform compared to the original waveform and the phase-shifted waveform for 5-tone multi-sines. It can be seen from these results that the PCA based method works perfectly to compensate for the frequency shift we imposed artificially.

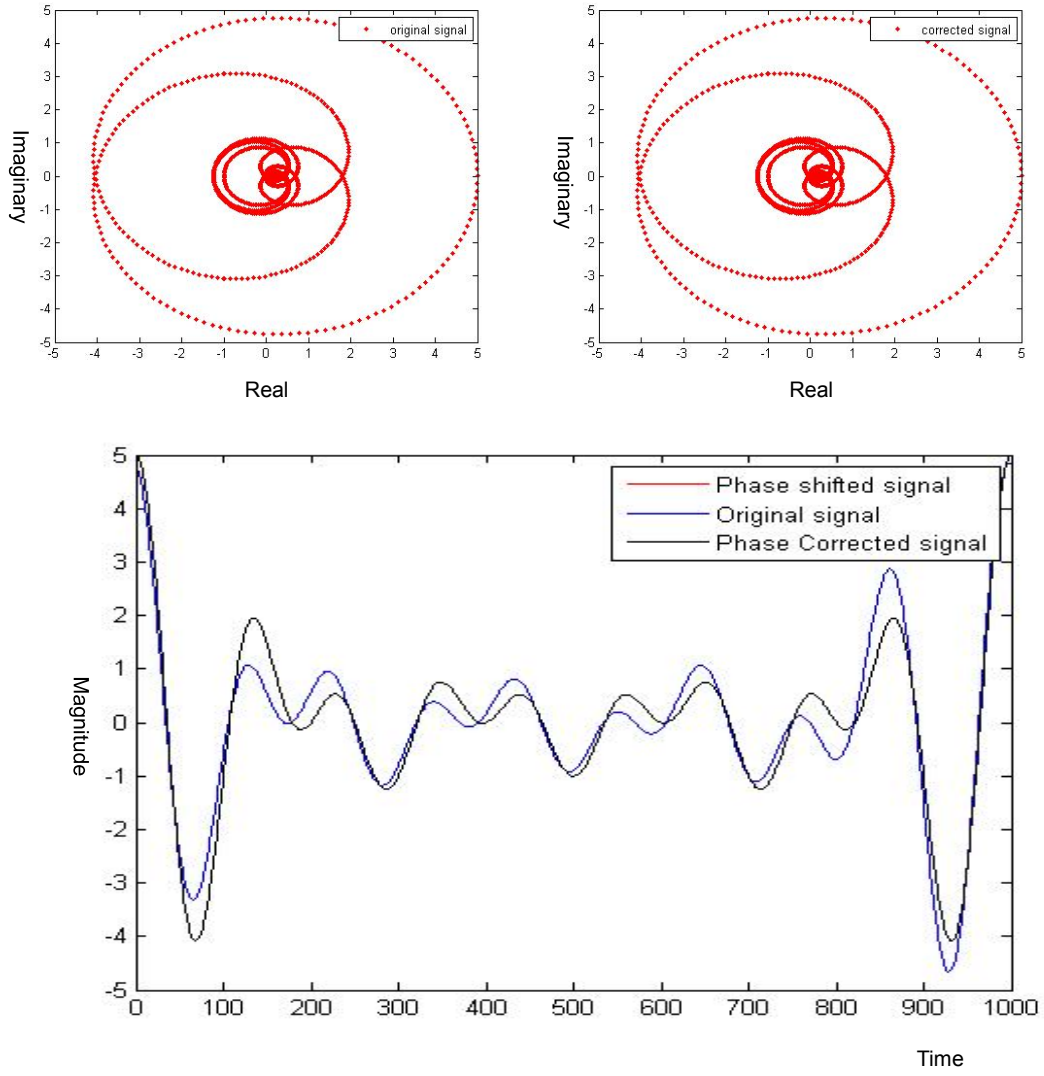

Figure 6.20 The phase correction results after PCA correction procedure. Both IQ diagram (up) and waveform (below) are perfectly aligned to the original signal

To further verify the applicability of our proposed PCA-based correction technique on very complicated excitation signals, a 50-tone multi-sines is employed as the test signal. The frequency shift correction procedure is applied and the results are shown below at figure 6.28. As can be seen in figure 6.28a, it will be very difficult to analyse the correspondent time-domain phase shift as the 50-tone multi-sines has no obvious IQ diagram shapes. However, after the PCA based correction process, as shown in figure 6.21b and 6.21c,

the corrected signal completely coincides with the original signal.

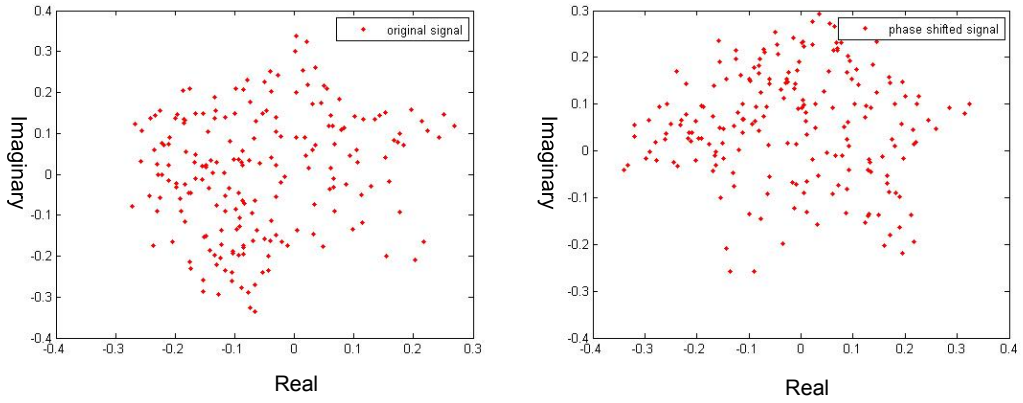

Figure 6.21a. The two signals before PCA correction procedure for 50-tone multi-sines. Obviously it is difficult to acquire the phase shift intuitively.

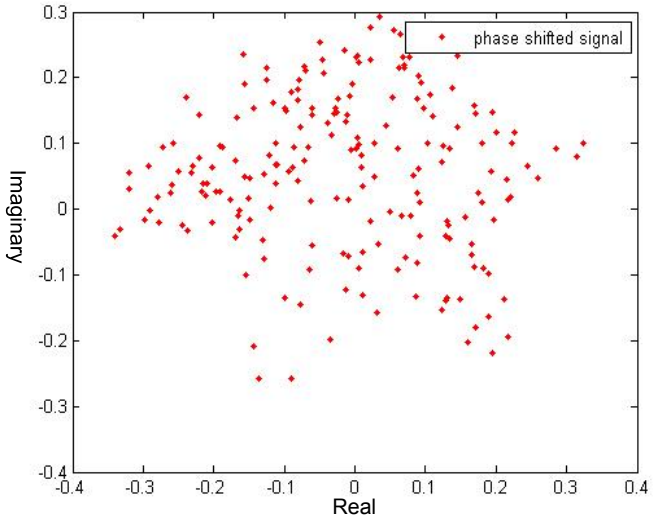

Figure 6.21b. After phase correction, the corrected signal's constellation diagram is almost a perfect match to the original signal(6.21a right)

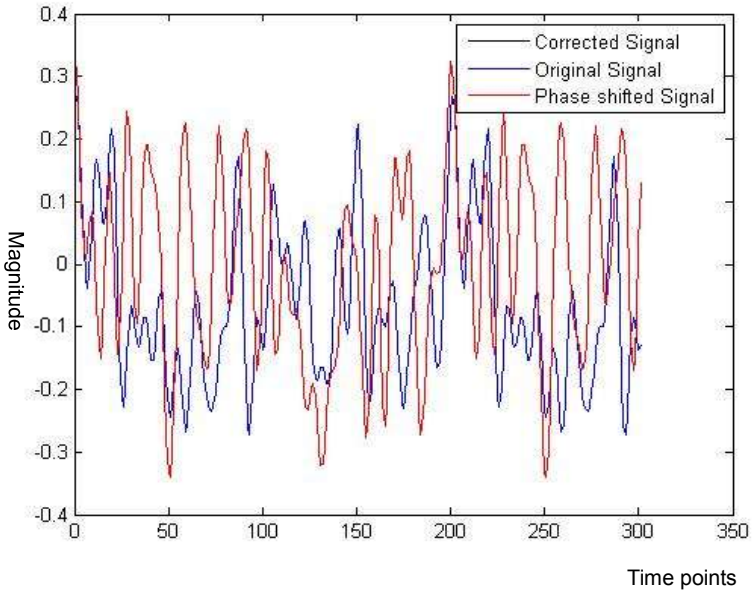

Figure 6.21c. After phase correction, the corrected signal's time domain waveform shape perfectly overlapped with original signal

6.4 **Conclusion**

In this chapter, we introduced an improved subsampling method that enables an accurate capture of multi-sines waveform, which is essential for Cardiff University's waveform measurement system. The validity of this method has been verified through the implentmentation in real measurement system. Hence the waveform measurement system can measure multi-sines stimulus which suggest its capablity has been extended to characterizing nonlinear behaviour excited by modulated signal source .

A phase correction method and a frequency-offset compensation method are further proposed to synchornize each capture of multi-sines which enables averaging of multiple measurements to get more accurate measurement resluts. These two methods, though not yet

being verified on real measurement system, are expected to enhance the performance of multi-sines waveform measurement system based on the good simulation results.

6.5 Reference:

[1] A. Sheikh, C. Roff, J. Benedikt, P. J. Tasker, B. Noori, P. Aaen, and J.Wood, "Systematic waveform engineering enabling high efficiency modes of operation in Si LDMOS at both L-band and S-band frequencies," in IEEE MTT-S Int. Microwave Symp. Dig., June 15–20, 2008, pp. 1143–1146.

[2] P. Wright, A. Sheikh, C. Roff, P. J. Tasker, and J. Benedikt, "Highly efficient operation modes in GaN power transistors delivering upwards of 81% efficiency and 12W output power," in IEEE MTT-S Int. Microwave Symp. Dig., June 15–20, 2008, pp.1147–1150.

[3] GSM/3G Market Update, online available at http://www.gsacom.com/gsm_3g/ Online Available: http://www.tek.com/products/signal_sources/awg7000/

[4] Jolliffe I.T. Principal Component Analysis, Series: Springer Series in Statistics, 2nd ed., Springer, NY, 2002, XXIX, 487 p. 28

7 Conclusion and future work

7.1 Conclusion

In summary, a novel, accurate and time-efficient way of designing a multi-sines stimulus signal to replace real-life modulated signals was demonstrated. It was demonstrated that with 50 tones, the multi-sines stimulus excites almost the same level of nonlinearity as real modulated signals do. This multi-sines design method also allows for the approximation of various types of modulation signal dependent on the user's needs.

By the investigation of the nonlinear behavior mechanism, a generalization was made, putting the nonlinear distortion into two categories according to their relationship to the original, namely correlated distortion and uncorrelated distortion. Existing figures of merit for evaluating the nonlinear behaviour were investigated regarding to their applicability to a multi-sines stimulus and also their capability of evaluating correlated distortion and uncorrelated distortion both in-band and out-of-band separately. It was found that although all prevalent figures of merit are incapable of measuring the in-band un-correlated distortion, a combination of EVM and ACPR would separate the in-band distortion and best describe the nonlinear behaviour of the device. Based on this conclusion, a PA was pushed into its compression zone with both real-life modulated signals and approximated multi-sines. The measured ACPR and EVM have shown good agreement with the multi-sines stimulus and its approximated modulated signal, which

proves that the designed multi-sines and real-life modulated signals have excited almost the same level of nonlinear distortion.

Existing techniques for designing a multi-sines stimulus were investigated, regarding their applicability to advanced RF measurement systems. The results obtained raise questions about its adaptability to various types of modulated signals. Consequently, three communication signals, namely IS-95 CDMA signals, 3GPP WCDMA test model-1 and 3GPP WCDMA uplink signals have been selected as the target signals to which multi-sines should approximate to, in order to prove the adaptability of our multi-sines design method. It has been shown that all these three signals can be accurately approximated via our design process, though the accuracy between the multi-sines and target signal may vary according to the statistical properties of the modulated signal.

The investigation of the multi-sines stimulus is compatible with the demanding requirements of advanced RF measurement systems which are capable of measuring the complete RF waveform including the harmonic and base-band frequencies but demanding a periodic stimulus signal. Moreover, the introduction of the multi-sines stimulus will enable the measurement system to handle high-power measurements which would be difficult and expensive if employing CW stimulus.

Cardiff University's waveform measurement system is such a system which allows for a simple and intuitive approach to address directly the mathematically and conceptually complex relationship between a non-linear device and its impedance environment and hence enable

the user to interact directly with the device and measurement system. A novel and quick sub sampling algorithm was proposed to efficiently use the memory of Sampling Oscilloscope and therefore allows for accurate multi-sine signal capturing which extend this measurement system's capability to handling multi-sines stimulus. This algorithm enables the large number of spectrum components introduced by the multi-sines stimulus to be accurately measured and displayed for further analysis. This algorithm has been verified in real measurement system where a Cree 10W device is used as the DUT. An averaging algorithm for the multi-sines stimulus was also proposed to "stabilize" the captured waveform. Furthermore, a PCA based phase compensating algorithm was also proposed to tackle the problem of frequency shift which may happen when the down-converted trigger frequency is not fully locked to the carrier frequency. These three techniques provided a base for the successful introduction of multi-sines stimulus to an advanced RF measurement system.

7.2 Further work

Despite the positive results obtained with not only the comparison between multi-sines and modulated signals but also waveform measurement systems employing the multi-sines stimulus, it should be emphasised that the assembling of a multi-sines stimulus to the waveform measurement system was merely a prototype built to assess its usefulness in the advanced RF measurement system. Its capabilities have not matured enough to fully replace CW stimulus yet. Furthermore, the multi-sines design method presented, significantly decreases the number of tones needed to approximate

the modulated signals, however it does not exploit the potential minimum number of tones possible. However, the development of this multi-sines design method and its application in a waveform measurement system gave valuable insights and ideas on how to proceed further.

7.2.1 Further decrease the number of tones of a multi-sines stimulus

The 50-tone multi-sines we designed to approximate the modulated signal will introduce over 300 spectral components if considering 7th order nonlinearity and 3rd order harmonics. This number will further increase to 1,500 when up to the 5th order harmonic are taken into consideration. This large number of spectral components will obviously lead to the difficulty of implementing load-pull techniques, as the variation of each spectral component will inevitably result in the variation of other spectral components in the load. To address this issue it is important to develop multi-sines with a fewer number of tones. Obviously the fewer the number of tones employed, the smaller the accuracy that will be achieved for the approximation of the modulated signals. Hence it is also important to investigate the relationship between the number of tones and accuracy in order to get a balance in this trade-off depending on the application.

7.2.2 Approximating other types of test signal

The modulated stimulus signals are crucial in understanding how complex-modulated signals are interacting with the non-linear PA characteristic. However, in the RF world there are other signals also being used as test signals such as a pulsed stimulus and a triangle-

wave stimulus. A triangle-wave signal can approximate modulated signal's PAPR but can avoid the generation of memory and thermal effects. Hence the AM-AM and AM-PM properties of the power amplifier can be accurately characterized therefore a memory-less polynomial pre-distortion method will be applied. One triangle-wave signal which has been successfully used in PA linearization is shown in figure 7.1.

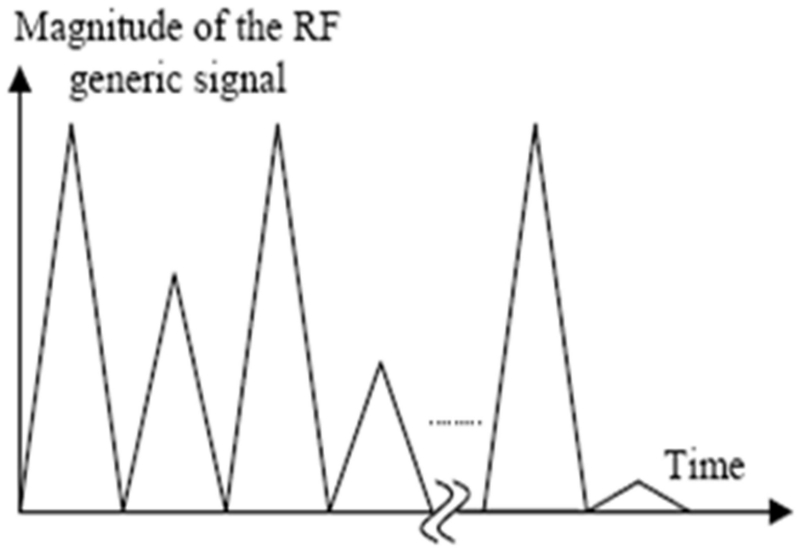

Figure 7.1 Magnitude of a triangle-wave signal[1]

Approximating this triangle-wave signal is fundamentally the same as approximating the communication signal. Some work has already been done and figure 7.2 shows some initial approximated multi-sines with 24, 36 and 40 tones.

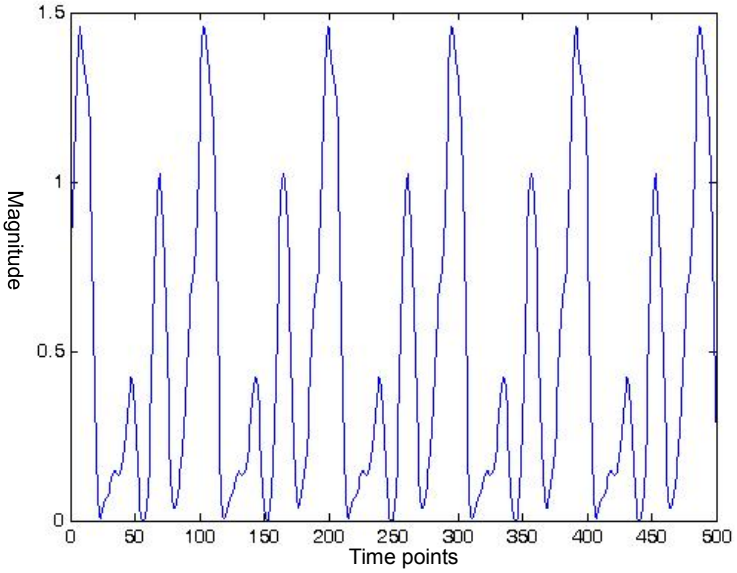

Figure 7.2a Approximated multi-sines triangle-wave signal with 24 tones

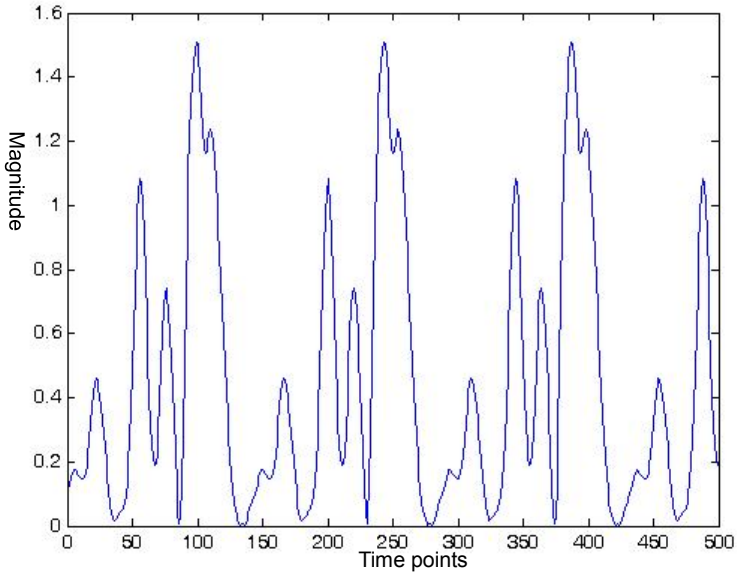

Figure 7.2b Approximated multi-sines triangle-wave signal with 36 tones

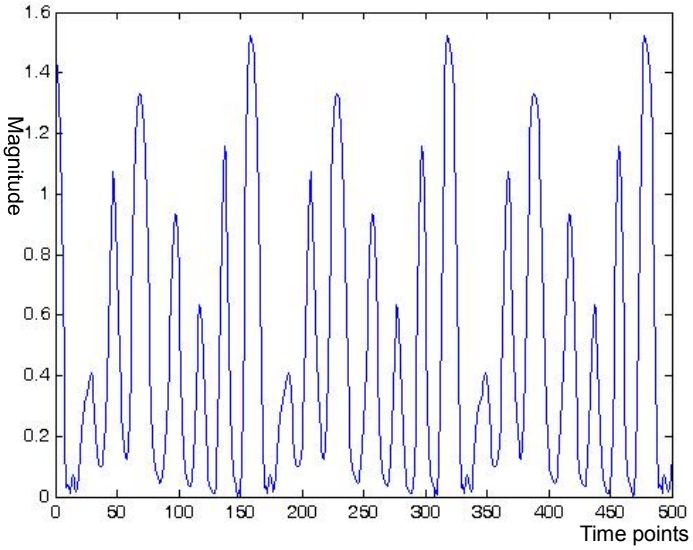

Figure 7.2c Approximated multi-sines triangle-wave signal with 40 tones

A pulsed stimulus is needed to test devices operating at higher power levels but not designed for continuous operation. These devices often lack adequate heat sinking for continuous operation thus could probably be damaged seriously; hence, it is being widely used today in device characterization, CAD modeling and system testing. Figure 7.3 shows a typical pulsed signal in both time-domain and frequency domain.

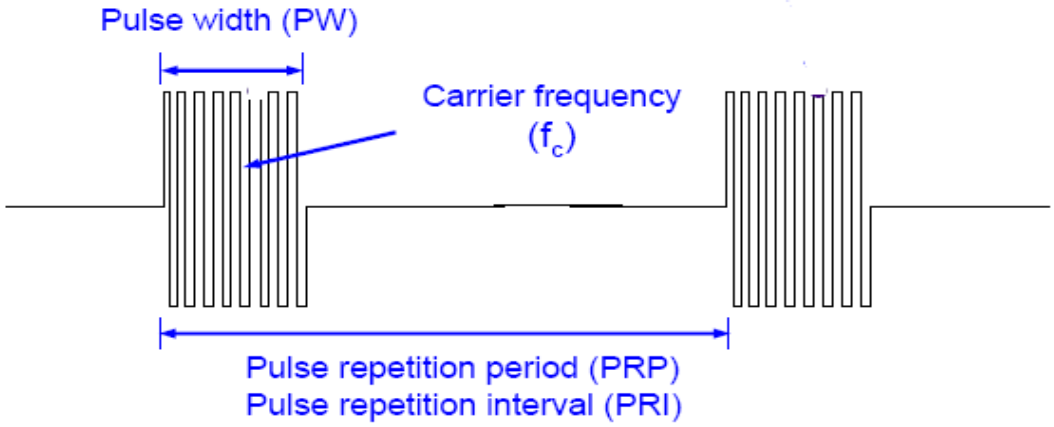

Figure 7.3a Time-domain illustration of pulsed stimulus

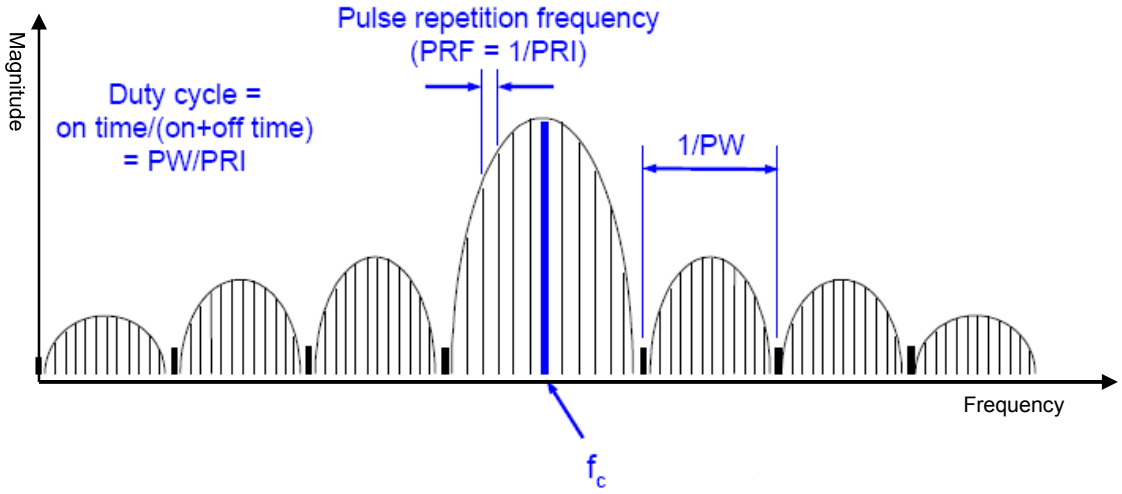

Figure 7.3b Frequency-domain illustration of pulsed stimulus

As it can be seen from the above figure, a pulsed signals' spectrum is more concentrated in the center of carrier, so it is possible to use a fewer number of tones to approximate the pulsed signal. Here we will illustrate how a 39-tone multi-sines stimulus has nicely approximated the shape of a pulsed CW stimulus, as figure 7.4 shows.

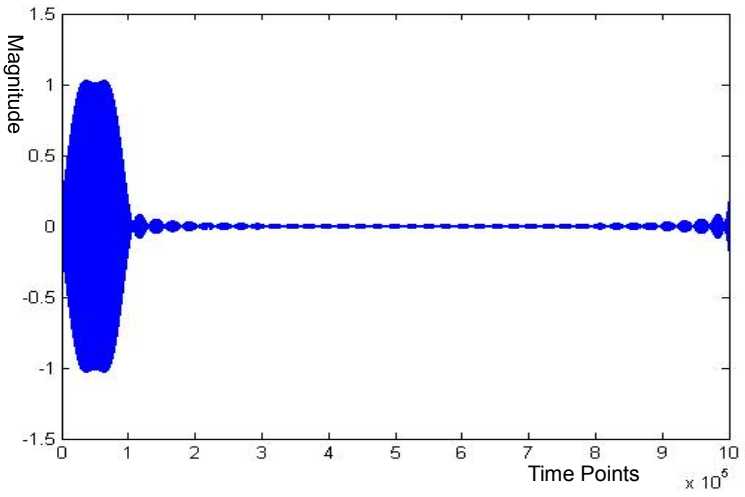

Figure 7.4 Using 39-tone multi-siness to approximate pulsed CW signal

During this multi-sines pulse signal design process, a triangle wave is employed to cancel the side-lobes of the pulse spectrum. As a result the number of tones needed to smooth the pulse will be significantly reduced. This process is graphically explained by figure 7.5.

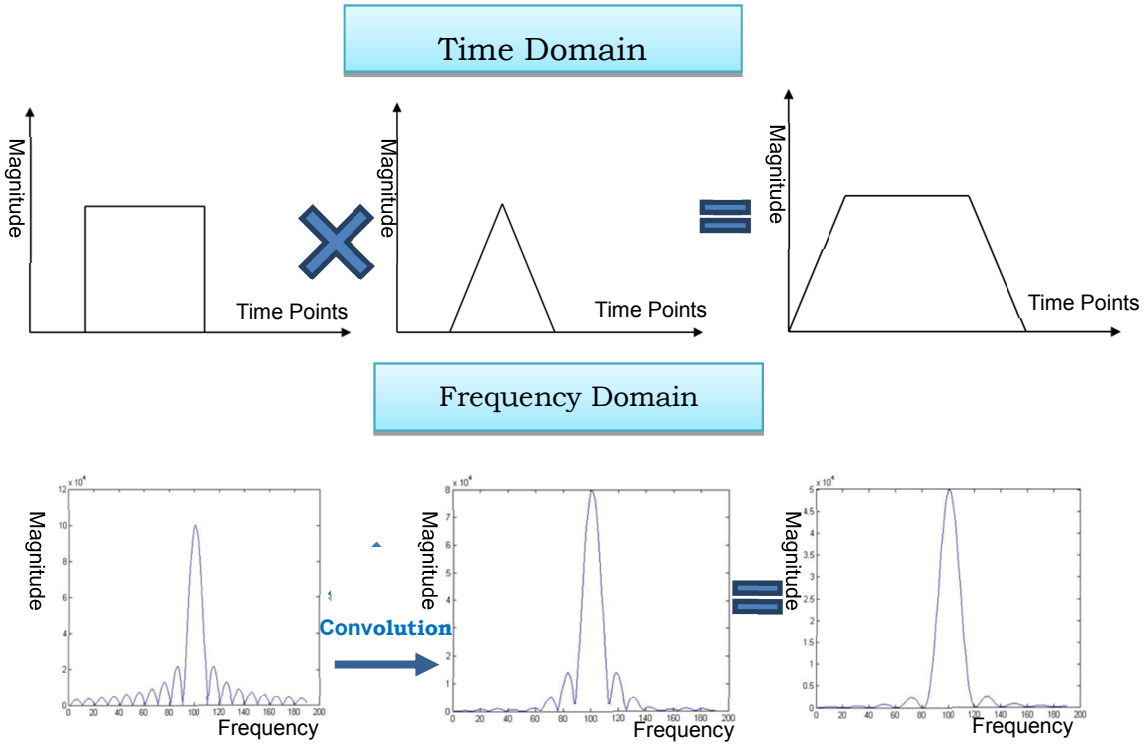

Figure 7.5 Employing triangle wave to reduce the number of tones needed for approximating pulse signals.

This multi-sines design algorithm is based on one of the basic signal processing rules that multiplies in the time domain corresponding to convolution in frequency domain. Hence as can be seen from the above figure, a pulse waveform multiplied by a triangle waveform will lead to their spectrum convolution in the frequency domain. Consequently, the amplitudes of the side-lobe frequency components

will be greatly compressed which provides the possibility of using a smaller number of tones to approximate a pulsed signal.

7.2.3 Integration of multi-sines stimulus into a waveform measurement system

The multi-sines design and measurement process presented in this work involves quite a few third-party pieces of software, such as Agilent Advanced Design System(ADS), Matlab, NI Labview and Microsoft Visual C#. This makes the entire multi-sines design and measurement process time consuming and difficult to debug potential problems. Clearly, this process needs to be concentrated into a single user interface to enable its implementation throughout the industrial world.

The Mesuro Company® [2] has introduced a software-driven measurement system which integrates RF waveform measurements with active harmonic source and load-pull; hence, for the first time, waveform engineering at high frequencies is possible for commercial purposes. The system modules include a wideband receiver, a wideband signal generator, an RF and baseband test-set and integrated software tools for s-parameter calibration and measurement. With these modules, users gain the control of the entire system for effective and automated measurements and display, control and analysis of measured waveform signals. A screenshot of Mesuro's software is shown at figure 7.6.

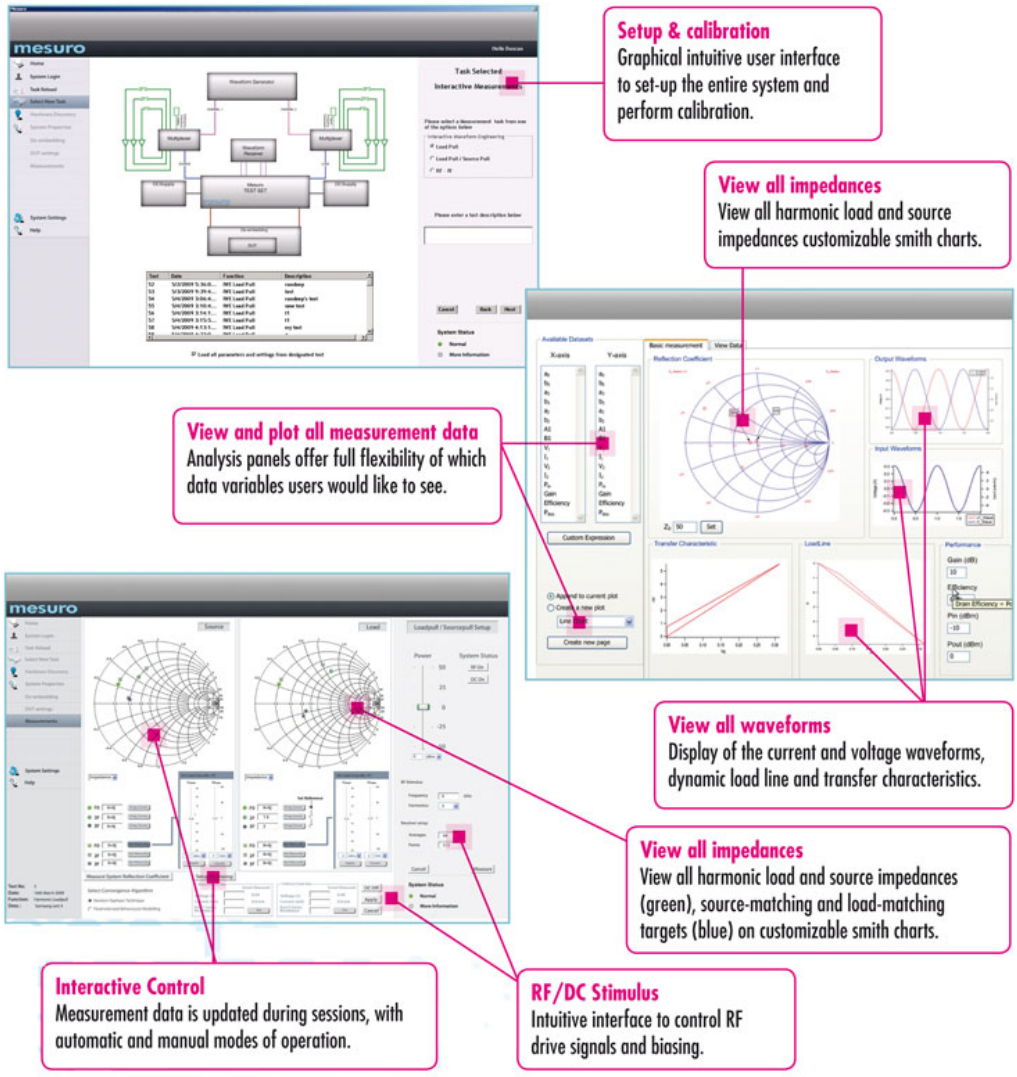

Figure 7.6 The snapshots of Mesuro's interactive measurement software[2]

However, the current version of the Mesuro software is only capable of dealing with CW stimuli. It is therefore important to integrate multi-sines stimuli into Mesuro's software to further increase the competitiveness of Mesuro's measurement solution. On the other hand, it also helps the multi-sines stimulus being widely accepted in industry.

More specifically, to incorporate multi-sines stimulus into Mesuro's software, the main works include:

1. Modification of the calibration module to incorporate multi-sines calibration.
2. Modification of the waveform de-embedding and correction engine for multi-sines waveform de-embedding.
3. Adding sub sampling technique into waveform receiver module, which is vital for multi-sines waveform collection.
4. Adding interactive multi-sines design and validation module to the users designing their own multi-sines stimulus.
5. Optimizing the software database, as multi-sines measurement contains far more spectrum information than CW measurement.

7.3 Reference:

[1] S. Bensmida, et al., "*Power Amplifier Memory-less Pre-distortion* for. *3GPP LTE Application*," European Microwave Conf. pp:1433-1436. Sept. 2009, Rome

[2]Available online at http://www.mesuro.com

Appendix.1 The introduction of waveform measurement system

1.1 The evolution from idea to practical waveform engineering and measurement

The lack of appropriate RF I-V waveform measurement tools has prevented waveform engineering directly being applied at microwave frequencies. So RF measurements have long been based on other measurable properties such as the DC I-V characteristic, bias dependent S-parameters, load-pull contours, etc.

A large proportion of existing RF measurement architectures are based around the established and mature technology of the Vector Network Analyser (VNA). Since at the low frequencies or DC, the voltage and current performance of a device can usually be measured with a parallel high impedance probe and a series low impedance probe respectively, these systems measure S-parameters to describe the behaviour of electrical networks when undergoing various steady state stimuli by small signals.

Fig. 1 gives an illustration of S-parameter in a two-port device. Where $a1$ and $a2$ are the incident signals and $b1$ and $b2$ are the reflection signals. S_{12} and S_{21} are called transmission ratios whilst S_{11} and S_{22} are called reflection ratios. S-parameters can be used to derive many commonly used design parameters such as the complex linear gain, stability, input/output return loss, and voltage reflection coefficient. In fact S-parameters completely describe the behaviour of a device under test (DUT) under linear conditions. It is this simplicity and ease of measuring the incident and reflected waves that make s-parameter convenient at microwave frequencies.

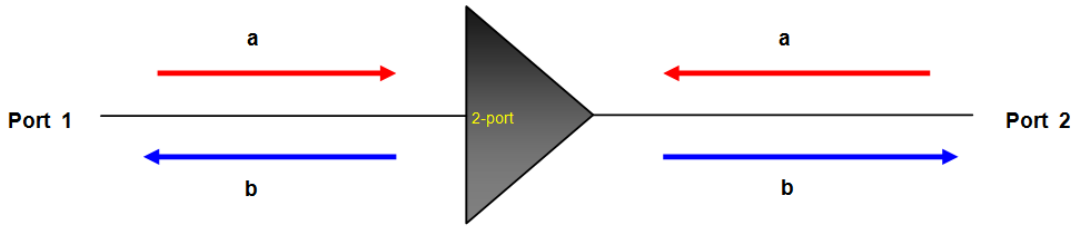

$$S_{21}=\frac{b_2}{a_1} \qquad S_{12}=\frac{b_1}{a_2} \qquad S_{11}=\frac{b_1}{a_1} \qquad S_{22}=\frac{b_2}{a_2}$$

Figure 1 S-parameter of two-port device

S-parameters are extremely popular for several reasons. First, they are easy to measure since the data is reliable and repeatable. Secondly, the data is also useful because it represents an intrinsic property of the device under test (DUT), independent of the measurement system used to provide the data. Moreover, the S-parameters of a two-port system are defined by ratios which mean the S-parameters are invariant with respect to the phase of the incident wave.

Despite the great success of S-parameters, they are severely limited as they are defined only for linear systems, or systems behaving linearly with respect to a small signal applied around a static operating point (e.g., fixed bias condition of a transistor) while virtually all real systems are nonlinear. Especially when the input excitation signal has a large amplitude variation as in modern modulated signals, the device will fall out of the scope for which linear S-parameters can apply.

In a word，measurement systems based on S-parameters are limited to when device is operated in the linear areas where there is no energy transfer from the stimulus frequency to other harmonic frequencies. However in reality devices are commonly operated far closer to compression, firmly in their non-linear regions in order to

acquire enhanced performance. Therefore S-Parameters are limited to when the device is working in linear conditions.

Standard large signal measurement, i.e. when the device is working in the nonlinear region, usually works in the frequency domain and measures the spectral re-growth by utilizing a spectrum analyser and/or power meter with narrowband tuneable filter to measure the magnitude of the spectral components. Typically, the usefulness of these measurements is further compromised by the required insertion of bandwidth-limiting components such as tuners or matching circuits. However, the lack of phase information still prevents us acquiring the voltage and current waveforms from such measurements. A more recent addition is the vector spectrum analyser, which can provide, in a frequency band around the carrier, information about the relative phase of the spectral components. However, during the process of tuning the instrument to the harmonic frequencies, the phase coherence is lost hence this solution still is of limited use in providing waveform information.

Hence large signal waveform measurement systems have been developed that operate in the time-domain. However an oscilloscope, which is the standard approach in low-frequency circuits, will usually struggle at RF frequencies. The first calibrated Digital Sampling Oscilloscopes (DSO)-based large signal waveform measurement system was presented just 20 years ago by Sipila in 1988 [2]. The measurement system uses a two-channel, high frequency sampling oscilloscope and collects only two of the four travelling waves namely the reflected input wave, $b1$, and the transmitted output wave, $b2$. Using knowledge of the S-parameters of the linear input and output coupling networks at fundamental and harmonic frequencies, the system could determine the required non-sinusoid waveforms.

Lott came up with a new frequency-domain-based waveform measurement system in the late 1980s [3]. In this case, a VNA was used to measure the individual spectral components sequentially, and a phase reference generator was used to establish a coherent phase reference. Improved error corrections can be acquired by having a magnitude and phase calibration. The setup allowed separate measurements of the fundamental and harmonic components. However, as only the output of the device is measured, this measurement approach is limited and only useful for devices and circuits that have, or have been pre-matched to a 50 Ω impedance. Hence it is unable to provide capabilities of engineering the waveforms by varying the load impedance. And again, the biggest limitation comes from the CW nature of the system, which means that the stimulus used in the measurement is still significantly different from the signals used in real life.

Barataud et al. presented a measurement setup in 1995 which is based around the VNA with extended capabilities [4]. In this setup, an off-the-shelf VNA is employed but modified in such a way that it could measure the four incident and reflected waves. This measurement architecture offers a more complete measurement solution than that presented by Lott [3] as it allows for calibrated measurement of both input and output voltage and current waveforms. In addition ports are made available for source and load impedance control allowing for waveform engineering at both the input and output of the device which is very useful in transistor performance optimization. The concepts of this system also form the basis of a further advanced VNA measurement solution that has recently emerged, specifically the PNA-X from Agilent, which is a VNA-based waveform measurement solution that utilizes a very accurate reference harmonic waveform signal generator with a

known phase characteristic attached to a fifth VNA channel to achieve phase coherence. However, due to the requirement of a frequency sweep for each measured harmonic, any architecture based around the VNA is inherently slow, and accurate phase measurement is difficult to achieve. Once again more importantly, device characterisation is limited only to CW performance and no option for the addition of multi-tone capabilities.

Other VNA vendors are presently developing similar solutions. In 1990, Kompa introduced a hybrid system integrating both a VNA and DSO [5]. This measurement system uses a modified network analyser one-path test-set for reference and test signal separation, yielding a simultaneous observation of stimulus and reflected waveforms. The concept of this system is to measure the relative phase relationship of the fundamental component using the high accuracy of the VNA, while absolute signal amplitudes are determined from the measured waveforms using a two channel sampling oscilloscope. The VNA also ensures a highly accurate method for extraction of the S-parameters during calibration. Additional accuracy is achieved during measurements at the fundamental waveform frequency as the VNA becomes part of the measurement and is constantly used to measure fundamental magnitude and phase. Again the measurement system has only two measurement channels, which are used to measure input stimulus and the transmission of the device. Reflected travelling waves are not measured. Instead, the integrated VNA is used during calibration to estimate the response of the input and output networks, thus introducing uncertainty into the measurements.

It was the introduction of the microwave transition analyser (MTA), a digitally triggered and synchronized time-domain DSO, by Hewlett Packard (Agilent Technologies) in 1992 that became the optimum

instrument for time domain based RF waveform measurement systems [6]. This instrument operates as a wideband, time domain sampling oscilloscope in its main mode of operation, but has the capability to conduct narrow band swept frequency measurements and act as a VNA to measure S-parameters with a very high dynamic range. A major advantage of the MTA over traditional oscilloscope instruments is that its sampling rate is synthesized from a common master clock, which allows this dual channel dual mode MTA to perform phase relation analysis between two channels. Many measurement system architectures have been proposed on the basis of the MTA, and a further step was taken in 1995 where the Agilent research group modified two MTA instruments, combining them to form a single 4-channel instrument. This modified MTA was used as the basis of a large signal measurement architecture known as the NLVNA [7] [8].

More recently, advances in the bandwidth of real time sampling oscilloscopes (particularly in terms of receiver bandwidth) have made it realistic to base waveform measurement systems around real time oscilloscopes. Though real-time oscilloscopes offer a number of advantages over sub-sampling oscilloscopes, such as increased memory depth allowing measurement of more complex modulated signals and the ability to capture non-repetitive signals along with simplified triggering architectures, there is also a significant down side as real-time oscilloscopes use high-speed Analog-to-Digital converters and must move huge amounts of data into and out of memory. This means that their resolution is typically limited to 8 bits, which has a significant effect on overall dynamic range and the ability to look at in-band and out-of-band distortion terms, which are typically at very different power levels to the carriers.

To summarise, a number of systems offer modulated large-signal

measurement capabilities but no single one of them combines the collection of all signal components (base-band, in-band and harmonic band) along with the appropriately engineered receiver sampling approach to allow the detailed investigations required in modern microwave device characterisation. Hence for our waveform measurement system it is necessary to inherit the advantages of the above systems and compensate for their incapability.

1.2 Introduction of Cardiff University's waveform measurement system

David Williams [9] reported a system that was similar to the one presented in [6] but with enhanced and extended capabilities. The major extension was the waveform engineering capability by employing harmonic load-pull. The system architecture shown in Fig.2，which is the most basic large signal measurement setup at Cardiff University.

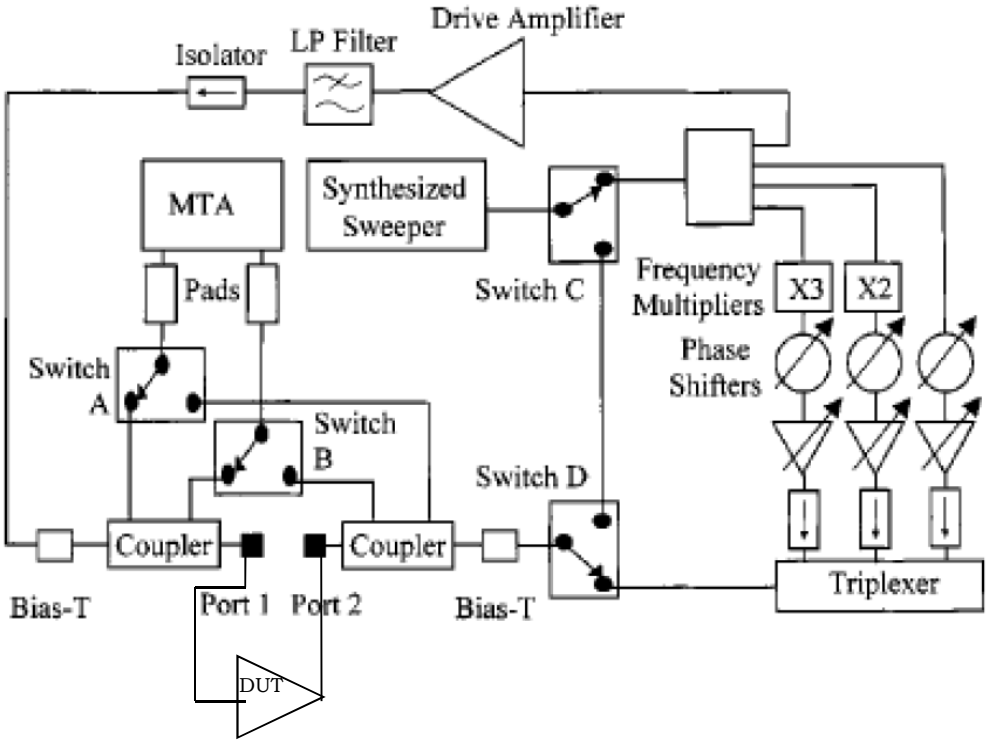

Figure 2 Schematic of implementation of Intial Cardiff waveform measurement system[9]

This system actually doesn't measure the current and voltage at each end of the device but measures the time-varying incident $a_n(t)$ and reflected/transmitted $b_n(t)$ voltage travelling waves at both ports of the DUT. Hence the integration of a four-channel MTA is necessary and the two switches are used to allow the 2-channel MTA capable of function as a multiplexed 4-channel receiver. However, switching strategy needs to be carefully designed to prevent the loss of synchronisation between the travelling waves. A phase handover measurement is performed to maintain the phase synchronisation. This requires switching one channel at a time to make sure there is always a common quantity being measured at any point of the measurement. In that case the phase offset when measuring these different travelling waves can be traced and corrected. These travelling wave energies are sampled by using two directional couplers at the device ports. The couplers also have attenuation and the amount of attenuation can be changed depending on the power of

the device being measured to protect the MTA from being overdriven when measuring high power transistor devices. The bias-T at the input and output are used for providing the required biasing to the device. Hence this system can be simplified as figure 3

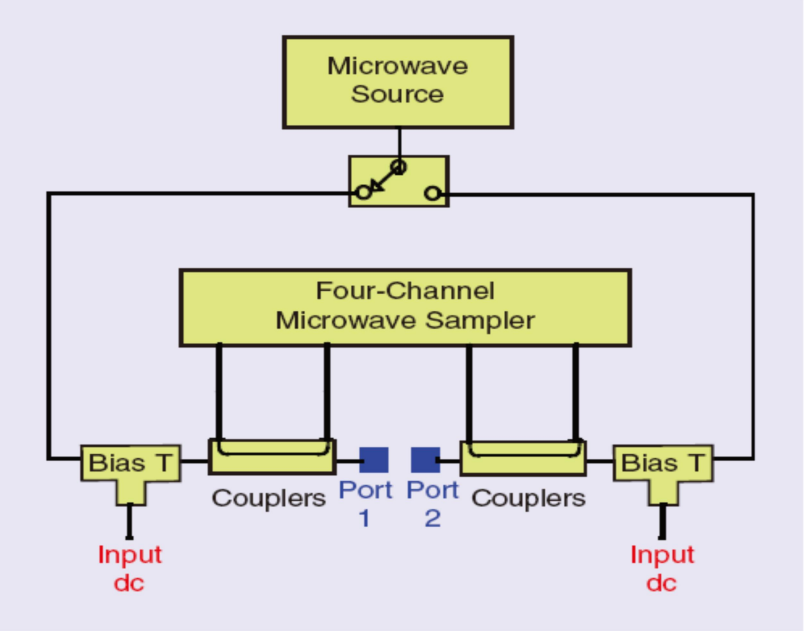

Figure 3 Simplified schematic of implementation of Cardiff waveform measurement system[10]

However, the biggest drawback of this architecture presented here is its incapability of measuring more complex modulation signals. Tudor Williams [11] replaced MTA receiver with a 4-channel sampling oscilloscope, modified to encompass both CW and multi-tone excitations. As the oscilloscope has 4 channels, the need for complex multiplexing and software control algorithms required to measure all four time synchronised incident and reflected travelling waves is removed. Thus simplifying the design and removing any measurement ambiguity relating to the relative phase measured at the input and output of the DUT. The measurement time is also dramatically reduced since only a single measurement is required to capture the necessary four travelling waves instead of the 3 measurements required with the two-channel MTA. He also performed appropriate changes in the setup architecture, by

incorporating bias tee to act as diplexer for both separating and combining the RF and IF (base band) signals, which is essential for multi-tone large signal characterization. The final measurement System Architecture is shown at figure 4.

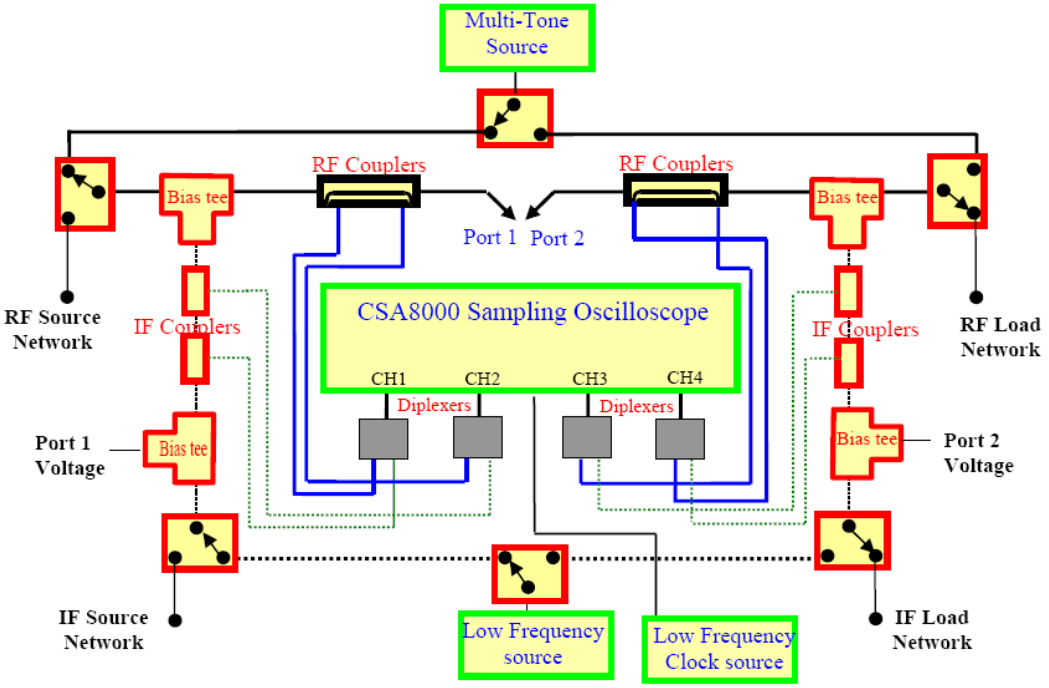

Figure 3 Basic schematic of a multi-tone time-domain-based measurement System Architecture, with Integrated RF and IF Capabilities [11]

1.3 The implementation of Active Load-Pull

This waveform measurement system also has integrated load-pull facilities. The RF PA design community has often emphasised the need for accurate measurements of key nonlinear performance parameters such as output power, gain, efficiency, linearity, etc. as a function of the fundamental load impedance, and to take it as the key design parameter. This is called load-pull which aims to find the fundamental load impedance with which the desired optimum performance is achieved. While PA designers are forced to tackle the increasingly demanding system requirements and thus consider more complex high-efficiency modes of operation, this black-box approach will become impractical as it requires a systematic

variation of many more parameters such as harmonic source and load impedances.

The active load-pull capability of Cardiff University's waveform measurement system provides a promising solution over this issue. In traditional passive load-pull setups, as shown in figure 5, the desired load is synthesized by varying the reflection coefficient of the impedance controlling element. Normally the load reflection coefficient is varied by tuning its phase and/or the amplitude with the help of passive tuner. There are a variety of tuners that have been developed over the years to achieve passive load-pull. For example, we can use a stub tuner and by varying the length of the stub and the position of the stub, we can adjust the magnitude and phase of reflection coefficient. Unfortunately, coverage of the impedance plane is limited by losses in these passive mechanical systems that effectively limit the achievable maximum magnitude of the reflected wave *a2*.

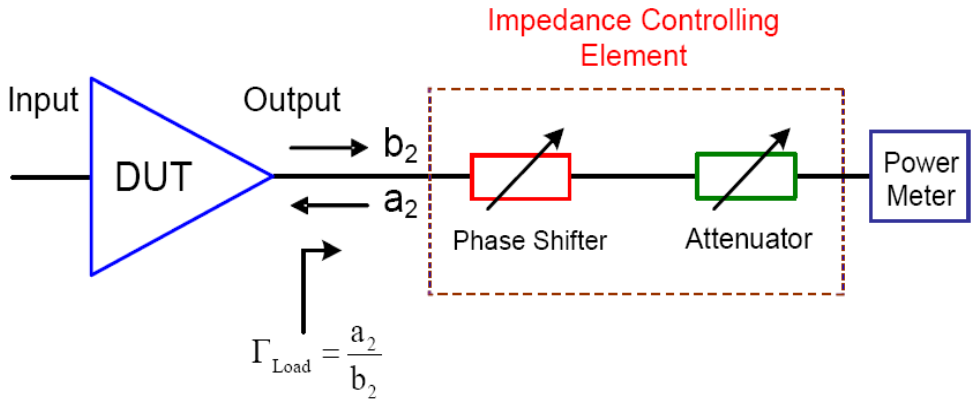

Figure 4 Basic schematic of passive load-pull technique

To overcome these losses, a number of active load-pull architectures have been proposed and investigated. In an active load-pull system these losses are overcome by amplifying the reflected wave *a2*. While signal amplification can address the problem of loss, hence allowing

unrestricted coverage of the impedance plane. When used in the preferred closed-loop architecture, they can introduce the potential for oscillation. This oscillation concern has limited the uptake of active load-pull.

Cardiff University's measurement system employs open loop active load-pull to tackle this problem. In this technique, the injected signal, *a*2, is from external RF signal generator and is independent of the transmitted signal, *b*2. Simple amplification of the signal from the RF signal generator ensures that the open-loop architecture can both overcome losses and achieve appropriate power levels. Figure 6a provides a simple illustration of open-loop active load-pull.

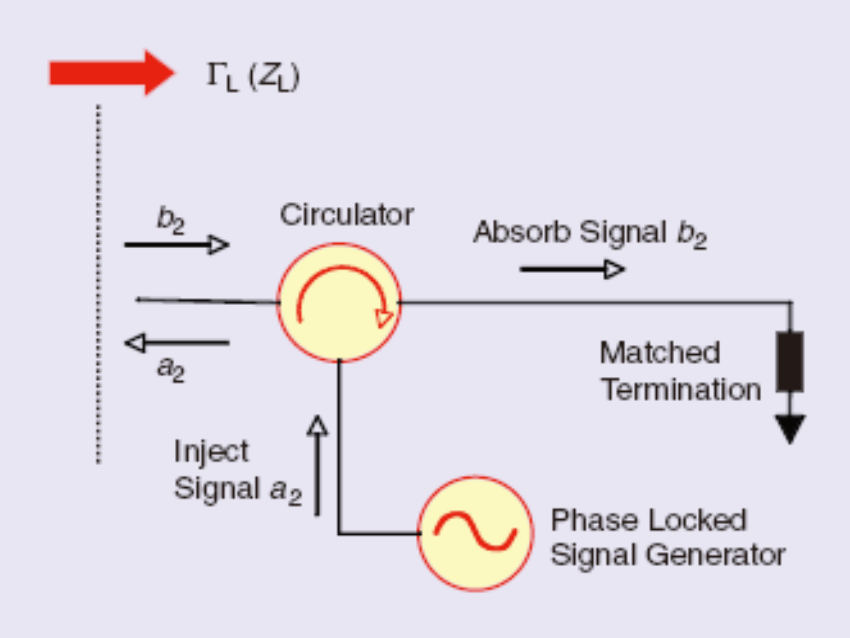

Figure 5a *Illustration of open-loop active load-pull technique [10]*

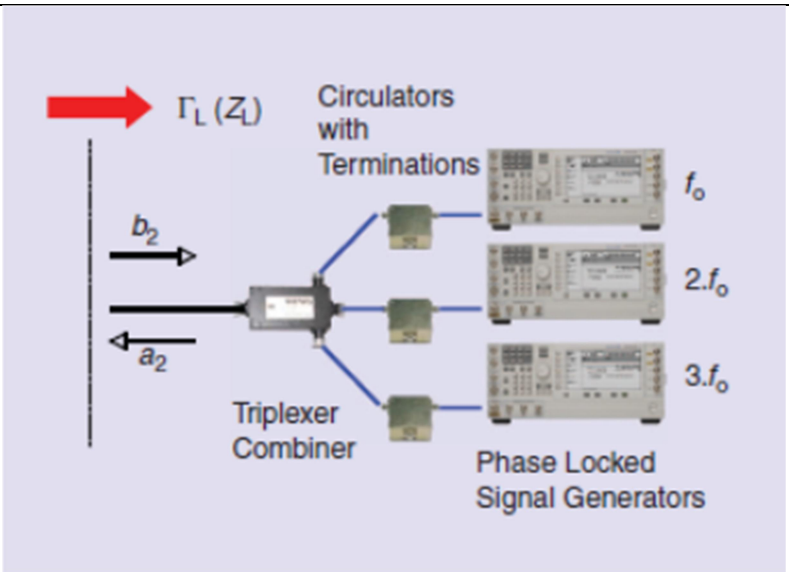

Figure 5b Illustration of open-loop active load-pull technique [10]

It is well understood that the harmonic signal content in an amplifier play a major role in defining the performance of microwave circuits and therefore it is a standard practice to consider their impact while designing microwave circuits and systems. Multi-triplexers are used to isolate the fundamental, 2nd harmonic and 3rd harmonic paths, thus the load impedance attached to each harmonic can be independently controlled [12]. This can be seen from figure 6b.

Recently envelope load-pull capability has also progressed on this measurement system to encompass a multi-sines stimulus. It functions by controlling the reflection coefficient with a feedback loop not at RF but at the down-converted baseband frequency. The premise of this approach is that by tracking the time varying amplitude and phase of the "envelope" of wideband modulated transmitted RF signals this active load-pull system can present a user control, frequency invariant load, even during multi-tone excitation. Figure 7 gives an illustration of envelope load-pull [13][14].

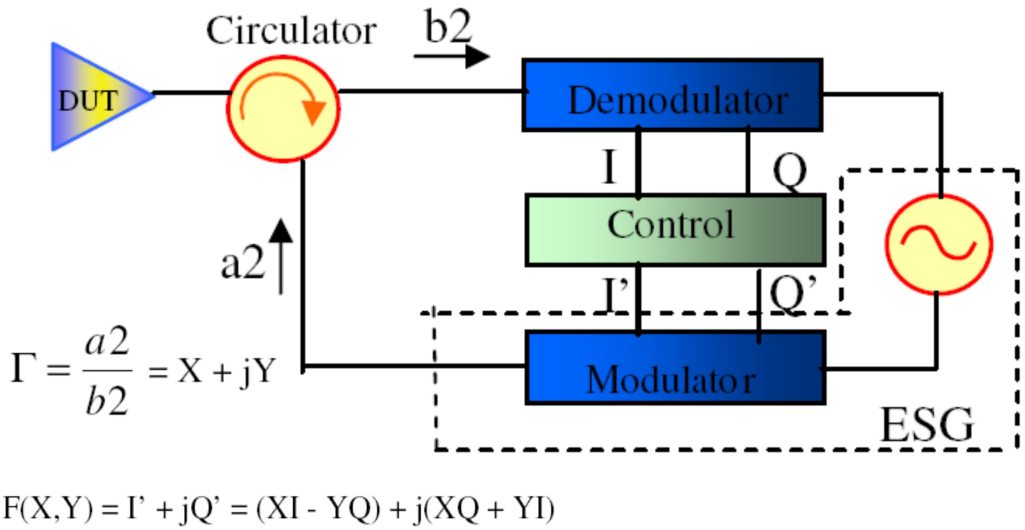

Figure 6 Illustration of envelope load-pull technique[13]

1.4 Application of waveform engineering

The measured RF I-V waveforms can be used in nonlinear device modelling as providing waveform information with the variation of bias or frequency to extract the necessary nonlinear state functions or model coefficients. Such models can then be used in nonlinear CAD simulators, mainly utilizing harmonic balance concepts, to compute nonlinear performance into arbitrary terminal impedances.

To name just few examples, Qi Hao [15] presents a "truth lookup model" developed to import non-linear measurement data into a non-linear CAD simulator. Its implementation in the Agilent ADS simulator has been verified on several different types of high frequency transistors. Aamir [16] outlines the use of a measurement based Look-Up Table (LUT) model for the design of a Doherty amplifier. It was shown that the LUT model was able to simulate the Doherty amplifier using well-established matching network design techniques. In this way, the Fourier coefficients of the measured input and output current waveforms are tabulated into a dataset after phase normalization and scaling. The dataset lookup parameters are typically DC bias voltages, frequency, magnitude of

the fundamental Fourier component of the input voltage waveform, and the complex load impedances of fundamental and harmonics. The LUT model has been implemented in commercial nonlinear CAD simulators, mainly utilizing harmonic balance concepts, and used, via a combination of data lookup and extrapolation, to compute nonlinear device performance into arbitrary terminal impedances. Moreover, on-going development is working on using X-parameters [17] or other parameters beyond S-parameters to extend the waveform lookup models over traditional nonlinear device models.

This measurement system can also be used in the field of transistor characterization to fully investigate the transistor's dynamic nonlinear response at RF frequencies. Chris. Roff provides a clarifying insight into DC–RF dispersion problems in GaN HFETs through RF waveform measurements performed across a range of RF load impedances and physical device modelling [18]. It has been shown that the virtual-gate surface charge created when devices are biased with high drain voltages can explain the different dispersion effects seen when different regions of the device I–V are probed by RF signals.

In the areas of amplifier design, these waveform measurement and engineering systems can be used to determine the appropriate impedance required to achieve a given performance. This performance is directly linked to the mode of operation (voltage and current waveforms) realized as this information can be directly measured. The experimental design object now becomes systematically adjusting the bias point, input RF drive level, and output and input terminal impedances to achieve a target waveform. Since this target waveform has been previously mathematically defined, once experimentally achieved, the associated RF power and efficiency predicted will automatically be observed [19]–[20]. Once

completed, linear CAD tools can then be employed to design a suitable matching network.

An inverse class-F design procedure was provided for obtaining very high efficiency performance at high power levels based on a GaN HEMT transistor[21]. Drain efficiencies above 81% have been achieved at 0.9 and 2.1GHz for 12W fundamental output power. Investigations into improvements in drain efficiency through increases in drain bias voltage have yielded drain efficiencies of up to 84% at 2.1GHz. In this inverse Class F solution a square output current waveform and a half rectified output voltage waveform is engineered, then the waveform measurement system provides the designer with the desired input and output matching circuit impedances necessary at the fundamental, second harmonic, and third harmonic. The designer now had all the information necessary to design an appropriate microwave matching circuit and assemble the PA. Once assembled, the amplifier was simply characterized, giving a measured performance that was identical to that predicted.

1.5 Reference

[5] Bossche, Marc Vanden; Verbeyst, Frans; Verspecht, Jan. "The Three Musketeers

[6] of Large Signal RF and Microwave Design-Measurement, Modeling and CAE", 53rd ARFTG Conference Digest-Spring, Volume 35, June 1999 Page(s):1 – 8

[7] Sipila, M.; Lehtinen, K.; Porra, V. "High-frequency periodic time-domain waveform measurement system" IEEE Transactions on Microwave Theory and Techniques, , Volume 36, Issue 10, Oct. 1988 Page(s):1397 – 1405

[8] Lott, U. **"**Measurement of magnitude and phase of harmonics generated in nonlinear microwave two-ports" IEEE Transactions on Microwave Theory and Techniques, Volume 37, Issue 10, Oct. 1989 Page(s):1506 – 1511

[9] Barataud, D.; Arnaud, C.; Thibaud, B.; Campovecchio, M.; Nebus, J.-M.; Villotte, J.P. "Measurements of time-domain voltage/current waveforms at RF and microwave frequencies based on the use of a vector network analyzer for the characterization of nonlinear devices-application to high-efficiency power amplifiers and frequency-multipliers optimization" IEEE Transactions on Instrumentation and Measurement, Volume 47, Issue 5, Oct. 1998 Page(s):1259 -1264.

[10] Kompa, G.; van Raay, F. "Error-corrected large-signal waveform measurement system combining network analyzer and sampling oscilloscope capabilities" IEEE Transactions on Microwave Theory and Techniques, Volume 38, Issue 4, April 1990 Page(s):358 – 365

[11] Van Raay, F.; Kompa, G. "A new on-wafer large-signal waveform measurement system with 40 GHz harmonic bandwidth" IEEE/MTT-S International Microwave Symposium Digest 1992, vol.3, Page(s):1435 – 1438.

[12] Verspecht, J.; Debie, P.; Barel, A.; Martens, L. "Accurate on wafer measurement of phase and amplitude of the spectral components of incident and scattered voltage waves at the signal ports of a nonlinear microwave device" IEEE/MTT-S International Microwave Symposium Digest 1995, Vol.3, Page(s):1029 – 1032.

[13] Verspecht, Jan; Verbeyst, Frans; Bossche, Marc Vanden "Network Analysis Beyond S-parameters: Characterizing and Modeling Component Behaviour under Modulated Large-Signal Operating Conditions" 30th European Microwave Conference Oct. 2000 Page(s):1 – 4.

[14] Williams D. J., "Non-linear Measurement System and Techniques for RF Power Amplifier Design," PhD thesis, 2003, Cardiff University.

[15] Tasker, P.J, "Practical Waveform Engineering", Microwave Magazine, IEEE Volume: 10 , Issue: 7, 2009, p65-p76

[16] Williams, T. V.; "A Large Signal Multi-tone Time Domain Waveform Measurement System with Broadband Active Impedance Control," PhD thesis, 2007, Cardiff University.

[17] D. J. Williams and P. J. Tasker, "An automated active source and load pull measurement system," in Proc. 6th IEEE High Frequency Postgraduate Student Colloquium, Sept. 9–10, 2001, pp. 7–12.

[18] S. J. Hashim, M. S. Hashmi, T. Williams, S. Woodington, J.Benedikt, and P. J. Tasker, "Active envelope load-pull for wideband multi-tone stimulus incorporating delay compensation," in Proc. 38th European Microwave Conf. (EuMC'08), Oct. 27–31, 2008 pp. 317–320

[19] M. S. Hashmi, A. L. Clarke, S. P. Woodington, J. Lees, J. Benedikt, and P. J. Tasker, "Electronic multi-harmonic load-pull system for experimentally driven power amplifier design optimization," in IEEE MTT-S Int. Microwave Symp. Dig., June 2009, pp. 1549–1552.

[20] H. Qi, J. Benedikt, and P. J. Tasker, "Data Utilization: From Direct Data Lookup to Behavioral Modeling," IEEE Trans. Microwave

Theory Tech., vol. 57, no. 6, pp. 1425–1432, June 2009.

[21] A. Sheikh, J. Lees, J. Benedikt, and P. J. Tasker, “Utilization of a measurement based CAD tool for enhanced PA design investigations,” in Proc. European Conf. Wireless Technology (EuWiT’08), Oct. 27–28, 2008, pp. 250–253 and 38th European Microwave Conf. (Eu-MC’08), Oct. 27–31, 2008, pp. 1671–1674.

[22] S. Woodington, T. Williams, H. Qi, D. Williams, L. Pattison, A.Patterson, J. Lees, J. Benedikt, and P. J. Tasker, “A novel measurementbased method enabling rapid extraction of a RF waveform look-up table based behavioral model,” in IEEE MTT-S Int. Microwave Symp. Dig., June 15–20, 2008, pp. 1453–1456.

[23] C. Roff, J. Benedikt, P. J. Tasker, D. J. Wallis, K. P. Hilton, J. O. Maclean, D. G. Hayes, M. J. Uren, and T. Martin, “Analysis of dc-RF dispersion in AlGaN/GaN HFETs using RF waveform engineering,” IEEE Trans. Electron Devices, vol. 56, no. 1, pp. 13–19, Jan.2009.

[24] C. Roff, J. Benedikt, and P. J. Tasker, “Design Approach for Realization of Very High Efficiency Power amplifiers,” in IEEE MTT-S Int. Microwave Symp. Dig., June 3–8, 2007, pp. 143–146.

Appendix.2 NI Labview program of measuring ACPR and EVM

As been introduced in the main chapters, the Labview programming environment will allow users to create virtual measurement devices which cater for their exact needs. In this project, although there are several virtual instruments have been developed, they are inherited from 4 main virtual instruments(VI). The functions of these 4 VIs are:

- Signal Generator for modulated signal generation. The modulated signal is generated from txt files which record the time-domain waveform information. This VI read I data and Q data from two separate files to generate baseband signals and then modulated to RF frequency.
- Signal Generator for multi-sines signal generation. This VI read multi-sines parameters such as frequency, amplitude and phase to generate multi-sines baseband signal and then modulated to RF frequency.
- Spectrum Analyser to measure ACPR. This VI performs like a standard spectrum analyser however specialized in ACPR calculation.
- Signal Analyser to fetch time-domain waveform data for EVM calculation. This VI demodulated the RF signal to baseband and records the time-domain waveform information into txt files. These files will be exported to Matlab to calculate the final EVM.

As introduced, a labview application is composed of front interface and background block based program. The detailed application files is

provided in the appended CD, so in here we will only introduce a simplified block flowchart in order to let the program files more understandable. Firstly, figure2.1~figure2.4 provide the interfaces of the above four virtual instruments.

Figure 2.5 provide the flowchart of the VI generating multi-sines signals. As we need to drive the DUT in various power levels, another VI is developed which inherited from this application but has automatic power control function. Figure 2.6 shows the flowchart of this new application. Other application's flowchart are also illustrated at figure2.7~ figure 2.9.

It is necessary to point out that, although NI labview provide a maximum possibility of freedom for people to design their own measurement instruments, and the GUI interface of labview also make it easy for people to program a labview application, the functions of final labview Virtual Instruments application still limited by National Instruments fundamental VIs. Which is somehow like programming a windows program with Visual C++ is actually limited by Microsoft Foundation Classes (MFC). Because of the copyright limitations, we can not include these fundamental VIs in the appended CD. Hence some NI fundamental VIs like SMT spectrum, ni5660, niRFSG, and niRFSA is necessary to fully access our developed applications.

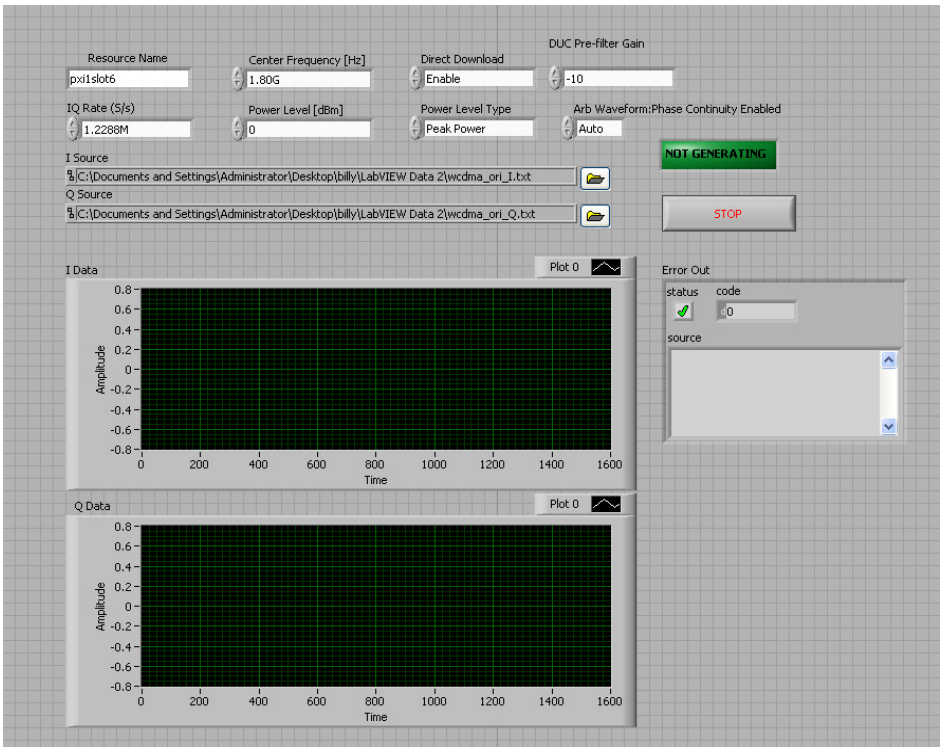

Figure 2.1 Front panel of Modulated signals Generation

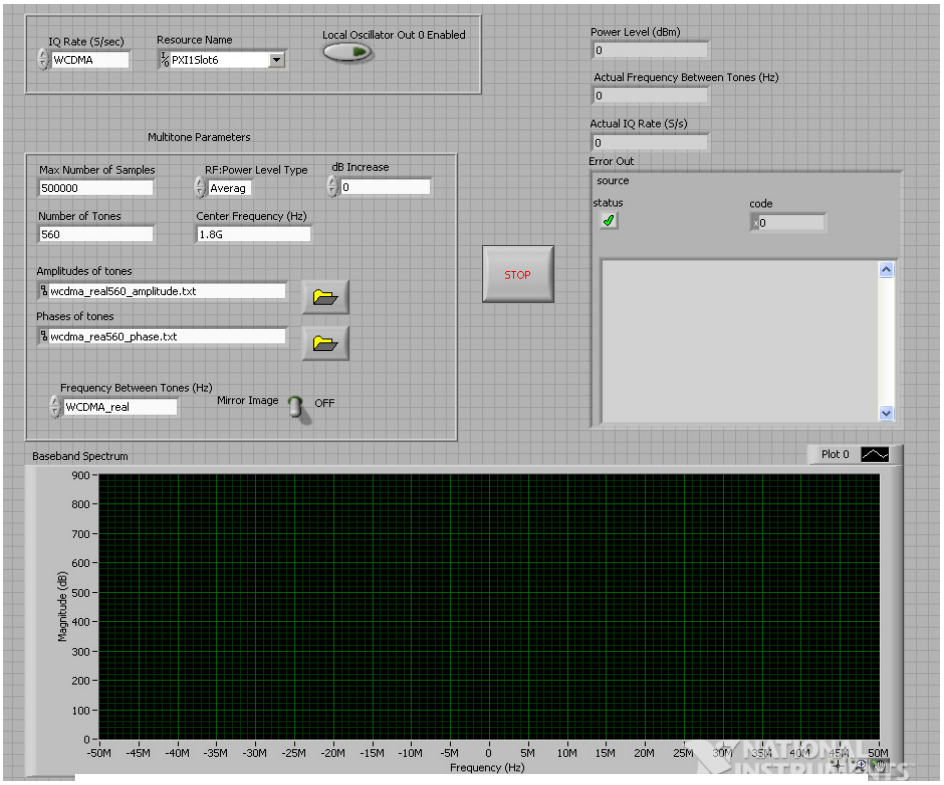

Figure 2.2 Front panel of Multi-sines Generation

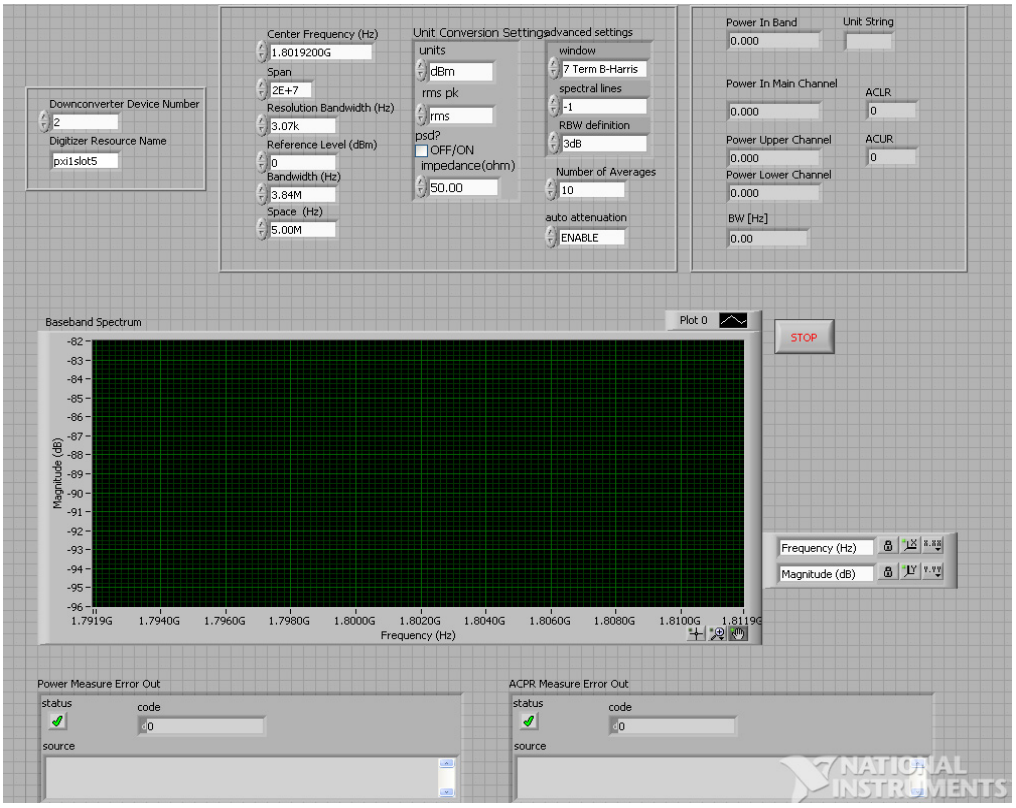

Figure 2.3 Front panel of measuring ACPR

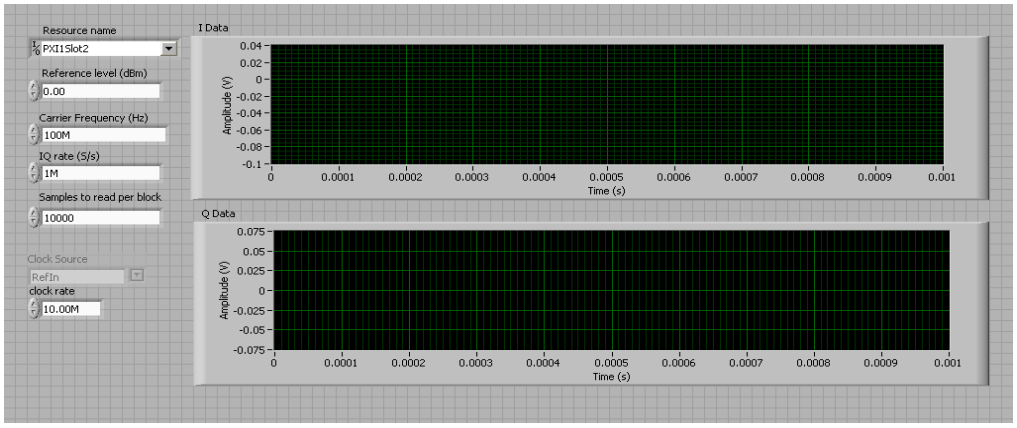

Figure 2.4 Front panel of Fetching IQ samples

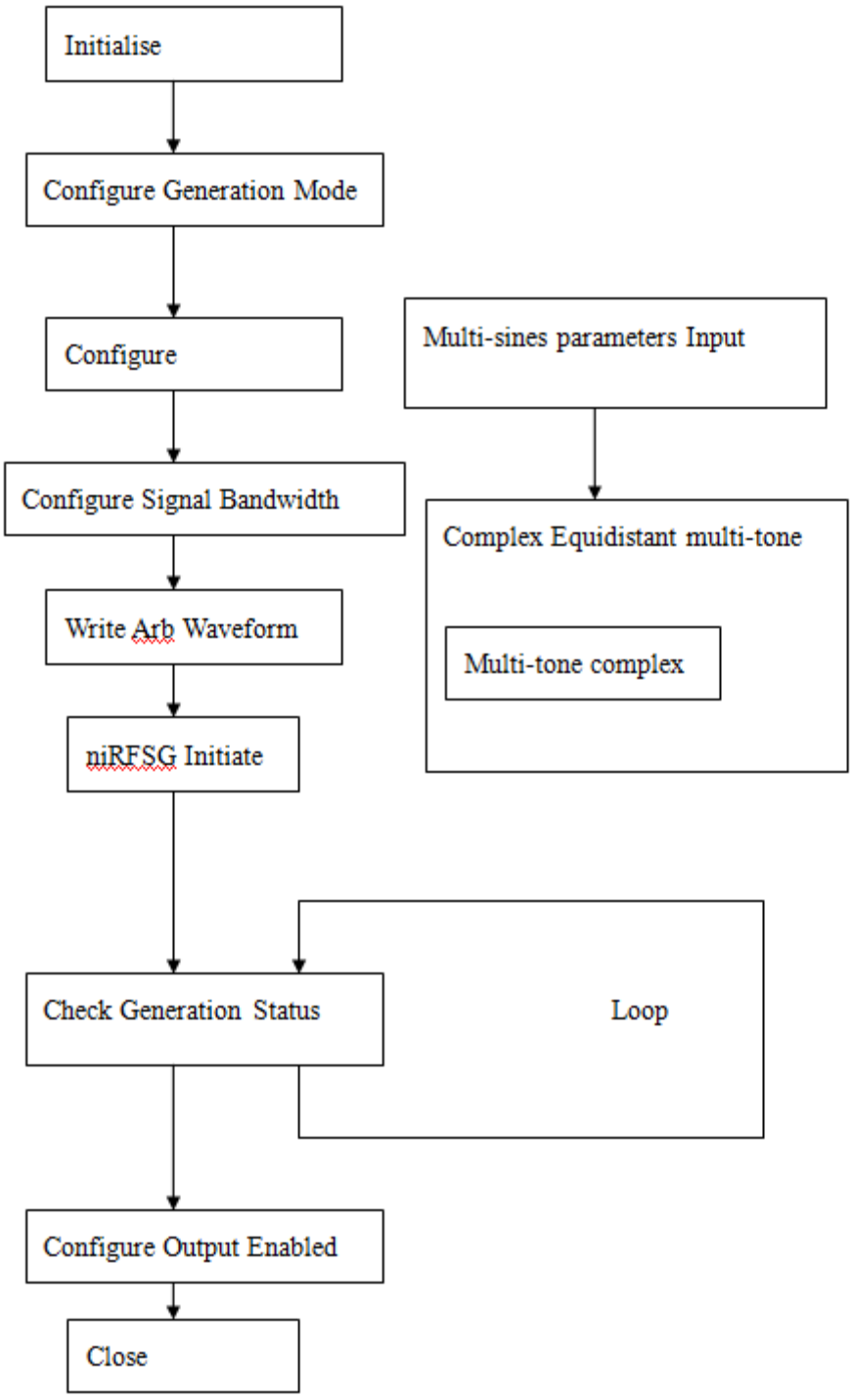

Figure 2.5 Simplified block diagram of Multi-sines Generation

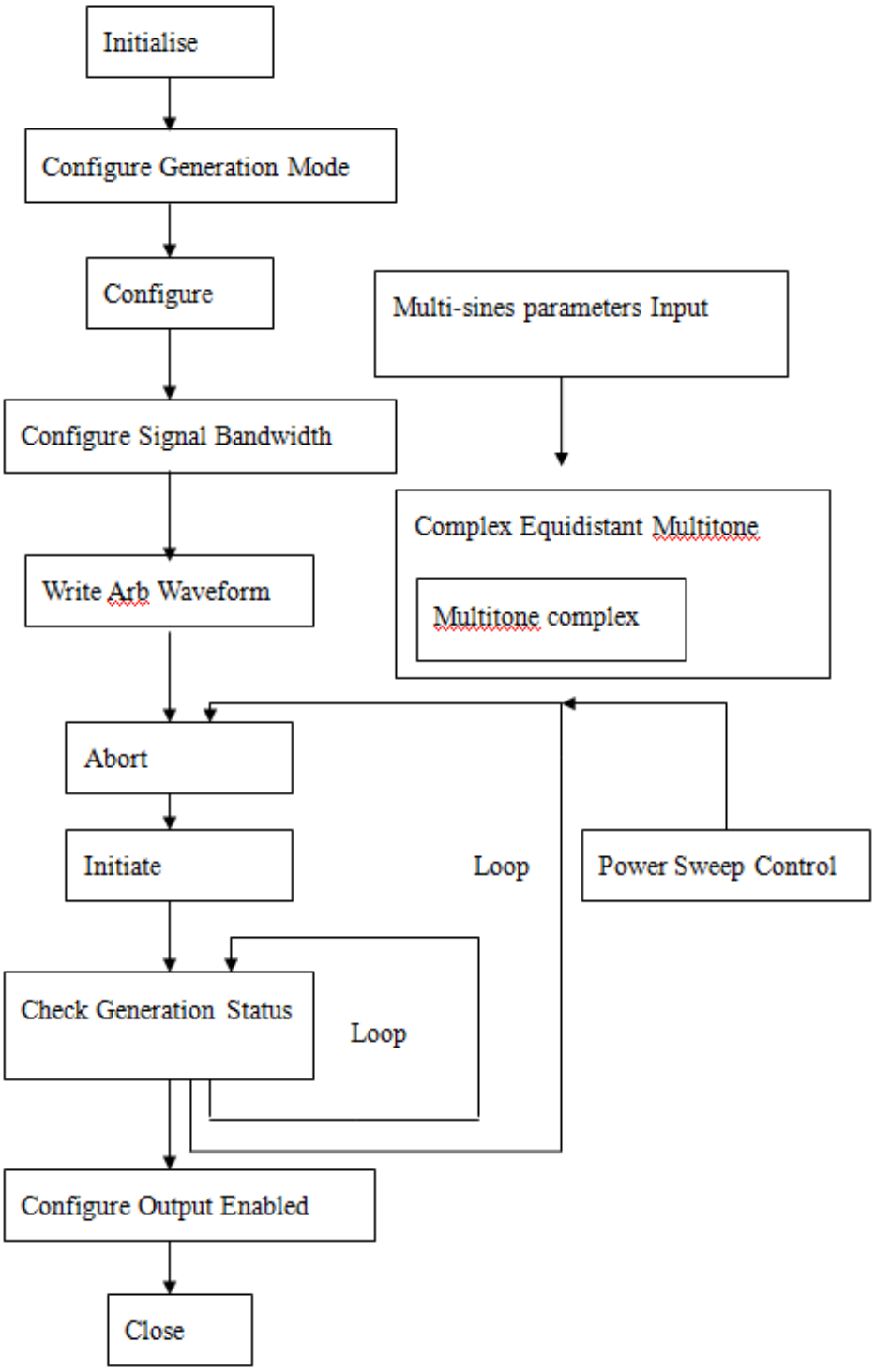

Figure 2.6 Simplified block diagram of Multi-sines Generation with power sweep

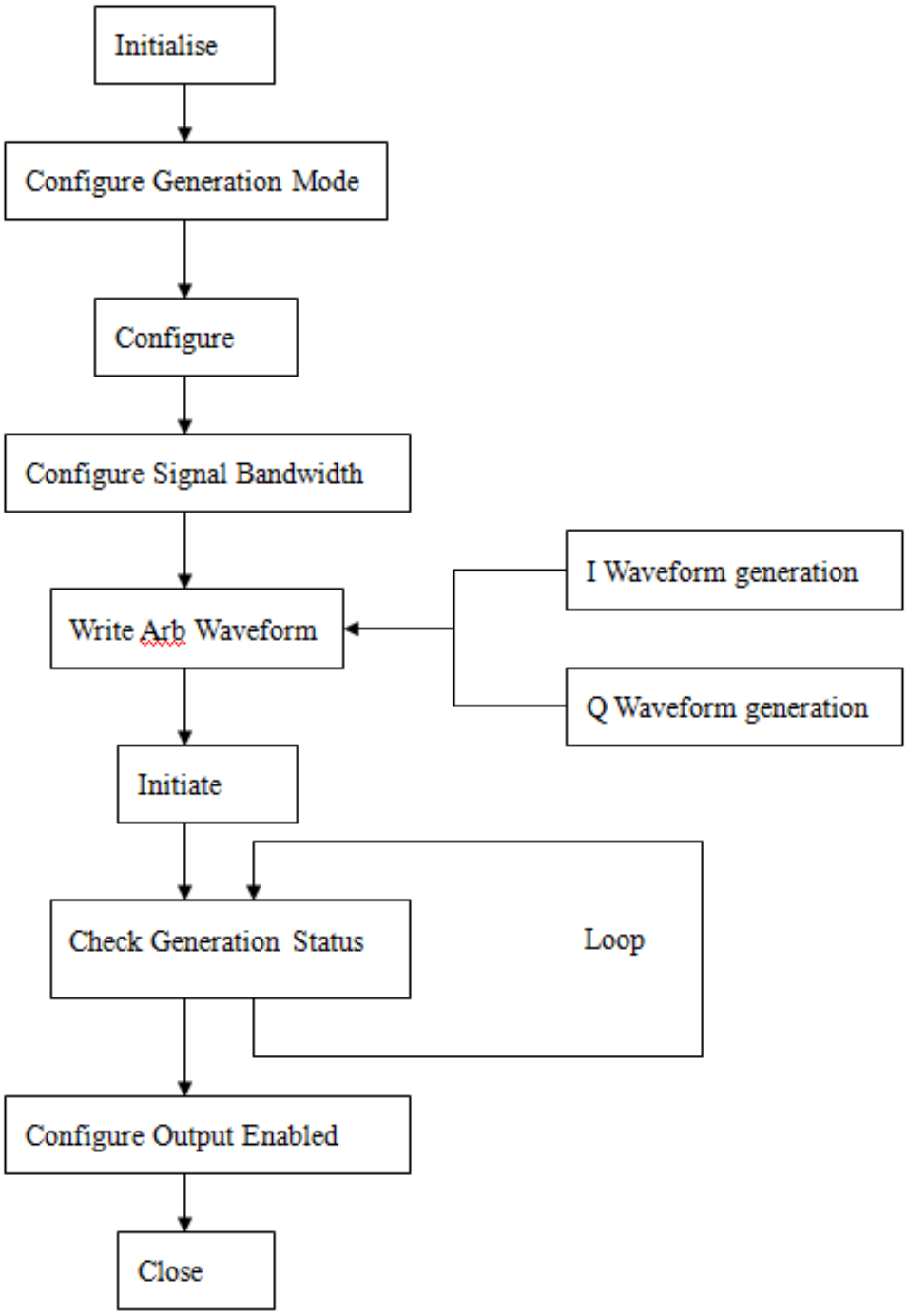

Figure 2.7 Simplified block diagram of Generating modulated signals from files

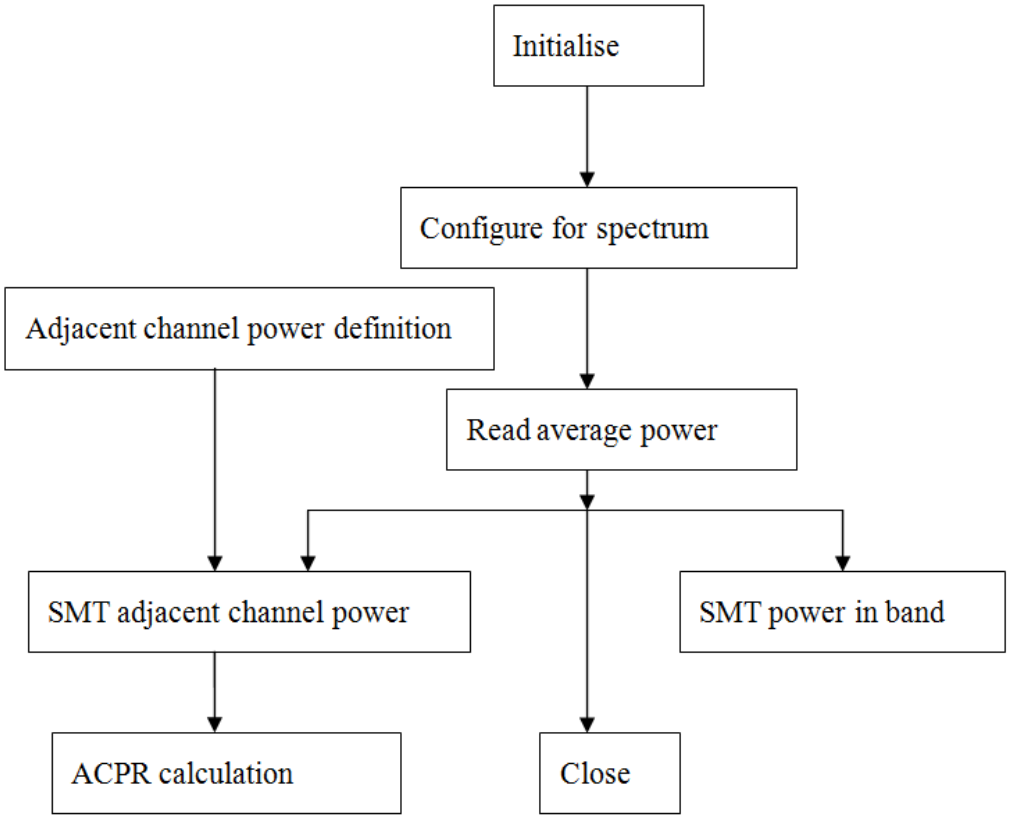

Figure 2.8 Simplified block diagram of Calculating ACPR

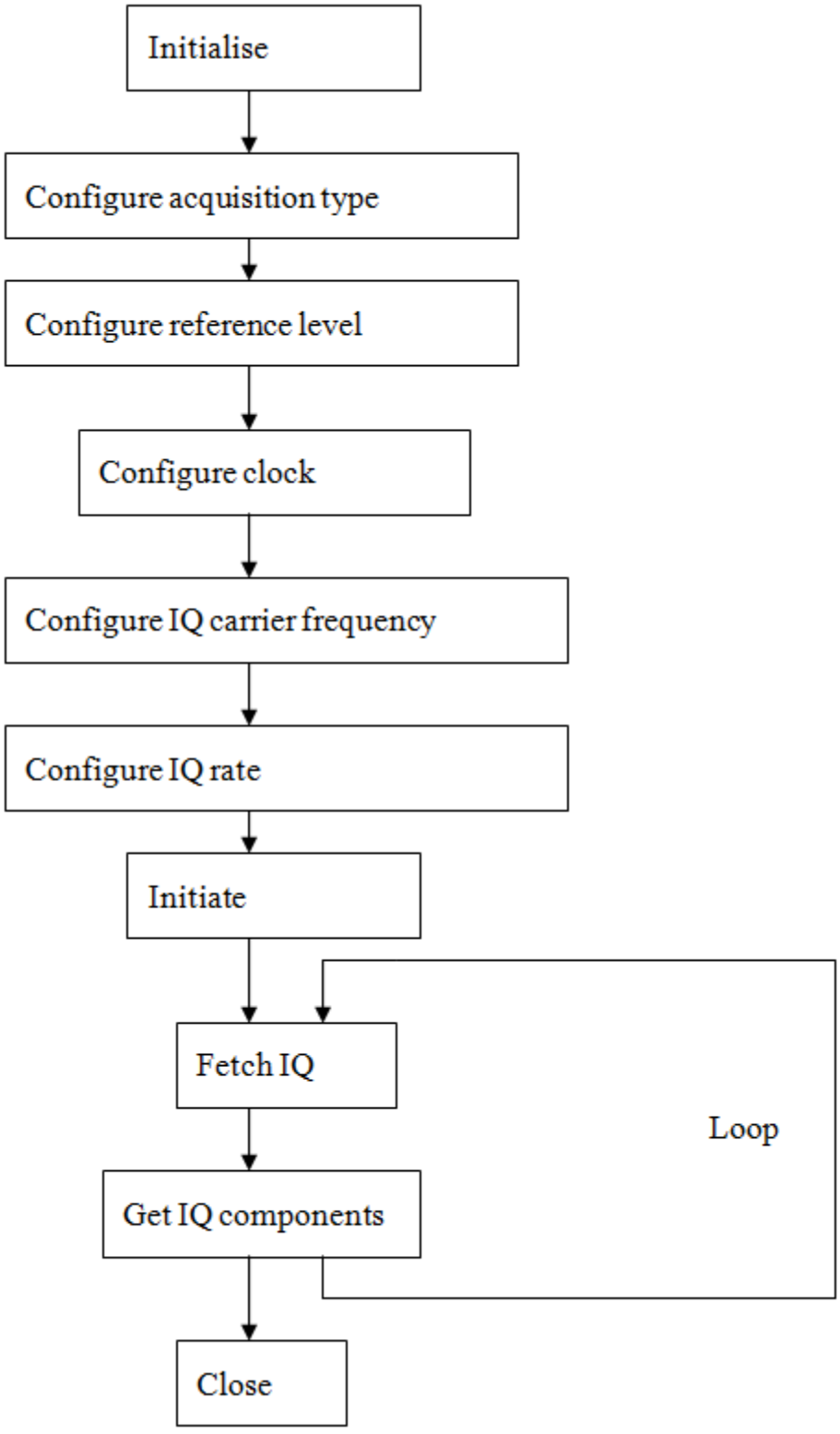

Figure 2.9 Simplified block diagram of Acquiring IQ data to calculate EVM